THE DEVELOPMENT AND IMPLEMENTATION OF MULTIPLE REFERENCE IMPACT TESTING

A thesis submitted to the

Division of Research and Advanced Studies
of the University of Cincinnati

in partial fulfillment of the
requirements for the degree of

MASTER OF SCIENCE

in the Department of Mechanical Engineering
of the College of Engineering

1994

by

William A. Fladung, Jr.

B.S.M.E., University of Cincinnati, 1990

Dr. Robert W. Rost, Committee Chair

Abstract

This thesis presents the development and implementation of Multiple Reference Impact Testing (MRIT), including issues related to data acquisition, data analysis, and test cases. MRIT is a modal testing method that measures frequency response functions (FRF) between a single, roving impactor and several, fixed response transducers which are the references of the FRFs. The fundamental theory of the MRIT method is justified by the principal of reciprocity which allows the impact positions to determine the spatial definition of the mode shapes.

The MRIT method is introduced in the context of modal testing methods and the implications of reciprocity are discussed. The testing equipment, signal processing techniques and testing procedures of impact testing are reviewed in relation to the requirements of the MRIT method. Additional concepts, such as selecting reference locations and input channel autoranging, and the limitation of the MRIT method are also addressed. The implementation of MRIT data acquisition has been accomplished with customized programming of a commercially available Fourier analyzer.

An analysis method based on the Complex Mode Indicator Function (CMIF) is proposed as a companion to MRIT. A derivation of CMIF and the associated parameter estimation algorithms is given, and practical considerations of CMIF are also discussed. Post-

processing techniques that address the limitations of the MRIT method are also outlined. The correction for the effects of the exponential window on the estimated system parameters is developed. The implementation of MRIT data analysis has been accomplished with a software package developed for the personal computer.

CMIF is demonstrated and the parameter estimation algorithms are verified with two analytical systems. Several experimental test cases are offered to illustrate many of the MRIT concepts, applications, testing procedures, and analysis techniques. The conclusion shows that MRIT is a practical, versatile, and useful testing method.

Preface

This all started with the seemingly innocent words spoken by Dave Brown, "You know what *we* need to do is ..." That was when Dave wanted to have an MRIT/Troubleshooting demonstration for the Technology Center at the Tenth IMAC. After IMAC, I started with some CMIF MATLAB scripts written by Pat Barney, borrowed the animation from Tony Severyn's SST program, and over the next year or so developed what became known as the MRIT Analysis Software. This software package has proliferated, and someday I may even update it for MATLAB version-4, with a graphical user interface. That year, Dave Brown and I wrote the MRIT papers for ISMA in Leuven and the Eleventh IMAC, and the following year I wrote two more IMAC papers related to MRIT with Dave, Bob Rost, and Jeff Poland.

Meanwhile, I was gaining experience on impact testing, but to develop a data acquisition system that was designed for impact testing would have meant creating custom software and hardware, something that was beyond the reach of my abilities. Then in the Spring of 1993, an HP-35670A four-channel analyzer arrived at SDRL, and I heard those infamous words again, "You know what *we* need to is ..." Now by writing an Instrument BASIC program for the analyzer, we could implement all the ideas for optimizing impact testing that before we had just been talking about. So for the next nine months, I worked on the MRIT Acquisition Software, with many iterations of testing and programming. This thesis is the compilation of everything I have done with Multiple Reference Impact Testing.

Table of Contents

List of Figures

List of Tables

Nomenclature

Matrix and Operator Notation

$[\cdot\cdot]$ matrix enclosed by brackets

$[\cdot\cdot]_{(m\times n)}$ or $\displaystyle\left[\cdot\cdot\right]_{(m\times n)}$ size of a matrix (m rows by n columns)

$[\cdot\cdot]^{T}$ transpose of a matrix

$[\cdot\cdot]^{H}$ Hermitian, or conjugate transpose, of a matrix

$[\cdot\cdot]^{-1}$ inverse of a matrix

$[\cdot\cdot]^{+}$ pseudo-inverse of a matrix

$\lceil\cdot\cdot\rfloor$ diagonal matrix

$\{\cdot\cdot\}$ column vector enclosed by braces

e^{at} exponential time function

j $\sqrt{-1}$

$y(t)$ time domain function

$Y(\omega)$ frequency domain function

$Y(\omega_k)$ discrete frequency domain function

$Y(s)$ Laplace domain function

$\Leftrightarrow$ denotes equivalence of time and Laplace or frequency domain functions with respect to Laplace or Fourier transforms and inverse transforms

$\wedge$ denotes an estimated system parameter, as defined in context

Roman Alphabet

a_0, a_1, a_2	frequency domain polynomial coefficients
A_{pqr}	residue of output DOF p and input DOF q for mode r
$[A]_r$	residue matrix for mode r
A_s	residue of principal mode of enhanced frequency response function s
$C_r(\omega_k)$	frequency domain single degree of freedom function for mode r
$D_{s,r}(\omega_k)$	modified frequency domain single degree of freedom function term defined for MDOF modal scale factor calculation
$eH_s(\omega_k)$	enhanced frequency response function for mode s at spectral line k
$h_{pq}(t)$	impulse response function output DOF p and input DOF q
$H_{pq}(\omega_k)$	frequency response function output DOF p and input DOF q at spectral line k
$[H(\omega_k)]$	frequency response function matrix at spectral line k
K_r	participation factor for rigid body mode r
$\{K\}$	participation factor vector for rigid body modes
$\{L_r\}$	modal participation vector for mode r
$[L]$	modal participation matrix
$[MAC]$	modal assurance criteria matrix
MAC_{ij}	modal assurance criteria value of vectors i and j
$\{MAC_s\}_k$	mode tracking modal assurance criteria vector for mode s at spectral line k
N	number of conjugate modes
N_i	number of input DOFs

N_o	number of output DOFs
p	output DOF subscript
q	input DOF subscript
$\{q_p\}$	vector of (x,y,z) modal coefficients of position p
Q_r	modal scale factor for mode r
T	time record length
$[T]$	transformation matrix
$\{U_n\}_k$	n^{th} left singular vector at spectral line k
$[U]_k$	left singular vector matrix at spectral line k
$\{U_s\}$	left singular vector associated with CMIF peak s
$\{V_n\}_k$	n^{th} right singular vector at spectral line k
$[V]_k$	right singular vector matrix at spectral line k
$\{V_s\}$	right singular vector associated with CMIF peak s
$w(t)$	time domain window function
$\lceil W_p \rfloor$	diagonal weighting matrix for position p
$\lceil W \rfloor$	composite diagonal weighting matrix
(x,y,z)	orthogonal coordinate axes
$(x_{p_o}, y_{p_o}, z_{p_o})$	(x,y,z) coordinates of position p relative to origin
x_p	x-direction motion of position p on a rigid body component
y_p	y-direction motion of position p on a rigid body component
z_p	z-direction motion of position p on a rigid body component

Greek Alphabet

β reciprocal of exponential window time constant

θ_1, θ_2 direction angles of local coordinate system

λ_r eigenvalue, or complex pole, of mode r ; $\lambda_r = \sigma_r + j\omega_r$

σ_r damping factor of mode r

$\sigma_{n,k}$ nth singular value at spectral line k

$\lceil \Sigma \rfloor_k$ singular value matrix at spectral line k

τ exponential window time constant

Ψ_x, Ψ_y modal coefficients in global coordinate system

Ψ_1, Ψ_2 modal coefficients in local coordinate system

$\Psi_{x_p r}$ x-direction modal coefficient of position p for mode r

$\Psi_{y_p r}$ y-direction modal coefficient of position p for mode r

$\Psi_{z_p r}$ z-direction modal coefficient of position p for mode r

$\{\Psi_r\}_p$ modal coefficients of position p for mode r

$[\Psi_p]$ modal coefficients of position p

$\{\Psi_r\}$ modal vector for mode r

$[\Psi]$ modal vector matrix

ω_k spectral line k

ω_r damped natural frequency of mode r

$\omega_{s'}$ spectral line nearest the frequency of mode s

Abbreviations

ADC   Analog-to-Digital Converter

CMIF   Complex Mode Indicator Function

DFT   Discrete Fourier Transform

DOF   Degree of Freedom

eFRF   Enhanced Frequency Response Function

FFT   Fast Fourier Transform

FRF   Frequency Response Function

IRF   Impulse Response Function

MAC   Modal Assurance Criteria

MDOF   Multiple Degree of Freedom

MIMO   Multiple-Input Multiple-Output

MRIT   Multiple Reference Impact Testing

MTC   Mode Tracking Criteria

PALS   Peak Auto-Location Sensitivity

SDF   Standard Data Format

SDOF   Single Degree of Freedom

SDRL   Structural Dynamics Research Lab

SFD   Squeeze Film Damper

SVD   Singular Value Decomposition

UMPA   Unified Matrix Polynomial Approach

Chapter 1   Introduction to MRIT

Multiple Reference Impact Testing (MRIT) does not imply impacting a test system with more than one hammer. Instead, the output(s) are taken as the references, rather than the input(s). MRIT is a modal data acquisition method in which frequency response functions (FRF) are measured between one roving impactor and several fixed response transducers. Because of the principle of reciprocity, the MRIT method produces a modal data set that is equivalent to a multiple-input data set and can be processed with multiple reference modal parameter identification techniques, but does not require a multiple-input FRF estimator.

For the past twenty-five years, impact testing has been one of the standard testing procedures for measuring FRFs. Historically, impact testing has proven to be a reliable and successful technique for field testing and troubleshooting vibration problems. The implementation of impact testing began in the mid-Sixties following the development of the Fast Fourier Transform (FFT). At that time, data was tape recorded in the field and then digitally processed with large, fixed-site computer systems. The development of the Fourier Analyzer system made the impact testing procedure practical because the measurements could be conveniently processed on-site. Although, the two channel systems that were available allowed only single reference measurements. Today, portable

analyzers and personal computers have extended the utility of impact testing and the availability of data acquisition systems.

Two significant developments occurring in the past five to ten years are the availability of multiple channel data acquisition systems and the development of multiple reference modal parameter estimation algorithms. Multiple Reference Impact Testing incorporates the application of these new developments to impact testing.[1] The advent of portable, multiple channel data acquisition systems has provided a platform for implementation of MRIT as practical and convenient method of acquiring modal data. The Complex Mode Indicator Function (CMIF) provides the basis of a simple but powerful multiple reference modal parameter estimation method that is compatible with MRIT. The scope of this body of work is the development, implementation, and integration of the MRIT acquisition and analysis procedures.

MRIT combines the beneficial features of the impact testing and Multiple-Input Multiple-Output (MIMO) testing methods. The advantages of impact testing are minimal equipment requirements and setup time, in-situ field testing, and testing systems while in operation. The setup time and equipment required for MRIT is considerably less than for MIMO testing. Testing a system in-situ, with operating boundary conditions, excludes the need for artificial support fixturing. The ability to test systems, such as rotating machinery, while in operation may be necessary if the dynamics of the system are dependent on the operational conditions. MRIT combines these advantages with the capability to measure multiple reference FRF data.

One of the underlying reasons for choosing the MRIT method is to couple multiple reference data acquisition with the convenience and utility of impact testing. This combination of features makes MRIT a particularly useful method for troubleshooting and field testing applications. MRIT is also an alternative to MIMO testing that may be more suitable for certain applications. For instance, MIMO testing may not be feasible for small, light-weight objects or very large structures. MRIT could also be used as a preliminary procedure for a large-scale MIMO modal investigation in a testing laboratory to identify modes of interest or to determine exciter locations. Since impact testing has been used principally for troubleshooting and field testing, the primary emphasis of this work is on techniques and procedures applicable to these testing situations.

To balance the advantageous aspects of the MRIT method, a few limitations must also be addressed: (1) In order to collect the measurements, the system under test must be impacted at many locations, and for several averages at each measurement location. By the nature of the techniques involved, impact testing is a labor intensive and repetitive task that requires a certain degree of skill and experience to accomplish successfully. Thus, any improvements in the implementation of the measurement process that reduce the testing time and effort will promote the usefulness of the method. (2) Although impact testing is a convenient method for collecting modal data, the characteristics of the impact force cause it to be a poorly suited type of excitation for measuring FRFs. To counteract this condition, specialized signal processing and measurement techniques are required to improve the quality of the measurements. (3) The physical constraints of a test structure may limit the possible measurements and, consequently, the response degrees of

freedom of the mode shapes. Alternative impacting techniques may allow obtaining additional measurements in the acquisition stage. Coordinate transformation and vector completion can produce more descriptive mode shapes in the analysis stage. Throughout the evolution of impact testing, substantial effort has been directed at the development of techniques to overcome these limitations associated with impact testing.

The organization of the remaining contents of this thesis is as follows. Chapter 2 presents the topic of MRIT acquisition, including a review of impact testing, as well as the theory of multiple reference impact testing. Chapter 2 also describes the implementation of MRIT acquisition software developed for a commercially available multiple channel analyzer. Chapter 3 presents the topic of MRIT analysis, consisting of the derivation of a multiple reference parameter identification method based on CMIF. Chapter 3 also describes the implementation of MRIT analysis software developed for the personal computer using a high-level numerical analysis programming application. Chapter 4 illustrates applications of the MRIT method with several representative test cases. Chapter 5 summarizes the current state of the development of Multiple Reference Impact Testing and discusses possible advancements for the future.

Chapter 2   MRIT Acquisition

Presented in this chapter are the conceptual principles and practical implications of Multiple Reference Impact Testing data acquisition. The MRIT method is introduced in the context of modal testing methods and the fundamental theory is established. The equipment requirements for impact testing are outlined, including details on the properties of impactors. The characteristics of the transient time signals associated with impulsive excitation and the signal processing techniques developed for impact testing are reviewed. The specialized impact testing procedures are explained, with emphasis on the importance of proper testing practices at each step of an MRIT test. The features of custom software developed for a multiple channel analyzer are described to demonstrate the practical implementation of the concepts presented in this chapter.

2.1   MRIT Theory

An FRF describes the input/output relationship between two degrees of freedom (DOF) of a system as a function of frequency. The *reference* for an FRF measurement can be either the input (excitation) DOF or the output (response) DOF. In this context, a reference is defined as a DOF that is common to the set of measurements. Modal analysis data can be collected by either roving the outputs with the inputs fixed or roving the

inputs with the outputs fixed.† For the former case, the inputs are the references, and the outputs determine the spatial definition of the mode shapes. For the latter case, the outputs are the references, and the inputs determine the spatial definition of the mode shapes. An input or output DOF is defined by the physical position at which a transducer is located and the orientation of the transducer in a defined coordinate system (i.e., point number and direction).

2.1.1   Modal Testing Methods

The fixed input alternative is the only feasible procedure for Multiple-Input Multiple-Output testing. The exciters are attached to the system under test at the input locations, and the references correspond to the force sensors that measure the input to the system applied by the exciters. FRFs are measured between the reference force transducers and the response transducers, typically accelerometers, mounted on the structure. The test system may be completely instrumented with response transducers at every output location, and all measurements acquired simultaneously, or a lesser number of response transducers may be roved about the output locations. The input locations of the exciters are generally chosen to excite all modes of the system and to supply an uniform distribution of excitation energy. The current state of MIMO data acquisition

---

† *Roving* an output means to position a response transducer (e.g., an accelerometer) on the system under test, acquire the measurement, and then move the response transducer to another position. *Roving* an input means to position the excitation device (e.g., a shaker or an impact hammer) on the system under test, acquire the measurement, and then move the excitation device to another position.

hardware and software allows for the multiple inputs to be applied simultaneously, which then requires a multiple-input FRF estimation algorithm[2,3].

For impact testing, both the fixed input and roving input alternatives are possible. For the fixed input procedure, the test system is repeatedly impacted at an input location while the response transducers are roved about the output locations. (Since less testing equipment is ordinarily used for an impact test than for a MIMO test, completely instrumenting the system with response transducers is not a common practice.) To collect multiple reference data with the fixed input procedure, the process is repeated for other input locations. Alternatively, the impacts could be made at all input locations before relocating the response transducers. To collect the complete set of measurements, the response transducers must be moved and remounted many times. Since only one input is applied at a time, a multiple-input FRF estimator is not required. Techniques for impacting at more than one input location at the same time have been developed[4,5] but are not as easily implemented as the MRIT method.

The roving input procedure is the basis of the Multiple Reference Impact Testing method. MRIT is a technique in which several response transducers are positioned on the test system and the impactor is roved to the input locations. A set of multiple reference FRFs is measured between the roving input and the array of fixed response transducers. The responses are the references because these are common to the complete set of measurements, and by assuming reciprocity (see Section 2.1.3) the input locations become the DOFs of the mode shapes. A multiple-input FRF estimator is not required

since there is only one input to the system and a set of single-input multiple-output FRFs are computed for each input location.

An equal number of measurement cycles are needed to complete an impact test with the fixed input procedure or the roving input procedure using the same equipment. For example, consider a test with ninety measurement locations and three references, using three response transducers. For the fixed input case, the response transducers will be relocated thirty times, and the three input locations will be impacted for each of the thirty relocations. For the roving input case, the three response transducers are not relocated during the test, but the input is roved to each of the ninety impact locations. For each case, a total of ninety measurement cycles is needed to complete the test. However, the roving input procedure has advantages over the fixed input procedure that result in a reduction in testing time and effort and a more consistent set of data. Moving the impactor to a new input location is much easier than remounting the response transducers. For the MRIT method, the reference transducers are positioned once at the beginning of the test and remain in those fixed locations throughout the test. Relocating the response transducers will also change the mass loading of the system. For MRIT method, the mass loading due to the reference transducers is constant for every measurement of the data set.

2.1.2   Reciprocity and the FRF Matrix

One of the basic assumptions associated with modal analysis is the condition of reciprocity. The fundamental assertion of the Maxwell-Betti principle of reciprocity[6,7] states that the output of a system at DOF p due to an input at DOF q is equivalent to the output of the system at DOF q due to an identical input at DOF p. Extending this definition to measured frequency response functions infers that the FRF of output DOF p with respect to input DOF q is equivalent to the FRF of output DOF q with respect to input DOF p.

The FRF matrix $[H(\omega_k)]$ is arranged as shown Equation 2-1, where N_i is the number of inputs, N_o is the number of outputs, and ω_k is the spectral line. The outputs are ordered down the columns and the inputs are ordered across the rows. Each row corresponds to an output DOF, and each column corresponds to an input DOF. The individual FRFs that comprise the matrix are expressed as $H_{pq}(\omega_k)$, where p denotes the output DOF and q denotes the input DOF.

$$[H(\omega_k)] = \begin{bmatrix} H_{11}(\omega_k) & H_{12}(\omega_k) & \cdots & H_{1N_i}(\omega_k) \\ H_{21}(\omega_k) & H_{22}(\omega_k) & \cdots & H_{2N_i}(\omega_k) \\ \vdots & \vdots & & \vdots \\ \vdots & \vdots & & \vdots \\ H_{N_o1}(\omega_k) & H_{N_o2}(\omega_k) & \cdots & H_{N_oN_i}(\omega_k) \end{bmatrix}_{(N_o \times N_i)} \tag{2-1}$$

An MRIT data set forms an FRF matrix in which the number of rows equals the number of references (fixed responses) and the number of columns equals the number of impact

9

DOFs, with $N_i \gg N_o$. A MIMO data set forms an FRF matrix in which the number of

columns equals the number of references (exciters) and the number of rows equals the

number of response DOFs, with $N_o \gg N_i$. For the MIMO case, a multiple-input FRF

estimator is required to measure the multiple reference FRFs if the inputs are applies

simultaneously. However, for the MRIT case, only a single-input FRF estimator is

required to measure the multiple reference FRFs simultaneously. Because of reciprocity

between the input and output DOFs, the rows and columns of the FRF matrix are

equivalent with respect to the frequency response of the system. An example of the

relationship between an MRIT and a MIMO FRF matrix is illustrated in Equation 2-2 for

data set of three references and nine impact locations.

$$
\begin{bmatrix}
H_{11} & H_{12} & H_{13} & H_{14} & H_{15} & H_{16} & H_{17} & H_{18} & H_{19} \\
H_{21} & H_{22} & H_{23} & H_{24} & H_{25} & H_{26} & H_{27} & H_{28} & H_{28} \\
H_{31} & H_{32} & H_{33} & H_{34} & H_{35} & H_{36} & H_{37} & H_{38} & H_{39}
\end{bmatrix}_{(3\times9)}
\Rightarrow
\begin{bmatrix}
H_{11} & H_{21} & H_{31} \\
H_{12} & H_{22} & H_{32} \\
H_{13} & H_{23} & H_{33} \\
H_{14} & H_{24} & H_{34} \\
H_{15} & H_{25} & H_{35} \\
H_{16} & H_{26} & H_{36} \\
H_{17} & H_{27} & H_{37} \\
H_{18} & H_{28} & H_{38} \\
H_{19} & H_{29} & H_{39}
\end{bmatrix}_{(9\times3)}
\qquad (2\text{-}2)
$$

$$MRIT \qquad\qquad\qquad\qquad MIMO$$

The reciprocal relationship between and MRIT and MIMO data set can also be

considered as simply transposing the FRF matrix. MRIT data is collected as a set of

many inputs and a few outputs, and by applying the reciprocity relationships, the data is

transposed into a set of many outputs and a few inputs. This is the form commonly

envisioned as multiple reference, or multiple input, data and processed by multiple

reference parameter identification algorithms. Again, the references of the MRIT data set are the output DOFs, which become the input DOFs after the reciprocal transposition.

2.1.3 Limitation of the MRIT Method

In order to perform a Multiple Reference Impact Test, the system must be impacted at numerous input locations. Furthermore, the basic concept of the MRIT method implies that each impact location becomes a DOF of the mode shapes. However, the geometric constraints of a test system can impose a limitation on the MRIT method by restricting the obtainable impact locations. As a result, the mode shape coefficients corresponding to the unmeasurable DOFs can not be determined. Supplemental measurement and post-processing techniques are available to overcome this consequence in many situations.

A triaxial reference will not produce triaxial responses at the impact locations. Rather, this corresponds to exciting the system in three orthogonal directions at one location. To obtain triaxial responses at a impact location, the impacts must be made in the three directions at that location. However, impacting in three orthogonal directions aligned with the defined global coordinate system may not be possible at some points of a structure. In addition, other potential impact locations may be inaccessible to a standard impact hammer. Coordinate transformation can resolve skewed and nonorthogonal impact directions into the global system. Post-processing the mode shapes with vector completion algorithms is possible to estimate unmeasurable mode shape coefficients. An

instrumented punch is an alternative type of impactor that permits impacting locations that would otherwise be unmeasurable. Coordinate transformation and basic vector completion methods are presented in Section 3.4. An example of an instrumented punch is introduced in Section 2.2.3.

2.2 Testing Equipment

Impact testing generally requires a minimal set of testing equipment to make FRF measurements or to perform a modal test. In most cases, the amount of equipment needed for an MRIT test is considerably less than for a similar MIMO test. The primary MRIT equipment includes a data acquisition system, an instrumented impactor, and several response transducers. Additional items such as cables, connectors, and possibly transducer power supplies are also necessary. A broad selection of hardware and software alternatives are commercially available to suit a variety of testing situations.

2.2.1 Data Acquisition Systems

A data acquisition system is a combination of hardware and software capable of performing the required signal conditioning, digitization, signal processing, FRF computations, and data management. Impact testing requires a data acquisition system that has the following capabilities:

1. Two or more input channels with analog-to-digital converters having a range of gain settings and anti-aliasing filters. (Although only two channels are required to measure an FRF, more than two channels are necessary to fully utilize the MRIT method, one channel for the impactor and one channel for each of the reference transducers.)

2. Fourier analysis functions such as FFT, autopower and crosspower spectrums, FRF, coherence, averaging, baseband and zoomband measurements, etc.[8,9]

3. Triggering on the input to synchronize the measurements.

4. Time domain windows of the type discussed Section 2.3.1.

5. High sampling rates that allow the system to operate as a digital oscilloscope.

6. Data storage in the data acquisition system or in a computer interfaced to the system.

Most data acquisition systems can be grouped into the categories of dedicated Fourier analyzers or computer-controlled front-end hardware. Some integrated analyzer/computer systems and programmable analyzers are also available. The key feature making a data acquisition system suitable for impact testing is portability.

Two-channel analyzers are a very common type of measurement system, and analyzers with more than two channels have recently been introduced in comparably sized packages. Dedicated analyzers offer a compact and durable data acquisition system choice for field testing situations. Analyzers typically have a limited data storage capacity and will usually require an auxiliary computer for the data analysis.

Many PC-based data acquisition systems have also become available in the past several years. Some are coupled with existing front-end hardware and others use specialized expansion boards. Laptop and notebook computers increase the portability of these systems. Computer-based systems provide expanded data storage capacity and can perform both the data acquisition and analysis functions. Although workstation-based data acquisition systems are available, these often provide more capabilities than are necessary for the typical impact testing situation, at the expense of portability.

Figures 2-1(a) through 2-1(e) present several representative models of data acquisition systems available for impact testing, which are described below:

a. A notebook computer interfaced to multiple channel front-end hardware.

b. A programmable four-channel analyzer of similar size as a standard oscilloscope.

c. A desktop computer with data acquisition channels installed in a disk drive bay.

d. A very compact and lightweight, battery-powered two-channel analyzer.
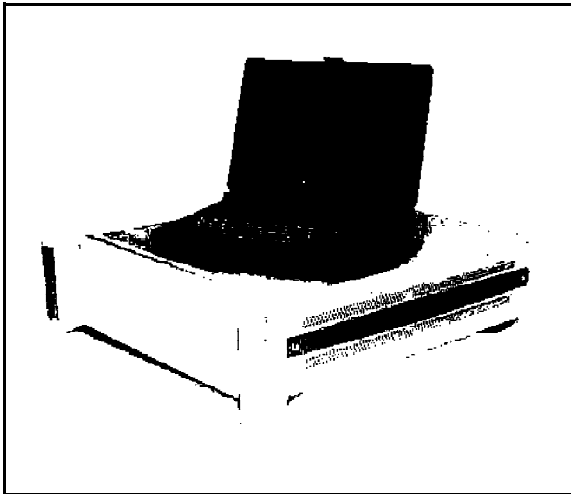
Figure 2-1(a). Personal Computer Based
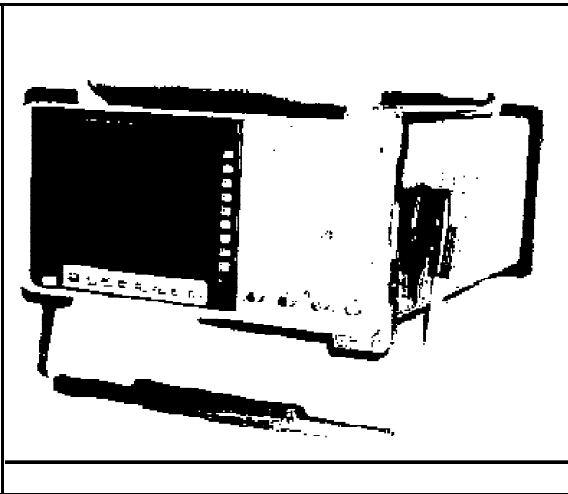
Figure 2-1(b). Multiple Channel Digital
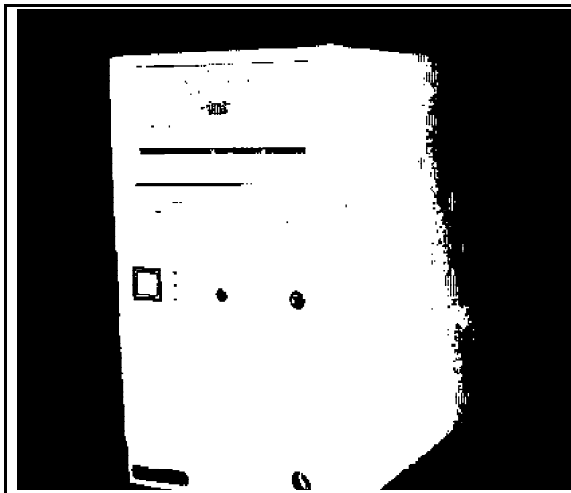
Figure 2-1(c). Personal Computer Based

The ruler is scaled for scale.
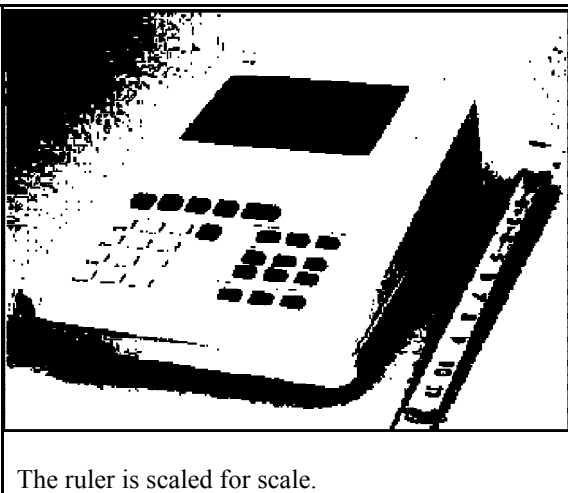
Figure 2-1(d). Small, Portable Digital

2.2.2   Impactors

A wide variety of impactors have been used with impact testing, ranging from small, uninstrumented ball bearings to instrumented masses weighing several thousand pounds. In fact, the only limitation in selecting an impactor is the imagination of the experimentalist. The instrumentation of an impactor is a force sensor at the striking end to measure the input to the system. An instrumented impactor is not required for the response ratio method[3] or techniques that process free decay measurements[10], but force measurements are required to compute FRFs. The considerations influencing the selection of an impactor include the size and construction of the test system, the level of energy needed to excite the system, and the frequency range of the measurements.

The most common type of impactor is an instrumented, hand-held hammer, of which. several sizes have been developed to meet different testing situations. A collection of typical impact hammers is shown in Figure 2-2. The advantage of an impact hammer is that it can very easily be moved to different locations on the test structure. Many other types of impacting devices have also been utilized for field testing.

Figure 2-2. Collection of Hand-Held Impact Hammers.

An impact hammer imparts a force due to the change of momentum of the hammer. The frequency content of the input force spectrum is controlled by the stiffness of the impact tip, the mass of the impactor, the impact velocity, and the compliance of the surface being struck. The stiffness of the impact tip is the dominant factor controlling the frequency range of the input spectrum. A softer tip, heavier impactor, and slower impact velocity decrease the frequency range. A harder tip, lighter impactor, and faster impact velocity increase the frequency range. An assortment of impact tips of varying stiffness are available to tailor the input spectrum. Additional mass can be added to the hammer to further modify the input spectrum. The impact velocity is controlled by the proficiency of the person doing the impacting. The magnitude of the impulse is determined by the mass of the impactor and the impact velocity.[11,12]

A proper input spectrum should drop between 10 and 20 dB across the frequency range. This guideline should normally provide that the excitation contains sufficient energy in the measurement frequency span while not exciting higher out-of-band modes. For zoomband measurements, the lower out-of-band modes will be excited because the lower bound of the force spectrum cannot be controlled.

Figure 2-3 illustrates the relationship between the duration of the impulse and the frequency span of the input spectrum. The short duration impulse (1) corresponds to a hard tip and results in a higher frequency range input spectrum. A long duration impulse (3) corresponds to a soft tip and results in a lower frequency range input spectrum. The intermediate duration impulse (2) corresponds to a medium stiffness tip and results in an

intermediate frequency range input spectrum. The difference in the spectrum levels is a function of the frequency distribution of the energy contained in the pulses.
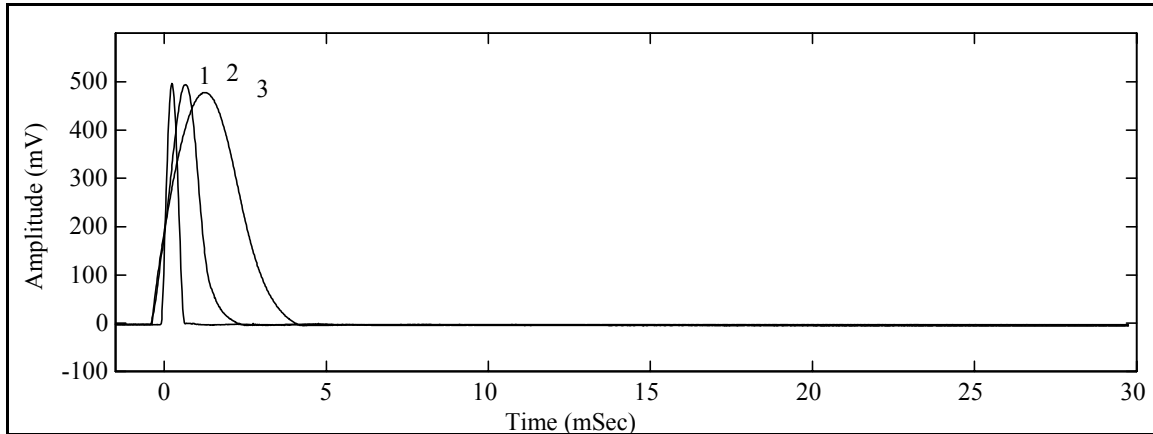
Figure 2-3(a). Impulse Time Records.
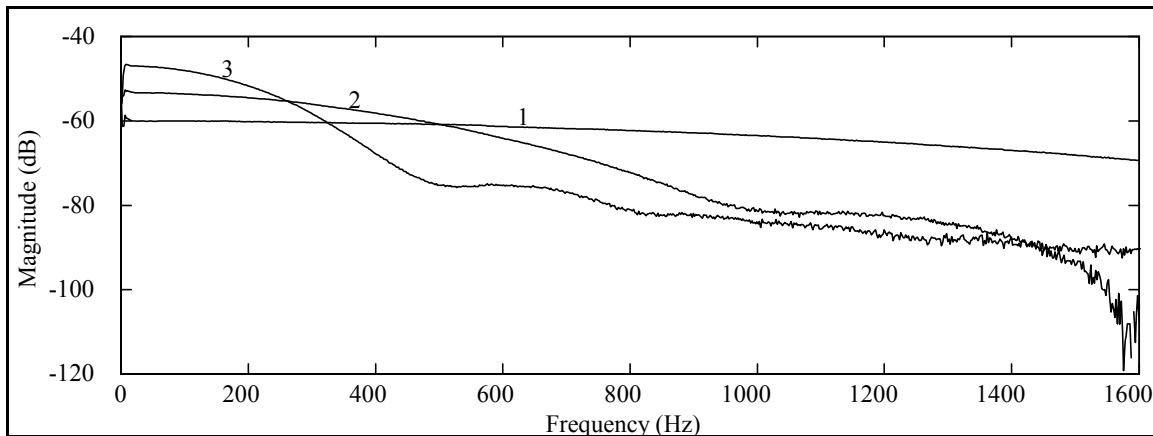
Figure 2-3(b). Input Power Spectrums.

The force imparted to the system is the force between the impact tip and the surface, but the force measured by the impactor load cell is the force at the interface of the tip and the transducer. The sensitivity of an impactor transducer depends upon the ratio of the effective mass of the impact tip to the total mass of the impactor. The effect mass of the

tip depends upon the material properties of tip and other, unpredictable factors. The recommended calibration procedure for an impactor is the ratio calibration method. The impactor should be calibrated in its testing configuration since the sensitivity is dependent of the properties of the tip and the impactor. Static calibration of the load cell is not an adequate method.[13-15]

2.2.3   Punch Impactors

As mentioned previously, the physical constraints of a test system can limit the obtainable measurements. For instance, impacting at some locations may not be possible with a conventional impact hammer. An instrumented punch is an alternative type of impactor that is useful for these situations. In the past, uninstrumented punches have been used out of necessity. The punch was struck with an instrumented hammer, and the signal from the impact hammer was taken to be the input to the structure. However, the force imparted to the system through the punch is not the same as the striking force. Understanding the properties of these forces is paramount to the need for and proper use of an instrumented punch impactor.

A model of an instrumented punch impactor which has been produced, called the Modal Punch[16], is shown in Figure 2-4. It is a 9/16 inch (15 mm) diameter anodized aluminum rod, and the length can be varied with extension sections. It is fitted with a modified load cell on one end and a side mounted 10-32 micro-dot connector on the other end, and the

electrical connection for the load cell is routed internally. The sections are assembled

with a 10-32 thread stud that serves as the mechanical and electrical connection.
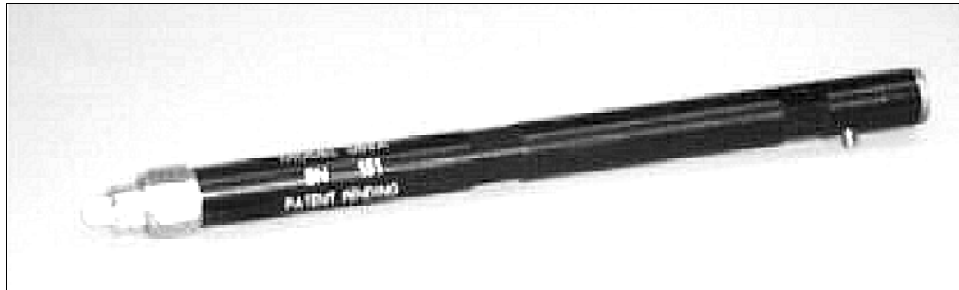
Figure 2-4. The Modal Punch.

The punch impactor is held against the surface of the test object and struck with a

standard impact hammer. The force imparted to the system is measured by the load cell

at the end of the punch in contact with the surface. Both the punch and the hammer can

be fitted with any of the standard impact tips, and the input force spectrum is controlled

by the combination of the tips. A detailed explanation of the Modal Punch force

characteristics is presented in Ref. [16].

The primary use of a punch impactor is to impact locations that are inaccessible to a

conventional impact hammer. It can also be used to precisely locate impacts to minimize

the variance of the impact location and to impact in a skewed direction (nonorthogonal to

the global coordinates) on the edge of a structure. Figure 2-5 shows a typical application

of the Modal Punch to impact on a recessed area of an automobile engine compartment.
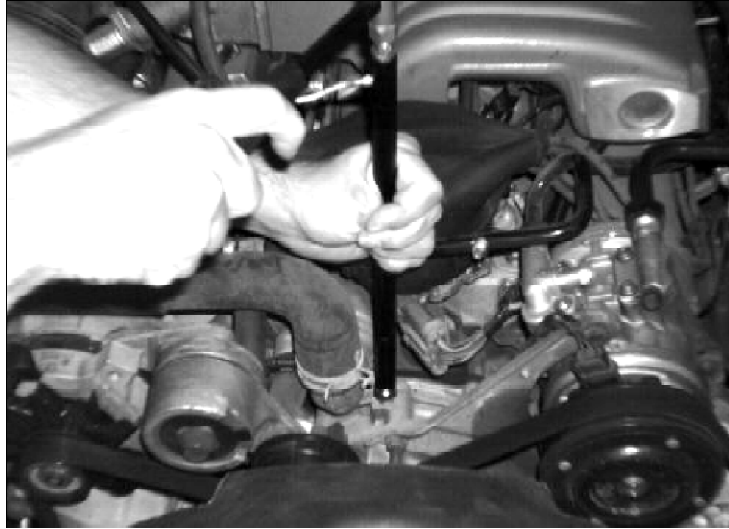
Figure 2-5. Typical Application of the Modal Punch.

An instrumented punch impactor such as the Modal Punch can expand the possibilities of impact testing. However, the following guidelines must be observed in order to obtain accurate measurements using this type of impactor:

1. The punch impactor should be fitted with a hard tip. A metal or hard plastic tip is recommended.

2. The shape of the impact pulse is tailored with the tip on the hammer.

3. The tip on the punch impactor must not be softer than the tip on the hammer. Tips of equal stiffness are acceptable.

4. The punch impactor should be calibrated in its testing configuration since the sensitivity is dependent on the tip combination.

2.2.4 Response Transducers

Accelerometers are the most common type of response transducer used for impact testing. However, other types of response transducers are more appropriate for certain applications. Proximity probes are used for rotating machinery and microphones have been used for small or lightweight objects. Due to the high acceleration levels experienced near the impact sites, accelerometers with sensitivities of 10 mV/g or 100 mV/g are usually preferred over more sensitive models. The ratio method is also the recommended calibration procedure for accelerometers.

2.2.5 Telemetered Input Channel

An auxiliary item of measurement equipment is a telemetered input channel for the impactor force transducer. A telemetry system consists of electronics that transmit and receive the measured voltage signal. Additional signal processing is required to compensate for the magnitude and phase distortion introduced by the electronics. Eliminating the wire from the impactor to the acquisition system allows for greater freedom of movement. Telemetering the force signal would be very convenient for testing large structures. Since the reference transducers are stationary during a test, telemetering these signals is not warranted.

Figure 2-6 shows a prototype model that has been developed to demonstrate the the feasibility of this type of testing hardware. The unit on the right is the transmitter, which is carried with the tester. The output of the impactor force transducer is connected to the

transmitter, which also contains the transducer power supply and signal conditioning. The unit on the left is the receiver, which is connected to the input channel of the acquisition system. The portability of this prototype model can be improved by reducing the size of the components, especially the transmitter.

Figure 2-6. Telemetered Input Channel System.

2.3   Signal Processing

Unfortunately, an impact force is a poorly conditioned input for exciting a system because it is impulsive and deterministic, both of which are often undesirable. The impulsive property produces high peak levels but low RMS levels due to the brief duration of the active input. This means that it can easily overload the input channels while imparting very little energy into the system. In addition, the low RMS value can result in a poor signal-to-noise ratio of the measured signals. Due to the impulsive characteristic of the impact force, specialized signal processing techniques are necessary to obtain accurate

measurements. The deterministic characteristic of the impact force affects the nonlinear behavior of systems and is discussed in Section 2.4.2.

2.3.1 Force and Exponential Windows

The force and exponential windows are time domain weighting functions that have been developed for impact testing.[13] These windows are designed to reduce the effects of leakage and improve the signal-to-noise ratio of the measured signals. In general, to improve impact testing FRF measurements, the force and exponential windows should almost always be applied to the time signals, with very few exceptions.

The purpose of the force window is to improve the signal-to-noise ratio of the input force signal by attenuating the data following the duration of the impact. After the impact, the impactor is no longer in contact with the surface and can not impart any excitation into the system. The data in the trailing segment of the unfiltered† time record consists of only electrical noise on the input channel. However, due to the short duration of the impulse, the total energy of the noise may be on the same order as the energy of the input force. The force window passes the initial segment of the time record containing the impact signal and suppresses the noise in the remainder of the time record. The force window is unity over the leading five to ten percent of the time record, has a steep cosine taper to zero, and is zero for the remainder of the time record. In some cases, the trailing

---

† The trailing segment of the filtered force time record also contains response to the anti-aliasing filter, see Section 2.3.3.

segment of the time record is set to the average value of the noise instead of zero. The force window is shown in Figure 2-7.
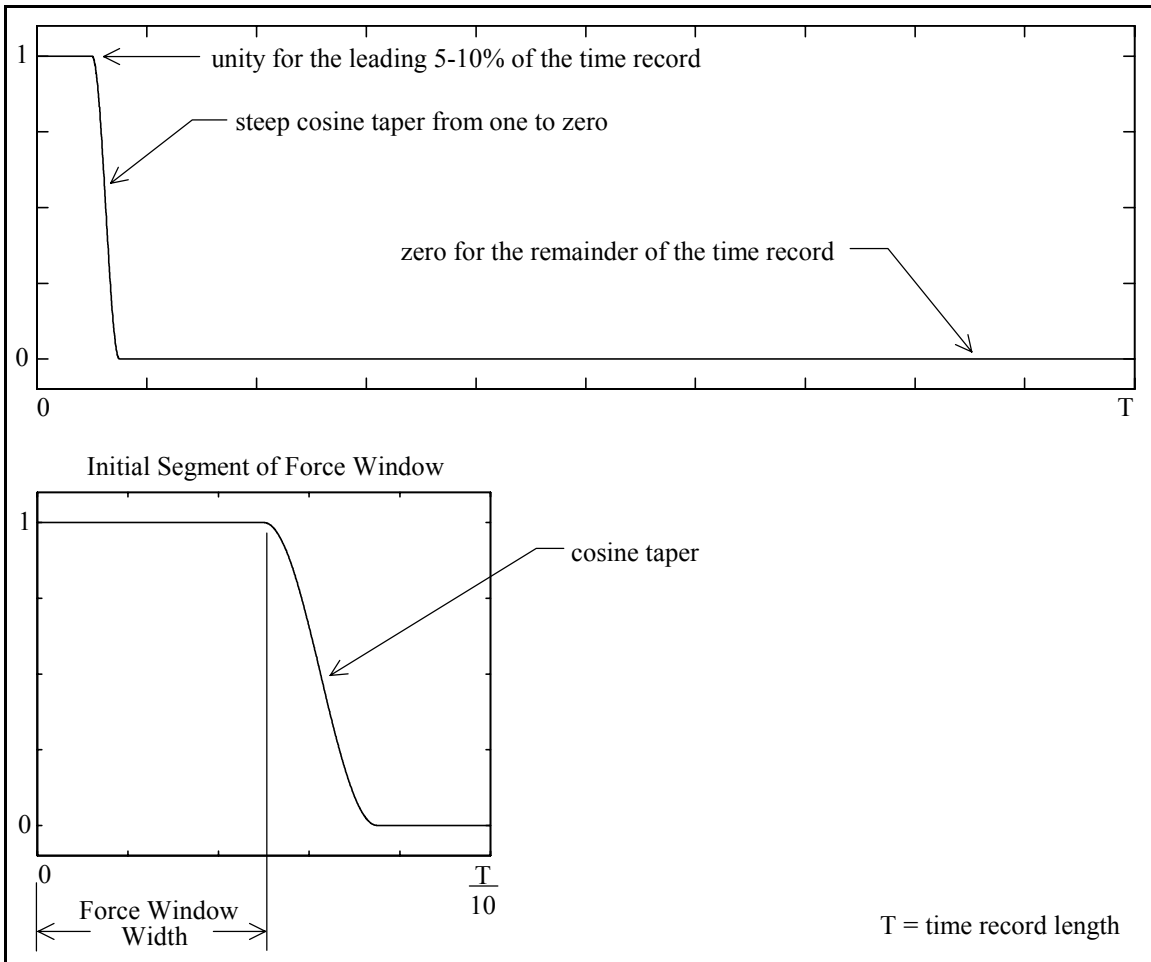
Figure 2-7. The Force Window.

The purpose of the exponential window is to reduce the effects of leakage on the response signals for lightly damped systems and to improve the signal-to-noise ratio of the response signals for heavily damped systems. For lightly damped systems, the exponential window should reduce the measured response at the end of the time record to approximately one percent in order to effectively reduce the distortion errors due to leakage, as shown in Figure 2-8. For heavily damped systems, the exponential window

25

should follow the damping of the system, as shown in Figure 2-9. In this case, the window will attenuate the noise on the measured output after the response has decayed due to system damping.
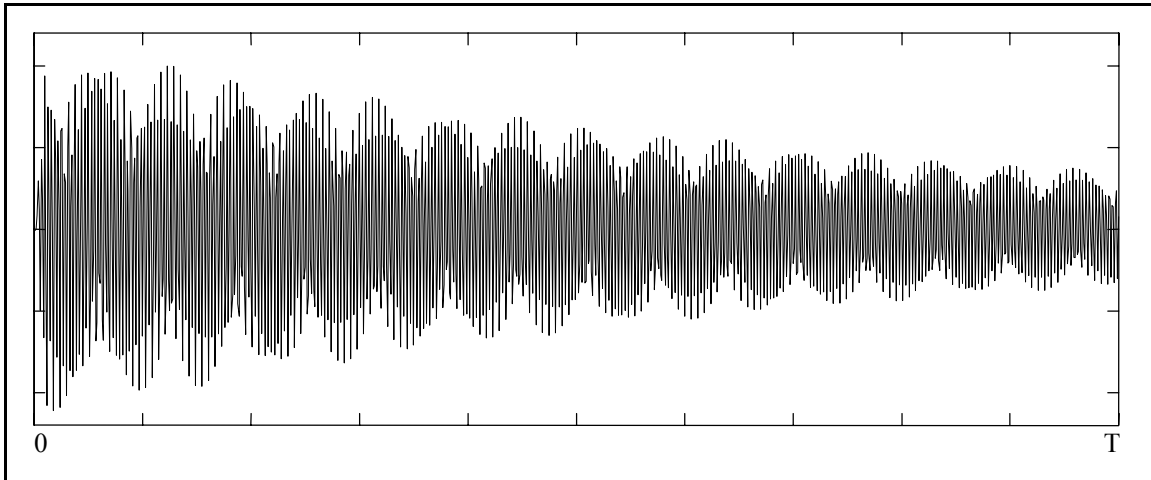
Figure 2-8(a). Unwindowed Response Signal of a Lightly Damped System.

exponential function
decayed to 1%

Windowed Response Signal
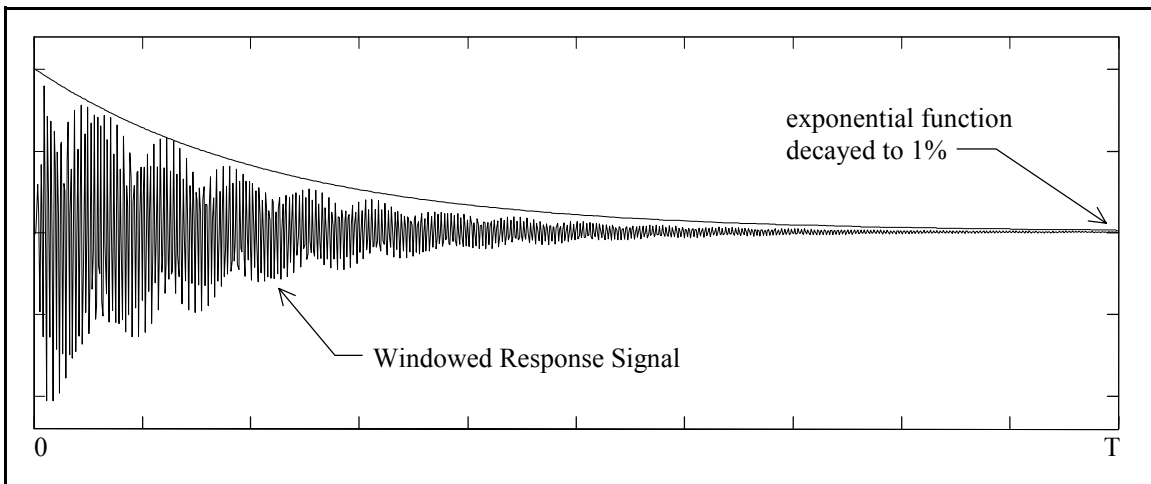
Figure 2-8(b). Windowed Response Signal of a Lightly Damped System and the
Exponential Window.

26
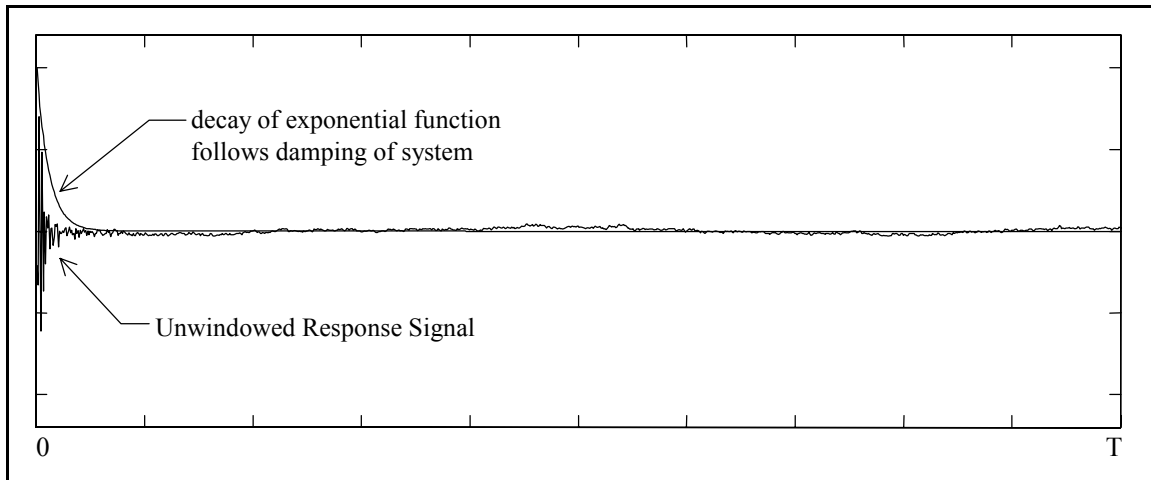
Figure 2-9. Unwindowed Response Signal of a Heavily Damped System and the Exponential Window.

The exponential window is simply an exponential function as defined by either of the two forms in Equation 2-3, where the parameter τ is the time constant of the exponential function. The time variable for the exponential function starts at zero, regardless if a pretrigger delay is used in the measurement.

$$w(t) = e^{\frac{-t}{\tau}} \quad \text{or} \quad w(t) = e^{-\beta t} \quad \text{where} \quad \beta = \frac{1}{\tau} \tag{2-3}$$

Multiplying the time signals by an exponential function increases the apparent damping of the measured system, which is equivalent to shifting the frequency axis of the associated spectra. If the exponential window is applied to the output signals, then it must also be applied to the input signal, in addition to the force window, to maintain a consistent damping shift of the FRF. The amount of added damping is determined by the exponential time constant. The effect of the exponential window is predictable and easily corrected in the subsequent parameter estimation, as explained in Section 3.3.

2.3.2 Periodic Noise

The force and exponential windows should normally be applied to the time signals when using impact testing. The exception to this rule is when the measured signals contain significant components of periodic noise. In this case, the windows will smear the periodic noise components, contaminating the adjacent spectral lines. The periodic noise components are undamped and, if not windowed, appear in the spectrum as narrow peaks. However, the exponential window increases the apparent damping of the measured signals, which results in broadening of the periodic noise peaks. The line shapes of the force and exponential windows are shown in Figure 2-10. The line shape of a time domain window determines the properties of the window in the frequency domain.
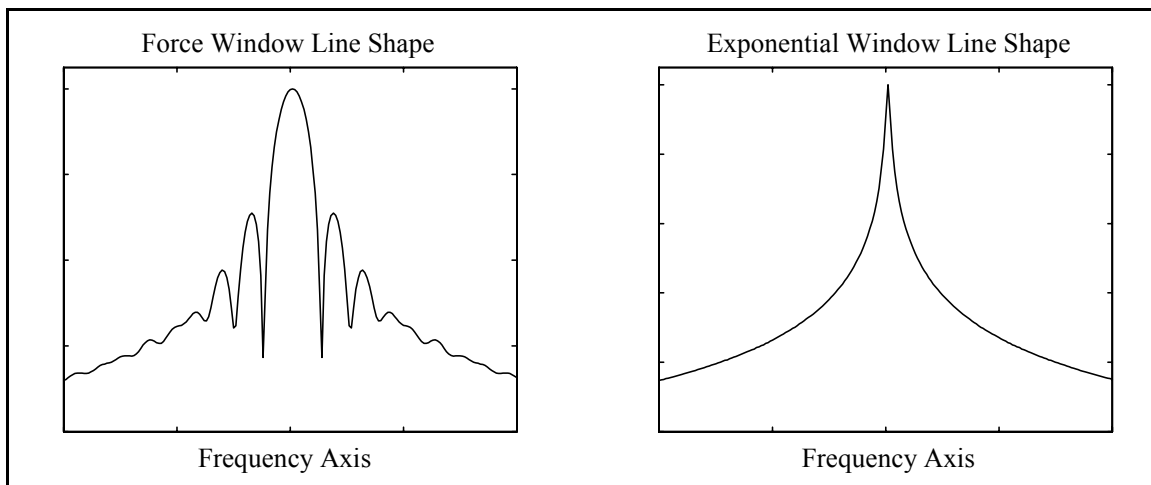
Figure 2-10. Line Shapes of the Force and Exponential Windows.

Because of the frequency domain effects of the windows, the periodic noise must be removed from the data before applying the windows in the time domain. If possible, the

noise sources should be eliminated by appropriate measurement practices. If the source of the noise can not be eliminated, then the periodic noise components can be removed by signal processing techniques described below[17]. The types of periodic noise commonly encountered with impact testing include the DC-component, electrical line noise, and periodic excitation sources.

A DC-component will generate a delta function at zero frequency in the spectrum of the data. The windows will smear this component over the adjacent spectral lines, which could obscure the low frequency data if the amplitude is large. The DC-component can be reduced by AC coupling the data acquisition channel, or it can be eliminated by removing the DC offset. With impact testing, this is done by using a pretrigger delay, measuring the DC offset from the pretrigger data, and subtracting the offset from the time record.

Electrical line noise due to ground loops is a common problem encountered with impact testing. Since impacting testing is largely a troubleshooting and field testing method, the test sites (e.g., factories and machine shops) often have inadequate electrical grounds for the testing equipment. Several methods can be used to reduce electrical noise in the measurements. The obvious solution is to improve the electrical grounds, but often this is not possible. One signal processing technique is to sample the data such that the electrical noise is periodic in the time period so that these components are not distorted by leakage. The data is Fourier transformed, without being windowed, and the data at the spectral line corresponding to the electrical noise is set to the average value of the two

adjacent spectral lines. The data is inverse Fourier transformed into the time domain and then the windows are applied. Another signal processing technique is to determine the magnitude and phase of the electrical noise components by curve-fitting the pretrigger data. This is easy to do since the frequencies of the electrical noise are well known and very precise. The electrical noise then is predicted and removed from the impact data before applying windows.

The response measurements are often contaminated with the responses caused by other excitation sources present in the testing environment. These sources are commonly due to periodic forcing functions such as rotating equipment. If possible, the test system should be isolated from these sources, but for many field testing situations this not possible. Again the signal processing technique utilizes the pretrigger data to predict and remove the periodic noise from the impact data . However, the frequencies of the noise components are not known and must be estimated in addition to the amplitude and phase.

Several methods are available to estimate the characteristics of the periodic noise signals: (1) The frequency of many noise sources can be determined by making measurements prior to beginning the impact test. This procedure is particularly useful for rotating equipment that operate at a constant speed, such as synchronous motors. (2) A tachometer mounted on the rotating equipment can provide a signal that can be used to estimate the frequency. (3) A Discrete Fourier Transform (DFT) can be used to estimate the frequencies from the pretrigger data. The advantage of the DFT verses an FFT is that any blocksize of data can be transformed to minimize leakage errors on the periodic

components. (4) The frequency of the periodic components can be estimated from the pretrigger data using an algorithm such as the complex exponential[18].

Once the frequencies of the periodic noise are determined, the amplitude and phase are computed from the pretrigger data using a process analogous to a time domain residue calculation[18,19]. The periodic noise synthesized from the estimated parameters is then extrapolated and subtracted from the impact data. The success of these techniques for removing periodic noise components from impact data is highly dependent on the frequency of the excitation source being constant throughout the measurement time period.

2.3.3   Filter Effects in the Force Signal

A positive voltage output of an force sensor registers compression of the transducer, and a negative voltage output registers tension. A measured impact signal should rise from zero to a positive peak as the transducer is compressed during the impact and then return to zero as the impactor leaves contact with the structure. However, inspection of the force measurement often reveals that the signal contains negative amplitudes and oscillates for several time samples after the initial pulse, as shown in Figure 2-11.
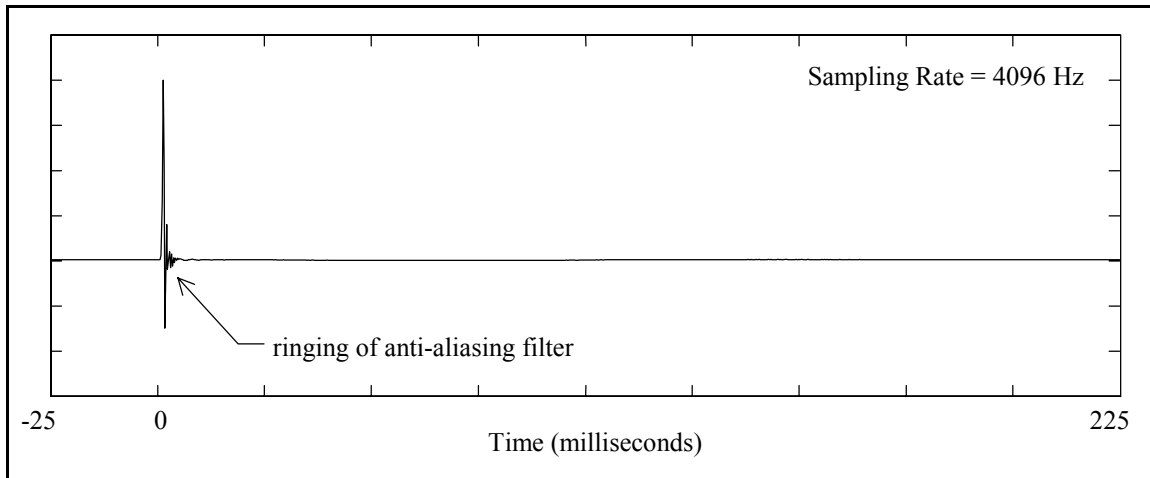
Figure 2-11. Measured Force Signal with Anti-Aliasing Filter Impulse Response Effects.

That the transducer could experience tension during an impact does not seem physically possible. This apparition in the force signal is produced by the convolution of the impulse response of the anti-aliasing filter(s) (analog and digital) and the measured impulse. An anti-aliasing filter is simply a low-pass filter which has an inherent impulse response[20], and the ringing of the filter appears as the oscillations in the force signal. The degree to which the anti-aliasing filter affects the force signal is a function of the frequency content of the input spectrum and the cutoff frequency of the filter[21].

The response signals are also filtered and will contain the same filtering effects as the force signal. Unlike the force signal, the effect is not noticeable in the response signal because it is obscured by the response data. The oscillations caused by the filters are a component of the measured force signal and should not be truncated by the force window.

32

2.4 Testing Procedures

Although impact testing seem to be a very straightforward method, specialized testing procedures are required to successfully conduct an impact test. Multiple Reference Impact Testing involves measuring the frequency response between a roving input and an array of fixed response transducers. The steps of an MRIT test include preparing the test system, mounting the reference transducers, configuring the data acquisition system, and collecting the measurements. Figure 2-12 is a schematic representation of a Multiple Reference Impact Test.

Obtaining impacts that are consistent in magnitude and alignment is an important concern. Consistent magnitude is related to impacting with approximately the same force level for each average so that the channel input ranges can be optimized, which is discussed in Section 2.4.5. Consistent alignment refers to impacting at the same point on the surface and normal to the surface, for each average at an impact location. All impacts should be normal to the surface because this is the assumed direction of the input DOF. For oblique impacts, the normal component is the principal direction of the input, but a tangential component is also produced as a function of the friction between the impact tip and the surface. In addition, oblique impacts often result in multiple impacts (see Section 2.4.6) because the impactor is likely to rebound across the surface. In general, misalignment of impacts, in both position and direction, will effect the FRF measurements and the accuracy of reciprocity between the input and output DOFs
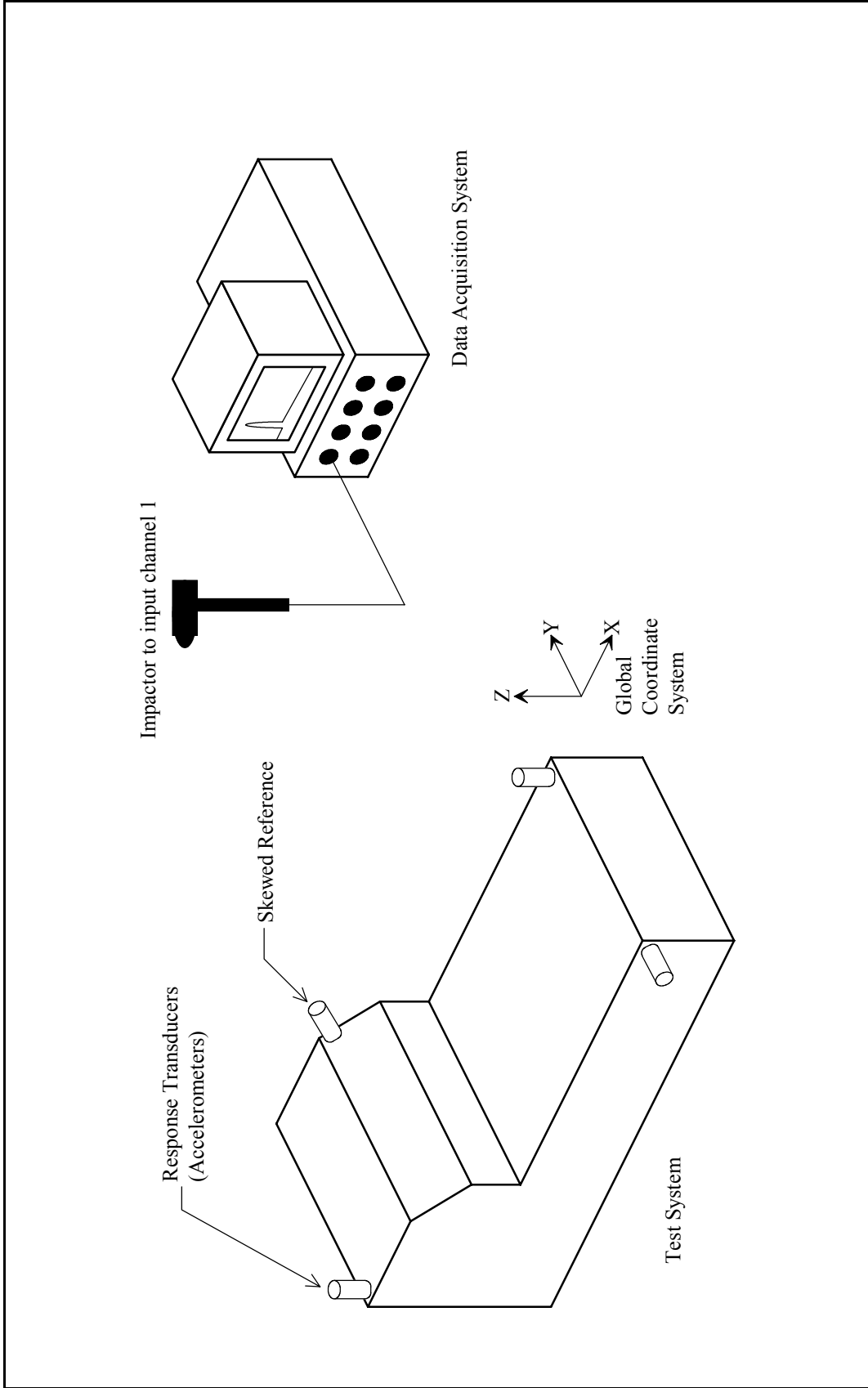
Figure 2-12. Schematic of a Multiple Reference Impact Test

2.4.1 Test Setup

One attractive feature of the MRIT method is the limited setup time needed to prepare for a test. The measurement equipment required for an MRIT test includes a data acquisition system of the type outlined in Section 2.2.1, an instrumented impactor, and the response transducers with the associated cables and power supplies. The impactor is connected to the first input channel of the data acquisition system and the response transducers are connected to the other input channels. The impactor is roved to each measurement location while the response transducers remain fixed during the test.

The preparation of a test system for an impact test does not ordinarily entail elaborate fixturing. The prescribed support fixturing depends on the test system and the testing conditions. For many field testing and troubleshooting situations, testing the system in situ, with operating boundary conditions, is either unavoidable or favorable. In most field testing situations, the test system can not be moved from its installation site and must be tested in place. When troubleshooting vibration problems, testing the system in the conditions under which it functions is preferred in order to evaluate its operational dynamics. In other situations, the test system may be supported by soft springs to simulate free-free boundary conditions or rigidly mounted to simulate fixed boundary conditions.

An important step in the test setup is selecting the locations for the reference transducers. The implications of reciprocity indicate that the locations of MRIT reference transducers are analogous MIMO exciter locations. Thus, the same guidelines for selecting exciter

locations for a MIMO test are applicable to selecting reference locations for an MRIT test. The possible locations for attaching an exciter to a structure are often limited by physical constraints and practical considerations, but greater flexibility is realized for the possible locations of MRIT reference transducers since they need only be mounted on the structure. The number of references is limited only by the number of channels of the data acquisition system. Typically, two to five references are sufficient for most applications. Since the data is acquired simultaneously, the incremental measurement time is minimal for additional references.

The reference transducers should be positioned on the test system such that the response of all modes of interest will be adequately observed. The references are defined by the location and orientation of the response transducers. The free edges of a structure, where the greatest motion is experienced, are popular choices for reference locations. Transducers should be oriented in all directions that significant response is expected to occur. However, the orientations of the references are not restricted to the directions of the global coordinate system, that is, skewed direction references are perfectly acceptable, provided driving point FRFs are measured. In addition, the distribution of the reference transducers should encompass all principal areas of the test system. The reference transducers in Figure 2-12 illustrate the result of these guidelines.

2.4.2   Nonlinearities

As mentioned in the section on signal processing, the impact force is impulsive and deterministic. Both of these properties are detrimental for measuring the frequency response of a nonlinear system when modal parameters are to be estimated. The high peak levels can overdrive the system and exaggerate its nonlinear response. Whereas randomized input functions will reduce the effects of nonlinearities with averaging, deterministic signals distort the measured FRFs. The degree of nonlinearity of a system can be evaluated with other deterministic measurements, such as swept-sine[11,22]. An impact is not a practical excitation for characterizing nonlinearities because the force level can not be precisely controlled.

Every effort should be made to linearize the system when making FRF measurements using impact testing to estimate modal parameters. All nonlinear components should be removed from the test system if possible. Static preloads applied with soft springs can tighten clearances and constrain the system into a more linear state. The springs should be soft enough so as to not appreciably change the dynamics of system. For example, when testing machine tools, a static preload can be applied simply by connecting the tool and workpiece to ground with nylon rope. The stiffness of the rope is orders of magnitude less than the stiffness of the machine tool. As a result, the low stiffness of preload in series with stiffness of the machine tool has a negligible effect on the machine tool dynamics. However, the rope is capable of exerting hundreds of pounds of preload.[13,14]

2.4.3   Pretest Measurements

Before the FRF collection process begins, an important set of preliminary measurements is recommended.   These measurements are necessary to determine the impactor properties, checkout the transducers and instrumentation, and ensure that the definition of the impact test is satisfactory.

The first pretest measurement is the autopower spectrum of the input force. The roll-off of the input spectrum is used to select the proper impactor and tip combination. Recall that the input spectrum should drop 10 to 20 dB across the measurement frequency span. The impactor is initially selected based on physical properties of the test system. Then the frequency range of the input spectrum is tailored by testing different impact tips and possibly additional mass attached to the impactor. The roll-off of the input spectrum is determined for each impactor configuration and compared to the recommended guideline. After the appropriate configuration of the impactor has been decided, the transducers can then be calibrated.

The next step is to configure the data acquisition system for high sampling rates (i.e., wide frequency span). The purpose is to operate the system as a digital oscilloscope in order to observe the initial segments of the time signals. A pretrigger delay should be used and the signals should not be windowed. If possible the anti-aliasing filters should be bypassed to eliminate any filtering effects that might obscure discontinuities in the signals. At the sampling rates associated with the actual impact test measurements, little detail of the time signals can be discerned. For instance, the duration impact pulse may

only be two or three time points. By viewing the time signals at high sampling rates, discontinuities or other anomalies in the signals that could indicate overloads, faulty wiring, or improper functioning of the instrumentation are detectable.

The last step is to setup the data acquisition system for the impact test measurements. First unwindowed time records are examined to determine the force window width and the exponential window time constant. Then time records are acquired with the windows applied to verify the effectiveness of the windows. The final pretest measurements are the driving point FRFs, which are examined for the expected magnitude and phase properties[23].

2.4.4   Triggering and Averaging

The measurements for an impact test are triggered on the positive slope of the force pulse so that the data acquisition begins upon impacting the test object. The triggering value of the force signal is commonly specified as a percentage of the input range. A pretrigger delay allows acquiring data that was measured before the impact in order to observe the leading edge of the time signals. All channels must have the same pretrigger delay time, otherwise a biased error in the phase of the FRFs will result. The force window must be constructed such that its width takes into account any pretrigger delay. These triggering functions are commonly available on modern data acquisition systems.

Typically five to ten averages are taken for an impact test. This relatively few number of averages is a compromise between improving the measurement quality and reducing the testing time. In order to collect high quality measurements, each average must be as good as possible. The ability to preview the time records for each average is a useful feature, which is available on many data acquisition systems. Measurement sets that contain overloads or multiple impacts should be rejected if possible. Any overloaded signals will adversely affect the quality of the measurements. Many data acquisition systems are equipped with overload detection circuitry. The implications of multiple impacts are discussed in Section 2.4.6. Rejecting an individual average is much less time consuming than restarting the measurement cycle.

2.4.5   Input Channel Autoranging

Attaining a high signal-to-noise ratio and avoiding overloads are critical concerns associated with impact testing. Thus, an important goal is optimizing the dynamic range of the analog-to-digital converter (ADC) for each input channel. If the range of the ADC is set too high, a poor signal-to-noise ratio will result. If the range of the ADC is set too low, overloads will occur. The ADC range of each input channel must be set according to the maximum voltage levels that will be measured on that input channel. Ideally, the peak amplitude of the measured signal should fall within the upper half of the input range.

Unfortunately, the standard autoranging function of most data acquisition systems is designed for continuous signals and is not effective for transient data. The customary procedure for impact testing has been to set the input channel ranges manually or to repeatedly impact while the system autoranges until no overloads are detected. However with a larger number of channels, optimizing the input ranges becomes much more time consuming. Thus for the MRIT method, the capability to autorange the input channels is a significant issue.

Adapting the autorange process to the properties of the impulsive excitation and transient response is actually very straightforward. The force reaches a maximum during the duration of the impact and then is near zero for the remainder of the time record. The transient response reaches a maximum at, or shortly after, the instant of the impact and then decays with time due to damping. Measuring the peak voltage amplitude of each time signal determines the appropriate input range for the corresponding channel. Measurements for autoranging should be triggered on the input, unwindowed, and unfiltered if possible. Autorange measurements should also be acquired at the highest available sampling rate because components of the signal above the impact test frequency range could cause overloading of the input channel. If overloading occurs during autoranging, then the range of the ADC must be increased. Normally the input channels can be autoranged with only a few impact cycles. Obviously, successful autoranging, as well as all impact testing, is greatly dependent on consistent impacts.

Autoranging the input channels at every impact location is not always necessary. The peak output level of any response transducer is a function of the proximity of the impact and also the direction of the impact. The response level will tend to increase as the impact location moves towards a transducer and tend to decrease as the impact location moves away from a transducer. The response level will generally be greater when the orientation of the transducer is parallel to the direction of the impact than when the orientation of the transducer is in another direction. In most cases, the response levels vary smoothly as the impact location progresses from point to point with the same impact direction. Often the range settings of the input channels are acceptable for several impact locations if impacts are made in the same direction, and autoranging is required less frequently.

2.4.6   Multiple Impacts

A proper impact signal should have one pulse at the beginning of the time record and then should be zero, excluding electrical noise and filter response, for the remainder of the time record. Multiple impacts occur when more than one pulse is measured in the time record. Multiple impacts can happen if the surface is not impacted sharply and cleanly or if the amplitude of vibration is large enough such that the rebounding surface contacts the hammer tip before the hammer rebounds away from the surface. This condition is most common with very lightly damped systems, in which case a lighter hammer should be used to reduce the possibility of multiple impacts. Multiple impacts should be avoided if

possible, because they can produce substantial measurement errors. Figures 2-13 through 2-15 illustrate the consequences of multiple impacts.

Figure 2-13(a) contains a proper, single impact time signal and the force window. The width of the force window is defined such that pulse in the initial segment of the time record is passed and the noise in the remainder of the time record is suppressed. Figure 2-13(b) contains the input spectrum of the windowed force signal from Figure 2-13(a) and also the output spectrum of the response. An exponential window is also applied to the time signals. Both spectra are smooth and noise-free across the frequency span. Figure 2-13(c) contains the H_1 FRF calculated from the spectra in Figure 2-13(b). For a single average, a single-input H_1 FRF is equivalent to division of the output spectrum by the input spectrum[2]. The data contained in Figure 2-13 demonstrates the proper measurement results and is a benchmark for comparison of the data contained in Figures 2-14 and 2-15.

Figure 2-14(a) contains a double impact time signal and the force window. The same force window that is shown in Figure 2-13(a) is applied to the double impact signal. The force window passes the first pulse but removes the second pulse. Figure 2-14(b) contains the input spectrum of the windowed force signal from Figure 2-14(a) and also the output spectrum of the response. An exponential window is also applied to the time signals. The input spectrum is similar to that of Figure 2-13(b) since the transformed signal consists of only the first pulse. However, the true input spectrum of the double impact has the shape of that shown in Figure 2-15(b). The lobes on the output spectrum

43

are caused by the response to the double impact. The combination of the input and output

spectra produce the FRF in Figure 2-14(c), which is highly contaminated with

measurement errors.

The measurement errors due to multiple impacts are actually introduced by the force

window, because the force window suppresses the second pulse in the force measurement

that is used in the FRF calculation. However, the response to this component of the input

exists in the output spectrum. Since the measured input does not accurately represent the

true input to the system, the response measurement that is used in the FRF calculation

contains response that is not due the measured input. As a result, the FRF calculated

from this data is not an accurate measurement of the frequency response of the system.

Figure 2-15(a) contains the same force signal as Figure 2-14(a), but in this case the width

of the force window is defined such that both pulses are included in the measured signal.

Figure 2-15(b) contains the input spectrum of the windowed force signal from Figure

2-15(a) and also the output spectrum of the response. An exponential window is also

applied to the time signals. The multiple impacts produce dropouts in the input spectrum

magnitude, and the frequency intervals of the dropouts are inversely proportional to the

time delay between the pulses. Although lobes are present in both input and output

spectra, errors are still present in the FRF. The low excitation levels at the dropout

frequencies lead to poor estimates of the FRF at those frequencies, as indicated by the

vertical lines in Figure 2-15(c). Thus, even if both pulses are included in the windowed

signals, inaccurate FRFs are produced. Although the errors in the FRF are not as severe

for this case as for the case in which the second pulse is removed from the force measurement, multiple impact should be avoided even if the force window does not truncate the true input to the system. Because only a few averages are typically taken for an impact measurement, one substandard average can adversely effect the averaged set of measurements.
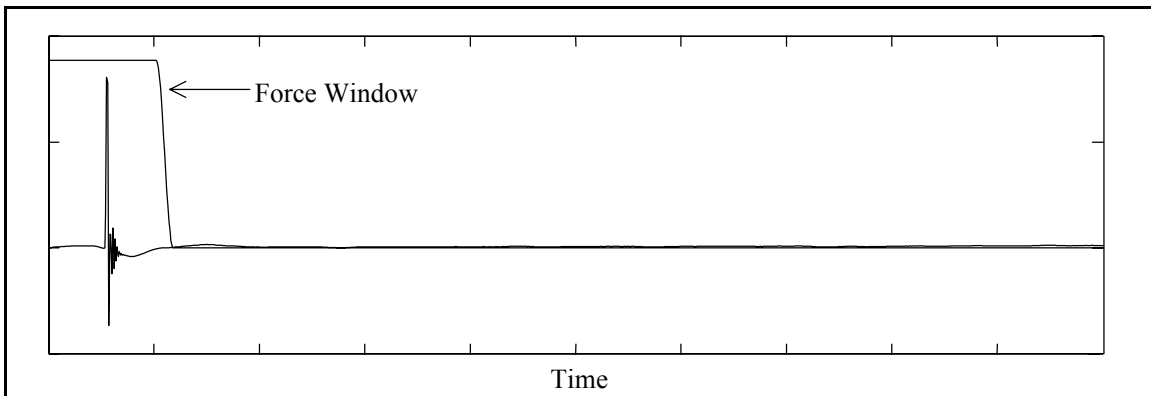
Figure 2-13(a). Single Impact Force Signal and Force Window.
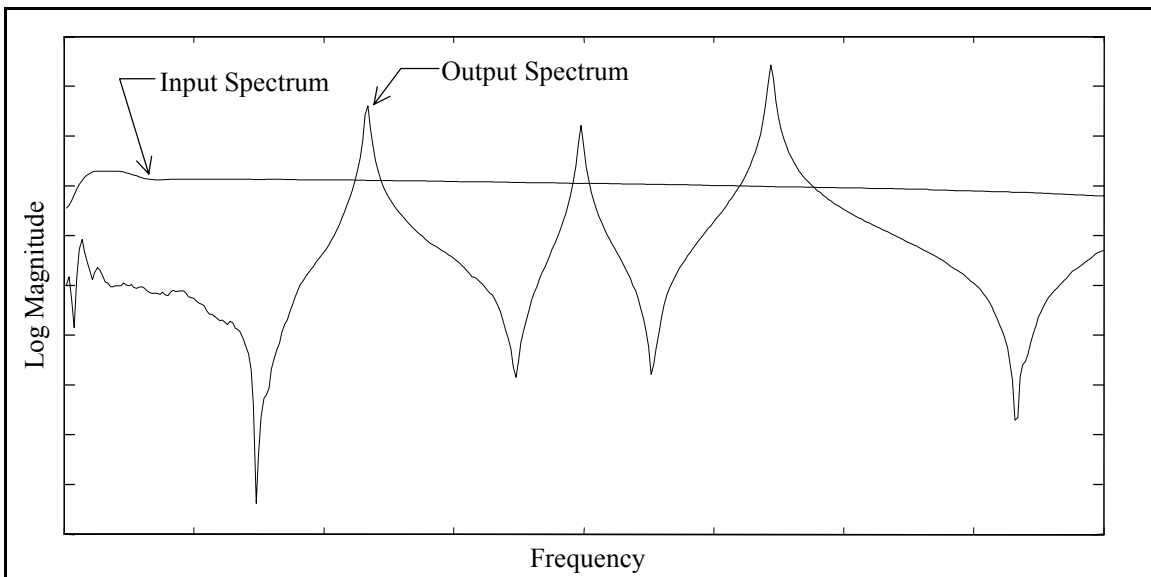
Figure 2-13(b). Single Impact Input Spectrum and Output Spectrum.
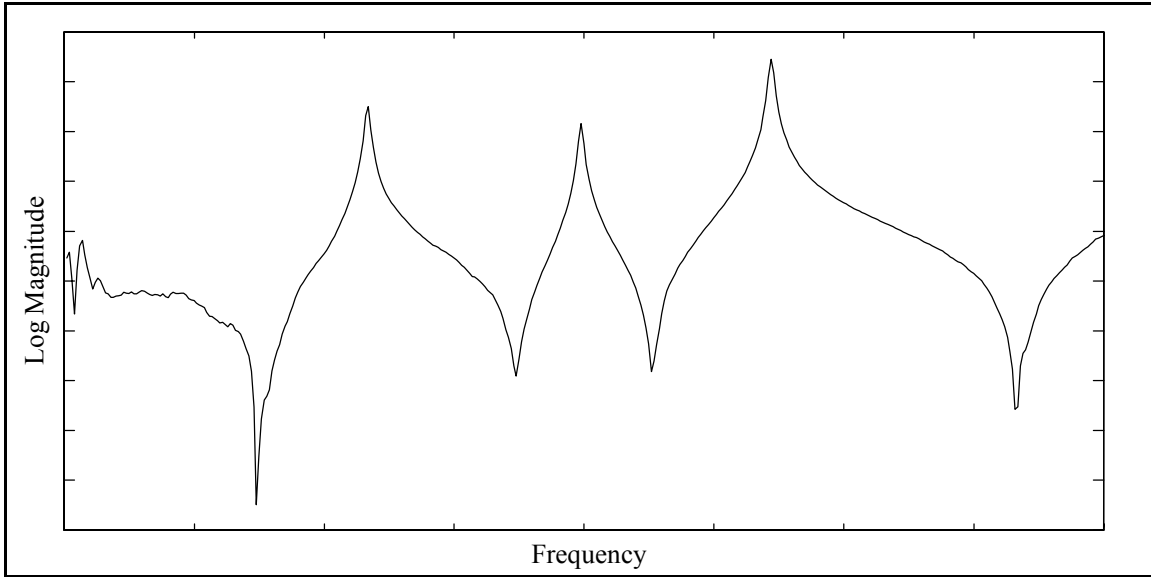
Figure 2-13(c). Single Impact Frequency Response Function.
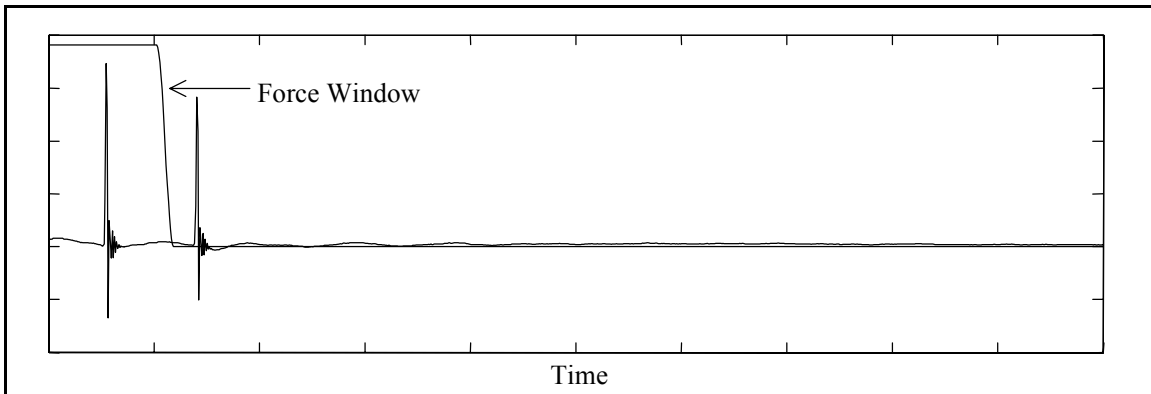
Figure 2-14(a). Double Impact Force Signal and Force Window.
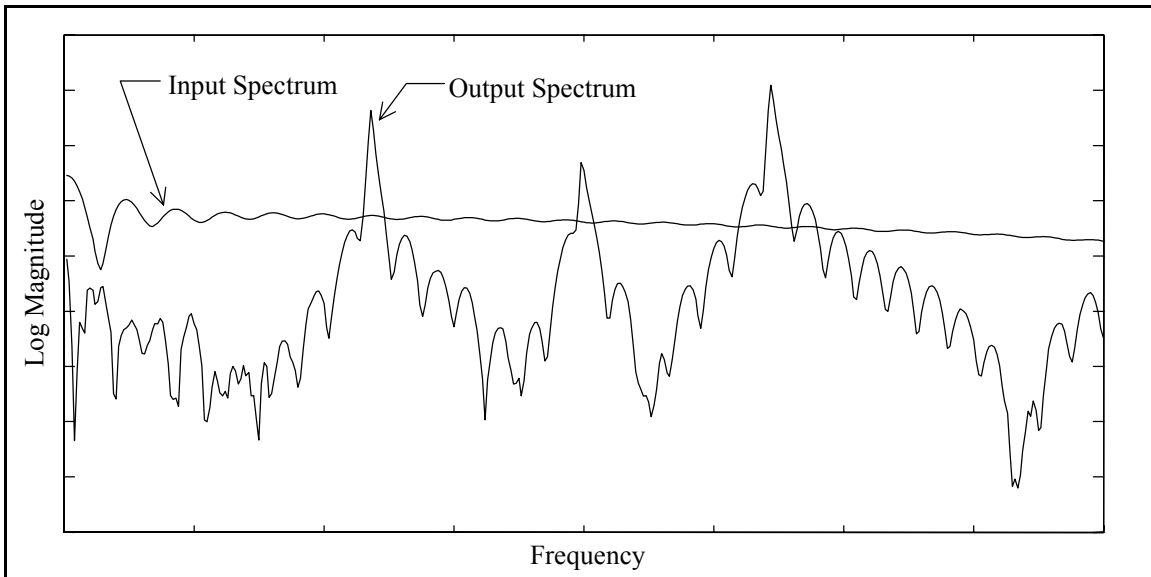
Figure 2-14(b). Double Impact Input Spectrum and Output Spectrum.
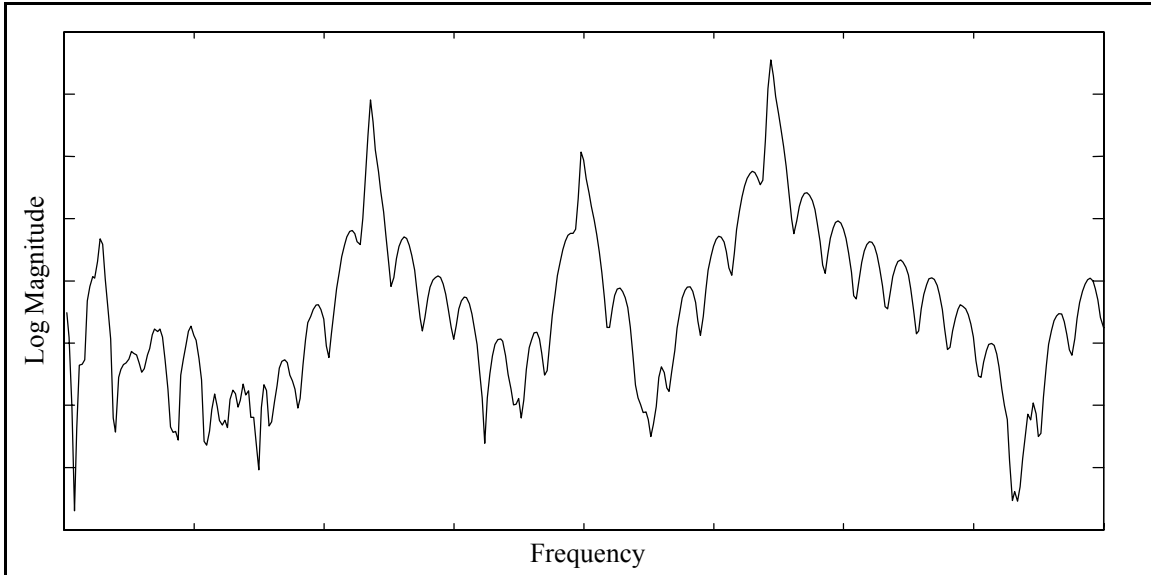
Figure 2-14(c). Double Impact Frequency Response Function.
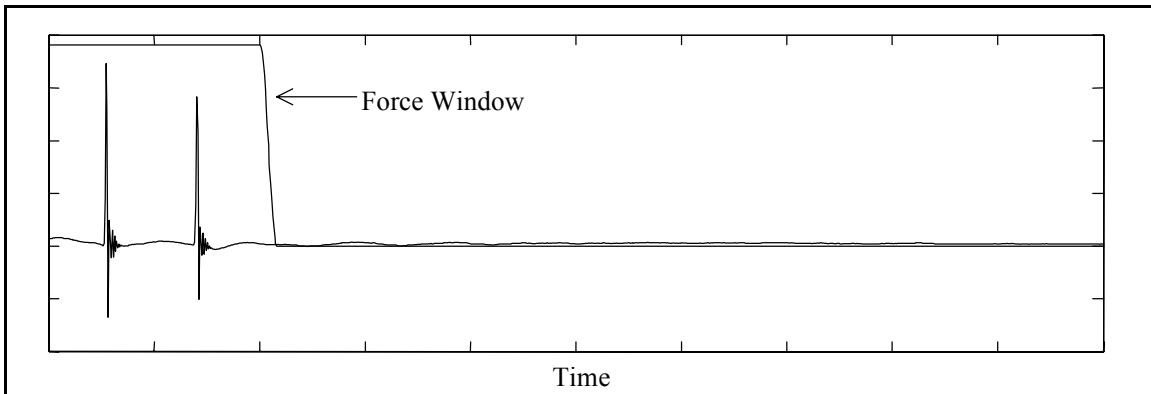
Figure 2-15(a). Double Impact Force Signal and Force Window.
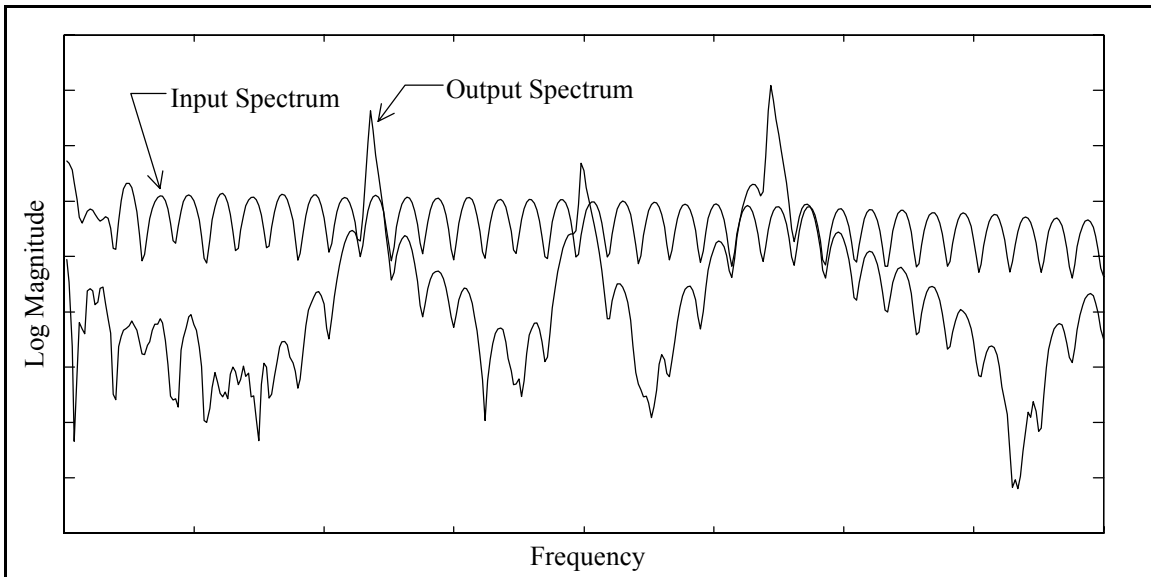
Figure 2-15(b). Double Impact Input Spectrum and Output Spectrum.
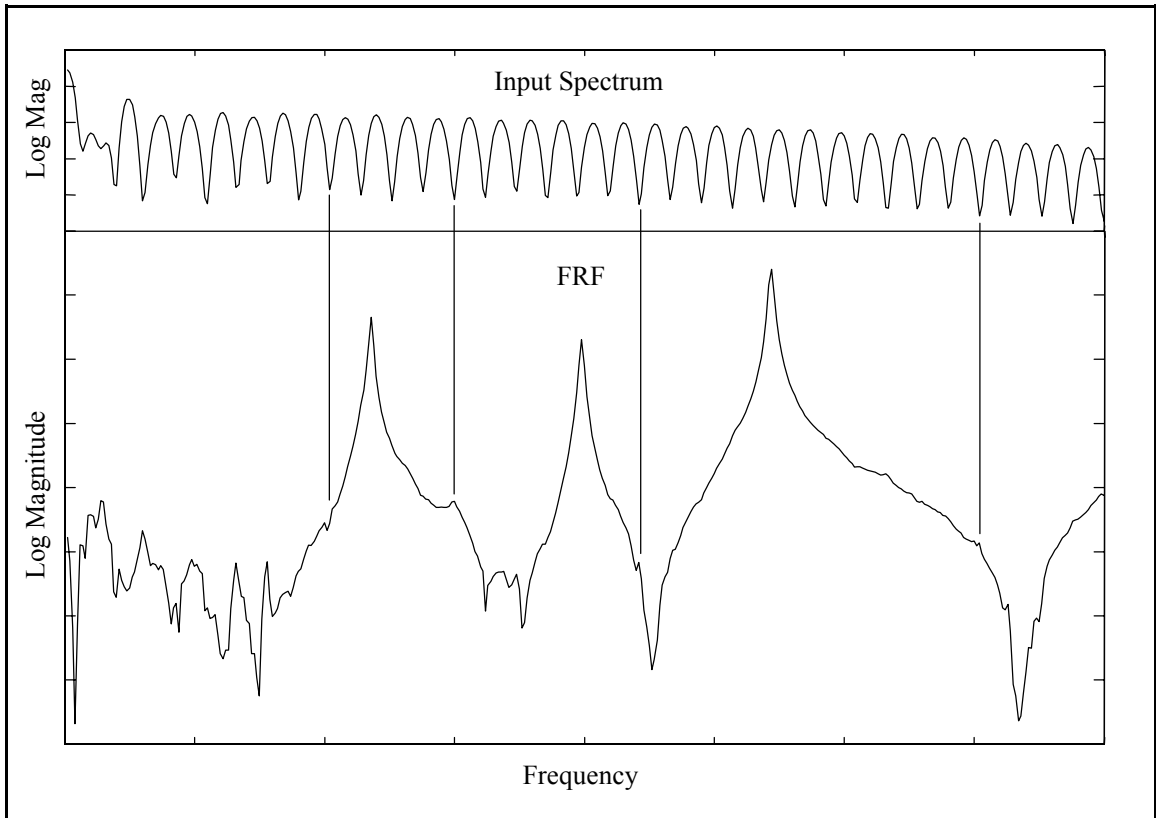
Figure 2-15(c). Double Impact Input Spectrum and Frequency Response Function.

2.5 Software Implementation

Modern data acquisition systems are designed to perform many diverse measurement functions. As a consequence of this intended versatility, the standard operation of a data acquisition system is often not fully optimized for impact testing. Furthermore, the MRIT method requires some specialized and unique measurement techniques that are not commonly provided. Therefore, modifications to the standard operation of a data acquisition system are necessary in order to accommodate the MRIT acquisition procedure.

As mentioned in the section on data acquisition systems, multiple channel and programmable dedicated Fourier analyzers have become commercially available. One such system, the Hewlett-Packard 35670A Dynamic Signal Analyzer (HP-35670), has recently been added to the inventory of the Structural Dynamics Research Lab (SDRL) at the University of Cincinnati, which is shown in Figure 2-1(b). The analyzer used for this thesis work was equipped with the following options: (1) four input channels, (2) Instrument BASIC programming, (3) additional one megabyte of nonvolatile RAM, and (4) eight megabytes of memory. Because of its four input channels, portability and programmability, this data acquisition system provides a platform for the practical implementation of the MRIT method. An Instrument BASIC program has been developed for HP-35670 to perform the MRIT data acquisition procedure.

2.5.1   Software Overview

Instrument BASIC is a programming language that supports the ordinary program functions such as mathematical and logical operations, input/output, graphics, etc. In addition, Instrument BASIC acts as a system controller residing in the analyzer and communicates with the analyzer via HP-IB commands.†   The interface bus used for Instrument BASIC is internal to the analyzer, not an external cable connection. The instructions sent by a program through the HP-IB essentially replace the analyzer's front-panel operations.[24-27]

---

† HP-IB is the Hewlett-Packard implementation of the IEEE 488 interface bus.

The MRIT Acquisition software customizes the analyzer explicitly for the intended purpose of performing MRIT data acquisition. The program utilizes functions provided by the analyzer and also creates additional, specialized features. The objective of the program is to optimize the MRIT data acquisition procedure by reducing the testing time and effort. Much of the emphasis in developing the program was directed at redressing many of the troublesome aspects of impact testing. Incorporated into the program are many features that facilitate collecting FRFs with impact testing. Some of the repetitive and error prone tasks commonly associated with impact testing have been automated. Many of the concepts presented in preceding sections of this chapter are also implemented in the program. The principal features of the MRIT Acquisition software that improve the convenience and utility of the MRIT method are described in the following sections.

The MRIT Acquisition software controls the built-in functions of the analyzer as well as provides additional capabilities to the analyzer and governs the testing process. The software is primarily menu driven using the soft-keys on the front panel of the analyzer. The performance of the analyzer is modified by arranging the relevant commands into an accessible structure of menus. Many common operations that may require a sequence of several front-panel key strokes are replaced with a single soft-key menu selection. While running, the Instrument BASIC program assumes control of the analyzer. The front panel function keys are disabled, except for entering alphanumeric responses to interactive prompts. Control of the analyzer is returned to the front panel upon exiting the program. A necessary consequence of customization is the loss of versatility as only a subset of the

analyzer functions are accessible during execution of the program. The software user's manual contains a detailed description of the program operation.

2.5.2 Test Management

Analyzers are a very portable and versatile measurement systems, but they usually lack the test management features provided by computer-controlled systems. The functions of an analyzer are typically arranged in a layered menu structure, but the organization of the functions is often inefficient for impact testing. Collecting measurements with an analyzer is a routine procedure, but the many repetitive tasks associated with impact testing are susceptible to careless errors. One of the principal benefits of the MRIT Acquisition software is the creation of a test management framework that governs the testing process, organizes the relevant measurement operations, and automates the repetitive tasks.

Upon starting the program, the analyzer is initialized for impact testing and the MRIT Main Menu and the MRIT State are displayed. The MRIT Main Menu controls the primary processes of the software, and the MRIT State consists of all parameters which define a test. However, an MRIT State is not the same as an instrument state because it includes information which is not applicable to the instrument state. The MRIT State can be saved to an ASCII file and then loaded into the software at a later time. The MRIT State is displayed on the screen, as shown in Figure 2-16, and is updated as the parameters are assigned. The default MRIT State parameters are assigned during

initialization of the software. The entries on the right are the general test parameters, the entries on the left are the measurement parameters, and the entries along the bottom are the channel information. The soft-key labels to the right of the display indicate the principal functions of the software. The diagram in Figure 2-17 depicts the general flow of the MRIT Acquisition software.
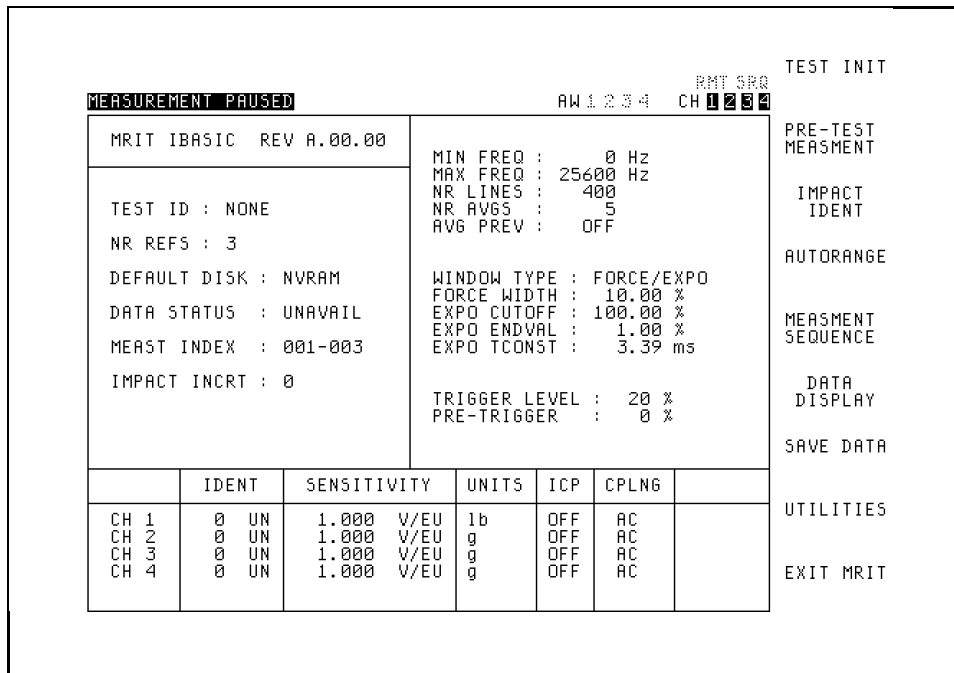
Figure 2-16. Default MRIT State Display and Main Menu.

2.5.3   Saving Data Files

The operation of saving data files, which is one of the most repetitive tasks of impact testing, has been automated. The acquired FRFs are saved to a set of Standard Data Format (SDF) files on disk, with a single key stroke. Each data file contains one FRF and the associated header information. The naming convention for the data files is *ABCDE123.DAT*. The first five characters of the filename (*ABCDE*) are the Test

TEST INIT	**Test Initialization.** Define the MRIT State parameters. Select Default Disk under Utilities. Save MRIT State file under Utilities when Test Initialization is completed.
AUTORANGE	**Auto-Range.** Auto-Range input range of active channels before performing Pre-Test Measurements.
PRE-TEST MEASMENT	**Pre-Test Measurements.** Acquire and evaluate Pre-Test Measurements before commencing FRF data acquisition.
IMPACT IDENT	**Impact Identification.** Enter point number and direction of next measurement location (or use automatic impact point number increment).
AUTORANGE	**Auto-Range.** Auto-Range input range of active channels for next measurement location, if necessary.
MEASMENT SEQUENCE	**Measurement Sequence.** Acquire Frequency Response Functions at measurement location.
DATA DISPLAY	**Data Display.** Review FRFs before saving data to SDF files on disk.
SAVE DATA	**Save Data.** Save FRFs to SDF files on disk. Data Status, Measurement Index, Impact Point Number, and Test-Log are updated.
EXIT MRIT	**Exit MRIT.** Terminate the software. Control is returned to the front panel. MRIT State information is cleared upon exiting.
UTILITIES	**Utilities.** Use Utilities as required to specify Default Disk, Save and Load MRIT State files, Display Test-Log, and Data File Transfer.

Figure 2-17. General Flow of the MRIT Acquisition Software.

Identification. Each data file generated during a test has the same Test Identification. The last three characters of the filename (*123*) are the Measurement Index. The Measurement Index ranges from 001 to 999 and is not required to be associated with a location on the test geometry. The customary practice of naming the data files from an analyzer according to the point number and direction of the measurement is not necessary because this information is stored in the data file header. Utilities to convert the SDF data files to other formats that are compatible with analysis software packages are readily available[28].

After each completed Save Data operation, the Measurement Index and Impact Point Number are incremented, the Data Status is updated, and entries are written to the Test-Log file. The Data Status is listed on the MRIT Display and indicates the condition of the FRF measurements present in the analyzer's memory. The Data Status can have the designations of *UNAVAIL(able)*, *ACQUIRED*, or *SAVED*. This feature is intended to reduce the possibility of losing measurements from memory before the FRFs are saved to data files on disk. The Test-Log file and the Impact (Point Number) Increment are described in Sections 2.5.4 and 2.5.5, respectively.

Although the MRIT method utilizes the principle of reciprocity, the data is saved as it was acquired. That is, the input and output identifications (point numbers and directions) stored in the header of the data files are not transposed. This decision is based on the premise that altering the data file measurement information can possibly lead to

complications and confusion. The reciprocity condition is invoked in the data analysis stage of the MRIT test.

The HP-35670 provides several data storage devices, and the MRIT data files can be saved to either a nonvolatile RAM disk or an internal 3.5-inch floppy disk. The nonvolatile RAM disk is the segment of the analyzer's random access memory allocated to retain its contents when the analyzer is turned off. The recommended procedure is to save the data files to the nonvolatile RAM disk if the additional one megabyte of nonvolatile RAM (1.1 megabyte total) is installed in the analyzer. Saving data files to the nonvolatile RAM disk takes only a few seconds, while saving data files to the internal disk can take a minute or more as the disk fills. Since saving data files to the nonvolatile RAM disk is much faster than saving data files to the internal disk, the interruption of the measurement cycle is minimized and the test time is reduced. A utility to transfer the data files from the nonvolatile RAM disk to the internal disk is provided. This will be necessary at the end of the test or when the nonvolatile RAM disk reaches full capacity during a test. The estimated time required to transfer a full nonvolatile RAM disk to the internal disk drive is seven minutes. Based on the data file capacity of the nonvolatile RAM disk and the quantity of measurements typically collected for an impact test, the down time for data file transfers should normally be just a small fraction of the total testing time.

2.5.4 The Test-Log File

Traditionally, recording the measured impact locations entailed manually compiling a list during the test. This practice has been automated by writing a Test-Log file to the nonvolatile RAM disk, which is updated after each completed Save Data operation. The Test-Log file produces a record of the test and documents the contents of each data file saved to disk. The Test-Log is an ASCII file that contains the index and identification of each FRF acquired and saved to a data file. The Test-Log provides an automated procedure for recording the measurements collected during a test that saves testing time and removes the chances for mistakes.

The Test-Log also provides a convenient means of monitoring the impact locations measured during the course of a test. The Test-Log information can be displayed on the screen to review the impact locations that have been measured at that stage of the test. The Measurement Indices and corresponding Impact Identification for each set of data files are listed. The contents of the Test-Log can be sorted by either Measurement Index or Impact Identification, as shown in Figure 2-18(a) and 2-18(b), respectively.

Figure 2-18(a). Test-Log Display Sorted by Measurement Index.

Figure 2-18(b). Test-Log Display Sorted by Impact Identification.

2.5.5   Test Definition

The MRIT State parameters listed Table 2-1 comprise all the information that defines a test. The test definition includes familiar parameters that are common to all measurement systems and also unique parameters that are specific the MRIT Acquisition software. The MRIT State parameters that improve standard functions or provide additional features are indicated by a checkmark (✓) and are explained below.

✓ Default Disk	Number of Averages
✓ Test Identification	Average Preview
✓ Measurement Index	Preview Time
✓ Number of References	Trigger Level
✓ Reference and Impact Identification	✓ Pretrigger Delay
✓ Impact Increment	✓ Window Type
Transducer Sensitivity	✓ Force Window Width
✓ Transducer Units	✓ Expo Window Cutoff
Minimum Frequency	✓ Expo Window End Value
Maximum Frequency	Input Channel Coupling
Number of Spectral Lines	ICP Power Supply

Table 2-1. MRIT State Parameters.

Default Disk. The Default Disk determines the storage device on which data files are saved. MRIT State files are also saved to and loaded from the Default Disk.

Test Identification. The Test Identification serves a simple but important test management function that associates the data files as members of a data set. The Test Identification is used to name the data files and the Test-Log file. Every data file collected during a test has the same Test Identification.

Measurement Index. The Measurement Index is also used to name the data files and contributes to the test management function. Each data file has a unique Measurement Index, which ranges from 001 to 999.

Number of References. The Number of References refers to the number of reference transducers that are to be measured. The Number of References determines the FRFs that are saved to data files, the entries that are written to the Test-Log, and the channels that are autoranged. The hardware and software support up to three references.

Reference and Impact Identification. The Reference Identifications define the point numbers and directions of the references. The Impact Identification defines the point number and direction of the current input. The Reference Identifications are defined once at the beginning of a test. The Impact Identification is redefined for every measurement cycle. The Reference and Impact Identifications are stored in the data file headers.

Impact Increment. The Impact Point Number is automatically incremented by the amount specified by the Impact Increment after each completed Save Data operation. If the impact locations proceed in sequential order with a constant direction, then the point number does not need to be entered manually, which conserves testing time.

Transducer Units.   The available units selections for the impactor force sensor and reference transducers are listed Table 2-2.   These include units for the common types of transducers used for impact testing, in both the English and SI systems.

Impactors	lb	N	
Accelerometers	g	m/s^2	$inch/s^2$
Proximity Probes	mil	m	inch
Microphones	psi	Pascal	

Table 2-2.   Units for Impact Testing Transducers.

Pretrigger Delay.   The Pretrigger Delay is specified as a percentage of the time record length, rather than as a time value.   The delay time is always negative, so that the measurements start before the impact.   The time record length is determined by the frequency span and the number of spectral lines, and if the time record length is modified, the delay time is also updated accordingly.   This feature is provided as a convenience such that the delay time does not need to be manually redefined if other measurement parameters are modified.   Figure 2-19 illustrates the definition of the Pretrigger Delay.
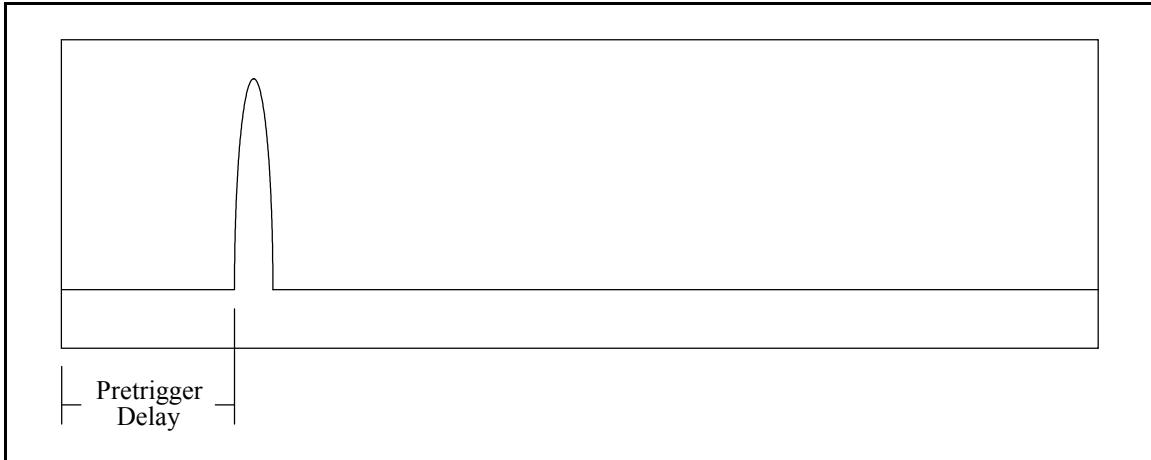
Figure 2-19. Definition of Pretrigger Delay.

Window Type. The uniform window and the force and exponential windows are available for impact testing. In almost all cases, the force and exponential windows will be used. The uniform window is included for measurements that contain periodic noise components, as discussed in Section 2.3.2. However, no signal processing techniques for removing periodic noise are presently implemented.

Force Window Width. The Force Width defines the duration of the force window and is specified as percentage of the time record length, rather than as a time value. The time record length is determined by the frequency span and the number of spectral lines, and if the time record length is modified, the Force Width time is also updated accordingly. This feature is provided as a convenience such that the force window duration does not need to be manually redefined if other measurement parameters are modified. The Force Width time is determined such that it also includes any Pretrigger Delay time. For example, if the Pretrigger Delay is 10% and the Force Width is 10%, the duration of the

force window will be 20% of the time record length. Figure 2-20 illustrates the definition
of the Force Width.
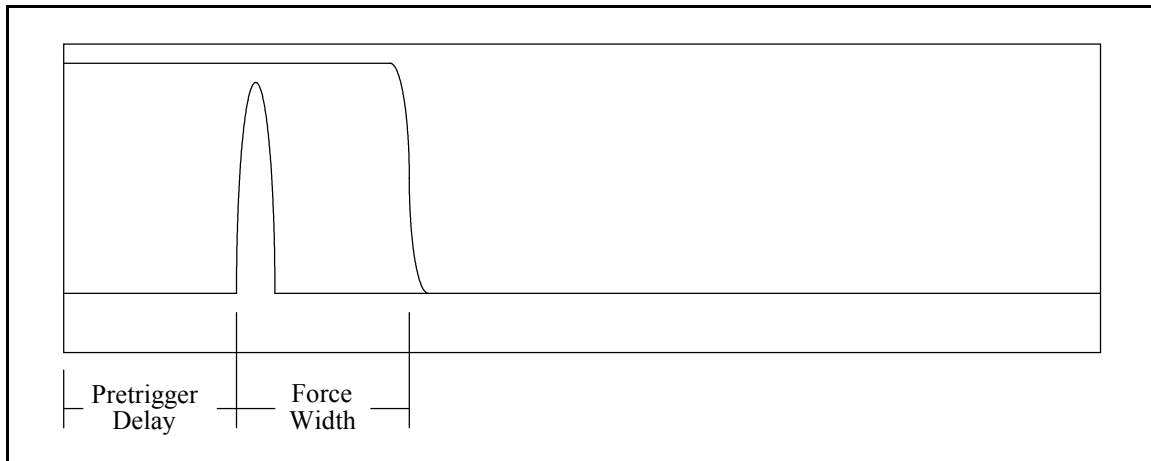
Figure 2-20. Definition of Force Window Width.

Exponential Window Cutoff and End Value. In some data acquisition software, the
exponential window is defined by specifying the time constant (τ) in seconds. In other
data acquisition software, the exponential window is defined by specifying the reciprocal
parameter (β) in radians per seconds. (Refer to Equation 2-3.) A common suggestion is
that the time constant should be one quarter of the time record length, which creates an
exponential function that decays to approximately two percent at the end of the time
record. However, this is not appropriate for heavily damped systems, as was explained in
Section 2.3.1. Although calculating either quantity (τ or β) for the desired exponential
window properties is not difficult, a much more intuitive definition for the exponential
window is proposed in Equations 2-4 and 2-5.

$$\exp\left(\frac{-ExpoCutoff(\%) * TimeRecordLength}{ExpoTimeConstant}\right) = ExpoEndValue(\%) \qquad (2\text{-}4)$$

or

$$ExpoTimeConstant = \frac{-ExpoCutoff(\%) * TimeRecordLength}{\ln(ExpoEndValue(\%))} \qquad (2\text{-}5)$$

The exponential time constant is calculated from the Expo Cutoff, the Expo End Value, and the time record length. The Expo Cutoff is defined as percentage of the time record length, and the Expo End Value is defined as percentage of unity. The exponential window has a value of unity at the beginning of the time record and will decay to the value specified by the Expo End Value at the percentage of the time record specified by the Expo Cutoff. For example, if the Expo Cutoff is 50% and the Expo End Value is 5%, the value of the window at the midpoint of the time record will be 0.05, for any time record length. By defining the exponential window in this manner, the properties of the window can very easily be specified. The time record length is determined by the frequency span and the number of spectral lines, and if the time record length is modified, the exponential time constant is also updated accordingly. Figure 2-21 illustrates the definition of the Expo Cutoff and Expo End Value.
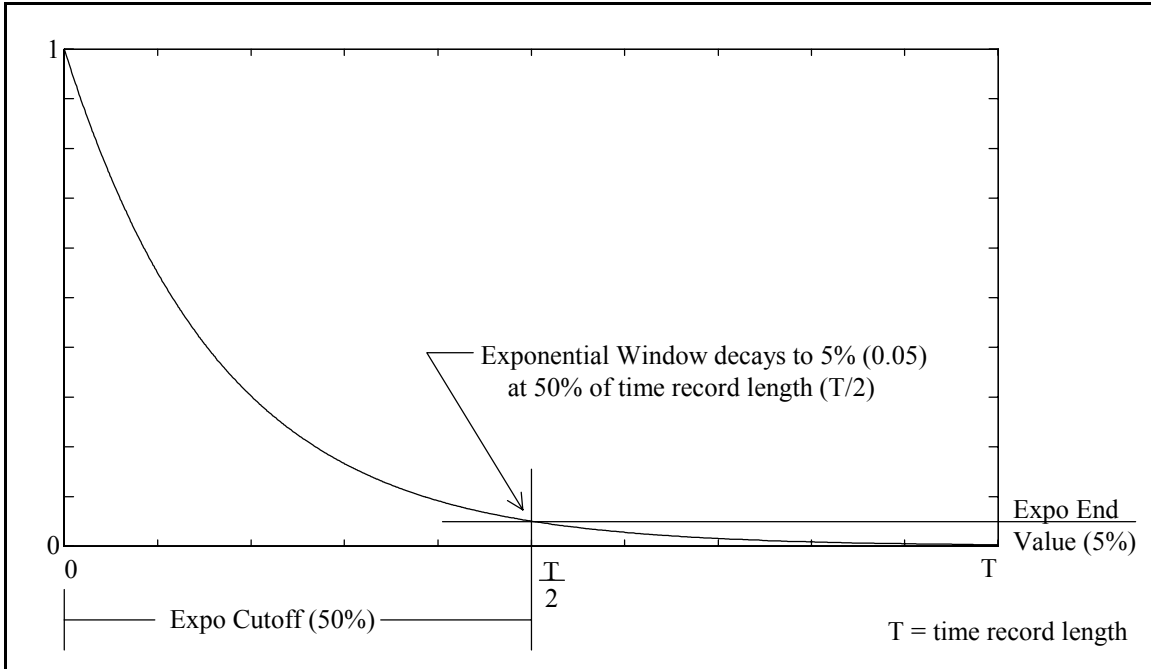
Figure 2-21. Definition of Exponential Window Cutoff and End Value.

2.5.6 Pretest Measurements

A suite of pretest measurements based on the concepts presented in Section 2.4.3 are integrated into the software. The pretest measurements include input autopower spectrum, digital oscilloscope, and windowed time signal measurements. The analyzer is initially set at the highest sampling rate possible for four input channels (25.6 kHz baseband frequency span) and the maximum spectral lines (800). Other baseband frequency spans are also possible for the input autopower spectrum and digital oscilloscope measurements. The attributes of the pretest measurements are described below.

Input Autopower Spectrum. The autopower spectrum of the input force is measured, as shown in Figure 2-22, for selecting the proper impactor and tip combination. In the top trace, the full frequency span is displayed. In the bottom trace, the test frequency span is displayed. Also in the bottom trace, relative markers are positioned at the spectral lines nearest the limits of the test frequency span. The relative markers measure the roll-off of the input spectrum magnitude across the test frequency span. The input spectrum roll-off is determined directly from the relative marker readout for every impact. Note that if the lower frequency limit is 0 Hz, the relative marker reference (indicated by the small square) is positioned at the second spectral line since a peak can sometimes occur at the DC spectral line of the input spectrum, which would cause an inaccurate roll-off value. The full frequency span of the upper trace reveals the input spectrum behavior above the test frequency limit.
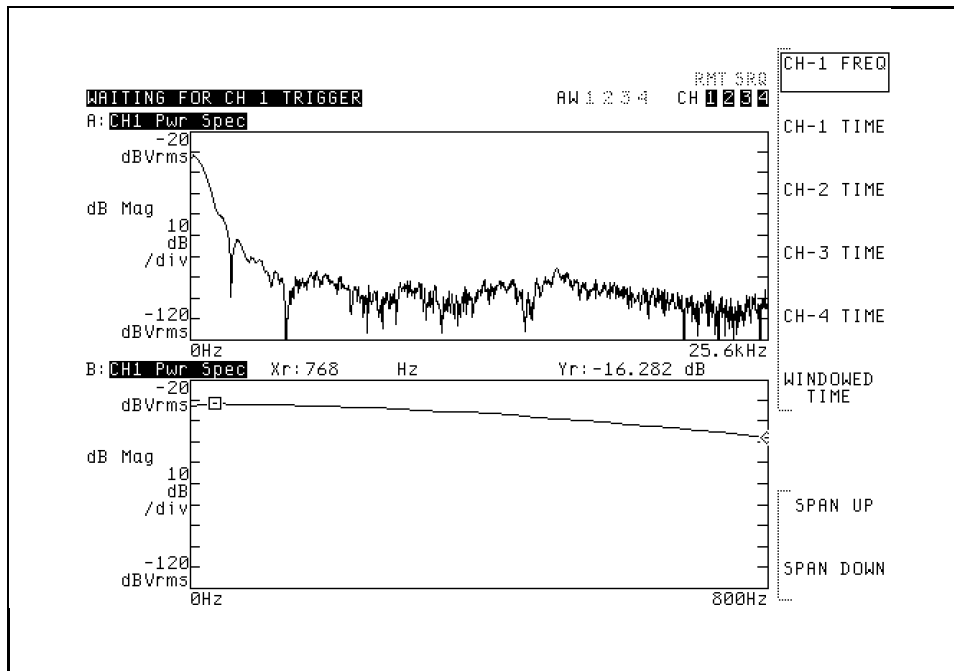
Figure 2-22. Input Autopower Spectrum Pretest Measurement.

Digital Oscilloscope. At high sampling rates the analyzer operates as a digital oscilloscope for observing detail in the initial segment of the time signals. The unwindowed time record of any of the four channels can be measured. A ten percent pretrigger delay is applied, and the measurements are displayed in volts. The time record of a force signal (channel 1) is shown in Figure 2-23. In the top trace the full time record is displayed. In the bottom trace, the display is expanded about the initial segment of the time record. The marker indicates the maximum measured voltage.
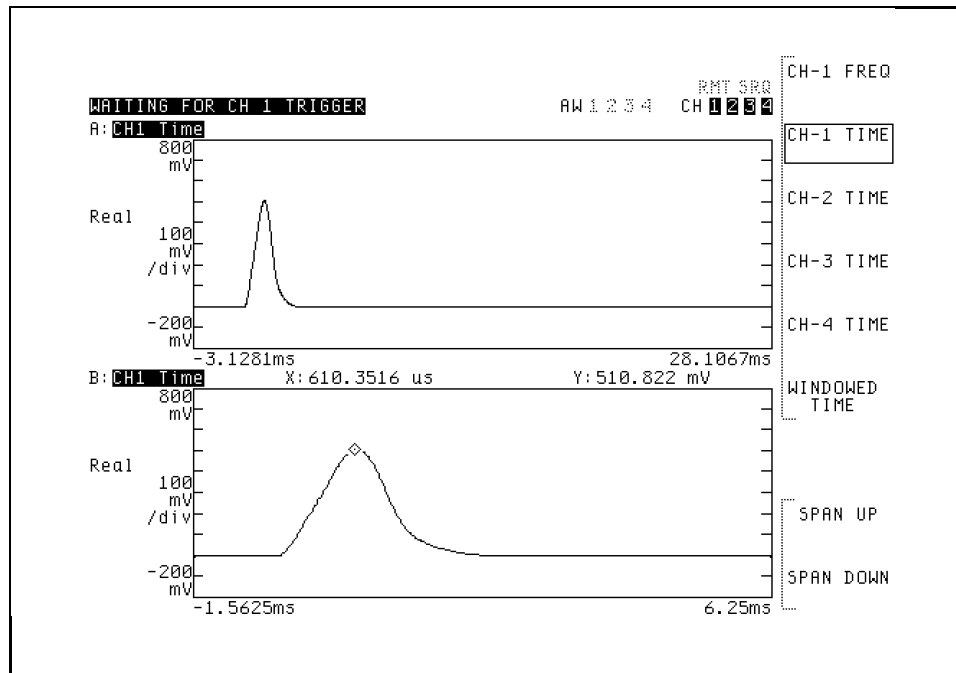
Figure 2-23. Digital Oscilloscope Pretest Measurement.

Windowed Time Signals. The windowed time signals of all four channels are measured and displayed as shown in Figure 2-24. The previously defined MRIT State parameters are applied for the measurements. The purpose of these measurements is to evaluate the

windowing of the time signals and to view the data as it will be acquired for the impact test.
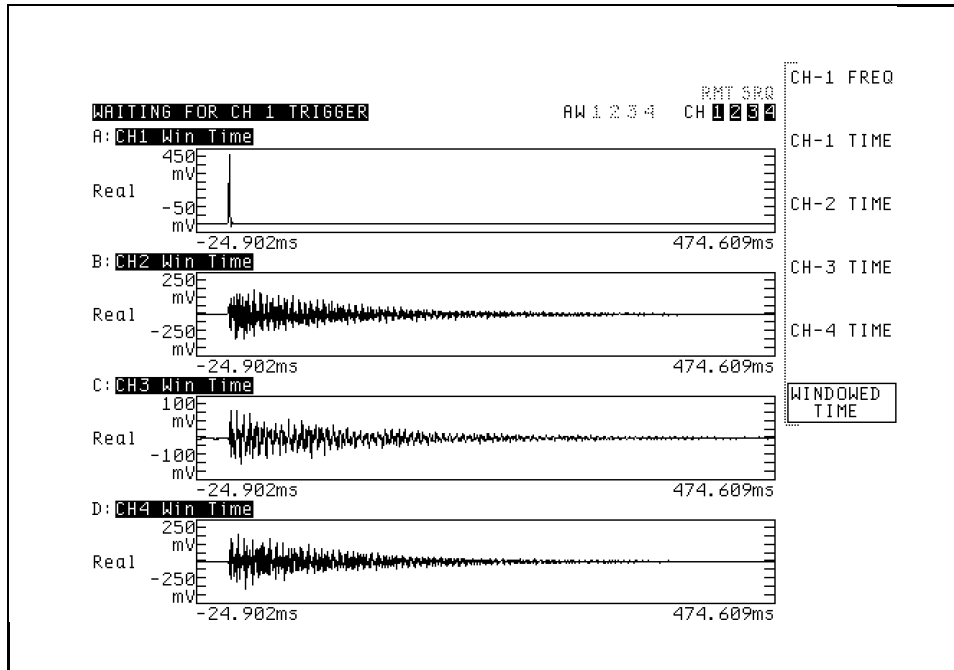
Figure 2-24. Windowed Time Signals Pretest Measurement.

2.5.7   Input Channel Autoranging

Input channel autoranging has been adapted to the properties of the transient impact time signals, as outlined in Section 2.4.5.   Unwindowed time records are acquired at a high sampling rate, triggered from the impact, and the maximum measured voltage of each channel is evaluated.   If the peak amplitude of a channel is greater than the input range, the input range is doubled.   Otherwise, the input range for a channel is determined by the peak amplitude and a parameter called the Auto-Range Over-Head.   The input range of the corresponding channel is assigned to the next higher available setting.

The input range of all four channels are assigned to one volt at the initialization of the program. Since the trigger level is defined as a percentage of the force channel (1) input range, a function to decrease the input range of this channel is provided in case the impact will not trigger the measurement at the current input range. The autoranging process is automatically completed when all the active channels are in-range, but the process may also be terminated at any other time if necessary. Since the force level should be relatively constant and the response levels usually vary smoothly, the current input ranges are maintained for subsequent autoranges.

The input range is based on the maximum (absolute value) measured voltage and the Auto-Range Over-Head. The peak amplitude is increased by the Auto-Range Over-Head to determine the input range. For example, if the peak amplitude is 1.0V and the Auto-Range Over-Head is 33%, the input range is calculated to be 1.33V. The overhead provides some margin of safety for the magnitude of the impact force. The analyzer's overload detection circuitry does not actually register an overload until a voltage of approximately 140% of the input range is detected, but this built-in margin of safety is not taken into account for the autoranging. The autoranging relationships for the default Auto-Range Over-Head of 33% are shown schematically in Figure 2-25. For an Auto-Range Over-Head of 33%, the peak amplitude will fall midway between half-range and full-range.
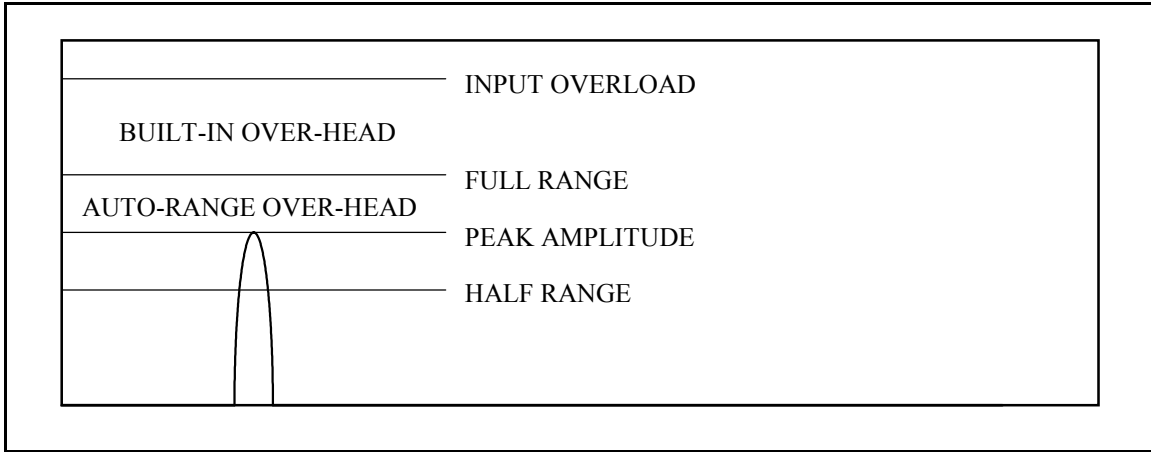
Figure 2-25. Autoranging Levels and Auto-Range Over-Head.

A graphical display represents the autoranging process, as shown in Figure 2-27, also refer to Table 2-3. For this example, two references have been specified (channels 1,2, and 3 are active), and only the active channels (as defined by the Number of References) are autoranged. After an impact, the peak amplitude is compared to the current input range for each channel. The input ranges are then reassigned and the display is updated with the new input ranges and the peak amplitudes. The horizontal blocks indicate the status of the channels. The channel status blocks are described in Figure 2-26.
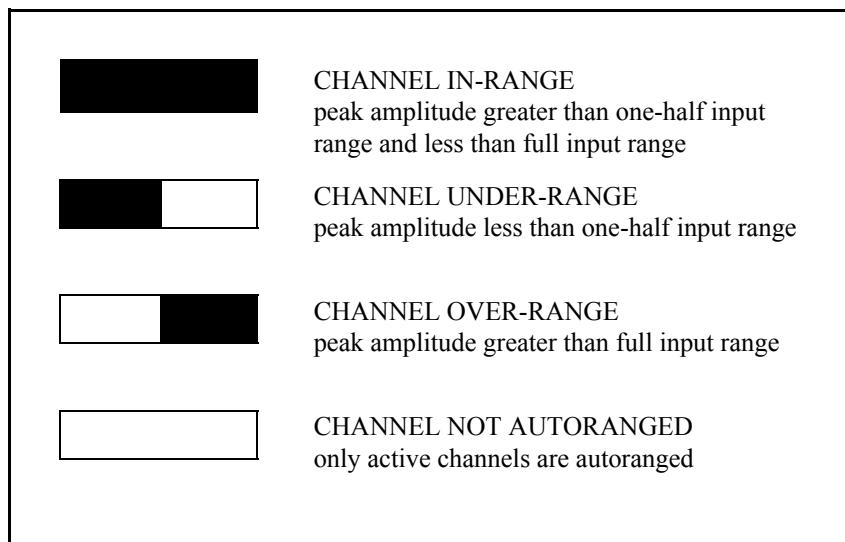
Figure 2-26. Autoranging Channel Status Blocks.

```
IMPACT FOR AUTO-RANGE . . .
                                                              OVER-HEAD
                                                   RMT SRQ
MEASUREMENT PAUSED                    AW 1 2 3 4   CH 1 2 3 4

     ┌──────────────────────┐     PEAK : 0.832 V
CH-1 │██████████████████████│     RANG : 1.260 V
     └──────────────────────┘
                                                           CHAN-1
                                                           RANG DOWN
     ┌──────────────────────┐     PEAK : 0.352 V
CH-2 │███████████           │     RANG : 0.502 V
     └──────────────────────┘

     ┌──────────────────────┐     PEAK : 1.326 V
CH-3 │            ██████████│     RANG : 1.998 V
     └──────────────────────┘

     ┌──────────────────────┐     PEAK :
CH-4 │                      │     RANG :
     └──────────────────────┘
                                                           ACCEPT
     OVER-HEAD : 33 %
```
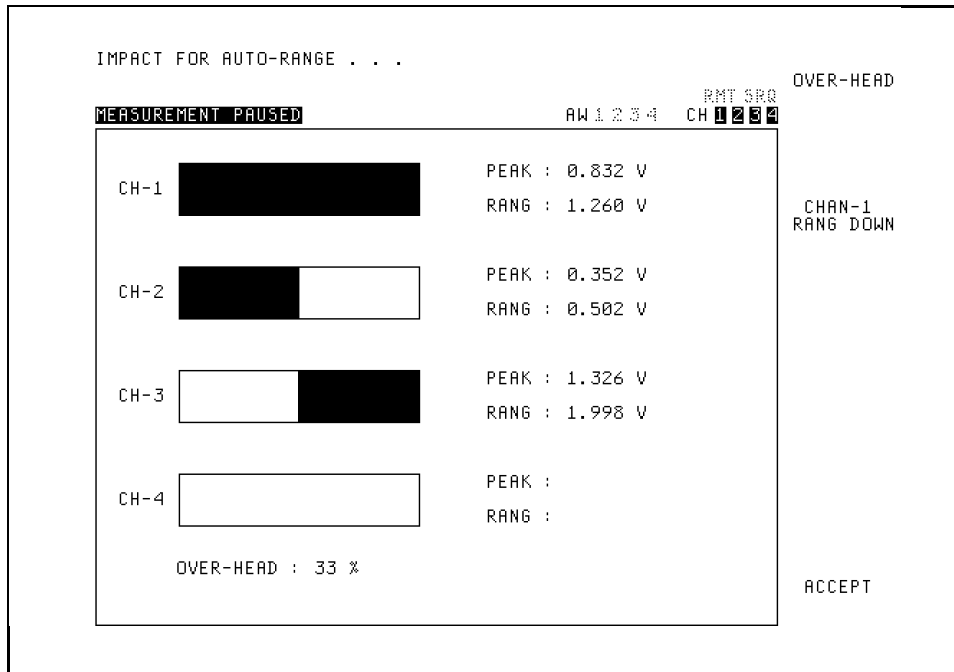
Figure 2-27. Graphical Autoranging Display.

CHANNEL	HALF RANGE	FULL RANGE	PEAK	PEAK x OVERHEAD*	NEW RANGE	CHANNEL STATUS
1	0.501	1.001	0.832	1.107	1.260	IN RANGE
2	0.501	1.001	0.352	0.468	0.502	UNDER RANGE
3	0.501	1.001	1.326	1.764	1.998	OVER RANGE
4	Channel 4 (Reference 3) is not autoranged for two references.					
						* Auto-Range Over-Head is 33%

Table 2-3. Autoranging Evaluation and Input Range Assignment.

2.5.8 Measuring and Displaying FRFs

The section of the software in which the FRFs are measured is called the Measurement Sequence. The sole purpose of Measurement Sequence is to efficiently collect the FRF measurement averages. The primary duty of the program during this operation is

controlling the built in functions of the analyzer. The data that is displayed while measuring FRFs are listed in Table 2-4. The Impact Identification is also displayed as a reminder of the current measurement point number and direction. If average previewing is enabled, the unwindowed time records of the four channels and soft-keys to accept or reject the average are displayed while the analyzer is waiting for a response. The Measurement Sequence automatically terminates upon completing the last average but can also be aborted prior to completing the averages.

Trace A	autopower spectrum of channel 1
Trace B	frequency response function of channel 2 and 1
Trace C	frequency response function of channel 3 and 1
Trace D	frequency response function of channel 4 and 1

Table 2-4. Measurement Sequence Displayed Data.

Because overloaded signals produce measurement errors, the overload rejection capability of the analyzer is enabled during the Measurement Sequence. The time records of all the channels are automatically rejected if an overload is detected on any channel. Functions are available to increase the input range of a channel that experiences recurring overloads and prohibits the collection of averages. This occurrence may indicate that autoranging is necessary.

After a set of measurements has been acquired, the FRFs can be reviewed before saving the data in the section of the software called the Data Display. The customary FRF

display formats are available, as listed in Table 2-5. The analyzer's display functions are coordinated such that the FRFs can be reviewed quickly. Any of the FRFs can be viewed by selecting the corresponding Reference number, and the the identification of the FRFs are indicated in the trace titles.

FRF Magnitude and Coherence
FRF Magnitude and Phase (with wrapped or unwrapped phase)
FRF Real and Imaginary
FRF Nyquist Diagram

Table 2-5. Data Display FRF Formats.

2.6   Chapter Summary

This chapter has surveyed the many concepts related to Multiple Reference Impact Testing data acquisition. MRIT is a testing method in which FRFs are measured between a single, roving impactor and multiple, fixed response transducers. The justification of this method is founded on a fundamental principle of mechanics that establishes a reciprocal relationship between an MRIT data set and a MIMO data set. The DOFs corresponding to the response transducers are the references of the FRFs because these are common to the set of measurements. Since the DOFs of the mode shapes are defined by the impact locations, the most significant limitation of the MRIT method is imposed by physical constraints of the test system that restrict the obtainable measurements.

The MRIT equipment includes a data acquisition system, an impactor, and reference transducers. The most important attributes for a data acquisition system to be compatible

with the MRIT method are multiple (more than two) channels and portability. An instrumented, hand-held impact hammer is the most common type of impactor, although other types of impactors have also been used for varied testing situations. In particular, an instrumented punch is a useful type of impactor for MRIT which can be used to obtain measurements that are not possible with a conventional impact hammer. Accelerometers are the most common type of reference transducer for impact testing, although microphones and proximity probes are more suitable for certain applications. An assortment of measurement hardware and software products have been developed for impact testing.

Although the impact is a very convenient excitation source, it is also an excitation source that has undesirable properties. Due to the characteristics of the impulsive force and transient response signals, specialized signal processing is required to obtain high quality impact measurements. Time domain windowing is a common technique available on all modern data acquisition systems. The force and exponential windows have been developed for impact testing to improve the signal-to-noise ratio and reduce leakage. Removing periodic noise components from impact data requires either supplemental data acquisition programming or post-processing.

MRIT is a measurement method that requires minimal setup time, fixturing, and equipment. These qualities make MRIT well suited for troubleshooting and field testing applications. Selecting reference locations is an important aspect of an MRIT test which is guided by engineering judgment and experience. The essential testing procedures for

an impact test include: (1) assessing and possibly modifying the linearity of the test system, (2) determining the correct impactor properties, (3) applying consistent impacts, (4) optimizing the dynamic range of the input channels, and (5) avoiding overloaded signals and multiple impacts. These practices are necessary to collect measurements that will produce valid results in the data analysis stage of an MRIT test.

Modern analyzers provide the basic capabilities for measuring FRFs with impact testing. However, additional capabilities are necessary to realize the full potential of the MRIT method. Implementation of MRIT data acquisition is possible with customized programming. The MRIT Acquisition software has been developed to integrate many of the concepts presented in this chapter into a practical procedure. The software controls the built-in functions and creates additional features to govern the testing process and automate repetitive tasks. The primary purpose of the software is to improve the utility of the MRIT method by reducing the testing time, effort, and errors.

Chapter 3   MRIT Analysis

Presented in this chapter are data analysis and post-processing methods that accompany Multiple Reference Impact Testing. An MRIT analysis method is proposed from the viewpoint of maintaining the fundamental intention of this modal testing method. The derivation of a multiple reference modal parameter estimation method based on the spatial decomposition of the FRF data set is documented in detail. Additional related data processing issues are discussed, and the correction for the exponential window is developed. Coordinate transformation and basic vector completion methods that address common MRIT measurement limitations are outlined. The features of a software package that has been developed are described to demonstrate the practical implementation of the MRIT analysis method presented in this chapter. The MRIT data sets used to illustrate the concepts and applications in this chapter are from test cases in Sections 4.1, 4.2, and 4.4.

3.1   Proposed Analysis Method

MRIT data is acquired as many sets of single-input, multiple-output FRFs. The principle of reciprocity allows an MRIT data set to be processed by modal parameter estimation software as an equivalent multiple-input, multiple-output data set. The reciprocity conditions are invoked in the data analysis stage by either transposing the input and

output DOF identifications (i.e., point number and direction pairs) for each measurement or by modifying the indexing in the algorithm. In either case, invoking reciprocity does not alter the data, but is only a matter of bookkeeping. The resulting data set typically consists of many output DOFs and a few input DOFs, which is the customary form for modal data.

A primary intention of the MRIT method is to collect multiple reference FRFs in a manner that balances testing time and effort with respect to the objective of the modal test. Therefore, an accompanying MRIT analysis method should maintain this approach of efficiency and practicality, as well as utilize the multiple reference information. Any multiple reference modal parameter estimation algorithm, such as Polyreference Time Domain[29], Eigensystem Realization Algorithm[30], or Polyreference Frequency Domain[31], could be used for the analysis of MRIT data. However, these methods may involve more processing complexity than is warranted in relation to the objective of a typical MRIT troubleshooting or field testing application. On the other hand, single degree of freedom (SDOF) and peak-picking, quadrature response methods do not process multiple reference data. The Complex Mode Indicator Function provides the basis of a modal parameter estimation method that is compatible with the concept of Multiple Reference Impact Testing. The CMIF analysis method is an uncomplicated but also robust procedure that processes multiple reference data.

3.2   The CMIF Analysis Method

CMIF was originally developed to indicate the existence and location of modes as an aid in model order determination[32]. However, the implementation of CMIF can be extended to estimate approximate modal parameters[33,1,34]. The term *estimate* refers to processing an over-determined set of experimental data that contains measurement noise. The term *approximate* refers to asserting some elementary assumptions in the development of CMIF as a modal parameter estimation method. The basic implementation of CMIF will locate the modes of the system to within the accuracy of the frequency resolution and produce unscaled mode shapes. A continuation of the CMIF formulation will produce complex poles (frequency and damping) and modal scaling, completing the set of modal parameters.

CMIF is a spatial domain algorithm which processes multiple reference FRF measurements. The characteristic space for a spatial domain algorithm is shown Figure 3-1, where the temporal DOF corresponds to the frequency domain for CMIF. The data is processed one temporal DOF (i.e., spectral line) at a time, and each input DOF - output DOF plane is processed independently. A spatial domain algorithm produces the spatial information, the mode shapes, in the first step and the temporal information, the poles, in the second step. In contrast, a time or frequency domain algorithm produces the temporal information in the first step and the spatial information in the second step. CMIF is classified as a zero-order model under the Unified Matrix Polynomial Approach (UMPA) of modal parameter estimation[19].
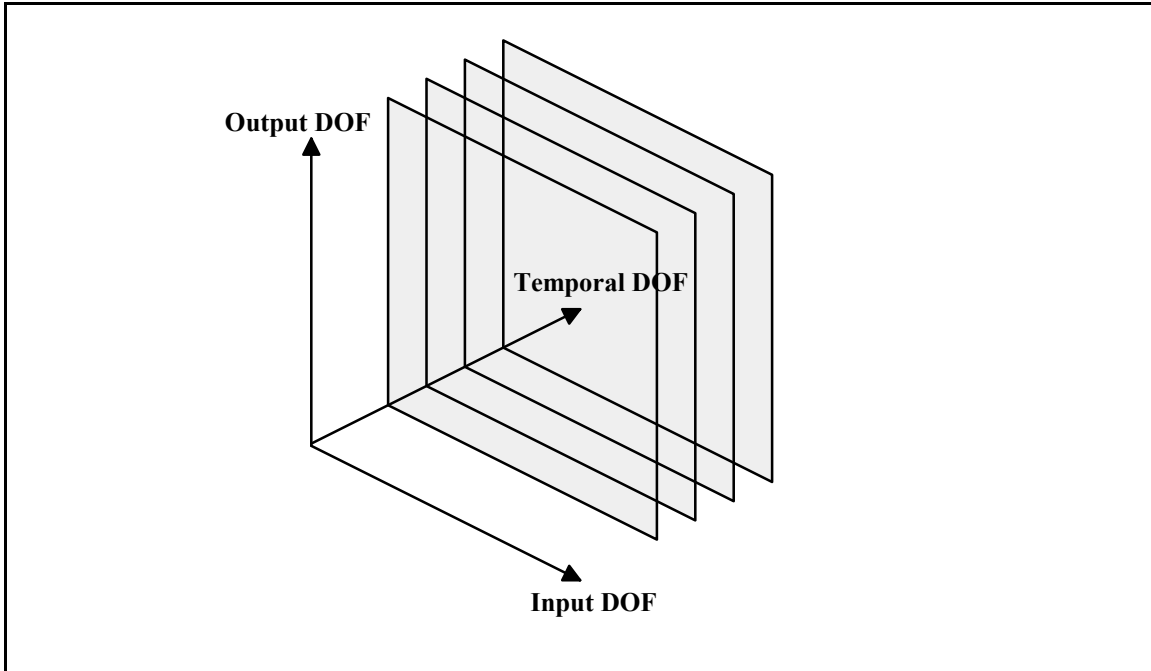
Figure 3-1. Characteristic Space for the Complex Mode Indicator Function.

The FRF matrix $[H(\omega_k)]$ is arranged as shown in Equation 3-1, where N_o is the number of outputs, N_i is the number of inputs, and ω_k is the spectral line. The outputs are ordered down the columns, and the inputs are ordered across the rows. Each row corresponds to an output DOF, and each column corresponds to an input DOF. The individual FRFs that comprise the matrix are expressed as $H_{pq}(\omega_k)$, where p denotes the output DOF and q denotes the input DOF. Each plane in Figure 3-1 corresponds to the FRF matrix at one spectral line. A fully populated FRF matrix is required to generate a CMIF.

$$[H(\omega_k)] = \begin{bmatrix} H_{11}(\omega_k) & H_{12}(\omega_k) & \cdots & H_{1N_i}(\omega_k) \\ H_{21}(\omega_k) & H_{22}(\omega_k) & & H_{2N_i}(\omega_k) \\ \vdots & \vdots & & \vdots \\ \vdots & \vdots & & \vdots \\ H_{N_o1}(\omega_k) & H_{N_o2}(\omega_k) & \cdots & H_{N_oN_i}(\omega_k) \end{bmatrix}_{(N_o x N_i)}$$

(3-1)

3.2.1 Processing the FRF Matrix

The Complex Mode Indicator Function is formed by computing the singular value decomposition (SVD) of the FRF matrix at each spectral line. SVD is a linear algebra technique in which a matrix is decomposed into the product of three matrices[35].

$$\underset{(N_o \times N_i)}{[H(\omega_k)]} = \underset{(N_o \times N_i)}{[U]_k} \underset{(N_i \times N_i)}{\lceil \Sigma \rfloor_k} \underset{(N_i \times N_i)}{[V]_k^H}$$

(3-2)

The columns of $[U]_k$ are the left singular vectors, which are mutually orthogonal with unity length. The columns of $[V]_k$ are the right singular vectors, which are mutually orthogonal with unity length. The notation ^{H} denotes the Hermitian (i.e., conjugate transpose) of the matrix. $\lceil \Sigma \rfloor_k$ is the singular value matrix, which is diagonal with real, non-negative elements in descending order. Since the singular value matrix is diagonal, the SVD can also be written as a summation.

$$[H(\omega_k)] = \sum_{n=1}^{N_i} \{U_n\}_k \sigma_{n,k} \{V_n\}_k^H$$

(3-3)

79

The columns of $[H(\omega_k)]$ are linear combinations of the left singular vectors, and the rows of $[H(\omega_k)]$ are linear combinations of the right singular vectors. The diagonal elements, the σ's, are the singular values of $[H(\omega_k)]$. The number of singular values equals the number of references.

A CMIF is a plot of the singular values as a function of frequency, usually on a log magnitude scale, with one curve for each singular value. The first CMIF curve is formed by the largest singular value at each spectral line, the second CMIF curve is formed by the second largest singular values, and so on. However, there is no direct connection between the CMIF curves and the references of the FRF data set. That is, the a CMIF curve does not correspond to a particular column of the FRF matrix.

The FRF matrix describes the multiple-input, multiple-output dynamics of a system as a function of frequency. From modal analysis theory, the FRF matrix of a linear, time invariant, multiple degree of freedom (MDOF) system can be expressed as [36]

$$[H(\omega_k)] = \sum_{r=1}^{2N} \frac{[A]_r}{j\omega_k - \lambda_r} = \sum_{r=1}^{2N} \{\Psi_r\} \frac{Q_r}{j\omega_k - \lambda_r} \{L_r\}^T \qquad (3\text{-}4)$$

$$\underset{(N_o \times N_i)}{[H(\omega_k)]} = \underset{(N_o \times 2N)}{[\Psi]} \left\lfloor \frac{Q_r}{j\omega_k - \lambda_r} \right\rfloor_{(2N \times 2N)} \underset{(2N \times N_i)}{[L]^T} \qquad (3\text{-}5)$$

where N is the number of conjugate modes, $[A]_r$ is the residue matrix for mode r, λ_r is the eigenvalue of mode r, Q_r is the modal scale factor for mode r, $[\Psi]$ is the modal vector matrix, and $[L]$ is the modal participation matrix. The frequency response is a superposition of the SDOF modes, and this form of the FRF matrix equation is valid for displacement over force FRFs. The columns of $[H(\omega_k)]$ are linear combinations of the modal vectors, and the rows of $[H(\omega_k)]$ are linear combinations of the modal participation vectors.

The singular value decomposition of Equations 3-2 and 3-3 and the modal decomposition of Equations 3-4 and 3-5 represent the same FRF matrix $[H(\omega_k)]$ at every spectral line. Near a resonance, as ω_k approaches λ_r , the SDOF function $\frac{1}{j\omega_k-\lambda_r}$ reaches a maximum. Since $\{\Psi_r\}$, $\{L_r\}$, and Q_r have constant values, the amplitude information in the modal representation of the FRF matrix is dependent on the SDOF functions. Similarly, since the left and right singular vectors have unity length at each spectral line, the amplitude information in the SVD representation of the FRF matrix is contained in the singular value matrix. Therefore, as the SDOF functions reach a maximum at resonance, so must the singular values. The peaks in the CMIF locate the damped natural frequencies of the system to the nearest spectral line. This result is illustrated in Figure 3-2, which shows a driving point FRF and the first CMIF curve of the circular plate (see Section 4.2).

Figure 3-2. Driving Point FRF and First CMIF Curve.

The singular value matrix, which has the form shown in Equation 3-6, contains important

information about the contents of the FRF matrix.

$$
\lceil \Sigma \rfloor_k = \begin{bmatrix} \sigma_1 & & & & \\ & \ddots & & & 0 \\ & & \sigma_d & & \\ & & & \sigma_{d+1} & \\ & 0 & & & \ddots \\ & & & & & \sigma_{N_i} \end{bmatrix}_k \tag{3-6}
$$

When processing experimental data, the significant singular vales (σ_1 ... σ_d) will be

several orders of magnitude greater than the non-significant singular values (σ_{d+1} ... σ_{Ni}).

This is the reason that the singular values are usually plotted on a log magnitude scale.

The number of significant singular values is an indication of the number of linearly

independent characteristics (i.e., modes) that measurably contribute to the content of the FRF matrix at each spectral line.

At every frequency, the response of a system is a linear combination of the modal vectors. At a resonance, the contribution of one mode dominates the content of the FRF matrix and the response is approximately the associated modal vector.

$$[H(\omega_{s'})] = \sum_{r=1}^{2N} \{\Psi_r\} \frac{Q_r}{j\omega_{s'} - \lambda_r} \{L_r\}^T \approx \{\Psi_s\} \frac{Q_s}{j\omega_{s'} - \lambda_s} \{L_s\}^T \tag{3-7}$$

In Equations 3-7 and 3-8, $\omega_{s'}$ denotes the spectral line nearest the frequency of mode s.

In comparison, the SVD representation near a resonance will have one significant singular value, which causes a peak in the first CMIF curve. Because the significant singular value is much greater than the other singular values, the terms other than the first do not appreciably contribute to the summation.

$$[H(\omega_{s'})] = \sum_{n=1}^{N_i} \{U_n\}_{s'} \sigma_{n,s'} \{V_n\}_{s'}^H \approx \{U_1\}_{s'} \sigma_{1,s'} \{V_1\}_{s'}^H \tag{3-8}$$

By assuming that the system response near a CMIF peak is dominated by the associated mode, a direct connection between the SVD of the FRF matrix and the modal parameters of the system is possible. The left singular vector corresponding to the significant singular value is an approximation of the modal vector. The associated right singular vector is proportional to the conjugate of the modal participation vector. The significant

singular value is related to the product of the modal scale factor and the SDOF function. The approximate mode shapes obtained from CMIF are essentially unscaled operating shapes.

3.2.2   Repeated Modes

The preceding development has concentrated on only single, or non-repeated, modes. However, since CMIF is a multiple reference algorithm, it can also detect and process repeated (or pseudo-repeated) and closely spaced modes[36]. For instance, the circular plate has many repeated modes of multiplicity two due to symmetry. At these resonances, two modal vectors dominate the response, and these two mode shapes are represented by the first and second left singular vectors. Then, there must be two significant singular values, and the first and second CMIF curves will peak at this frequency. The complete CMIF of the circular plate, with three references, is shown in Figure 3-3. This explanation extends directly for modes of greater multiplicity, and CMIF can resolve a repeated mode of multiplicity no greater than the number of references. For the limiting case in which each CMIF curve peaks at a spectral line, the multiplicity of the mode can not be uniquely determined because it may be greater than the number of references.
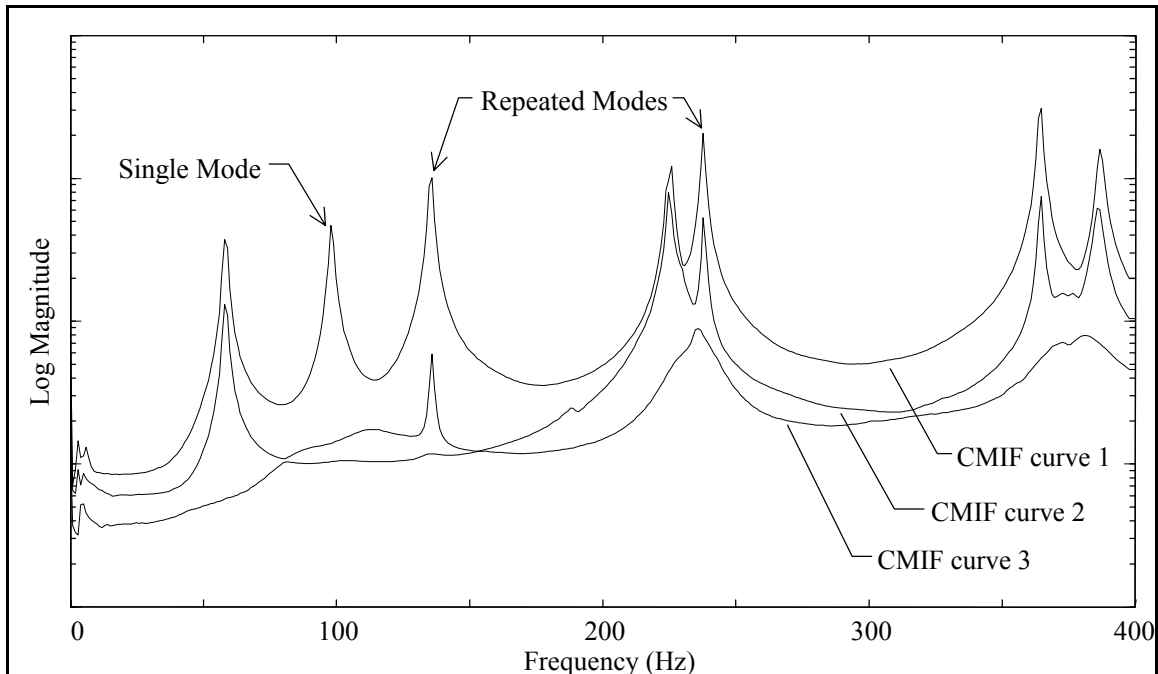
Figure 3-3. Repeated Modes with CMIF.

3.2.3 Enhanced FRFs

At this point, the CMIF analysis method has located the modes of the system to the nearest spectral line and produced unscaled mode shapes. By utilizing the spatial information obtained in the first step, the system poles and modal scale factors can be estimated with SDOF techniques. The left and right singular vectors at the CMIF peaks are used to create an enhanced frequency response function[3,37] (eFRF) for each mode. The set of eFRFs are then used in the estimation of the pole and scale factor of each mode. An eFRF is a weighted summation of the measured FRF data, in which the singular vectors are the weighting functions. The singular vectors create a discrete modal filter[37] that transforms the data from the physical space to the modal space. To calculate

the eFRF for mode s, $eH_s(\omega_k)$, the FRF matrix is pre-multiplied by the left singular vector $\{U_s\}$ and post-multiplied by right singular vector $\{V_s\}$ at each spectral line.

$$eH_s(\omega_k) = \underset{(1 \times N_o)}{\{U_s\}^H} \underset{(N_o \times N_i)}{[H(\omega_k)]} \underset{(N_i \times 1)}{\{V_s\}}$$

$$= \{U_s\}^H \left[\sum_{r=1}^{2N} \{\Psi_r\} \frac{Q_r}{j\omega_k - \lambda_r} \{L_r\}^T \right] \{V_s\} \qquad (3\text{-}9)$$

$$= \sum_{r=1}^{2N} \{U_s\}^H \{\Psi_r\} \frac{Q_r}{j\omega_k - \lambda_r} \{L_r\}^T \{V_s\}$$

The effect of this operation is to attenuate the contribution to the summation of all modes except mode s, thus enhancing this mode. (In Equation 3-9, the modal vectors are assumed to be scaled to unity length.) The degree of enhancement is dependent on the inner product of the left singular vector and modal vectors. If the modal vectors are mutually orthogonal, then the eFRF will be completely decoupled. Otherwise, if the modal vectors are not orthogonal with respect to $\{U_s\}$, then those modes have some contribution to the eFRF for mode s. When r equals s, the vectors are parallel and the principal mode is not attenuated. The eFRF formulation can accommodate repeated modes because the left singular vectors at a spectral line are mutually orthogonal. An effective eFRF should approximate an SDOF function near the principal mode since this data is used in the pole and scaling algorithms.

Figure 3-4 illustrates the typical results of the eFRF formulation for the 238 Hz mode of the circular plate. The solid line is the eFRF from the complex CMIF calculation, and the dashed line is the eFRF from the quadrature CMIF calculation (see Section 3.2.8).
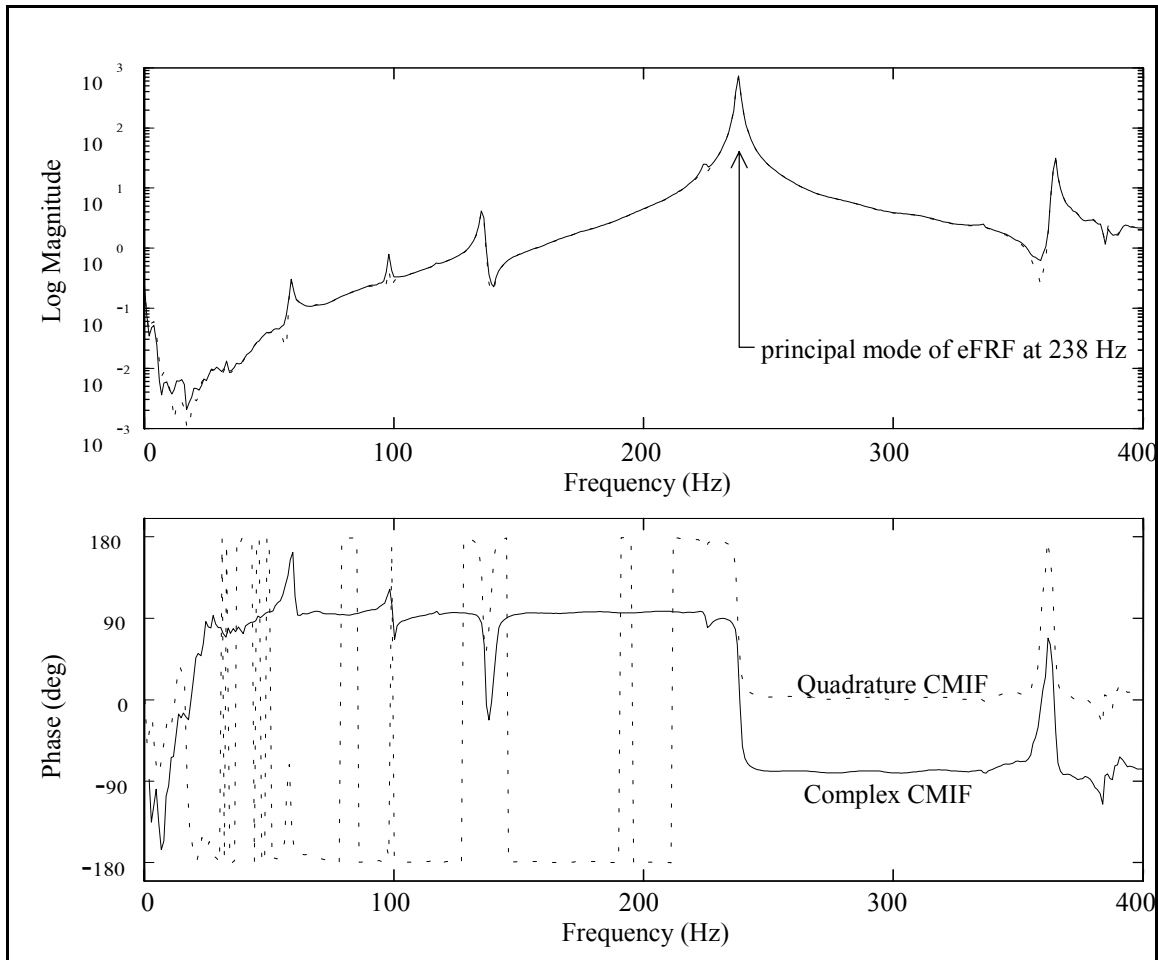
Figure 3-4. Enhanced Frequency Response Function.

The magnitudes of the two eFRF are basically identical, but the phases are shifted. The eFRF from the quadrature CMIF calculation is formed with a real left singular vector, and its phase is between 0 and 180 degrees (disregarding phase wrap), as is expected for an SDOF mode. The eFRF from the complex CMIF calculation is formed with a complex left singular vector, and its phase is shifted by approximately 100 degrees (for this case;

in general, the phase shift of a eFRF can be any value). This can happen because, although the relative phase among the coefficients of the vector is a property of the system, the entire vector can be scaled by a complex scalar with unity magnitude but arbitrary phase[†], which results in the phase shift of the eFRF. A phase shift is commonly observed in eFRFs formed with complex left singular vectors and is a function of the SVD algorithm. This phase shift in the eFRFs is a concern because it seems to have an effect on the accuracy of the estimated poles and scale factors. Possible techniques to address the eFRF phase shift are suggested in Chapter 5.

3.2.4   Calculation of Poles

The poles are calculated from the eFRFs using a scalar, second-order, frequency domain polynomial algorithm.

$$(j\omega_k)^2 eH_s(\omega_k)a_o + (j\omega_k)^1 eH_s(\omega_k)a_1 + (j\omega_k)^0 eH_s(\omega_k)a_2 = 0 \tag{3-10}$$

Taking a_0=1, since this is a homogeneous equation, and writing in matrix form yields

$$\begin{bmatrix} a_1 & a_2 \end{bmatrix} \begin{bmatrix} j\omega_k eH_s(\omega_k) \\ eH_s(\omega_k) \end{bmatrix} = \omega_k^2 eH_s(\omega_k) \tag{3-11}$$

[†] The phase shift of the left singular vector is compensated by an opposite phase shift of the corresponding right singular vector such that the true phase of the FRF matrix is maintained. (A singular value is always a non-negative, real number.)

This expression is valid for all frequencies, and more equations are generated by including several spectral lines near the peak. The polynomial coefficients are computed using a pseudo-inverse solution. The eigenvalues of the companion matrix formed with the polynomial coefficients are the conjugate poles of the associated mode.

$$Companion\ Matrix = \begin{bmatrix} -a_1 & -a_2 \\ 1 & 0 \end{bmatrix} \qquad (3\text{-}12)$$

This procedure is performed for each eFRF to produce the set of poles. Since CMIF locates the modes to the nearest spectral line, the frequency of the poles should fall within one spectral line of the peak. This condition is useful for evaluating the validity of the estimated poles.

3.2.5 Calculation of Modal Scale Factors

Direct calculation of modal scaling is an alternative to a residue calculation which is possible because the mode shapes are available from the first step. The scale factors are also calculated from the eFRFs by modifying Equation 3-9 to form Equation 3-13. In this algorithm, the modal vectors are taken to be the left singular vectors, and the modal participation vectors are taken to be the coefficients of the left singular vectors at the reference DOFs. An SDOF method or an MDOF method can be used for the scaling calculation.

$$eH_s(\omega_k) = \sum_{r=1}^{2N} \{U_s\}^H \{\Psi_r\} Q_r C_r(\omega_k) \{L_r\}^T \{V_s\} \qquad (3\text{-}13)$$

for displacement / force FRFs : $\qquad C_r(\omega_k) = \dfrac{1}{j\omega_k - \lambda_r}$ (3-14)

for velocity / force FRFs : $\qquad C_r(\omega_k) = \dfrac{\lambda_r}{j\omega_k - \lambda_r}$ (3-15)

for acceleration / force FRFs : $\qquad C_r(\omega_k) = \lambda_r + \dfrac{\lambda_r^2}{j\omega_k - \lambda_r}$ (3-16)

SDOF Method. The SDOF method assumes that each eFRF consists of a single mode and includes only the positive frequency pole.

$$eH_s(\omega_k) = \{U_s\}^H \{\Psi_s\} Q_s C_s(\omega_k) \{L_s\}^T \{V_s\}$$ (3-17)

Although this is a scalar equation with one unknown (Q_s), a least squares solution for the scale factor is formed by generating equations from spectral lines near the peak.

$$\begin{Bmatrix} eH_s(\omega_1) \\ \vdots \\ eH_s(\omega_K) \end{Bmatrix} = \{U_s\}^H \{\Psi_s\} \{L_s\}^T \{V_s\} \begin{Bmatrix} C_s(\omega_1) \\ \vdots \\ C_s(\omega_K) \end{Bmatrix} Q_s$$ (3-18)

This procedure is repeated for each eFRF to produce the set of modal scale factors.

MDOF Method. If the single mode assumption is not made, all modes are included in the modal scaling calculation. The MDOF model better describes the eFRF data, but at the expense of increased computation time.

$$eH_s(\omega_k) = \Sigma_{r=1}^{2N} Q_r D_{s,r}(\omega_k) = \begin{bmatrix} D_{s,1}(\omega_k) & \cdots & D_{s,2N}(\omega_k) \end{bmatrix} \begin{Bmatrix} Q_1 \\ \vdots \\ Q_{2N} \end{Bmatrix} \qquad (3\text{-}19)$$

where, $D_{s,r}(\omega_k) = \{U_s\}^H \{\Psi_r\} C_r(\omega_k) \{L_r\}^T \{V_s\}$

A set of simultaneous equations in matrix form is generated, and the vector of modal scale factors is computed using a pseudo-inverse solution. Again, the equations are generated by including spectral lines near the peak.

$$\begin{Bmatrix} eH_s(\omega_1) \\ \vdots \\ eH_s(\omega_K) \end{Bmatrix} = \begin{bmatrix} D_{s,1}(\omega_1) & \cdots & D_{s,2N}(\omega_1) \\ \vdots & & \vdots \\ D_{s,1}(\omega_K) & \cdots & D_{s,2N}(\omega_K) \end{bmatrix} \begin{Bmatrix} Q_1 \\ \vdots \\ Q_{2N} \end{Bmatrix} \qquad (3\text{-}20)$$

Although the scale factors for all the modes are included in the model, only the Q_s associated with the eFRF is retained. This procedure is repeated for each eFRF to produce the set of modal scale factors.

3.2.6   Physical Interpretation of CMIF

The mathematical justification of the CMIF analysis method was presented in Section 3.2.1. The singular value decomposition of the FRF matrix can also be interpreted from a more physical point of view by comparing the left singular vectors to the columns of the FRF matrix.

At every frequency, the columns of the FRF matrix are linear combinations of the mode shapes. Near a resonance, the system response is dominated by the contribution of one mode but also contains some contribution from the other modes. The quadrature response method is a common SDOF technique in which the imaginary part of a column of the FRF matrix at a resonant peak is taken as an approximate mode shape[23]. A multiple reference FRF matrix has several columns, and any of the columns can be taken as the mode shape. For repeated modes, each column of the FRF matrix is a different linear combination of the contributing mode shapes, but an SDOF response vector method can not decouple the mode shapes.

Another property of SVD is that the matrix of left singular vectors $[U]$ forms an orthonormal basis for the columns of the FRF matrix. That is, SVD decouples the vectors that comprise the columns of the FRF matrix, which are the contributing mode shapes. The first left singular vector represents the most significant vector contained in the columns of the FRF matrix, which at resonance is the associated mode shape. The other left singular vectors represent the secondary contributions to the columns of the FRF matrix. For repeated modes, SVD separates the mode shapes into an orthonormal set of left singular vectors. In effect, the mode shapes obtained from CMIF can be thought of as 'multiple reference response vectors'.

Each spectral line of the FRF matrix is processed independently to form the CMIF, and the peaks in the CMIF curves coincide with the modes of the system. Additional information can be obtained from CMIF by examining the relative magnitudes of the

singular values as a function of frequency. Comparison of Equations 3-7 and 3-8 infers that the relative magnitudes of the CMIF peaks are proportional to the relative magnitudes of the modes. The CMIF magnitude at a peak indicates the overall response of the system for the corresponding mode normalized to a unit input at the reference DOFs. CMIF peaks with a large relative magnitude correspond to modes that have a high overall response from the included reference DOFs. CMIF peaks with a small relative magnitude correspond to modes that have a low overall response from the included reference DOFs. For a fixed input data set, the overall response of a mode is related to the ability of the inputs to excite the mode. For a fixed output data set, the overall response of a mode is related to the ability of the outputs to observe the mode.

Figure 3-5 shows a representative CMIF plot that illustrates some typical relative peak magnitudes[†]. The peak marked (1) is much lower than the other peaks in the first curve, which implies that this mode is not measured (either excited or observed) as well as the other modes. The peak marked (3) lies below the first curve, which implies that this mode does not dominate the response near its resonant frequency. The contribution of the mode at the peak marked (2) exceeds the contribution of the mode at peak (3). Since there is not a peak in the first curve at the same frequency, peak (3) does not indicate a repeated mode. The peaks marked (4) and (5) correspond to a repeated mode, but the overall response of the two modes is unequal since peak (5) is lower than peak (4). Although the validity of modal parameters associated with CMIF peaks with very low

---

† This data was generated from the five DOF M-C-K system in Section 4.1.2. The residue matrix for each mode of the original system was scaled to generate a data set with the attributes shown in Figure 3-5.

relative magnitudes may often be suspect, examination of the mode shapes may reveal how to better measure these modes.
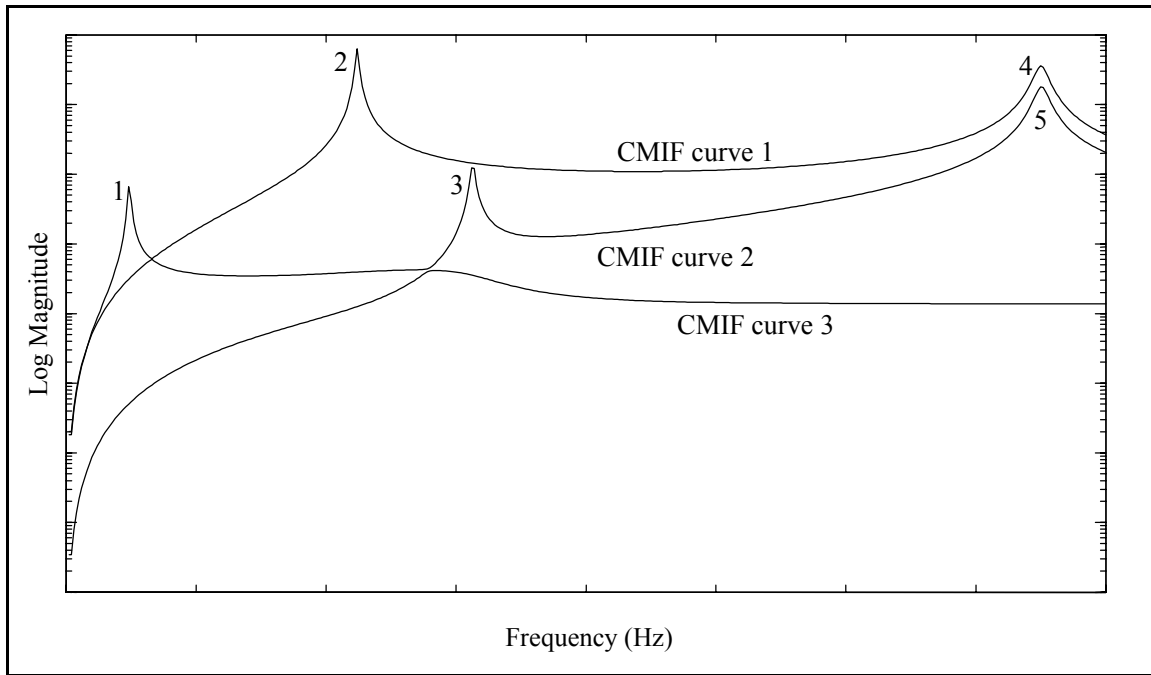
Figure 3-5. Typical Relative Magnitudes of CMIF Peaks.

3.2.7 CMIF Crossover Effect

The modes of the system are indicated by CMIF peaks, but not every peak indicates a mode. Measurement noise, leakage, nonlinearities, and the CMIF crossover effect can also create peaks in the CMIF curves. The CMIF crossover effect is caused by the succession of the dominant mode in the system response as a function of frequency. Consider the relationship of the two CMIF peaks marked (1) and (2) in Figure 3-6 as the

independent frequency variable increases from left to right[†]. The first CMIF curve corresponds the mode with largest contribution to the system response at each spectral line. The influence of a mode increases to a maximum as the frequency approaches its resonance, then decreases as the frequency recedes. As the influence of mode (1) is decreasing, the influence of mode (2) is increasing, and at some frequency the contribution to the system response from both modes will be equal. However, due to the finite frequency resolution the CMIF curves do not actually intersect. A CMIF crossover can be recognized by a dip (i.e., negative-slope to positive-slope inflection) in the upper CMIF curve at the same spectral line as the peak (i.e., positive-slope to negative-slope inflection) in the lower CMIF curve.
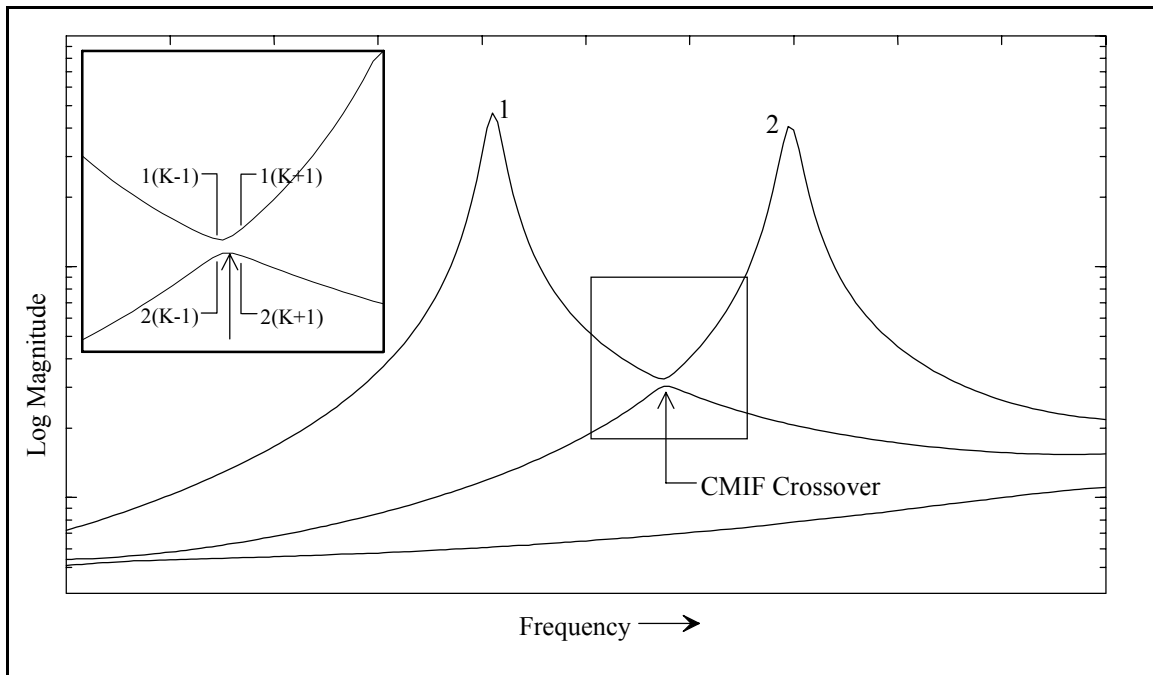
Figure 3-6. CMIF Crossover Effect.

---

† This data is from the test case in Section 4.4.

The existence of a CMIF crossover can be evaluated by comparing the left singular vectors at the spectral lines adjacent to the peak in question. Refer to the insert in Figure 3-6, where K denotes the spectral line of the possible crossover, and (1,2) refer to the first and second CMIF curves, respectively. Since the dominant mode shape does not change significantly near a resonance, the vectors from the lower CMIF curve at the adjacent spectral lines should be similar to the vector at the peak, as well as to one another. The modal assurance criteria (MAC)[3], which is the normalized inner product of two vectors, determines the similarity of the vectors. If the MAC value for the vectors at 2(K-1) and 2(K+1) is near unity, then this peak indicates a mode, otherwise the peak is caused by the CMIF crossover effect. The vectors from the upper CMIF curve at the adjacent spectral lines can also be included in the MAC comparisons. At a CMIF crossover, the vectors at 1(K-1) and 2(K+1) will be similar and the vectors at 2(K-1) and 1(K+1) will be similar. Mode tracking, which is discussed in Section 3.5.4, is another technique to examine CMIF crossovers. Note that a CMIF crossover can occur between any two CMIF curves, not just the first and second.

3.2.8   CMIF Processing Options

In the definition of the CMIF calculation, the complex values of the FRF matrix are processed in the SVD computation. One processing option is to use only the imaginary values (quadrature) of the FRF matrix in the SVD computation. A CMIF computed from the quadrature FRF matrix versus a CMIF computed from the complex FRF matrix is analogous to the imaginary part of an FRF versus the linear magnitude of an FRF. In

general, the quadrature CMIF has narrower peaks, better separation of closely spaced peaks and amplification of low peaks, but is usually noisier, in comparison to the complex CMIF. The effects of the quadrature CMIF calculation are typically more pronounced for heavily damped systems. SVD of the complex FRF matrix can produce complex singular vectors, but SVD of the quadrature FRF matrix produces real (normal) singular vectors.

CMIF overlapping is another processing option, which can reduce the effects of leakage and other measurements errors in the estimation of the mode shapes. This techniques is based on the condition that the dominant mode shape does not change significantly near a resonance. At each spectral line, the SVD is computed of a matrix that is assembled by augmenting adjacent spectral lines of the FRF matrix.

$$\left[\ [H(\omega_{k-n})] \ \cdots \ [H(\omega_k)] \ \cdots \ [H(\omega_{k+n})] \ \right]_{(N_o \times (2n+1)N_i)} = [U]_k \lceil \Sigma \rfloor_k [V]_k^H \qquad (3\text{-}21)$$

where, $\qquad [U]_k$ is $N_o \times (2n+1)N_i$

$$\lceil \Sigma \rfloor_k \ \text{is} \ (2n+1)N_i \times (2n+1)N_i$$

$$[V]_k \ \text{is} \ (2n+1)N_i \times (2n+1)N_i$$

The number of singular values calculated from the augmented matrix is $(2n+1)N_i$, but only the first N_i singular values are retained. As in the standard CMIF calculation, SVD decouples the vectors that combine to form the columns of the FRF matrix. By

97

processing several sets of similar vectors, an averaged estimate of the mode shape is obtained. The additional left singular vectors account for noise and errors in the measurements and also the presence of other modes. In general, CMIF overlapping tends to smooth the noise on the CMIF curves, but also broaden the peaks. A potential complication with overlapping is that sometimes false peaks may appear in the lower CMIF curves. These spurious peaks can be evaluated with MAC and mode tracking. CMIF overlapping can be extended to simulate additional references by retaining singular values to form more CMIF curves[34].

3.3   Exponential Window Correction

As mentioned in Section 2.3.1, the exponential window increases the apparent damping of the measured FRFs, but the estimated poles can be easily corrected for this effect. The exponential window is an exponential function as defined by either of the two forms in Equation 3-22, where τ is the time constant of the exponential function.

$$w(t) = e^{\frac{-t}{\tau}} \qquad \text{or} \qquad w(t) = e^{-\beta t} \qquad \text{where} \qquad \beta = \frac{1}{\tau} \tag{3-22}$$

The time constant determines the decay rate of the exponential function and the apparent increase in damping of the measurements. The exponential window is applied to the output signals and also to the input signal so that both signals used to compute an FRF have the same change in damping. Applying the exponential window to the input signal does not cancel the effect of the window from the computed FRFs.

The following series of equations explains the effect of the exponential window on the estimated poles. In this derivation, the Laplace variable (s) is used, but the Fourier transform is equivalent to the Laplace transform evaluated at the imaginary ($j\omega$) axis. The effect of the exponential window is governed by the shift property of Laplace and Fourier transform theory[9]. Multiplying a time signal $y(t)$ by an exponential function shifts the independent variable of the associated spectrum $Y(s)$.

$$\text{If} \qquad y(t) \Leftrightarrow Y(s) \qquad\qquad \text{then} \qquad\qquad e^{at}y(t) \Leftrightarrow Y(s-a) \qquad\qquad (3\text{-}23)$$

The windowed input (f_q) and output (x_p) time signals are transformed to the frequency domain, where q denotes the input DOF and p denotes the output DOF.

$$e^{\frac{-t}{\tau}}f_q(t) \Leftrightarrow F_q\!\left(s+\frac{1}{\tau}\right) \qquad\qquad \text{and} \qquad\qquad e^{\frac{-t}{\tau}}x_p(t) \Leftrightarrow X_p\!\left(s+\frac{1}{\tau}\right) \qquad\qquad (3\text{-}24)$$

Since the FRF is computed from the shifted input and output spectra, it is a function of the same independent variable. The FRF is inverse transformed to the impulse response function (IRF), where $h_{pq}(t)$ is the IRF of the true (i.e., unwindowed) system.

$$H_{pq}\!\left(s+\frac{1}{\tau}\right) = \frac{X_p\!\left(s+\frac{1}{\tau}\right)}{F_q\!\left(s+\frac{1}{\tau}\right)} \qquad\qquad \text{and} \qquad\qquad H_{pq}\!\left(s+\frac{1}{\tau}\right) \Leftrightarrow e^{\frac{-t}{\tau}}h_{pq}(t) \qquad\qquad (3\text{-}25)$$

The IRF can be written as a summation of damped exponential terms, where λ_r is the complex eigenvalue of mode r, A_{pqr} is the residue of DOF pair (p,q) for mode r, and the

caret notation (^) denotes a parameter associated with the measured (i.e., windowed) system.

$$e^{\frac{-t}{\tau}} h_{pq}(t) = \hat{h}_{pq}(t) \tag{3-26}$$

$$e^{\frac{-t}{\tau}} \sum_r e^{\lambda_r t} A_{pqr} = \sum_r e^{\hat{\lambda}_r t} \hat{A}_{pqr} \tag{3-27}$$

Equating the like terms in Equation 3-27 and inserting the real and imaginary parts of the eigenvalues yields the correction for the exponential window, where ω_r and σ_r are the damped natural frequency and damping factor of mode r, respectively.

$$e^{\frac{-t}{\tau}} e^{\lambda_r t} = e^{\hat{\lambda}_r t} \qquad \text{and} \qquad A_{pqr} = \hat{A}_{pqr} \tag{3-28}$$

$$-\frac{1}{\tau} + \lambda_r = \hat{\lambda}_r \tag{3-29}$$

$$-\frac{1}{\tau} + \sigma_r + j\omega_r = \hat{\sigma}_r + j\hat{\omega}_r \tag{3-30}$$

$$\sigma_r = \hat{\sigma}_r + \frac{1}{\tau} \qquad \text{and} \qquad \omega_r = \hat{\omega}_r \tag{3-31}$$

Equations 3-28 and 3-31 indicate that the damped natural frequencies and residues of the measured system are identical to those of the true system and the difference of the damping factors between the true and measured systems is a function of the exponential window time constant. The effects of the exponential window described in the above equations are illustrated on the complex plane in Figure 3-7. Since the damping factors

of natural system are expected to be negative, the damping factors of the measured system will have larger negative values than that of the true system, which causes the apparent increased damping in the measurements. Note that since the measured FRFs are computed from data modified by the exponential window, residue and modal scaling calculations and FRF synthesis should use the uncorrected poles. Another possible effect of the exponential window which should be noted is that it may complicate separation of closely spaced modes due to the increased damping.
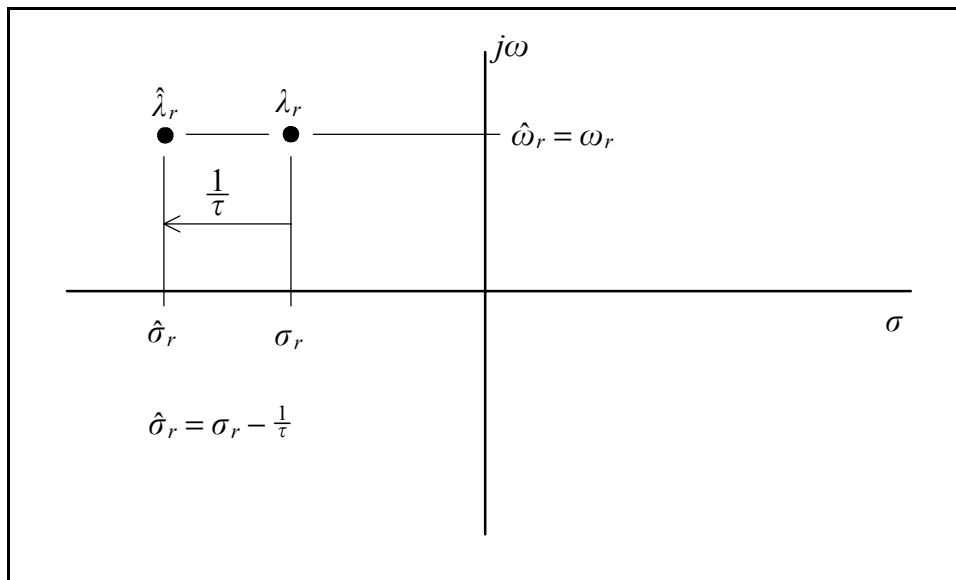
Figure 3-7. Correction for the Exponential Window on the Complex Plane.

3.4   Coordinate Transformation and Vector Completion

An inherent property of the MRIT method is that each impact DOF becomes a DOF of the mode shapes. However, obtaining three orthogonal measurements in the defined global coordinate directions at every point of the test geometry may not be possible due to the physical constraints of the test system. Since the modal coefficients of the unmeasurable DOFs can not be determined, the motion of some points on the animated display will not be completely or correctly described. The missing measurement DOFs may cause the animated mode shape to appear misleading. Sometimes the missing DOFs can be supplied mentally by the analysts, other times the missing DOFs can cause confusion. Coordinate transformation and vector completion are post-processing techniques that can produce more descriptive mode shapes.

Coordinate transformation resolves the directions of the measured DOFs into the global coordinate system, but adds no new information. Vector completion estimates unmeasurable mode shape coefficients from the measured DOFs by constraining the motion to an assumed pattern. Much work has been done in the area of modal vector completion for the general case[38,39]. However, since MRIT is largely a troubleshooting and field testing method, a few basic techniques are suitable for this application. As such, the discussion of coordinate transformation and vector completion methods will be addressed to situations commonly encountered in impact testing[17].

3.4.1   Coordinate Transformation

Since the impact force is primarily normal to the surface of contact, the orientation of the surface defines the direction of the input.   As a consequence, impacting in a global coordinate direction is sometimes not possible.   In this case, the direction of the mode shape DOFs are assigned by the orientation of a local coordinate system.   The local coordinate axes are defined by the local geometry of the test system and may not be orthogonal.   However, the animated mode shapes are usually displayed relative to an orthogonal set of global coordinate directions. The direction of the measured mode shape DOFs can be transformed into the global coordinates, and the transformation is determined by the geometry of the test system.

Figure 3-8 shows an example in which the directions of the measurements are skewed relative to the global directions and are nonorthogonal.   The directions of the local coordinate axes are defined by the angle relative to the global x-axis.   The third axes of the local system is parallel to the z-axis of the global system.
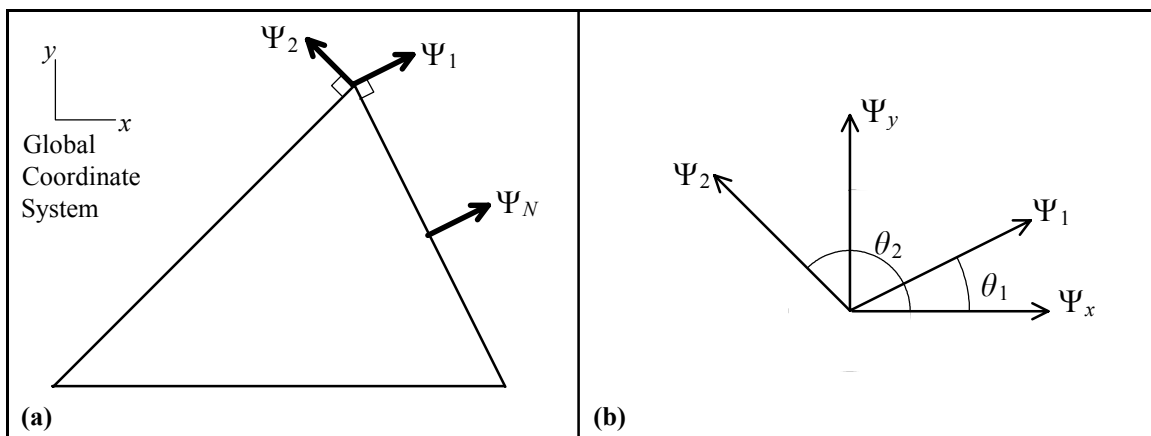
Figure 3-8. Skewed and Nonorthogonal Local Coordinate System.

The relationship between the local coordinate system and the global coordinate system is determined from the geometry.

$$\Psi_1 = \Psi_x \cos\theta_1 + \Psi_y \sin\theta_1 \tag{3-32}$$

$$\Psi_2 = \Psi_x \cos\theta_2 + \Psi_y \sin\theta_2 \tag{3-33}$$

Combining Equations 3-32 and 3-33 to form a matrix equation yields

$$\left\{ \begin{array}{c} \Psi_1 \\ \Psi_2 \end{array} \right\} = \left[\begin{array}{cc} \cos\theta_1 & \sin\theta_1 \\ \cos\theta_2 & \sin\theta_2 \end{array} \right] \left\{ \begin{array}{c} \Psi_x \\ \Psi_y \end{array} \right\} = [T] \left\{ \begin{array}{c} \Psi_x \\ \Psi_y \end{array} \right\} \tag{3-34}$$

where $[T]$ is the transformation matrix. Taking the inverse of Equation 3-34 produces the global x-y mode shape coefficients from the local measured directions.

$$\left\{ \begin{array}{c} \Psi_x \\ \Psi_y \end{array} \right\} = [T]^{-1} \left\{ \begin{array}{c} \Psi_1 \\ \Psi_2 \end{array} \right\} \qquad \text{where,} \qquad [T]^{-1} = \frac{\left[\begin{array}{cc} \sin\theta_2 & -\sin\theta_1 \\ -\cos\theta_2 & \cos\theta_1 \end{array} \right]}{\cos\theta_1 \sin\theta_2 - \sin\theta_1 \cos\theta_2} \tag{3-35}$$

Since the local axes are nonorthogonal, the transformation matrix is not orthogonal. However, if the local axes are orthogonal,

$$\theta_2 = \theta_1 + 90 \quad \text{and} \quad \theta = \theta_1 \tag{3-36}$$

the result is the familiar orthogonal transformation matrix and its inverse.

$$[T] = \begin{bmatrix} \cos\theta & \sin\theta \\ -\sin\theta & \cos\theta \end{bmatrix} \quad \text{and} \quad [T]^{-1} = [T]^T = \begin{bmatrix} \cos\theta & -\sin\theta \\ \sin\theta & \cos\theta \end{bmatrix} \quad (3\text{-}37)$$

In order to describe the motion of a point in a plane, two independent directions must be measured. Resolving a single skewed DOF, such as Ψ_N in Figure 3-8, into its components in the global coordinates does not completely describe the motion. To do so constrains the motion perpendicular to the measured direction to be zero, when in fact it is unknown.

In the preceding development, the third axis of the local and global coordinate systems were parallel. If the local coordinate system is rotated in three dimensions, three measured DOFs are required to transform the local coordinates into the global coordinates. The resulting transformation is the product of two 2-dimensional transformation matrices.

3.4.2   Slave DOF Completion Method

A very common type of unmeasurable DOF is encountered on the interior of a surface. Since the primary direction of an impact force is normal to the surface of contact, impacting tangent to a surface is not possible. Figure 3-9 shows the measurable and unmeasurable DOFs of a rectangular beam as a typical example.
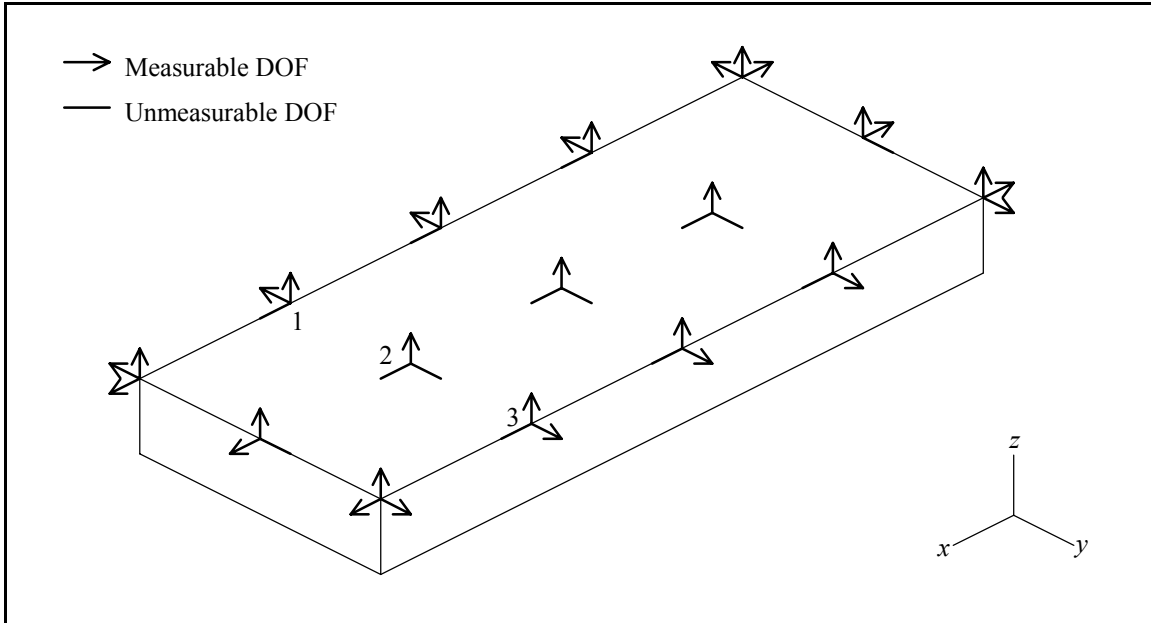
Figure 3-9. A Rectangular Beam with Unmeasurable DOFs.

All measurements normal to the top surface and along the edges are possible. The vertical bending modes can be adequately described with z-direction DOFs. However, the horizontal bending modes will appear as shown in Figure 3-10(a), where the points along the centerline of the beam have no motion in the y-direction. A reasonable assumption to make is that no relative displacement of a line of points across the top surface is expected in the frequency range of interest. Then the y-direction motion of the points along the centerline can be approximated from the y-direction motion of the points along the edges. For example, the y-direction mode shape coefficient of point *2* could be set equal to that of point *1*, point *3*, or the average of points *1* and *3*. The resulting completed mode shape is shown in Figure 3-10(b).
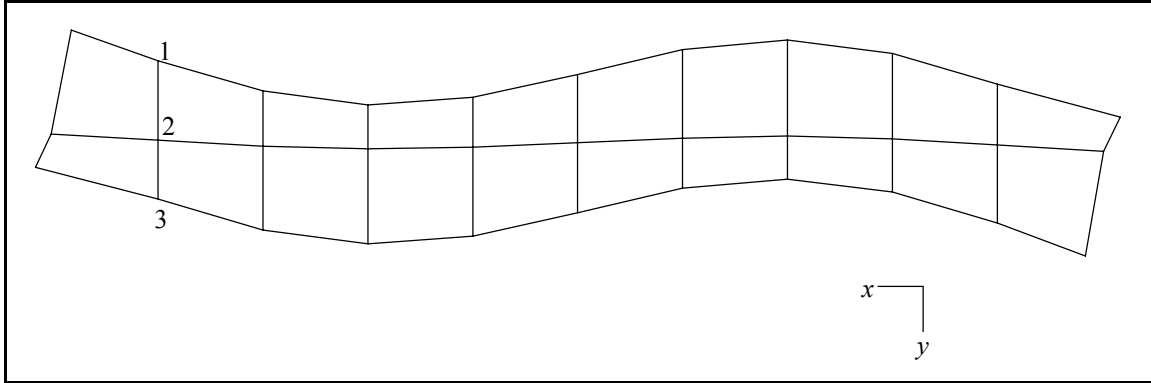
Figure 3-10(a). Measured Horizontal Bending Mode Shape.
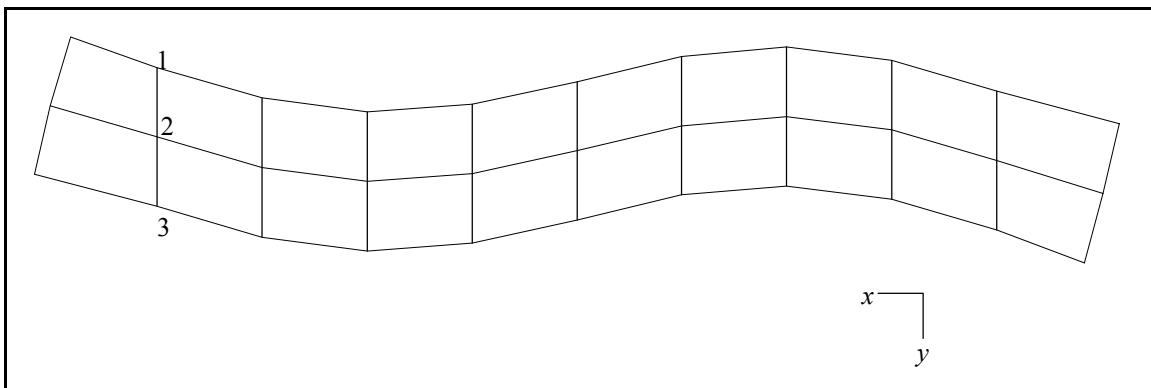
Figure 3-10(b). Completed Horizontal Bending Mode Shape.

3.4.3   Rigid Body Completion Method

The motion of a system is described by the superposition of its modal vectors. If a component of a system behaves as a rigid body in some frequency range, its motion can be fully described by six rigid body mode shapes. If the measured DOFs do not adequately describe the motion of the component, the rigid body modes shapes can be expanded to determine the unmeasurable DOFs[40]. The six rigid body mode shapes in rectangular coordinates are:

107

1. translation along the *x*-axis   4. rotation about the *x*-axis

2. translation along the *y*-axis   5. rotation about the *y*-axis

3. translation along the *z*-axis   6. rotation about the *z*-axis

The three dimensional motion of any point p on the component can be described by the linear combination of the rigid body mode shapes.

$$\begin{Bmatrix} x_p \\ y_p \\ z_p \end{Bmatrix} = \sum_{r=1}^{6} \begin{Bmatrix} \Psi_{x_p r} \\ \Psi_{y_p r} \\ \Psi_{z_p r} \end{Bmatrix} K_r = \sum_{r=1}^{6} \{\Psi_r\}_p K_r \tag{3-38}$$

where x_p, y_p, z_p are the *x*-, *y*-, *z*-direction motion of point p, respectively, $\{\Psi_r\}_p$ is the modal coefficients of point p for rigid body mode r, and K_r is the participation factor for rigid body mode r. The participation factors represent the contribution of each rigid body mode to the total motion. In matrix form this becomes

$$\begin{Bmatrix} x_p \\ y_p \\ z_p \end{Bmatrix} = \begin{bmatrix} \Psi_{x_p 1} & \Psi_{x_p 2} & \Psi_{x_p 3} & \Psi_{x_p 4} & \Psi_{x_p 5} & \Psi_{x_p 6} \\ \Psi_{y_p 1} & \Psi_{y_p 2} & \Psi_{y_p 3} & \Psi_{y_p 4} & \Psi_{y_p 5} & \Psi_{y_p 6} \\ \Psi_{z_p 1} & \Psi_{z_p 2} & \Psi_{z_p 3} & \Psi_{z_p 4} & \Psi_{z_p 5} & \Psi_{z_p 6} \end{bmatrix} \begin{Bmatrix} K_1 \\ K_2 \\ K_3 \\ K_4 \\ K_5 \\ K_6 \end{Bmatrix} \tag{3-39}$$

The contributions to motion in the *x*-direction are translation along the *x*-axis, rotation about the *y*-axis, and rotation about the *z*-axis.

$$x_p = \Psi_{x_p 1} K_1 + \Psi_{x_p 5} K_5 + \Psi_{x_p 6} K_6 \tag{3-40}$$

Figure 3-11 illustrates the contributions to the x-direction motion. Right-hand rotations are taken to be positive. The position of point p is given by the coordinates $(x_{p_o}, y_{p_o}, z_{p_o})$.

(a)

(b) Translation along the x-axis.

(c) Rotation about the z-axis.

(d) Rotation about the y-axis.
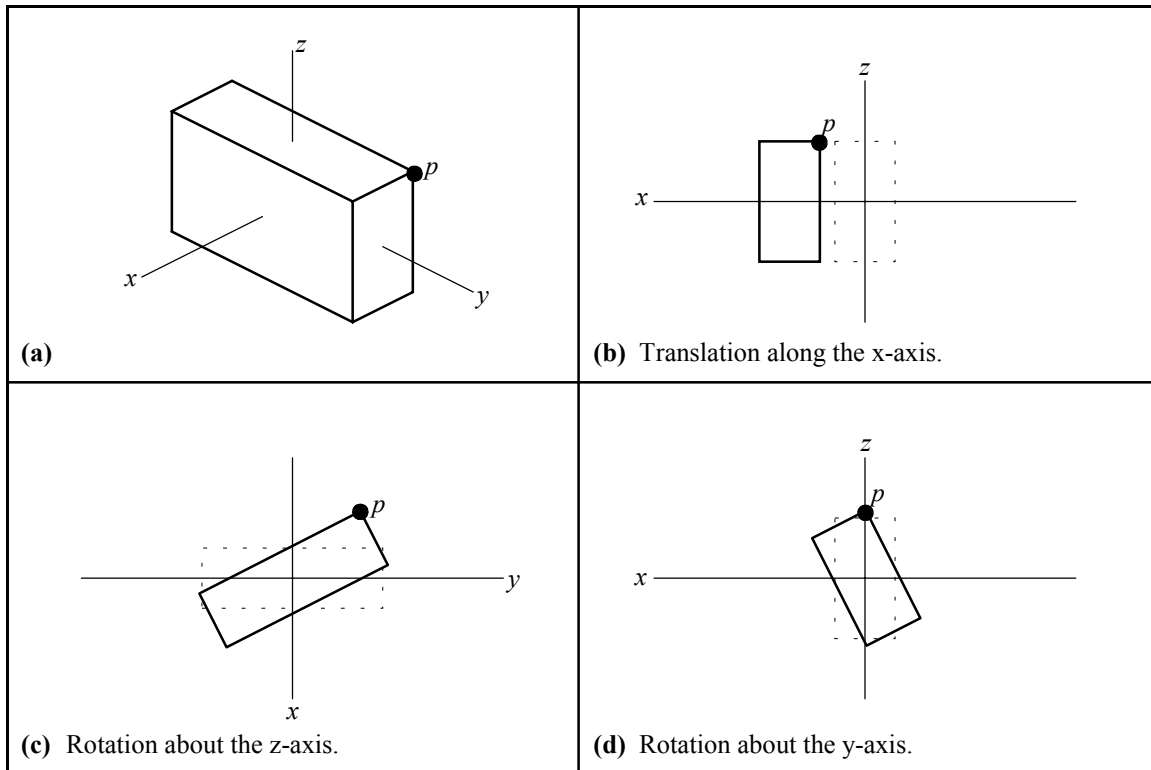
Figure 3-11. *X*-Direction Rigid Body Motion.

A modal vector defines only the relative displacement of the points on the body. The participation factors define the absolute scaling of the modes. All points on the body experience the same x-direction motion due to translation along the x-axis, as shown in Figure 3-11(b). The modal coefficient due to rotation about the z-axis is dependent on the y-coordinate relative to the origin (y_{po}), as shown in Figure 3-11(c). The modal coefficient due to rotation about the y-axis is dependent on the z-coordinate relative to the origin (z_{po}), as shown in Figure 3-11(d). The motion in the x-direction can also be written as

$$x_p = (1)K_1 + z_{p_o}K_5 - y_{p_o}K_6 \qquad (3\text{-}41)$$

The motions in the y-direction and z-direction are determined in the same manner.

$$y_p = \Psi_{yp2}K_2 + \Psi_{yp4}K_4 + \Psi_{yp6}K_6 = (1)K_2 - z_{p_o}K_4 + x_{p_o}K_6 \qquad (3\text{-}42)$$

$$z_p = \Psi_{yp3}K_3 + \Psi_{yp4}K_4 + \Psi_{yp5}K_5 = (1)K_3 + y_{p_o}K_4 - x_{p_o}K_5 \qquad (3\text{-}43)$$

Substituting the above expressions in Equation 3-39 yields

$$
\begin{Bmatrix} x_p \\ y_p \\ z_p \end{Bmatrix} =
\begin{bmatrix}
1 & 0 & 0 & 0 & z_{p_o} & -y_{p_o} \\
0 & 1 & 0 & -z_{p_o} & 0 & x_{p_o} \\
0 & 0 & 1 & y_{p_o} & -x_{p_o} & 0
\end{bmatrix}
\begin{Bmatrix} K_1 \\ K_2 \\ K_3 \\ K_4 \\ K_5 \\ K_6 \end{Bmatrix}
\qquad \text{or} \qquad \{q_p\} = [\Psi_p]\{K\} \qquad (3\text{-}44)
$$

Equation 3-44 shows that the rigid body modal matrix $[\Psi_p]$ is completely determined by the coordinates of point p. The elements of $\{q_p\}$ are the modal coefficients of the measured DOFs at point p on the rigid body component of the system. Equation 3-44 needs to be modified to account for missing measurement DOFs in the motion vector $\{q_p\}$, which is done with a (3x3) diagonal weighting matrix.

$$\lceil W_p \rfloor\{q_p\} = \lceil W_p \rfloor[\Psi_p]\{K\} \qquad (3\text{-}45)$$

where, $\quad (W_p)_{11} = 1$ if x_p exists, else $(W_p)_{11} = 0$

$$(W_p)_{22} = 1 \text{ if } y_p \text{ exists, else } (W_p)_{22} = 0$$

$$(W_p)_{33} = 1 \text{ if } z_p \text{ exists, else}(W_p)_{33} = 0$$

This is a set of three equations for six unknown participation factors. More equations are generated by including other measured DOFs on the component.

$$\lceil W \rfloor \begin{Bmatrix} \{q_1\} \\ \{q_2\} \\ \vdots \\ \{q_N\} \end{Bmatrix} = \lceil W \rfloor \begin{bmatrix} [\Psi_1] \\ [\Psi_2] \\ \vdots \\ [\Psi_N] \end{bmatrix} \{K\} \quad \text{or} \quad \lceil W \rfloor \{q\} = \lceil W \rfloor [\Psi] \{K\} \tag{3-46}$$

$$\text{where,} \quad \lceil W \rfloor = \begin{bmatrix} \lceil W_1 \rfloor & & & \\ & \lceil W_2 \rfloor & & \\ & & \ddots & \\ & & & \lceil W_N \rfloor \end{bmatrix}$$

The participation factors are calculated using a pseudo-inverse solution.

$$\{K\} = [\lceil W \rfloor [\Psi]]^{+} \lceil W \rfloor \{q\} \tag{3-47}$$

Once the participation factors are known, the motion of any point on the rigid body component can be estimated from Equation 3-44 by substituting the coordinates of that point into the rigid body modal matrix.

In order to determine the rigid body motion, the measured DOFs must be sufficient to describe the rigid body mode shapes. This condition is satisfied if the rigid body modal

matrix [Ψ] has full rank. Figure 3-12 shows two possible examples. In Figure 3-12(a) the measured DOFs are able to describe three translations, but only two rotations since the point are collinear. In this case the rigid body modal matrix does not have full rank, but the pseudo-inverse solution will attempt to compute the motion based on the available rigid body mode shapes. In Figure 3-12(b) the measured DOFs are able to describe all translations and rotations, and the rigid body modal matrix has full rank.

(a)   **(b)**
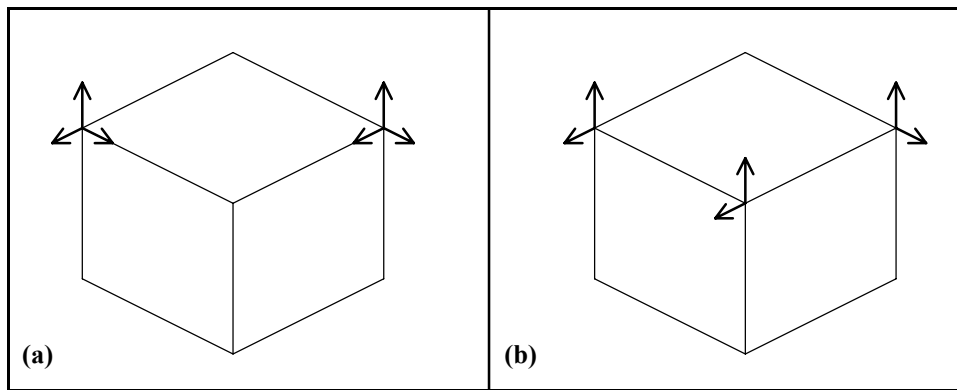
Figure 3-12. Measured DOFs for Rigid Body Motion.

Note that the slave DOF method is a special case of the rigid body method for translation in one direction. In addition, the rigid body completion method can be extended to also include deformation modes in the modal matrix [Ψ], but these techniques are beyond the scope of this thesis.

3.5 Software Implementation

A software package has been developed to implement, evaluate, and investigate the CMIF analysis method. The programs were developed using MATLAB® version 3.5k and MS-DOS® version 5.00 on a 33-MHz 486-PC with 16 megabytes of RAM. The MRIT Analysis software is a collection of over sixty MATLAB functions and scripts, several executable programs, and a few initialization files. An animation program is also included with the software package.[†] The personal computer was chosen as the platform for the software because of its portability. MATLAB was chosen as the principal programming environment because of its intrinsic matrix-based operations and graphics capabilities.

3.5.1 Software Overview

MATLAB is a technical computing software package that provides a high-level programming language in which the default variable type is a matrix. MATLAB supports the ordinary program functions such as mathematical and logical operations, input/output, graphics, etc. In addition, MATLAB provides access to sophisticated matrix computational algorithms, such as singular value decomposition. Operating system

---

† The animation program is a subset of the Spatial Sine Testing project developed by A.J. Severyn, Ph.D. at SDRL.

MATLAB is a registered trademark of The Math Works, Inc.

MS-DOS is a registered trademark of Microsoft Corporation.

commands and external programs can also be executed from within MATLAB. The MATLAB software is required to run the MRIT Analysis software.[41]

The MRIT Analysis software is designed to process a set of multiple reference FRFs from data conversion to animated mode shapes. Although it is intended for MRIT data sets, fixed input data sets are also accepted. The software implements the CMIF analysis method presented in this chapter. However, coordinate transformation and vector completion are not currently integrated into the software package. Data management functions and supplemental utilities are also provided. The principal features of the MRIT Analysis software related to the CMIF analysis method are described in the following sections. The software user's manual contains complete documentation of the software package.

The MRIT Analysis software is primarily operated from text menus displayed on the screen. (MATLAB version 3.5k does not support a graphical user interface.) The menu selections are arranged in the general order of execution and are issued by entering the number of the selection at the keyboard prompt. Additional user input is entered with interactive prompts, and the mouse is used for some basic graphical input. The animation program is operated by issuing mnemonic commands from the keyboard. The MRIT Analysis Main Menu and CMIF Analysis Menu, which are shown in Figures 3-13 and 3-14, respectively, control the principal processes of the software.

```
 ┌──────────────────────────────────────────────────────────────────────┐
 │ UC-SDRL        MULTI-REFERENCE IMPACT TESTING ANALYSIS     rev. 2.5    │
 ├──────────────────────────────────────────────────────────────────────┤
 │  DATA DIRECTORY :                                                      │
 │  MRIT DATA FILE :                                                      │
 │  RESPONSES :                 FREQUENCY RANGE :                         │
 │  REFERENCES :                SPECTRAL LINES :                          │
 ├──────────────────────────────────────────────────────────────────────┤
 │  1. Load MRIT Data File           9. Analysis Frequency Range         │
 │  2. Analysis Data Set Sieve      10. List Data Header                  │
 │  3. CMIF Analysis                11. Save Work-Space                   │
 │  4. Peak-Pick Analysis           12. Load Work-Space                   │
 │  5. Data Management              13. Resume Work Session               │
 │  6. Static Data Display                                                │
 │  7. Utilities                    99. Keyboard                          │
 │  8. Animation                     0. Exit                              │
 ├──────────────────────────────────────────────────────────────────────┤
 │                                                                        │
 └──────────────────────────────────────────────────────────────────────┘
```

Figure 3-13. MRIT Analysis Main Menu.

```
 ┌──────────────────────────────────────────────────────────────────────┐
 │ UC-SDRL                  CMIF ANALYSIS                    MRIT 2.5     │
 ├──────────────────────────────────────────────────────────────────────┤
 │   1. Calculate CMIF              10. FRF Synthesis                     │
 │   2. Select Peaks                11. Write Animation File              │
 │   3. Sort Peaks                  12. Write Modal Parameter File        │
 │   4. List Peaks                  13. List Data Header                  │
 │   5. Modal Assurance Criteria    14. Save Work-Space                   │
 │   6. Mode Tracking               15. Load Work-Space                   │
 │   7. Modal Parameter Calculation 16. Animation                        │
 │   8. List Poles                  99. Keyboard                          │
 │   9. Review CMIF Plot             0. Exit                              │
 ├──────────────────────────────────────────────────────────────────────┤
 │                                                                        │
 └──────────────────────────────────────────────────────────────────────┘
```

Figure 3-14. CMIF Analysis Menu.

Before any analysis is possible, the FRF data set must be converted into a MATLAB binary data file (a MAT-file). The MRIT Analysis software can convert SDF[28] files and Universal File[42] Dataset 58 files.† The filename convention for SDF files is the same as

---

† A Hewlett-Packard SDF conversion program is included with the MRIT Analysis software. A Universal

   File Dataset 58 conversion program, which was developed by P.S. Barney, Ph.D. at SDRL, is included

   with the MRIT Analysis software.

for the MRIT Acquisition software, which allows for a set of data files to be converted sequentially. The conversion process assembles an MRIT Data File, which is a MAT-file containing the FRF measurements, header information, frequency range, and exponential window time constant of the data set. The reciprocity conditions are applied by manipulation of the input and output DOF point numbers and directions in the header information. Once the MRIT Data File is assembled, it can then be loaded into MATLAB for analysis.

In general, the CMIF analysis proceeds as follows. First, the CMIF is calculated for the FRF data set. Next, the peaks in the CMIF curves that correspond to modes of the system are selected. The MAC and Mode Tracking functions are provided to evaluate the selected peaks. The selection and evaluation of CMIF peaks is normally an iterative process. After a set of valid peaks has been selected, an animation file can be written. An animation file is a MAT-file that contains the mode shapes, frequencies, and response DOF identifications and is read by the animation program. The left singular vectors at the selected CMIF peaks are the mode shapes, and the frequencies at this stage are the spectral line frequencies of the selected CMIF peaks. The analysis can continue to the calculate the system poles and modal scale factors. The mode shapes are examined in the animation program. The diagram in Figure 3-15 depicts the primary procedures of the MRIT Analysis software.

3.5.2 CMIF Calculation

The first step in the CMIF analysis is to calculate the Complex Mode Indicator Function for the FRF data set. Either the complex or quadrature processing option can be specified. The CMIF overlapping option is also available, and extra singular values can be retained to simulate additional references. At each spectral line, the FRF data is assembled into the form of the FRF matrix defined in Equation 3-1, and the SVD is computed as defined in Equation 3-2. For this first step, the SVD algorithm returns only the singular values to form the CMIF. The singular vectors are computed only for the selected peaks.

3.5.3 Selecting CMIF Peaks

The next step in the CMIF analysis is selecting the CMIF peaks that correspond to modes of the system. Peaks can be selected from any of the CMIF curves, but the CMIF curves are considered individually. The peaks can be auto-located or manually located in the CMIF curves. The auto-location of peaks is based on determining if the CMIF curve goes through a positive-slope to negative-slope inflection at each spectral line. A parameter called the Peak Auto-Location Sensitivity (PALS) defines the number of spectral lines to either side of the spectral line in question that are examined to determine if a peak exists. A peak is auto-located if one and only one positive-slope to negative-slope inflection is found within the sliding window defined by the PALS. Measurement noise and processing effects often cause jagged peaks in the CMIF curves which do not indicate

```
┌─────────────────┐          ┌──────────────────────────────────────┐
│                 │          │ Convert the FRF data set into a MAT-file │
│  Convert Data   │          │ with the  MRIT Data File format.  The    │
│                 │          │ reciprocity conditions are applied during the │
└─────────────────┘          │ data conversion process.                 │
        │                    └──────────────────────────────────────┘
        ▼
┌─────────────────┐          ┌──────────────────────────────────────┐
│  Load MRIT      │          │ Once the data set is converted into an MRIT │
→ │  Data File      │        │ Data File, it can be loaded into MATLAB  │
│                 │          │ for analysis.                            │
└─────────────────┘          └──────────────────────────────────────┘
        │
        ▼
┌─────────────────┐          ┌──────────────────────────────────────┐
│  Calculate CMIF │          │ Calculate the CMIF for the data set.  Specify │
│                 │          │ either complex or quadrature processing  │
│                 │          │ option.  The overlap processing option is │
└─────────────────┘          │ also available.                          │
        │                    └──────────────────────────────────────┘
        ▼
┌─────────────────┐          ┌──────────────────────────────────────┐
│  Select Peaks   │          │ Peaks in the CMIF are automatically      │
│                 │          │ located.  Then select the peaks corres-  │
│                 │          │ ponding to modes of the system with the  │
└─────────────────┘          │ mouse.  Peaks can also be manually located. │
        │                    └──────────────────────────────────────┘
        ▼
┌─────────────────┐          ┌──────────────────────────────────────┐
│  MAC and        │          │ Evaluate the validity of the CMIF peaks  │
│  Mode Tracking  │          │ with MAC and Mode Tracking.  Iterate the │
│                 │          │ selection of peaks as necessary.         │
└─────────────────┘          └──────────────────────────────────────┘
        │
        ▼
┌─────────────────┐          ┌──────────────────────────────────────┐
│  Calculate      │          │ eFRFs are formed.  Poles are calculated  │
│  Poles          │          │ with an SDOF frequency domain algorithm. │
│                 │          │ Review eFRFs.  Iterate the selection of  │
│                 │          │ peaks as necessary.  Scale factors can also │
└─────────────────┘          │ be calculated.                           │
        │                    └──────────────────────────────────────┘
        ▼
┌─────────────────┐          ┌──────────────────────────────────────┐
│  Write          │          │ Write an animation file (a MAT-file) after │
│  Animation File │◄         │ selecting a set of valid peaks or calculating │
│                 │          │ poles.  The left singular vectors at the │
└─────────────────┘          │ selected CMIF peaks are the mode shapes. │
        │                    └──────────────────────────────────────┘
        ▼
┌─────────────────┐          ┌──────────────────────────────────────┐
│  Animation      │          │ Examine the animated mode shapes.        │
│                 │          │                                          │
└─────────────────┘          └──────────────────────────────────────┘
```

Figure 3-15. Primary Procedures of the MRIT Analysus Software.

modes of the system. Setting the PALS to a larger value will filter out the spurious peaks from the peak auto-location. Figure 3-16 illustrates the peak auto-location process with examples. In Figure 3-16(a), one peak will be auto-located; in Figure 3-16(b), no peak will be auto-located; in Figure 3-16(c), one peak will be auto-located since the negative-slope to positive-slope inflection is not a peak; in Figure 3-16(d), no peak will be auto-located since three peaks exist in the window. A vertical cursor is located at every peak in the CMIF curve that meets the PALS, and the mouse is used to select the peaks that correspond to modes of the system. After the peaks are selected, they can be sorted according to frequency, CMIF curve, or singular value magnitude.
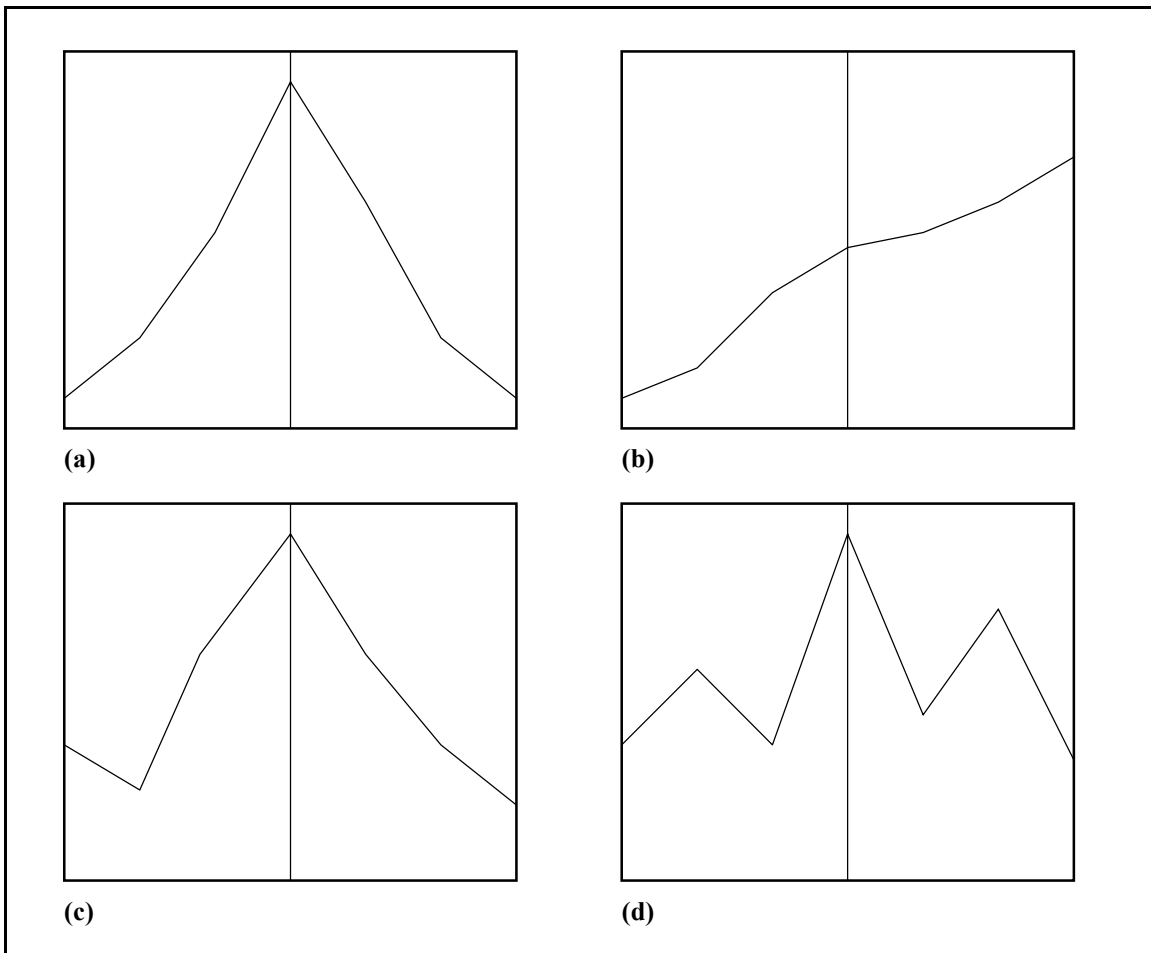
Figure 3-16. CMIF Peak Auto-Location.

3.5.4 MAC and Mode Tracking

Measurement noise, processing effects, CMIF crossovers, low peaks, and other irregularities can possibly complicate the selection of peaks that correspond to modes of the system. MAC and Mode Tracking are intended to assist in the selection of a valid set of CMIF peaks. The purpose of the MAC function is to determine the uniqueness or similarity of the mode shapes. The purpose of the Mode Tracking function is to determine the range of influence of the modes and to detect CMIF crossovers.

The MAC matrix is formed from the inner products of all combinations of the mode shapes. In general, the vectors in a MAC calculation are normalized to unity length, but left singular vectors are unity length by definition. For this case, in matrix form

$$\underset{(N \times N)}{[MAC]} = \underset{(N \times N_o)(N_o \times N)}{[\Psi]^H \, [\Psi]} \qquad (3\text{-}48)$$

where, $[\Psi] = \begin{bmatrix} \{U_1\} & \cdots & \{U_N\} \end{bmatrix}$, $MAC_{ij} = \{U_i\}^H \{U_j\}$

and, N is the number of modes. The MAC matrix is symmetric, and a MAC value is a scalar ranging from zero (0) to one (1). The MAC value between a vector and itself is always one, and if all other MAC values associated with that vector are low, the mode shape is unique. High MAC values indicate similarity between the two vectors, which may be due to spatial aliasing or the CMIF crossover effect. Some typical results of the MAC function are displayed as shown in Figure 3-17. The plots show the MAC of one mode shape with respect to all other mode shapes, with one plot for each of the selected

CMIF peaks. Figure 3-17(a) indicates that the first mode shape is unique. Figure 3-17(b)

indicates that the sixth and seventh mode shapes are similar.
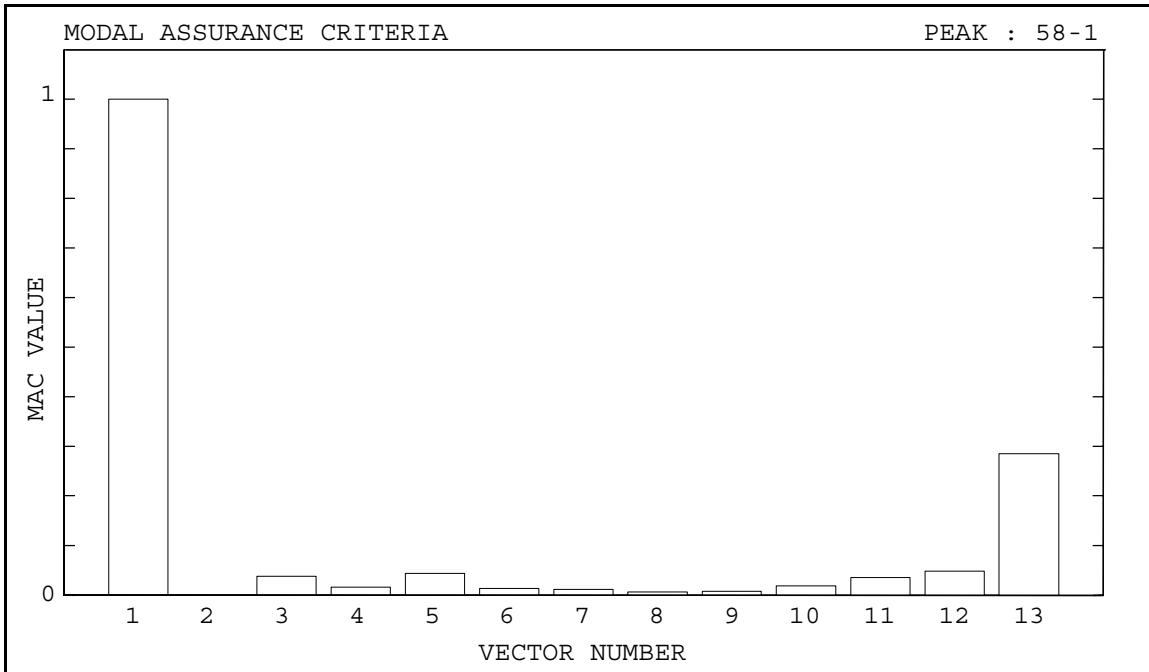
Figure 3-17(a). MAC Display, Unique Mode Shape.
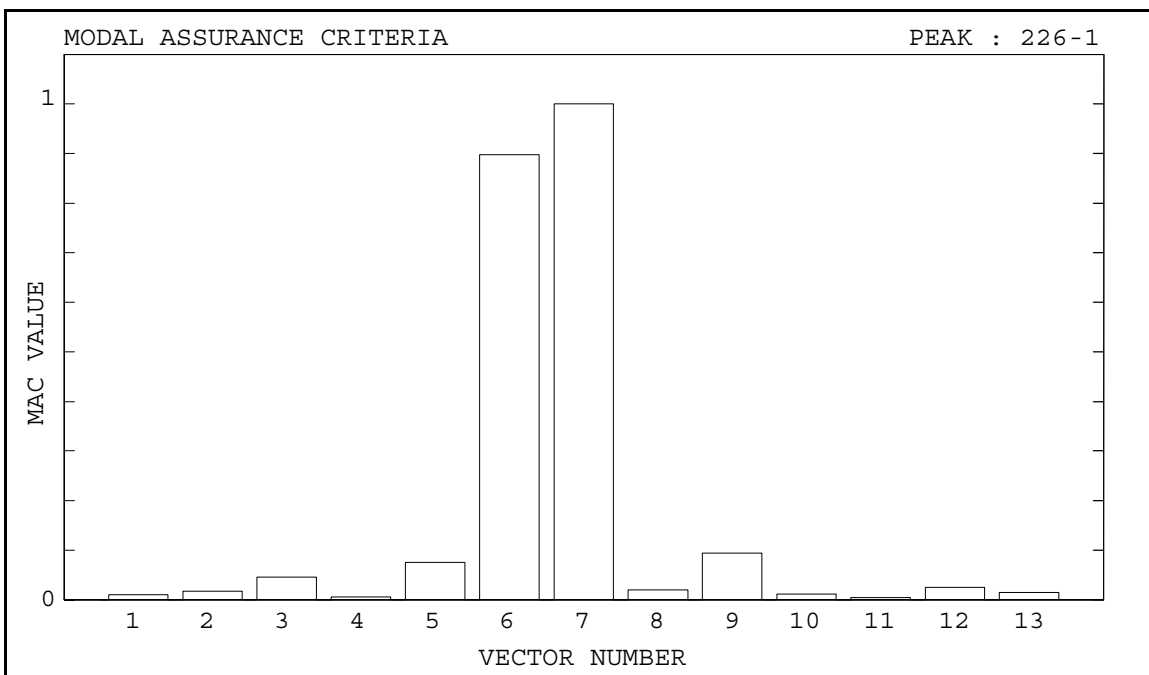
Figure 3-17(b). MAC Display, Similar Mode Shapes.

Mode Tracking compares the mode shape associated with a selected CMIF peak to the left singular vectors of the FRF matrix at contiguous spectral lines. The comparison is based on a MAC-type calculation, formed by

$$\{MAC_s\}_k = \{U_s\}^H \left[\ \{U_1\} \ \cdots \ \{U_{N_i}\} \ \right]_k \tag{3-49}$$

where s denotes the mode number and k denotes the spectral line. A high MAC value indicates similarity between vectors, and a parameter called the Mode Tracking Criteria (MTC) defines the minimum MAC value for tracking modes. Mode Tracking starts at the spectral line of the CMIF peak and proceeds in both directions, increasing and decreasing frequency. The mode is considered to track at a spectral line if one and only one MAC_s value in Equation 3-49 is greater than or equal to the MTC, and the tracking of a mode continues until the MTC is no longer satisfied. Some typical results of the Mode Tracking function are displayed as shown in Figure 3-18. The plots display the track of the mode indicated by the vertical cursor, with one plot for each of the selected CMIF peaks. The dashed lines are the CMIF curves, and the solid line is the track of the mode. In some cases, the mode track will continue across a CMIF crossover, as shown in Figure 3-18(a). In other cases, the mode track will stop at the CMIF crossover, as shown in Figure 3-18(b). The behavior of Mode Tracking is dependent on the properties of the FRF data and the MTC.
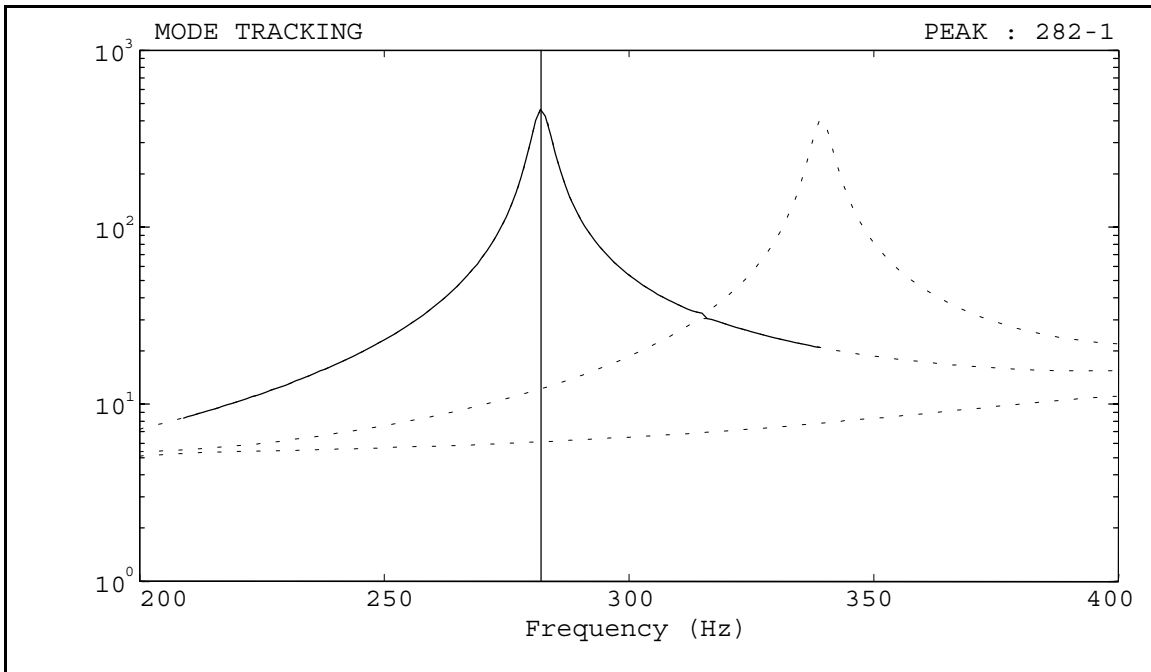
Figure 3-18(a). Mode Tracking Display.
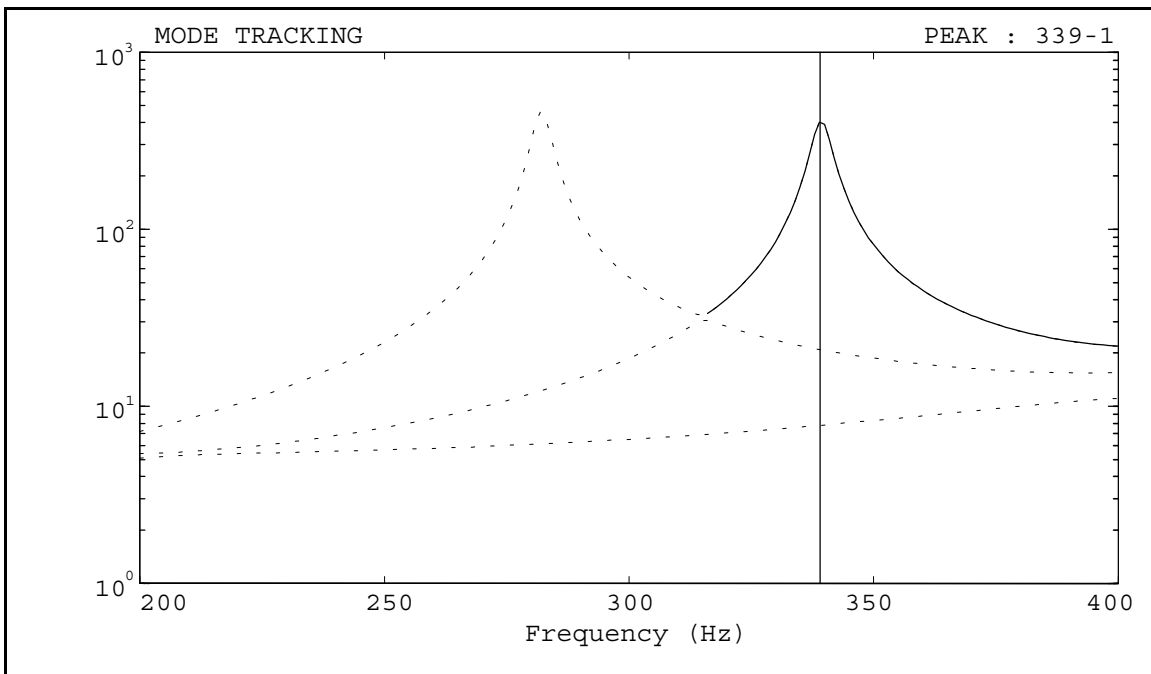
Figure 3-18(b). Mode Tracking Display.

123

3.5.5   Modal Parameter Calculation

A set of eFRFs is generated from Equation 3-9 using the left and right singular vectors at the selected CMIF peaks. The pole of each mode is estimated from the corresponding eFRF using the algorithm in Section 3.2.4. The damping factors are corrected for the effects of the exponential window as indicated in Section 3.3. The modal scale factors can be calculated using the SDOF method or the MDOF method outlined in Section 3.2.5.

The frequency and damping ratio for each mode are listed, as shown in Figure 3-19. Further evaluation of the selected CMIF peaks is possible from the list of estimated poles†. The entries in the **PEAK** column denote the spectral line frequency and also the number of the CMIF curve from which the peaks were selected. As mentioned in Section 3.2.4, the frequency of the pole estimated from an eFRF should fall within one spectral line of the peak. As an example, the frequency of mode 4 is more than three spectral lines from the associated peak, which could indicate an invalid CMIF peak. The damping values should also be examined for negative damping values, as in mode 5, and damping values that are not of approximately the same order as the rest, as in mode 13. The selected CMIF peaks corresponding to any anomalies in the frequency or damping values should be reexamined.

---

† The poles in Figure 3-19 are from the circular plate test case in Section 4.2. The values discussed above have been modified to illustrate some examples of possible results. The frequency resolution of this data set is one (1) Hertz.

MODE	PEAK	FREQ (Hz)	DAMP (%)
1	58-1	58.2581	1.014
2	58-2	58.6537	1.005
3	98-1	98.3036	0.764
4	136-1	132.6279	0.498
5	136-2	136.0337	-0.723
6	225-1	224.8996	0.529
7	226-1	225.9115	0.348
8	238-1	237.9126	0.279
9	238-2	238.1505	0.309
10	365-1	364.6167	0.181
11	365-2	364.8485	0.200
12	386-2	386.7700	0.396
13	387-1	387.3283	34.292

Figure 3-19. CMIF Analysis Estimated Poles Listing.

The eFRFs can also be reviewed as shown in Figure 3-20, with one plot for each selected CMIF peak. The solid line is the computed eFRF, and the dashed line is a synthesized, single degree of freedom eFRF. The SDOF eFRF is generated from a variation of Equation 3-17, which assumes that the eFRF is composed of only one mode.

$$eH_s(\omega_k) = eA_s C_s(\omega_k) \qquad (3\text{-}50)$$

The term eA_s in Equation 3-50 is the residue for principal mode of the eFRF, and the SDOF function $C_s(\omega_k)$ is given by Equation 3-14, 3-15, or 3-16. A least squares solution for eA_s is formed by generating equations from spectral lines near the peak. This technique is very similar to the modal scale factor SDOF method in Section 3.2.5. The purpose of synthesizing the SDOF eFRF is to compare the computed eFRF to a completely decoupled eFRF. Ideally, the computed eFRF should match the synthesized

125

eFRF near the peak since the algorithms for estimating the poles and scale factors process this data.

ENHANCED FREQUENCY RESPONSE FUNCTION   PEAK : 238-1
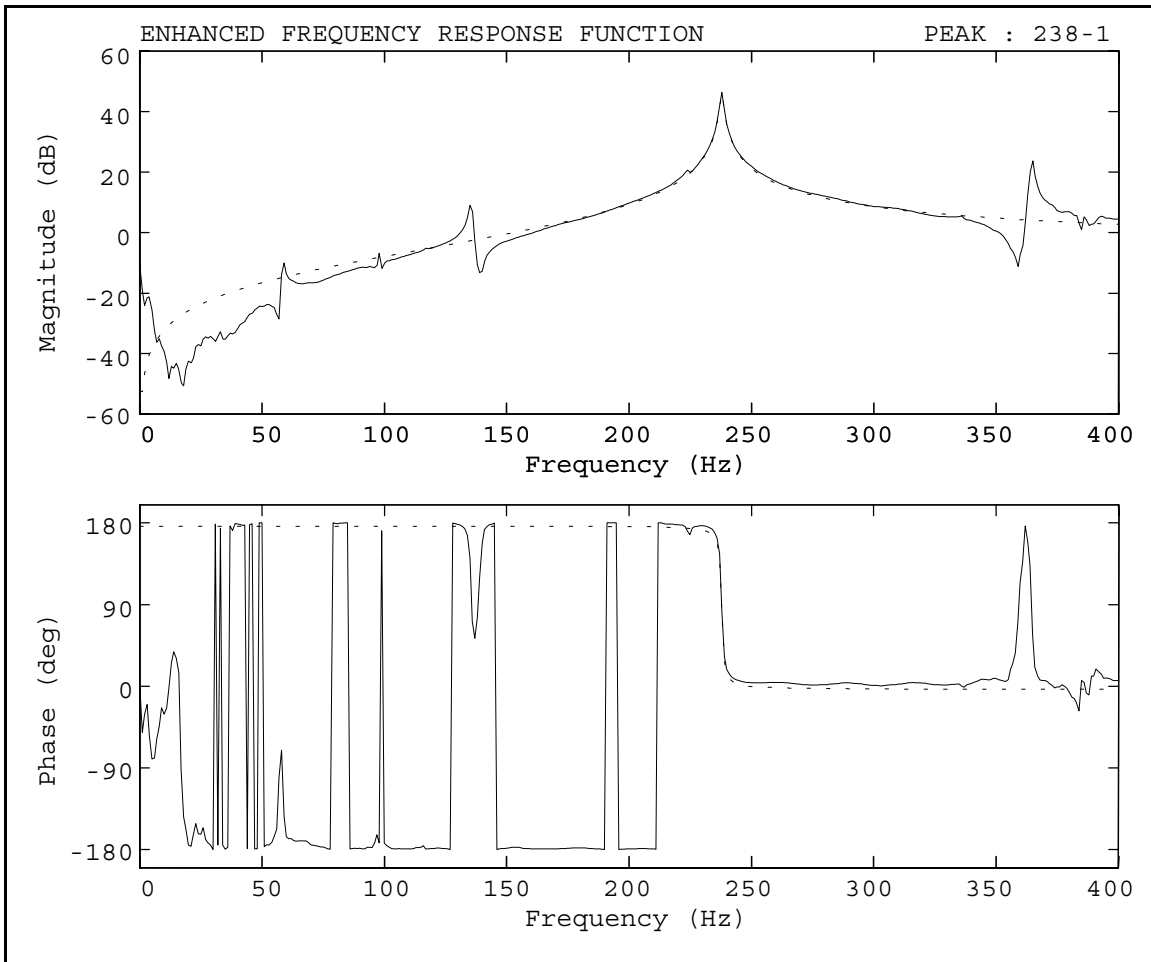
Figure 3-20. Enhanced Frequency Response Function Display.

3.6   Chapter Summary

This chapter has presented the analysis method and post-processing techniques that are appropriate for Multiple Reference Impact Testing.   The principle of reciprocity is realized by manipulation of the input and output DOF identifications of the FRFs.   The CMIF analysis method is an effective companion for the MRIT method because it is

efficient, practical, and multiple reference. The CMIF analysis method fills a position between sophisticated, multiple degree of freedom and multiple reference parameter estimation algorithms and simple, single degree of freedom and single reference peak-picking techniques.

The CMIF analysis method is a spatial domain algorithm and a zero-order UMPA model. The basic formulation locates the modes of the system to the nearest spectral line and produces approximate mode shapes. CMIF is formed from the singular values of the FRF matrix at each spectral line. A connection exists between the SVD of the FRF matrix and the dynamic properties of the system. The peaks in the CMIF coincide with the modes of the system, and the left singular vectors at the CMIF peaks are approximate mode shapes. For repeated modes, more than one CMIF curve peaks at the same frequency.

The CMIF formulation can be extended to produce system poles and modal scaling. The spatial information obtained from the first step is used to generate a set of enhanced frequency response functions. The objective of the eFRF formulation is to create an SDOF function for each mode which can be used for estimating the poles and scale factors. The effectiveness of the eFRF calculation is influenced by the spatial definition of the mode shapes. Since the form of an eFRF near the principal peak is predominately a single mode, an SDOF algorithm is adequate for calculating the poles. The exponential window affects only the estimated damping factors, which are corrected by adding the reciprocal of the time constant. The modal scale factors can be estimated from the eFRFs using an SDOF algorithm and an MDOF algorithm.

The relative magnitudes of the CMIF peaks is related to the relative overall system response for each mode and provides information about the measured FRF data set. SVD of the FRF matrix decouples the vectors that combine to form the columns into the left singular vectors. The CMIF mode shapes are not truly modal vectors but are essentially unscaled operating shapes or multiple reference response vectors. The CMIF crossover effect can create peaks in the lower CMIF curves as result of a transition of the dominant mode in the system response. The quadrature CMIF calculation and CMIF overlapping are processing options which are useful variations for some applications.

The most significant limitation of the MRIT method is imposed by physical constraints of a test system that restrict the obtainable impact DOFs. Because each impact DOF becomes a mode shape DOF, any unmeasurable DOFs could possibly degrade the information provided by animated mode shapes. The purpose of coordinate transformation and vector completion is to create more descriptive mode shapes which provide a clearer understanding of the dynamics of the system. Coordinate transformation resolves skewed and nonorthogonal orientations of measured impact DOFs into the global coordinate system. A few basic vector completion methods are sufficient for the common MRIT situations. The slave DOF completion method assumes that there is no relative displacement along a surface and assigns the motion of unmeasured DOFs to that of measured DOFs. The rigid body completion method extrapolates the motion of a subset of measured DOFs on a rigid body component to other points on the component.

The MRIT Analysis software has been developed to integrate many of the techniques presented in this chapter into a practical procedure. The software manages a multiple reference FRF data set through data conversion, CMIF analysis, and mode shape animation. The CMIF analysis method is an expedient procedure which requires minimal user interaction and experience. The most important step in the procedure is selecting a set of CMIF peaks that correspond to modes of the system. In its most basic form, the CMIF analysis method is almost a completely automated procedure. However, additional processing options and evaluation techniques are often necessary to improve the effectiveness of the method.

Chapter 4 MRIT Test Cases

Presented in this chapter are several analytical and experimental test cases which illustrate many of the Multiple Reference Impact Testing concepts and applications discussed in the preceding chapters. Two analytical systems demonstrate CMIF and validate the modal parameter estimation methods. Each experimental test case illustrates a few unique and interesting aspects of MRIT applications, testing procedures, and analysis techniques. A brief outline of the testing conditions is given for the experimental test cases. The equipment used for these MRIT test cases includes PC-based acquisition systems, Fourier analyzers, and an assortment of impactors and reference transducers. The MRIT Analysis software described in Section 3.5 was used to process the data sets.

4.1 Analytical Systems

Two analytical, lumped parameter, mass-spring-damper systems are used to examine the MRIT analysis method proposed in Chapter 3. A one DOF system is used to validate the pole and modal scaling estimation algorithms and the exponential window correction. A five DOF system is used to demonstrate the CMIF analysis method. Both systems were created and analyzed in MATLAB.

4.1.1　One DOF System

Since the pole and modal scaling estimation algorithms are based on an SDOF model, a one DOF system is appropriate for validation. The properties of the one DOF system are shown in Figure 4-1, and its analytical modal parameters are listed in Table 4-1. The system was designed for the specified undamped natural frequency and damping ratio.

The displacement over force FRF of the system was synthesized for a frequency span of 0-512 Hz and frequency resolution of 1 Hz, which is shown in Figure 4-2. The complex conjugate pair of poles was calculated from the FRF using the algorithm in Section 3.2.4. Since this system has only one mode, the enhanced FRF formulation is unnecessary. The modal scale factors were calculated using both the SDOF method and MDOF method algorithms in Section 3.2.5. The residue was then calculated from

$$A_{111} = Q_1 \Psi_1 \Psi_1 \qquad (4\text{-}1)$$

where, the modal coefficient Ψ_1 is the left singular vector (which is in this case a scalar) at the peak, and Q_1 is the modal scale factor of the positive frequency pole. The set of simultaneous equations for all three algorithms was generated by including ten spectral lines on either side of the peak. The results are listed in Table 4-2 and confirm that the SDOF parameter estimation algorithms are accurate for noise-free, analytical, SDOF data.

To examine the exponential window correction, the impulse response function of the SDOF system was synthesized, as shown in Figure 4-3(a). The sampling parameters were

specified such that the response does not decay to near zero at the end of the time period. An exponential window was applied to the IRF, as shown in Figure 4-3(b). The window was defined such that it decayed to one percent at the end of the time period. The windowed IRF was then Fourier transformed to create an FRF[†]. The FRF of the windowed and unwindowed system are compared in Figure 4-4. The FRF of the windowed system was then processed by the pole and scaling algorithms, and the results are listed in Table 4-3, which show that the estimated poles can be corrected for the exponential window to determine the true damping of the system, as indicated in Section 3.3.

Figure 4-1.
One DOF System Test Case.
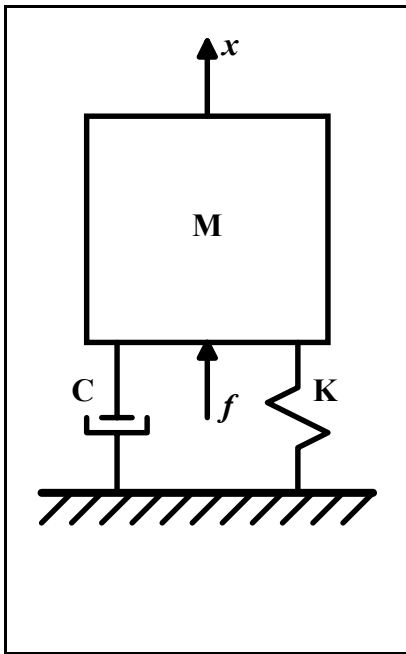
Mass	1
Stiffness	1.5791×10^6
Damping	5.0265
Eigenvalue (rad/s)	$-2.5133 \pm j\, 1.2566 \times 10^3$
Residue	$-5.4189 \times 10^{-23} \pm -j\, 3.9789 \times 10^{-4}$
Undamped Natural Frequency	200 Hz
Damped Natural Frequency	199.9996 Hz
Damping Ratio	0.2 %

Table 4-1. One DOF System
Analytical Modal Parameters.

---

† The IRF that was transformed to create the FRF in Figure 4-4 was oversampled by a factor of sixteen in order to sufficiently eliminate the effects of aliasing which would contaminate the data. The IRFs shown in Figure 4-3 has been decimated consistent with the frequency bandwidth of the corresponding FRF.
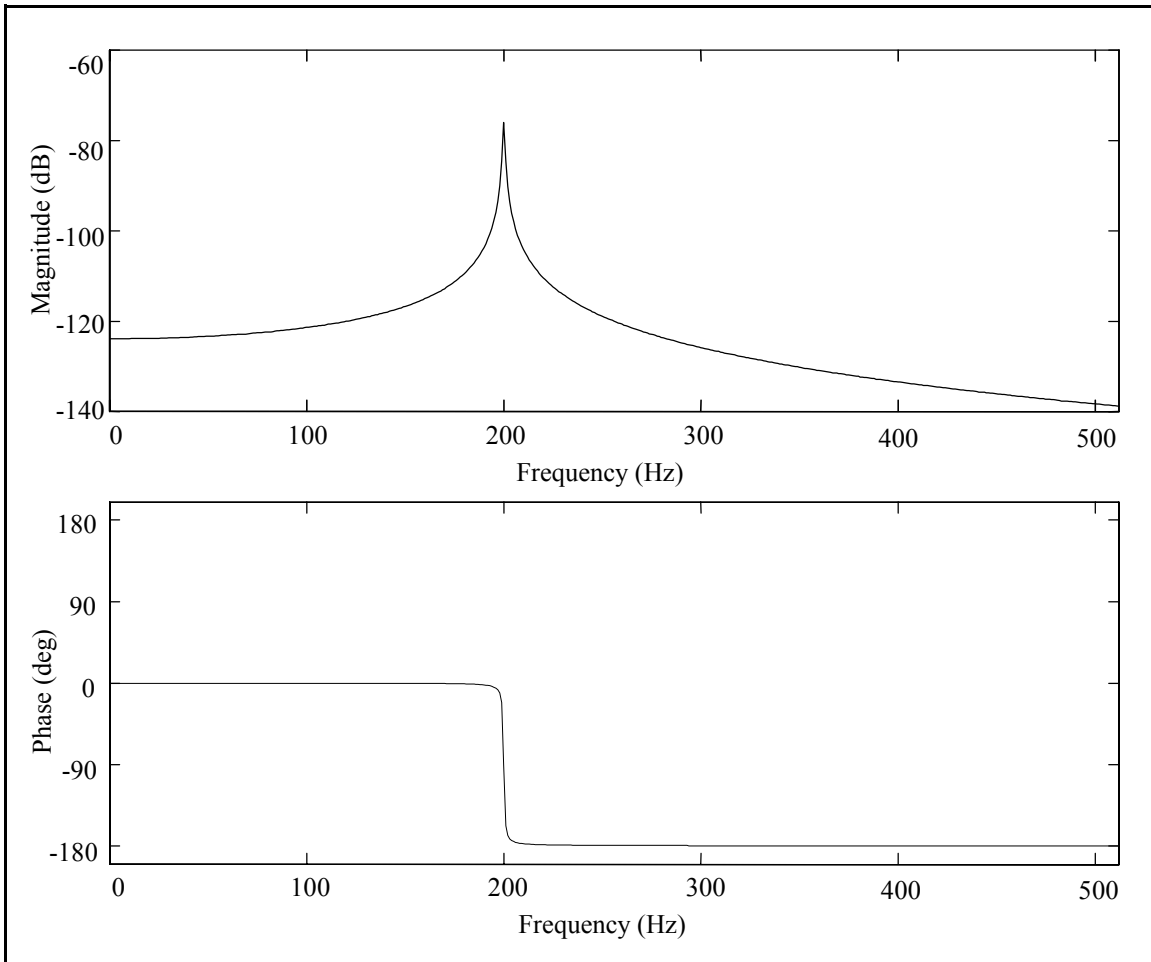
Figure 4-2. One DOF System FRF.

	Estimated Parameters	Analytical Parameters
Eigenvalue (rad/s)	$-2.5133 + j\ 1.2566 \times 10^3$	$-2.5133 \pm j\ 1.2566 \times 10^3$
Undamped Natural Frequency (Hz)	200	200
Damped Natural Frequency (Hz)	199.9996	199.9996
Damping Ratio (%)	0.2	0.2
Modal Coefficient	$5.7023 \times 10^{-15} - j\ 1.0000$	
Scale Factor (SDOF)	$-9.0527 \times 10^{-7} + j\ 3.9787 \times 10^{-4}$	
Scale Factor (MDOF)	$2.7582 \times 10^{-11} + j\ 3.9789 \times 10^{-4}$	
Residue (SDOF)	$-2.7582 \times 10^{-11} - j\ 3.9789 \times 10^{-4}$	$-5.4189 \times 10^{-23} \pm - j\ 3.9789 \times 10^{-4}$
Residue (MDOF)		

Table 4-2. One DOF System Estimated Modal Parameters.

134
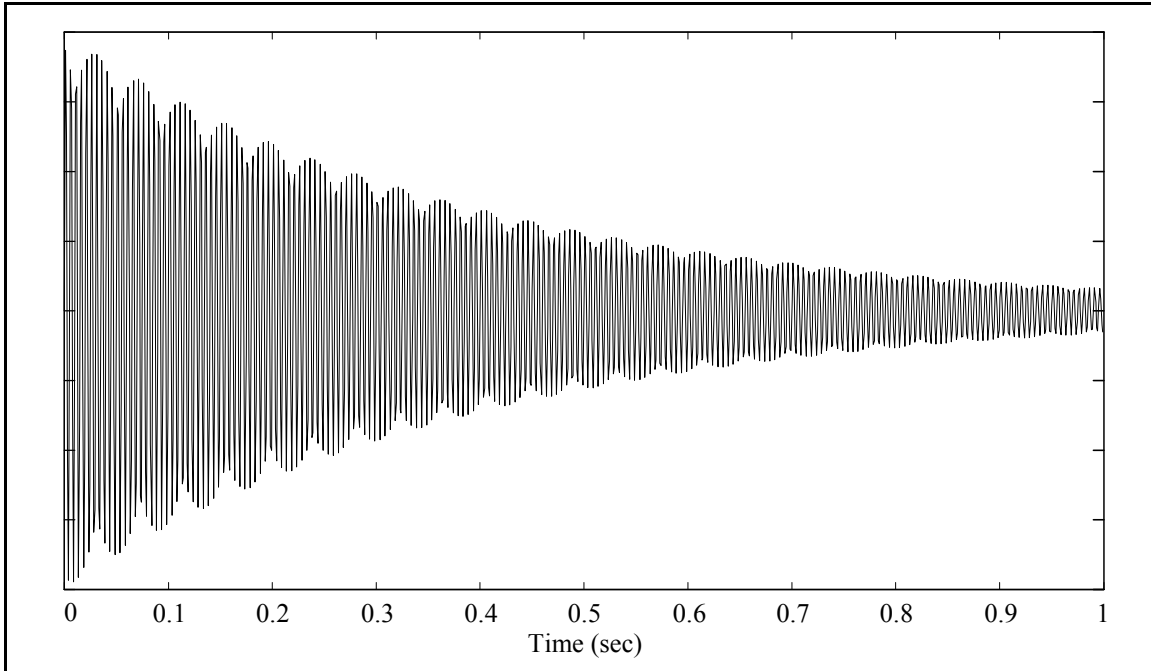
Figure 4-3(a). One DOF System Unwindowed IRF.
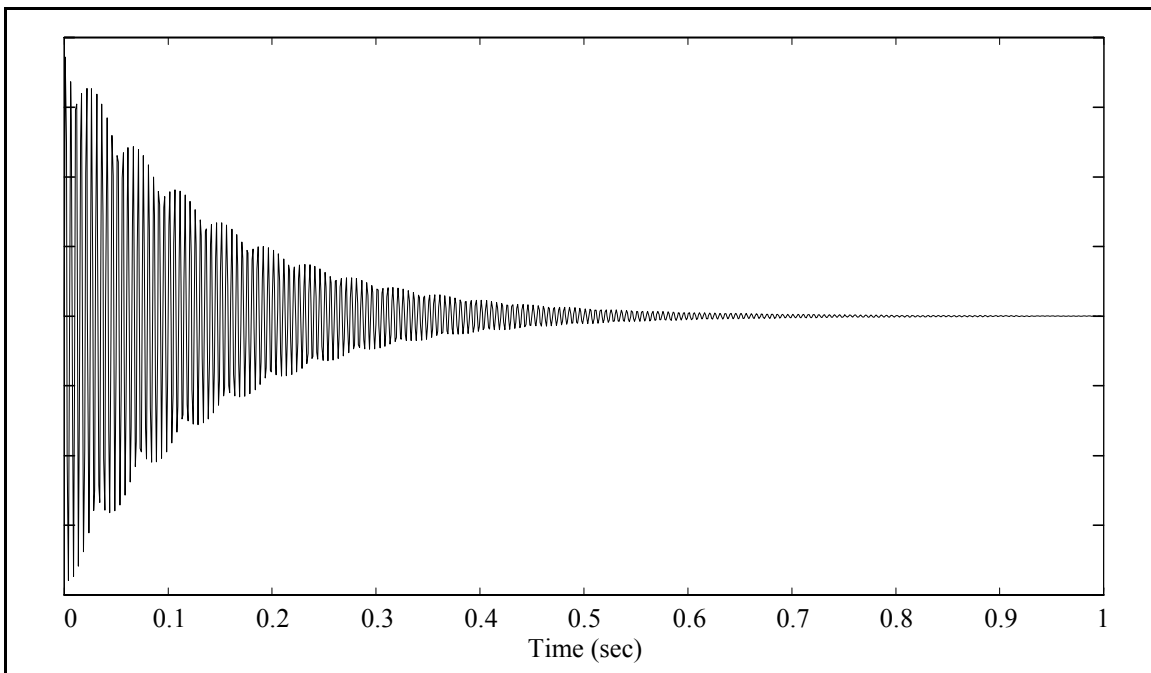
Figure 4-3(b). One DOF System Windowed IRF.
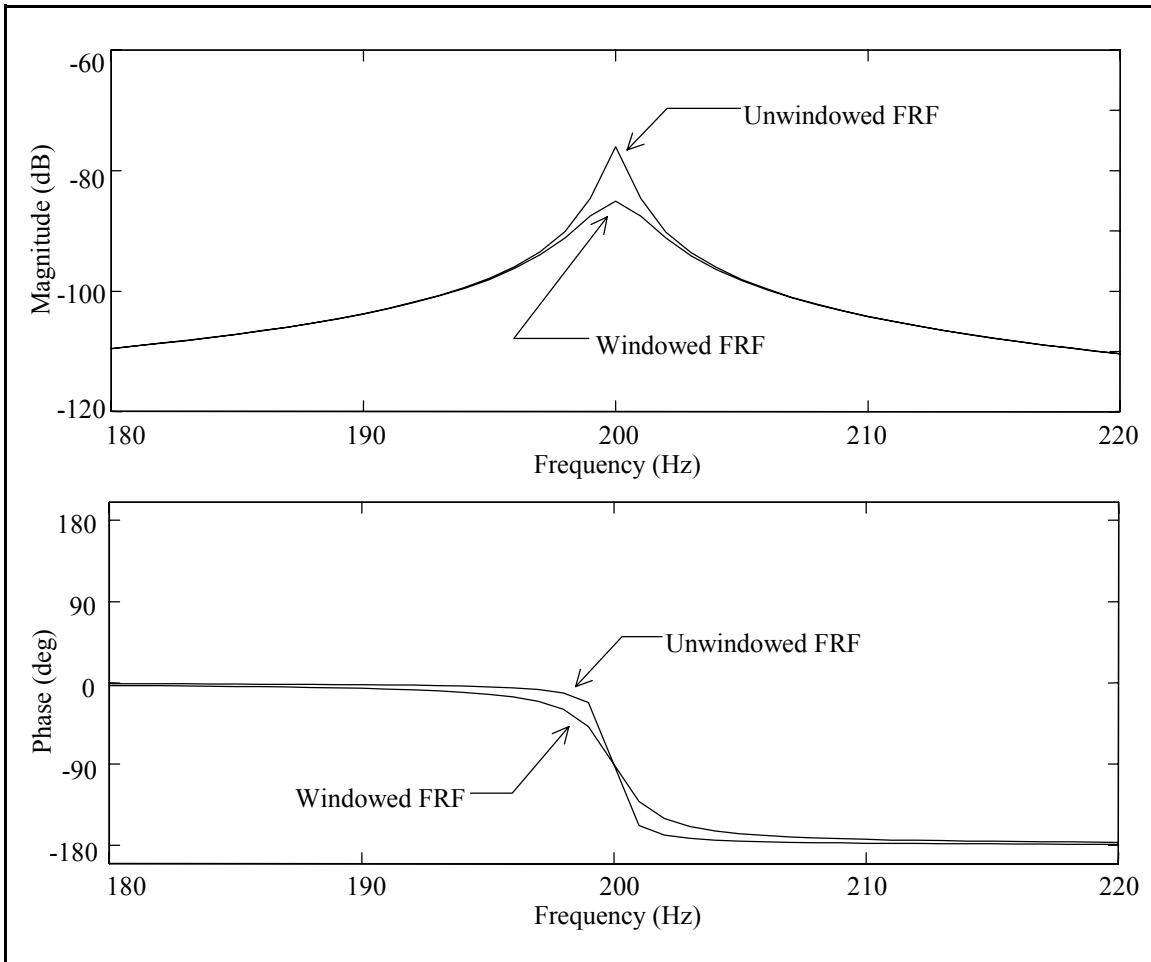
Figure 4-4. One DOF System Windowed and Unwindowed FRFs.

	Uncorrected Parameters	Corrected Parameters
Exponential Time Constant	0.2171 (sec) or 4.6052 (rad/s)	
Eigenvalue (rad/s)	$-7.1187 + j\ 1.2566 \times 10^3$	$-2.5135 + j\ 1.2566 \times 10^3$
Damping Ratio (%)	0.5665	0.2000
Undamped Natural Frequency (Hz)		200
Damped Natural Frequency (Hz)		199.9996
Modal Coefficient		$2.4759 \times 10^{-3} - j\ 9.9999 \times 10^{-1}$
Scale Factor (SDOF)		$-1.1234 \times 10^{-5} + j\ 3.9739 \times 10^{-4}$
Scale Factor (MDOF)		$1.9789 \times 10^{-6} + j\ 3.9756 \times 10^{-4}$
Residue (SDOF)		$1.3202 \times 10^{-5} - j\ 3.9732 \times 10^{-4}$
Residue (MDOF)		$-1.0351 \times 10^{-8} - j\ 3.9757 \times 10e^{-4}$

Table 4-3. One DOF System Estimated Modal Parameters,
Corrected for the Exponential Window.

4.1.2   Five DOF System

The five DOF system is shown in Figure 4-5, and its analytical modal parameters are listed in Table 4-4.   The system was intentionally designed to have two very closely spaced (i.e., pseudo-repeated) modes.   The acceleration over force FRFs of the system were synthesized for a frequency span of 0-512 Hz and frequency resolution of 1 Hz.   The full data set was processed with the CMIF analysis method, and since this is a multiple DOF system, the enhanced FRF formulation was performed.   The estimated poles from the complex and quadrature CMIF processing options are listed in Table 4-4.   Since data from a MDOF system was processed by an SDOF pole estimation algorithm, exact agreement with the analytical eigenvalues is not necessarily expected.   The quadrature CMIF calculation appears to give slightly better results, which is most probably attributed to the eFRF phase issue discussed in Section 3.2.3.

Figure 4-6 is the superposition of the SDOF functions for the FRF of input/output DOF pair (1,1).   The dashed lines are the SDOF modes, the solid line is the composite FRF, and the numbers by the SDOF curves denote the mode.   Figure 4-7(a) is the CMIF of the data set for a complete five by five FRF matrix (i.e., references 1,2,3,4,5).   The solid line is the first CMIF curve, and the dashed lines are the lower four CMIF curves.   Several observations can be made from these two plots: (1) The relative magnitudes of modes four and five (the repeated modes) are equal, which causes the first and second CMIF curves to coincide at this peak.   (2) The CMIF curves actually intersect at the crossover points, instead of creating a dip in the upper curve and a peak in the lower curve. (3) By following the CMIF curves across the crossover points, the tracks of the modes are

evident over the full frequency range. (4) Comparison of the SDOF functions and the CMIF mode tracks reaffirms the connection between singular value decomposition of the FRF matrix and the modal properties of the system.

Figures 4-7(b-e) are the CMIFs of the system for several different combinations of references. The solid line is the first CMIF curve, and the dashed lines are the lower CMIF curves. For each data set there are fewer references than modes, which is much more typical for experimental data sets, and the mode tracks are not apparent across the full frequency range. In each CMIF, the first and second CMIF curves coincide at the peak of the repeated modes. The third CMIF curve in (c) and (d) confirms that the multiplicity of the mode is two.
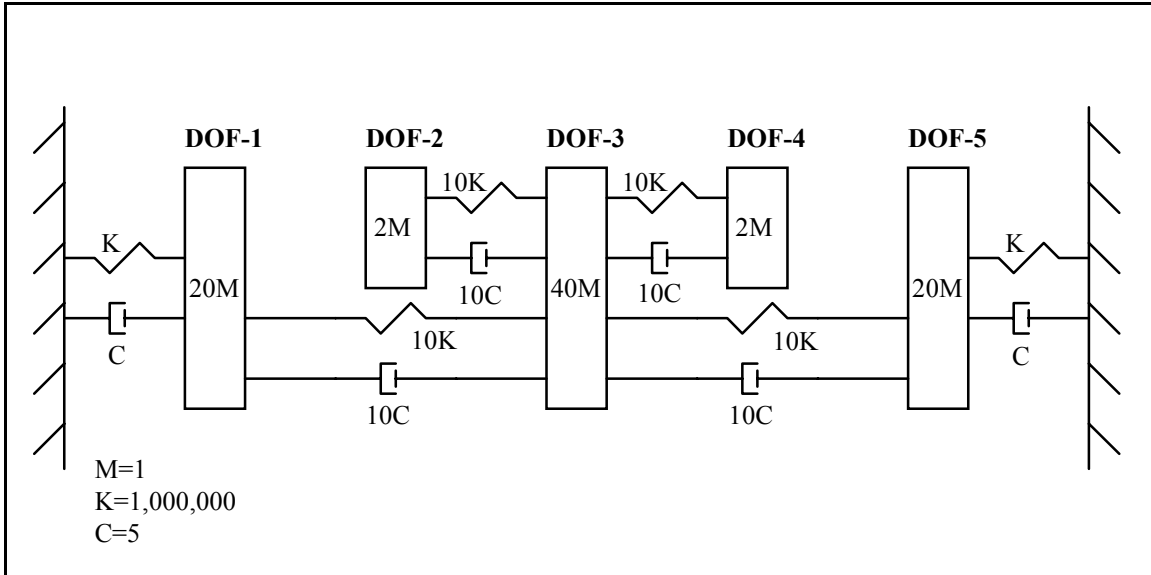
Figure 4-5. Five DOF System Test Case.

Mode	Analytical		Estimated			
			CMIF - Complex		CMIF - Quadrature	
	Damped Natural Frequency (Hz)	Damping Ratio (%)	Damped Natural Frequency (Hz)	Damping Ratio (%)	Damped Natural Frequency (Hz)	Damping Ratio (%)
1	24.2716	1.6772	24.1930	1.4072	24.2667	1.6756
2	111.9800	0.5312	111.9312	0.5299	111.9662	0.5308
3	156.4503	0.5001	156.4058	0.4909	156.4331	0.4998
4	375.1021	0.6953	375.0590	0.6948	375.1139	0.6952
5	375.2866	0.6955	375.2445	0.6943	375.2991	0.6954

Table 4-4. Five DOF System Analytical and Estimated Modal Parameters.
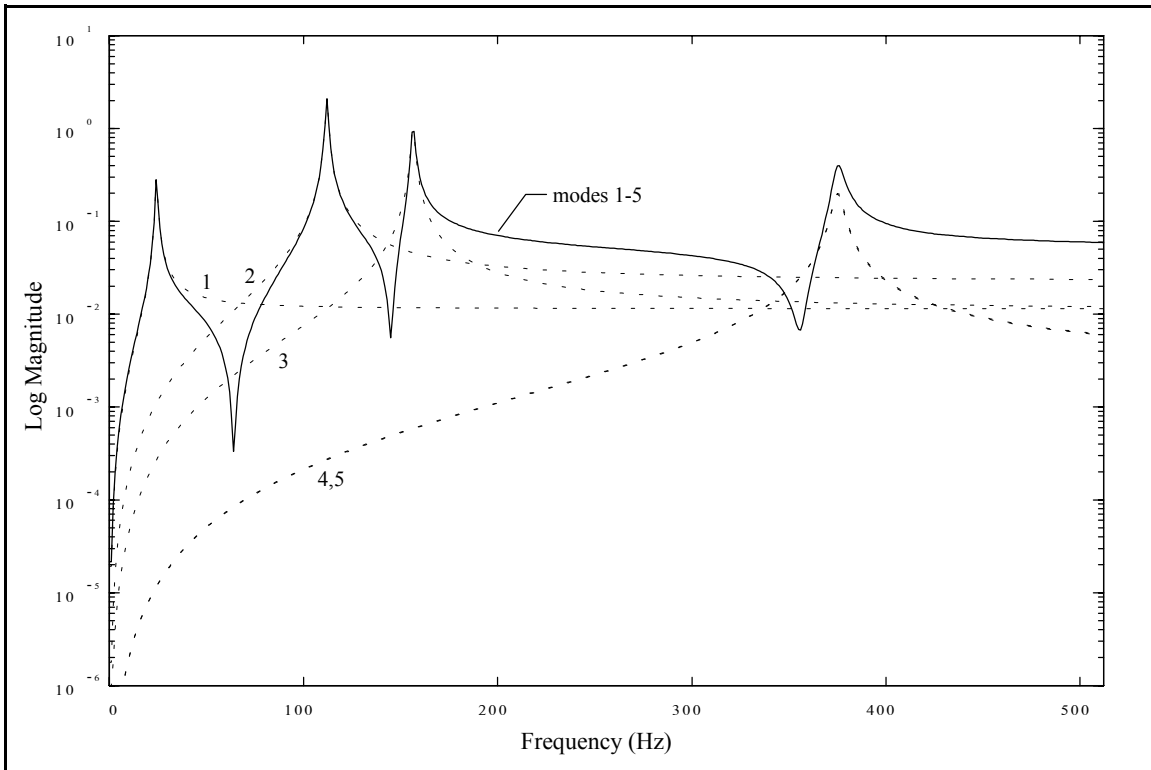
Figure 4-6. Five DOF System Superposition of Modes for FRF (1,1).
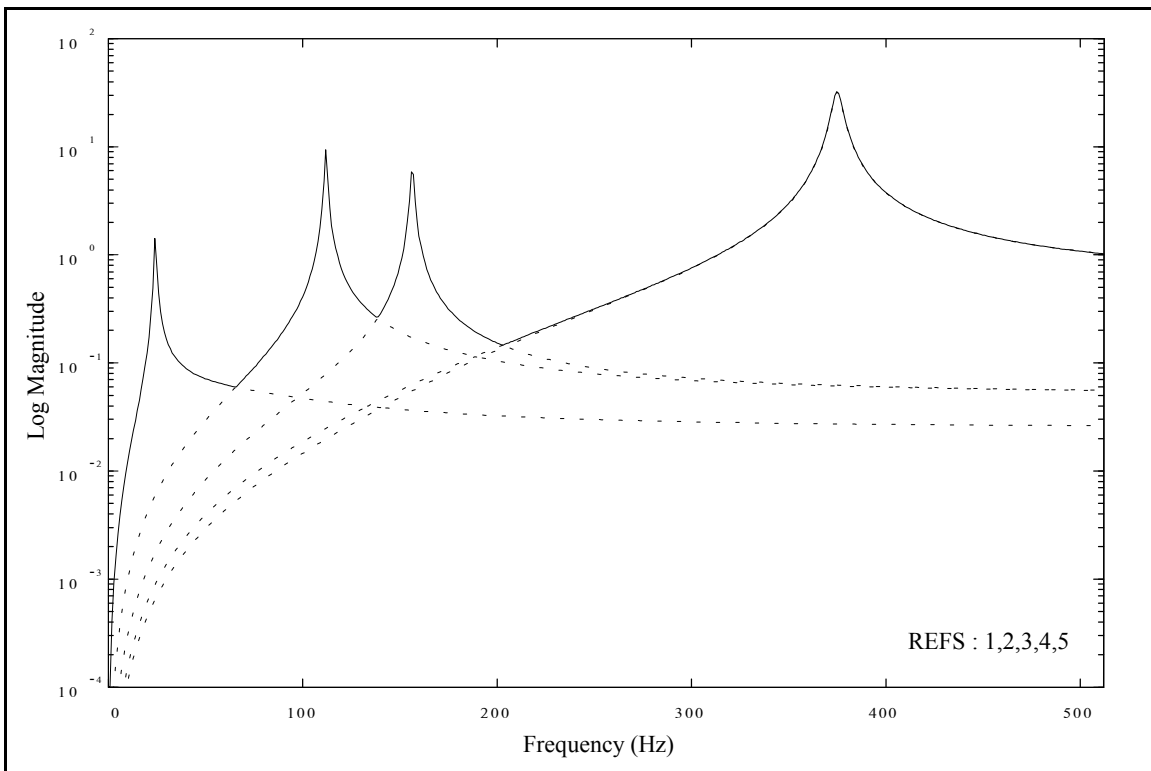
Figure 4-7(a). Five DOF System CMIF (References 1,2,3,4,5).

140
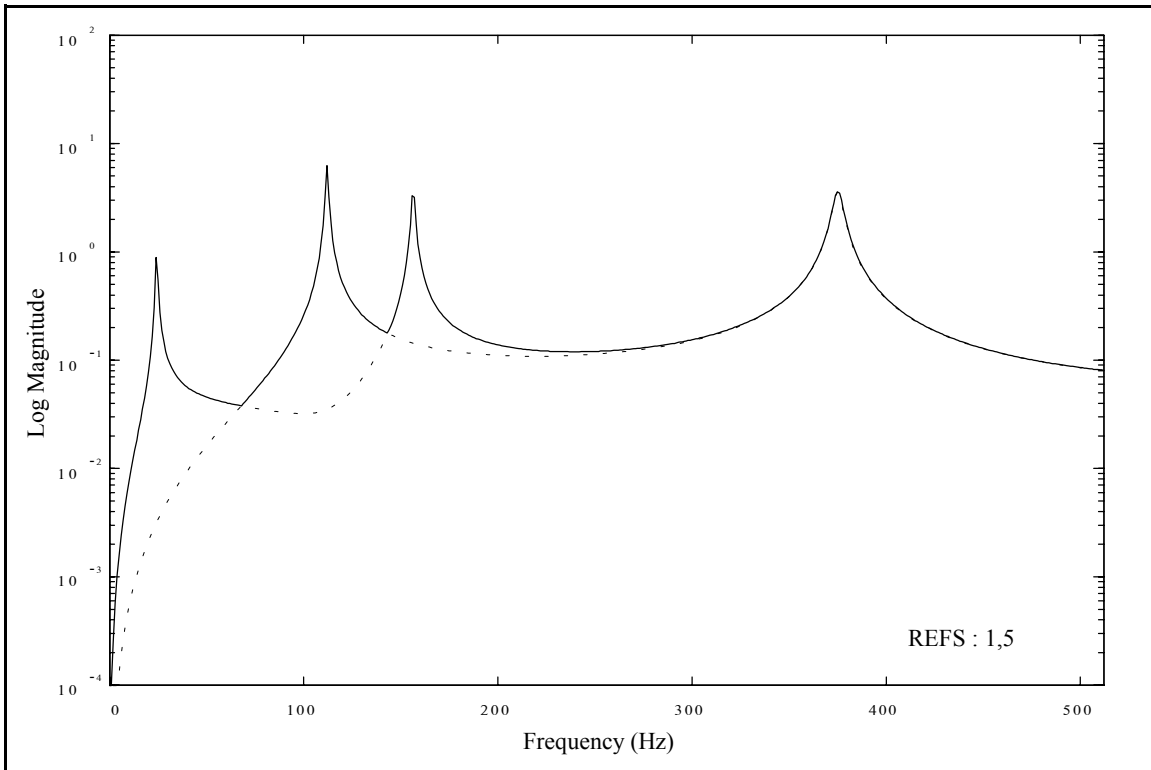
Figure 4-7(b). Five DOF System CMIF (References 1,5).
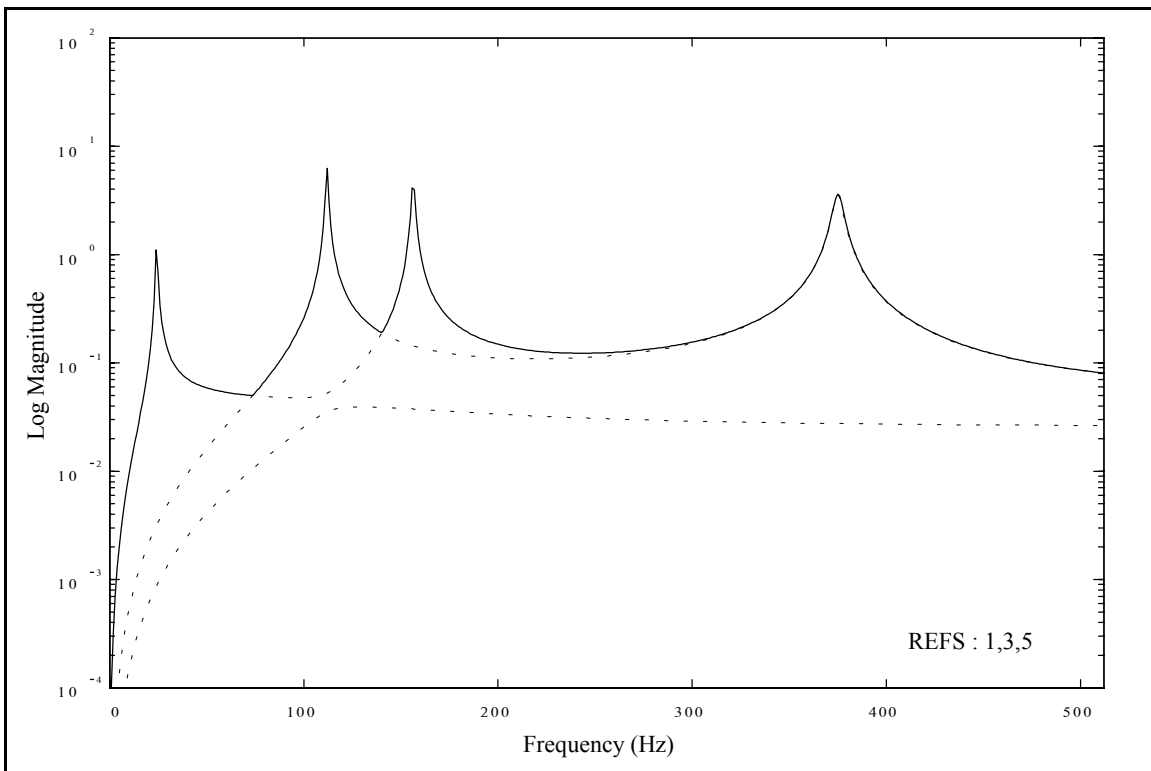
Figure 4-7(c). Five DOF System CMIF (References 1,3,5).

141
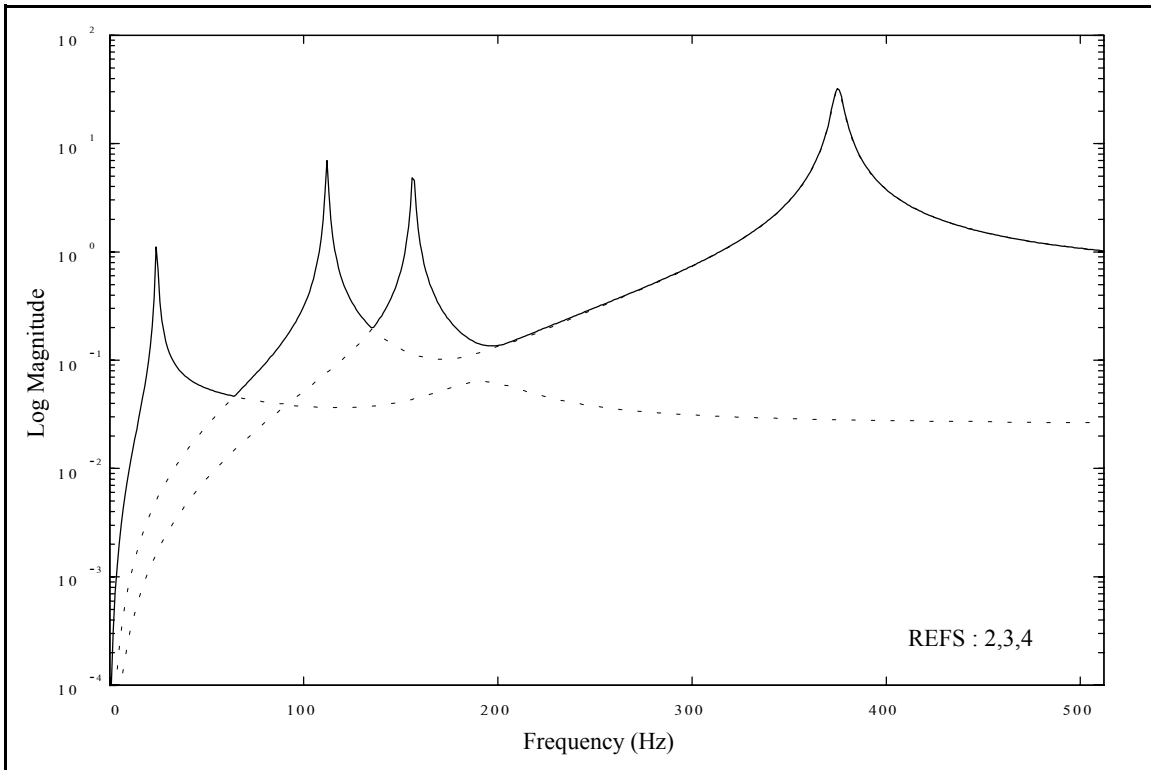
Figure 4-7(d). Five DOF System CMIF (References 2,3,4).
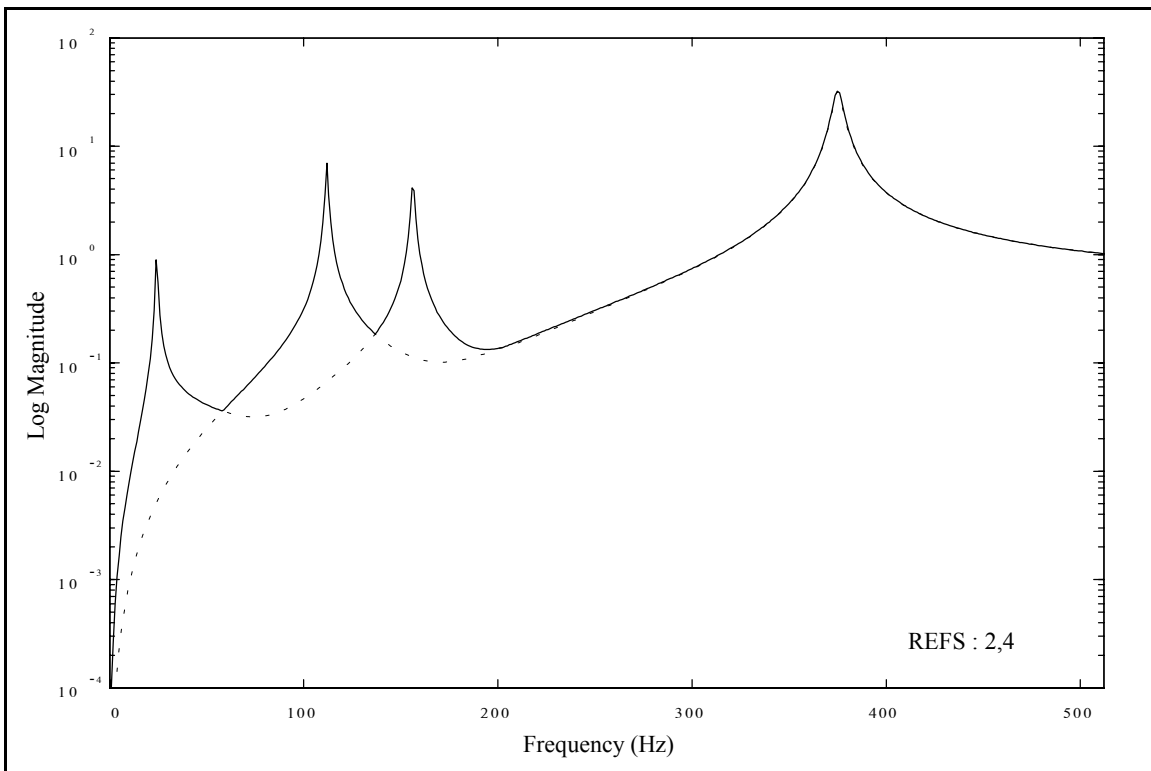
Figure 4-7(e). Five DOF System CMIF (References 2,4).

142

4.2   Circular Plate

The circular plate (c-plate) is a 30-inch diameter, 1/4-inch thick, aluminum disk with a 2-inch hole in the center. The c-plate is a simple, lightly damped structure, that has many repeated modes of multiplicity two due to symmetry. The data from this test case was used to illustrate the CMIF and eFRF concepts in Chapter 3. The c-plate is pictured in Figure 4-8(a), and the test definition is listed in Table 4-5. The test geometry and reference locations are shown in Figure 4-8(b), where the numbers next to the points on the test geometry indicate the reference locations. Measurements were made only in the z-direction, normal to the top surface.

The CMIF of the data set is shown in Figure 4-9, where the vertical cursors locate the selected CMIF peaks and the solid line is the CMIF curve from which peaks have been selected. The estimated system poles corresponding to the selected CMIF peaks are listed in Table 4-6.[†] All modes except mode 3 are repeated (or nearly repeated) mode pairs. The mode shapes for modes 1 and 2 are shown in Figure 4-10.

A case in which a crossover occurs at a peak in the CMIF is shown in Figure 4-11. The dashed lines are the CMIF curves and the solid lines are the mode tracks of the peaks at 224-1 and 226-1. The frequencies of these two modes are separated by more than one spectral line, and the second curve does peak at the same spectral line as the first curve. Peak auto-location would have selected the peaks at 225-2 and 226-1 as two, distinct modes. However, the mode tracking reveals that the peak at 225-2 is not a valid peak, but

---

† CMIF peaks are referenced by the spectral line frequency and the CMIF curve.

is actually caused by the CMIF crossover effect. If the peak at 225-2 had been selected, the mode shape would have been the same as that of the peak at 226-1. Because of the very close spacing and relative magnitudes of the two peaks, the crossover is not evident by a dip in the upper curve at the same spectral line as the peak in the lower curve.

Figures 4-12 through 4-15 illustrate some examples of the CMIF processing options with the c-plate data set. Figure 4-12(a) is the complex CMIF calculation, and Figure 4-12(b) is the quadrature CMIF calculation. Note that the CMIF from the quadrature calculation is not as smooth as the CMIF from the complex calculation, but the peaks are better separated and the low magnitude peaks are increased. The CMIFs in Figure 4-13 were generated with an overlap of one spectral line (i.e., n=1 in Equation 3-21). The CMIFs in Figure 4-14 were generated with an overlap of three spectral lines (i.e., n=3 in Equation 3-21). Overlapping has smoothed the CMIF curves, especially for the quadrature calculation, and broadened the peaks. The smoothing and broadening tend to increase with overlapping more spectral lines. Note that an effect of CMIF overlapping is the creation of peaks in the lower CMIF curves below the primary peaks. The CMIFs in Figure 4-15 were generated from the data set of only the references at (1,-z) and with an overlap of one spectral line. In this case the extra singular values were retained to simulate additional references. Note that CMIFs with simulated references do indicate the repeated modes, but are also very noisy and distorted.

144
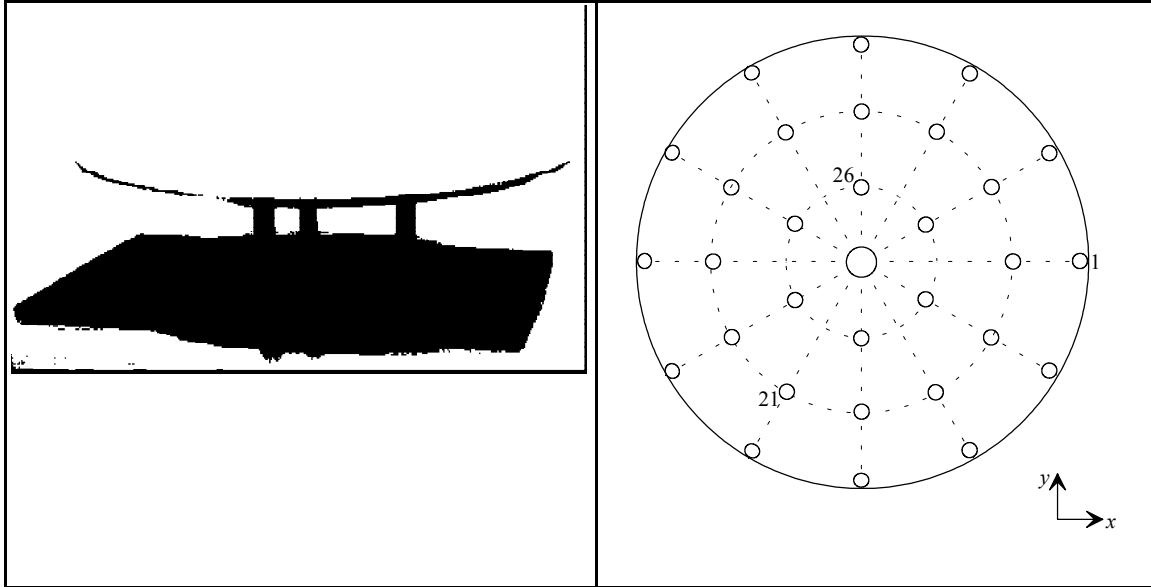
Figure 4-8(a). Circular Plate Test Case.   **Figure 4-8(b).** Circular Plate Geometry and Reference Locations

No. References	3
No. Impact Locations	30
Data Acquisition System	PC with multi-channel front-end hardware
Impactor	lightweight impact hammer
Reference Transducers	(3) lightweight accelerometers (10 mV/g)
Frequency Range	0 - 400 Hz at 1 Hz

Table 4-5. Circular Plate Test Definition.

Mode	CMIF Peak	Frequency (Hz)	Damping (%)
1	58-1	58.1145	0.9972
2	58-2	58.5125	1.0137
3	98-1	98.1985	0.7615
4	136-1	135.5605	0.4933
5	136-2	135.9728	0.7189
6	224-1	224.5758	0.4244
7	226-1	225.8632	0.3471
8	238-1	237.8753	0.2780
9	238-2	238.1114	0.3099
10	365-1	364.5917	0.1811
11	365-2	364.8232	0.1993
12	386-2	386.7126	0.3976
13	387-1	387.2919	0.2914

Table 4-6. Circular Plate Estimated Frequencies and Damping.
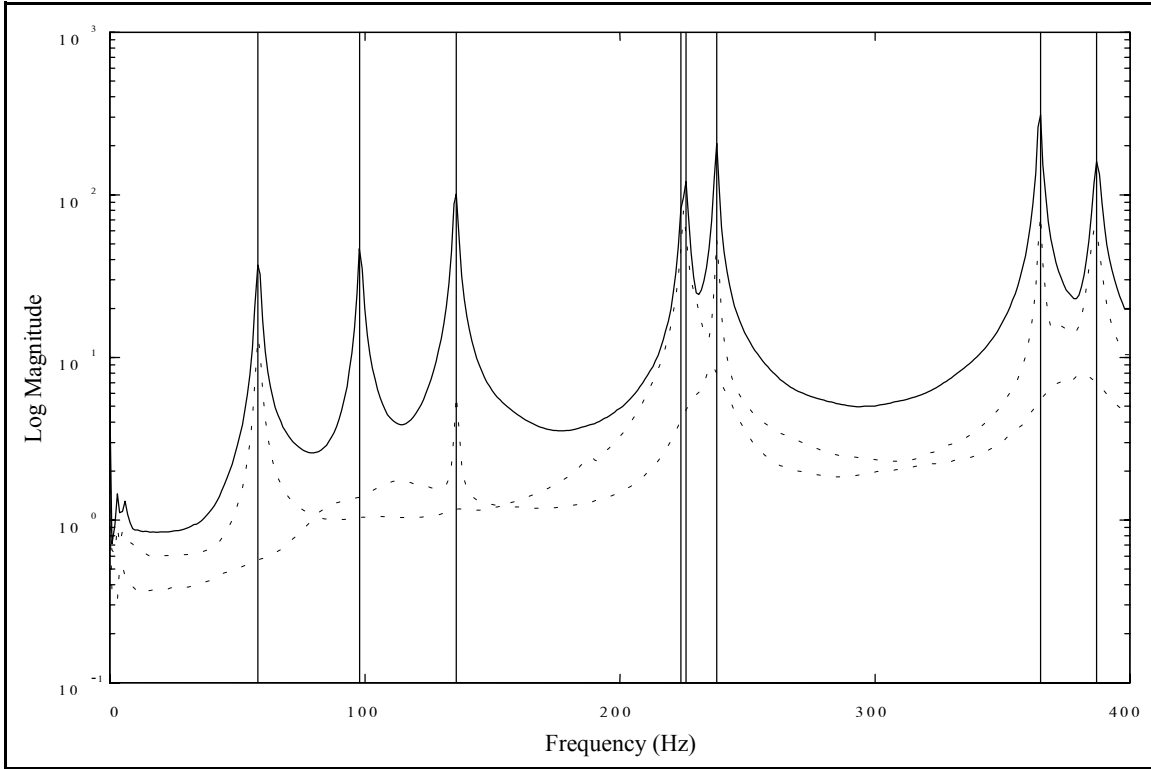
Figure 4-9(a). Circular Plate CMIF, Curve 1 Selected Peaks.
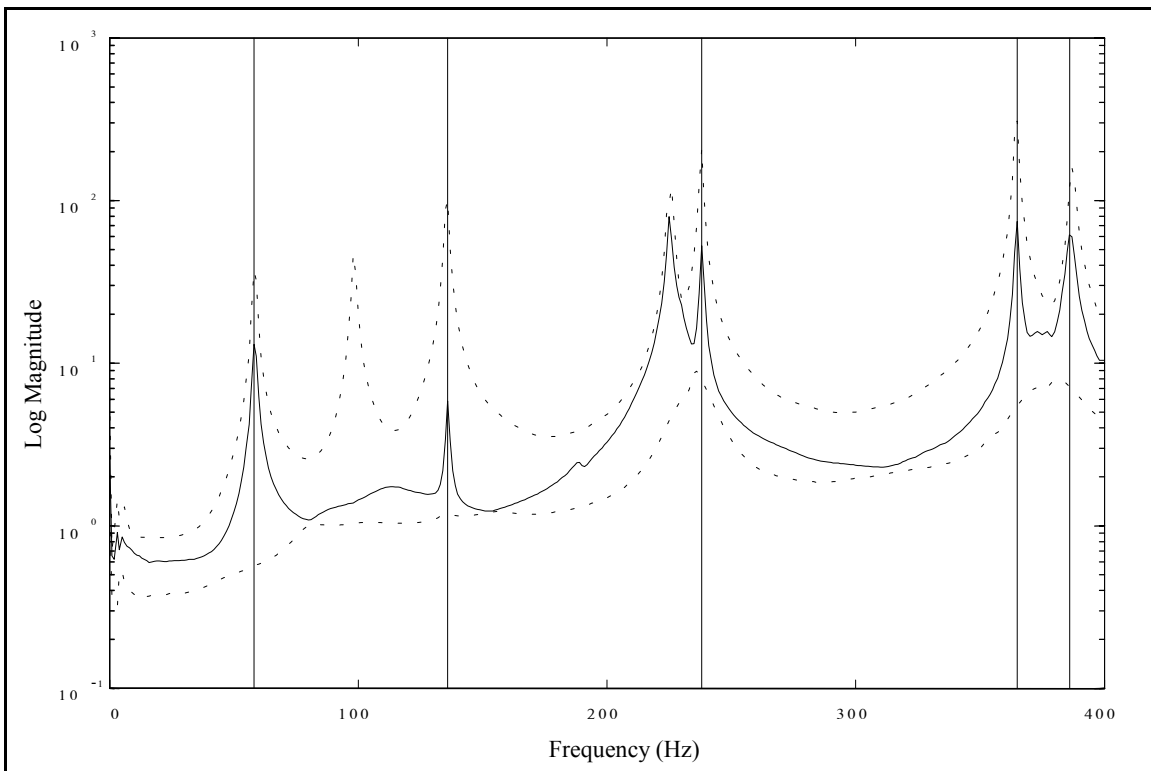
Figure 4-9(b). Circular Plate CMIF, Curve 2 Selected Peaks.

146
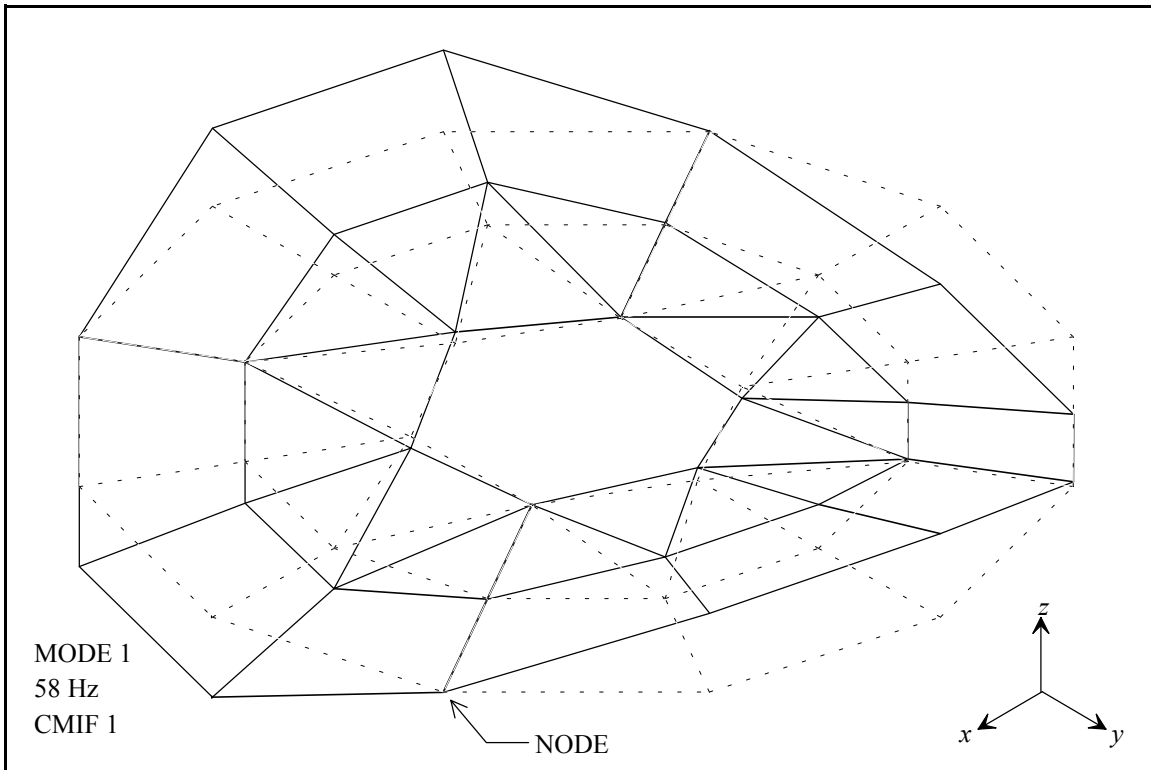
Figure 4-10(a). Circular Plate Mode Shape (58-1).
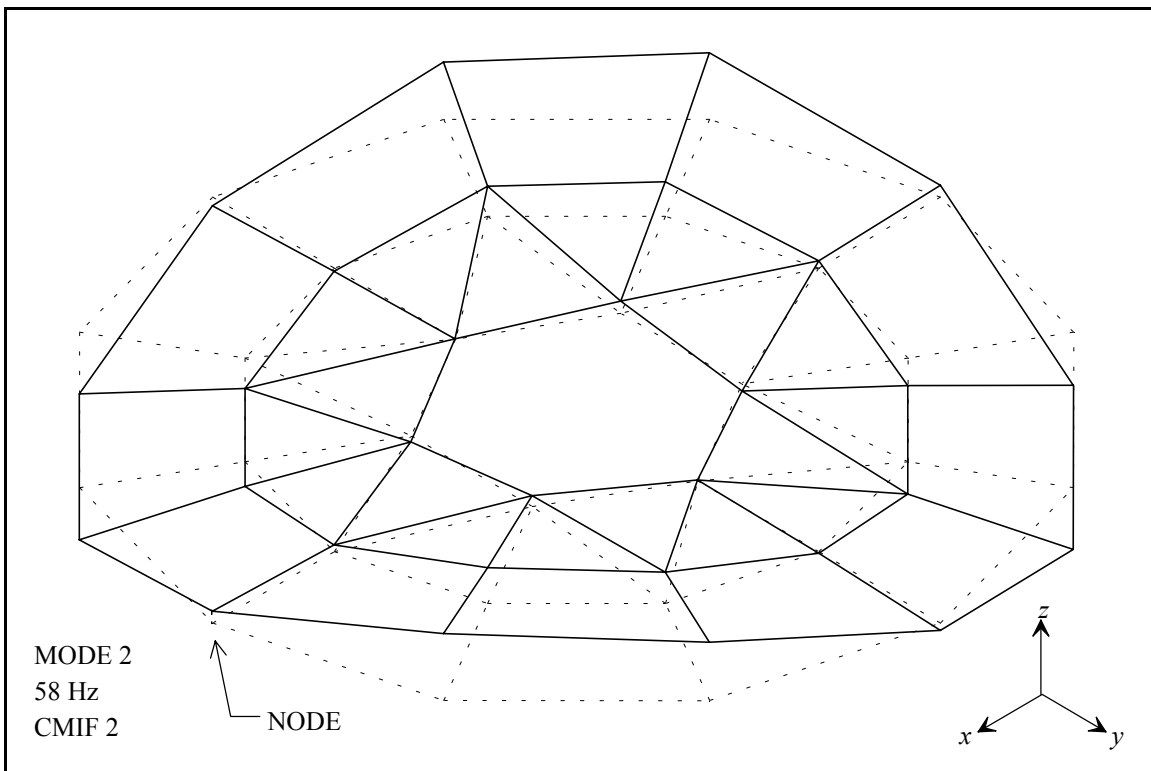
Figure 4-10(b). Circular Plate Mode Shape (58-2).
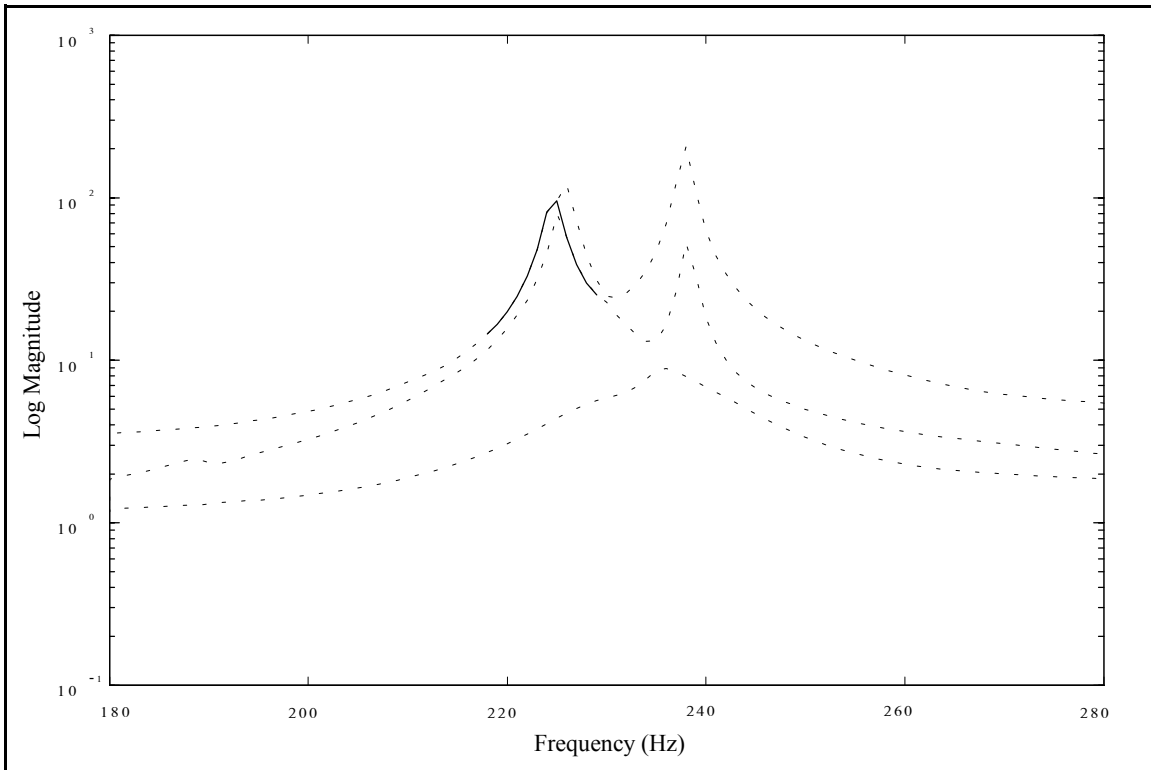
Figure 4-11(a). Circular Plate CMIF, Mode Tracking of Crossover at Peak (224-1).
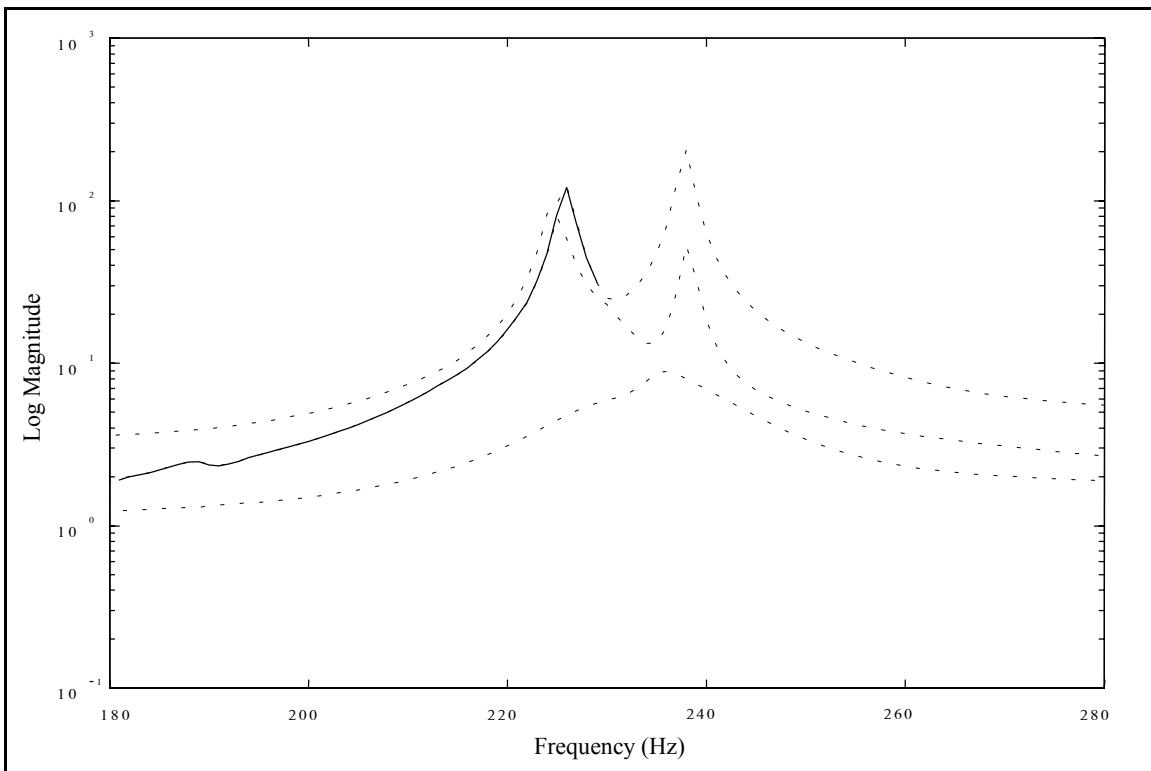
Figure 4-11(b). Circular Plate CMIF, Mode Tracking of Crossover at Peak (226-1).

148
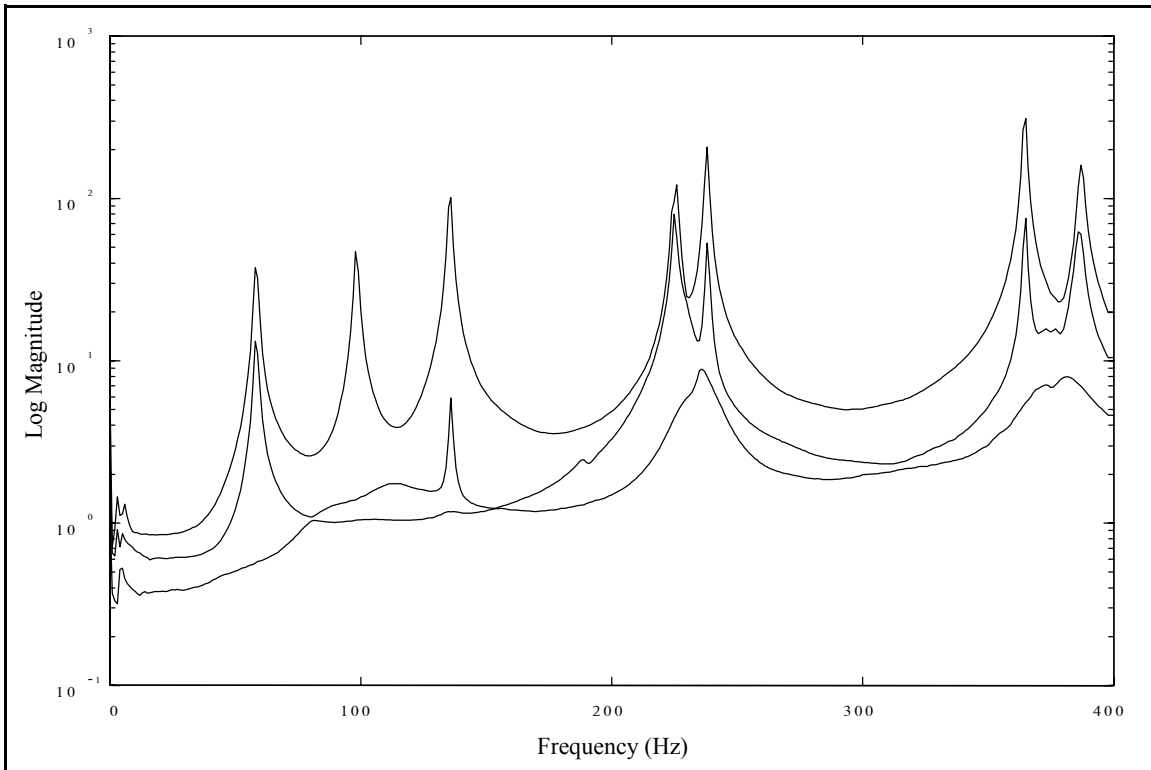
Figure 4-12(a). Circular Plate CMIF, Complex Calculation.
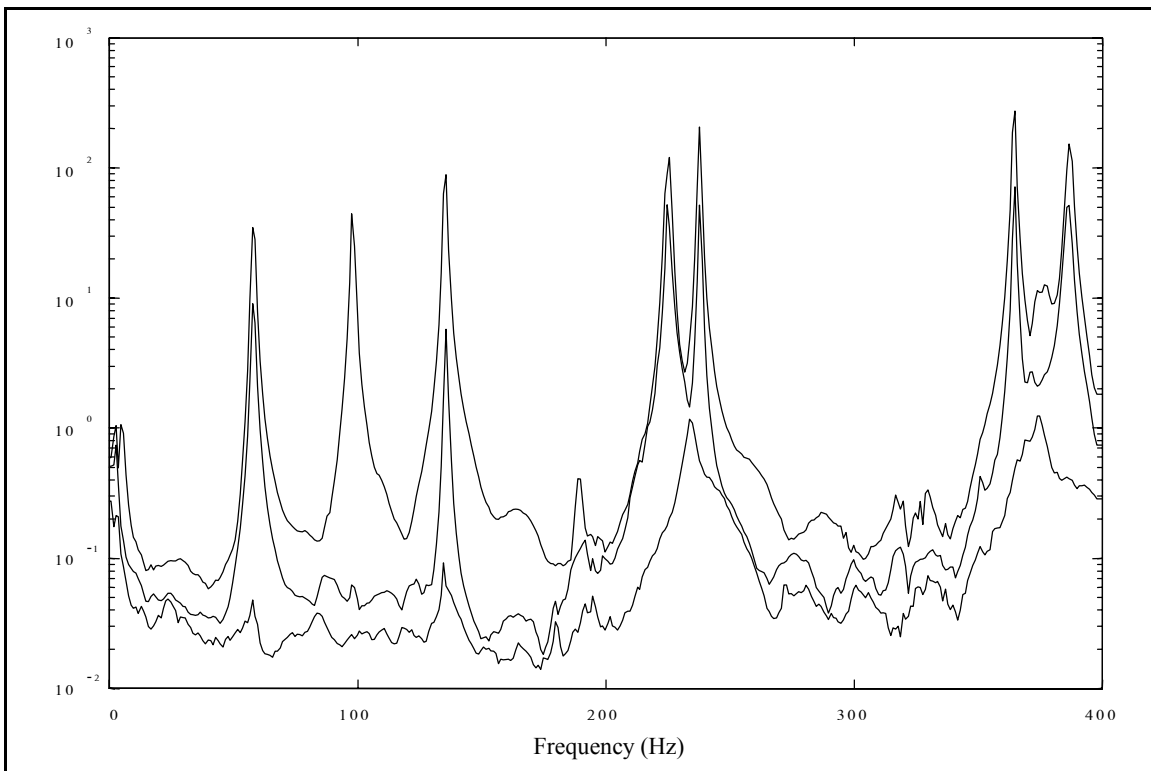
Figure 4-12(b). Circular Plate CMIF, Quadrature Calculation.

149
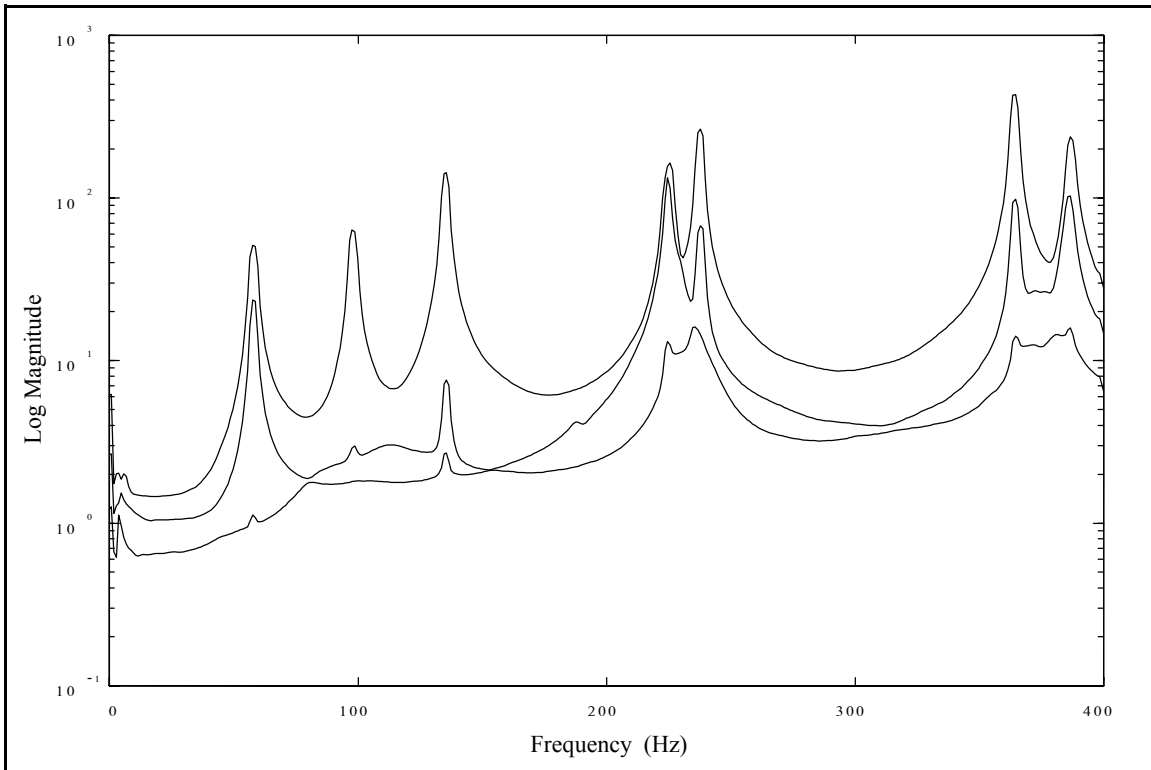
Figure 4-13(a). Circular Plate CMIF, Overlap 1 Spectral Line, Complex Calculation.
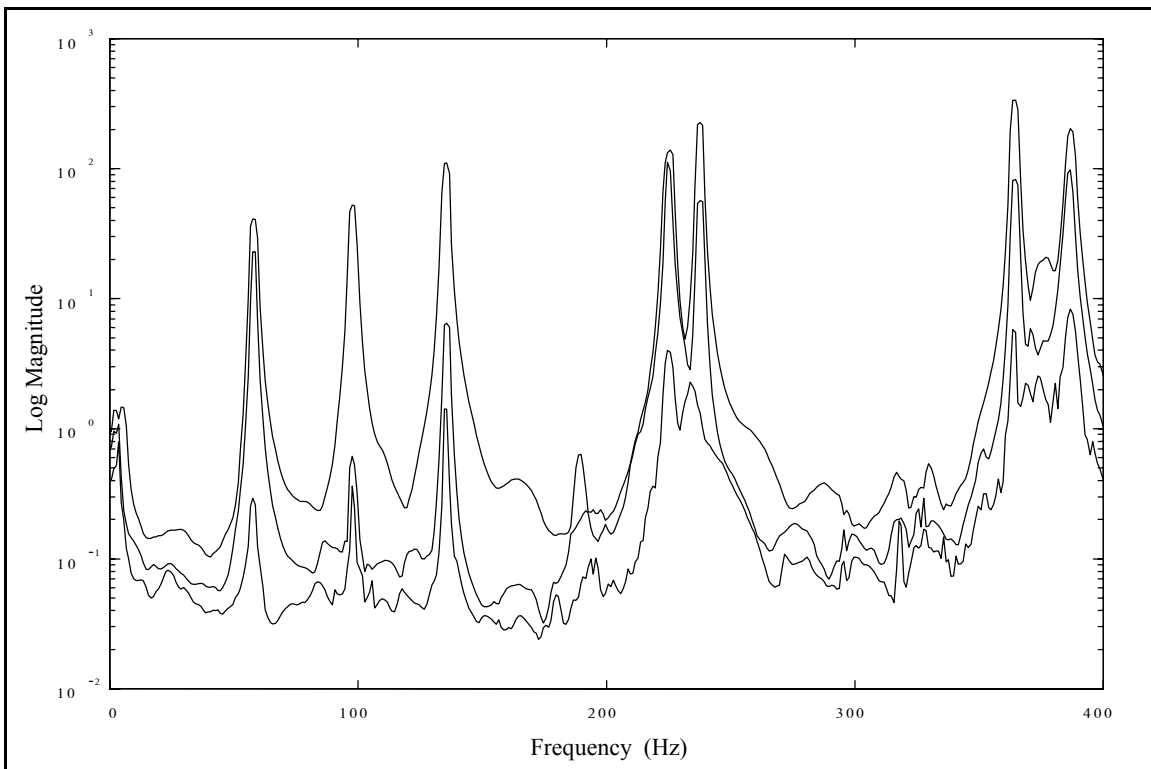
Figure 4-13(b). Circular Plate CMIF, Overlap 1 Spectral Line, Quadrature Calculation.

150
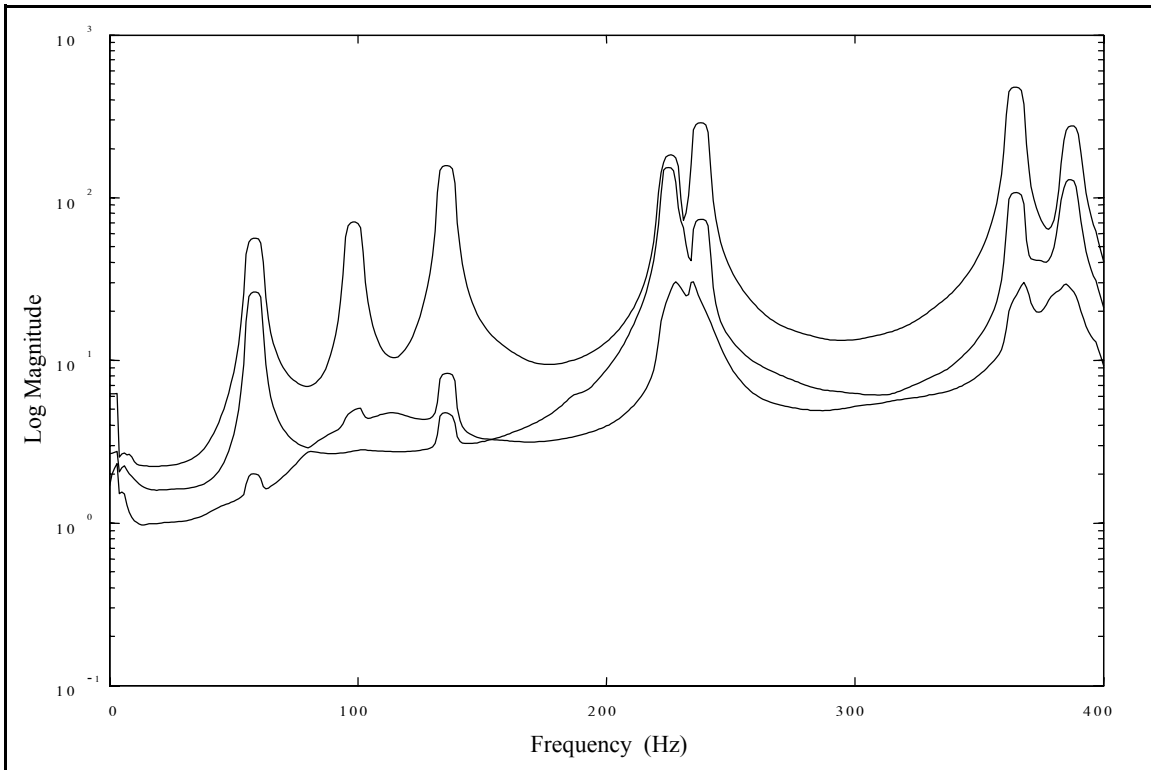
Figure 4-14(a). Circular Plate CMIF, Overlap 3 Spectral Lines, Complex Calculation.
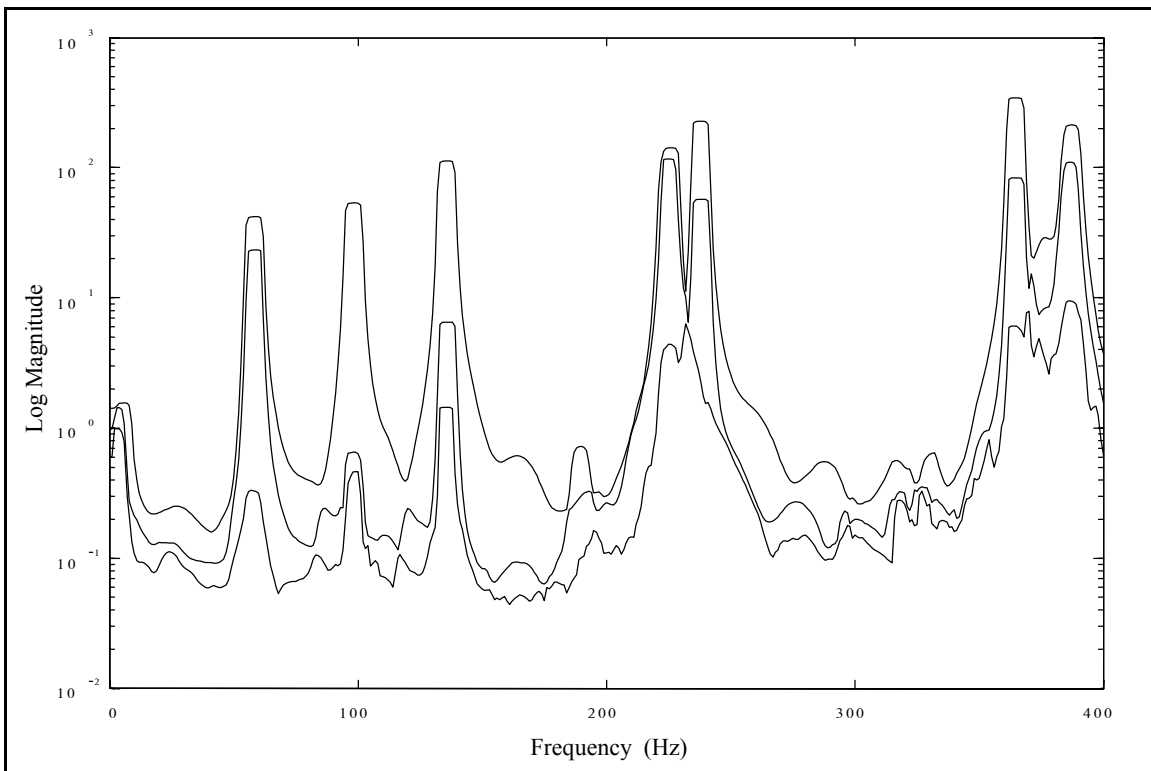
Figure 4-14(b). Circular Plate CMIF, Overlap 3 Spectral Lines, Quadrature Calculation.

151
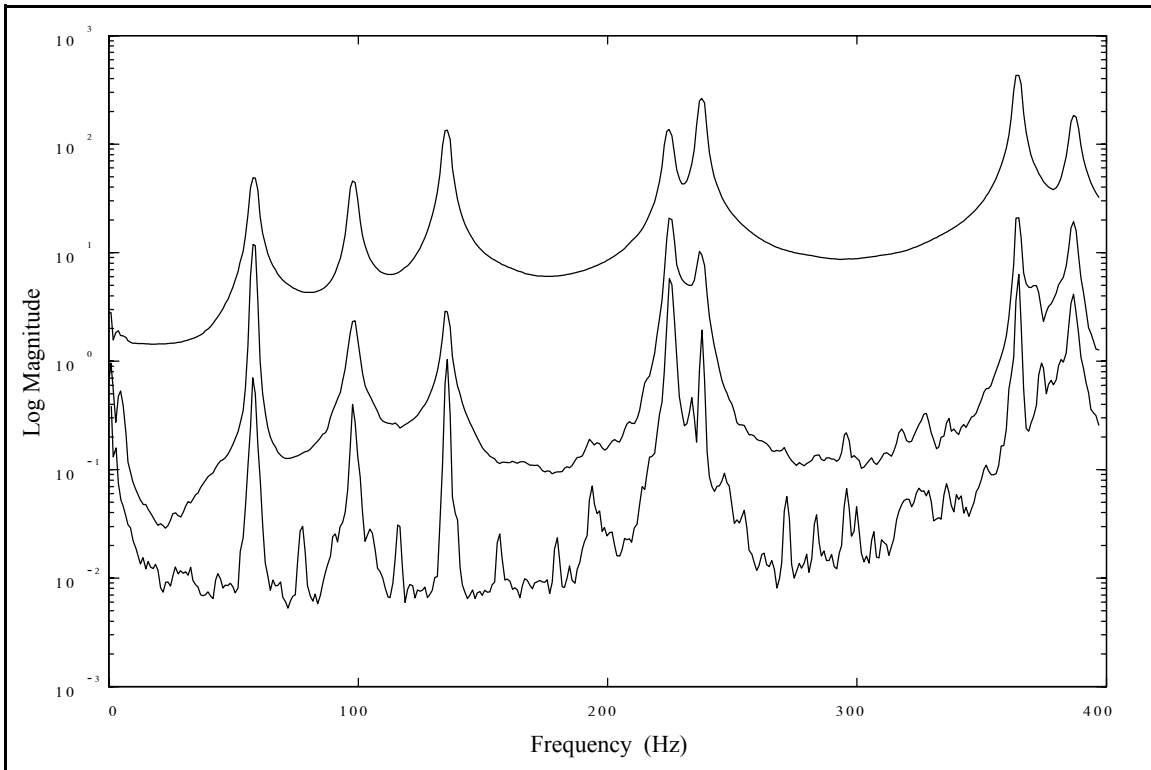
Figure 4-15(a). Circular Plate CMIF, Overlap 1 Spectral Line, 2 Simulated References, Complex Calculation.
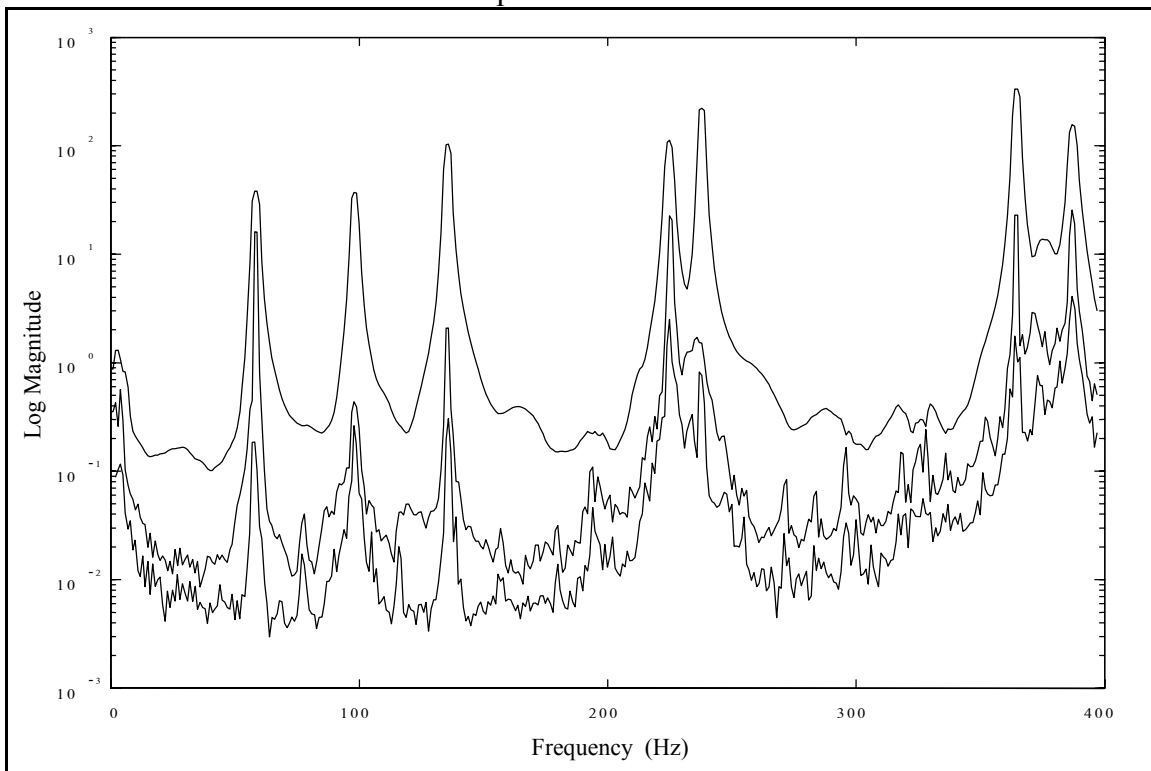
Figure 4-15(b). Circular Plate CMIF, Overlap 1 Spectral Line, 2 Simulated References, Quadrature Calculation.

152

4.3   Machine Tool

A small machine tool lathe was tested as an exercise of a typical application of the MRIT method for troubleshooting or field testing. The test definition is listed in Table 4-7, and the test object is pictured in Figure 4-16. The lathe was tested in situ, no support fixturing was necessary. To minimize nonlinearities due to clearances, a static preload was applied by inserting a soft rubber wedge between the tool holder and workpiece. The test geometry and reference locations are shown in Figure 4-17. The testing time was approximately eight hours; including equipment setup, pretest measurements, calibration, geometry layout, data acquisition, and preliminary analysis. Two people can conduct this type of test efficiently; one to do the impacting and one to operate the data acquisition software.

This "real-world" system is much more complicated than a simple circular plate and is also much more heavily damped. These properties are evident in the CMIFs of this data set, which are shown in Figure 4-18. The CMIF curves are not very smooth, and the peaks are broad, rounded, and not clearly distinct, yet usable mode shapes, frequencies and damping can be extracted from this type of data.

No. References	6
No. Impact Locations	112
Data Acquisition System	PC with multi-channel front-end hardware
Impactor	1-lb impact hammer
Reference Transducers	(6) accelerometers (100,1000 mV/g)
Frequency Range	0 - 400 Hz at .5 Hz

Table 4-7. Machine Tool Test Definition.
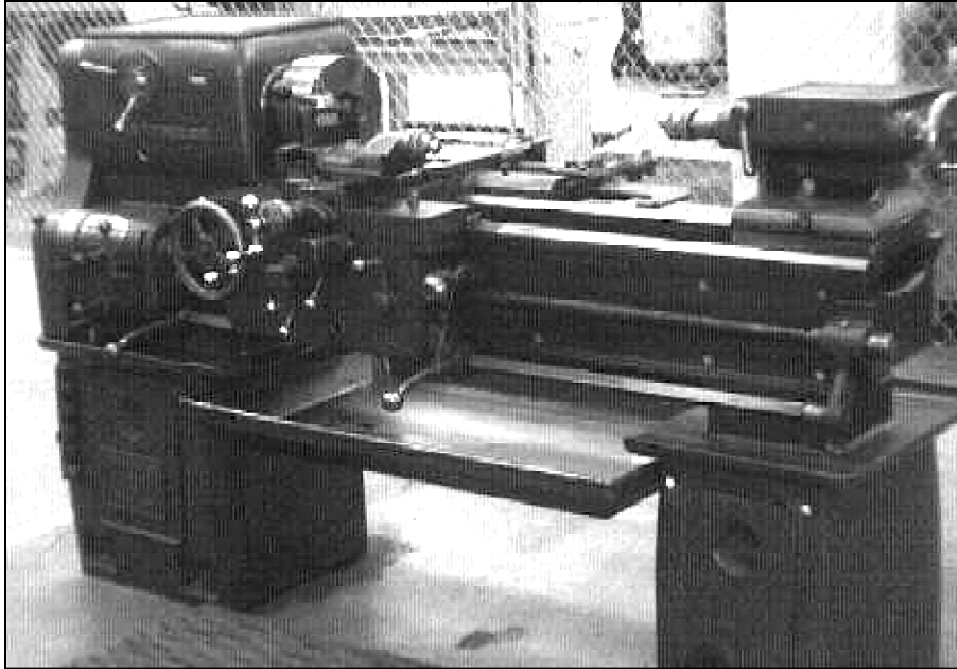
Figure 4-16. Machine Tool Test Case.

REFERENCES	
20	$-x$
19	z
16	$-x$
16	z
33	$-x$
25	$-x$

Overall Dimensions: 80(L) x 48(H) x 24(W) in.
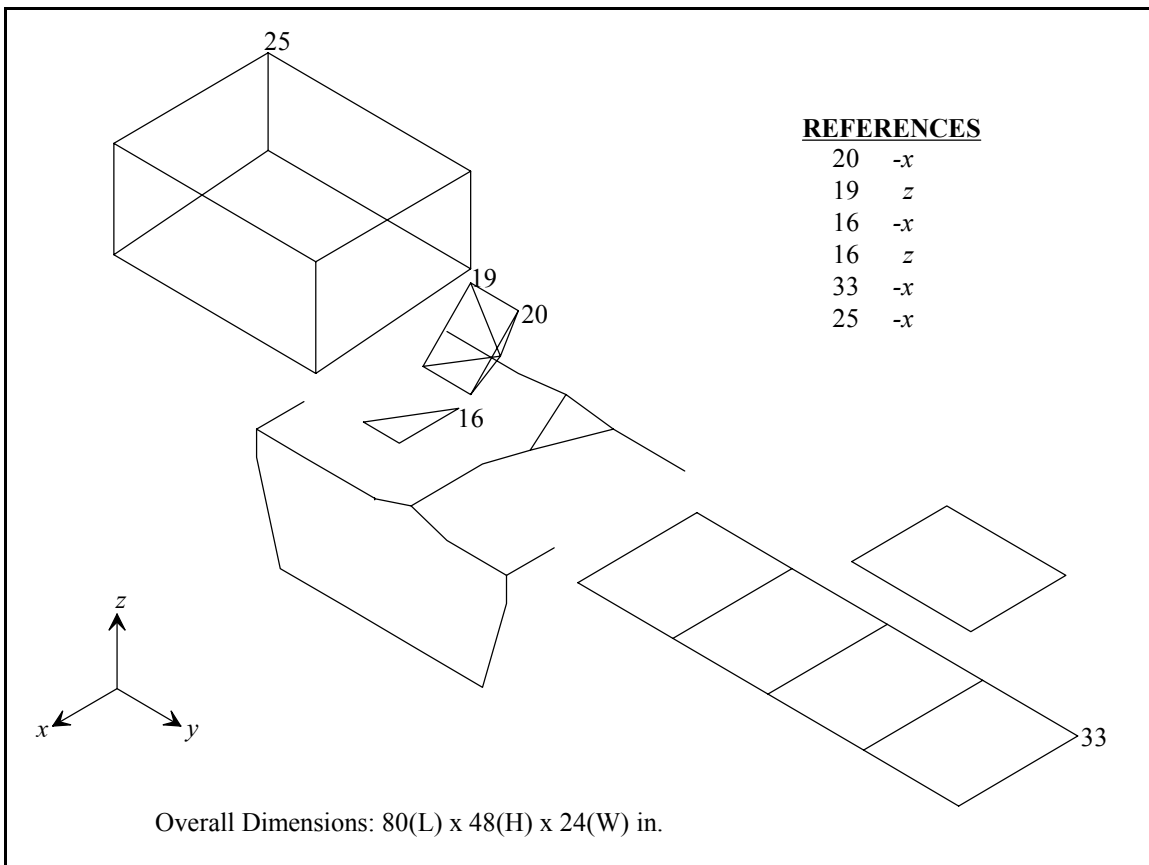
Figure 4-17. Machine Tool Geometry and Reference Locations.
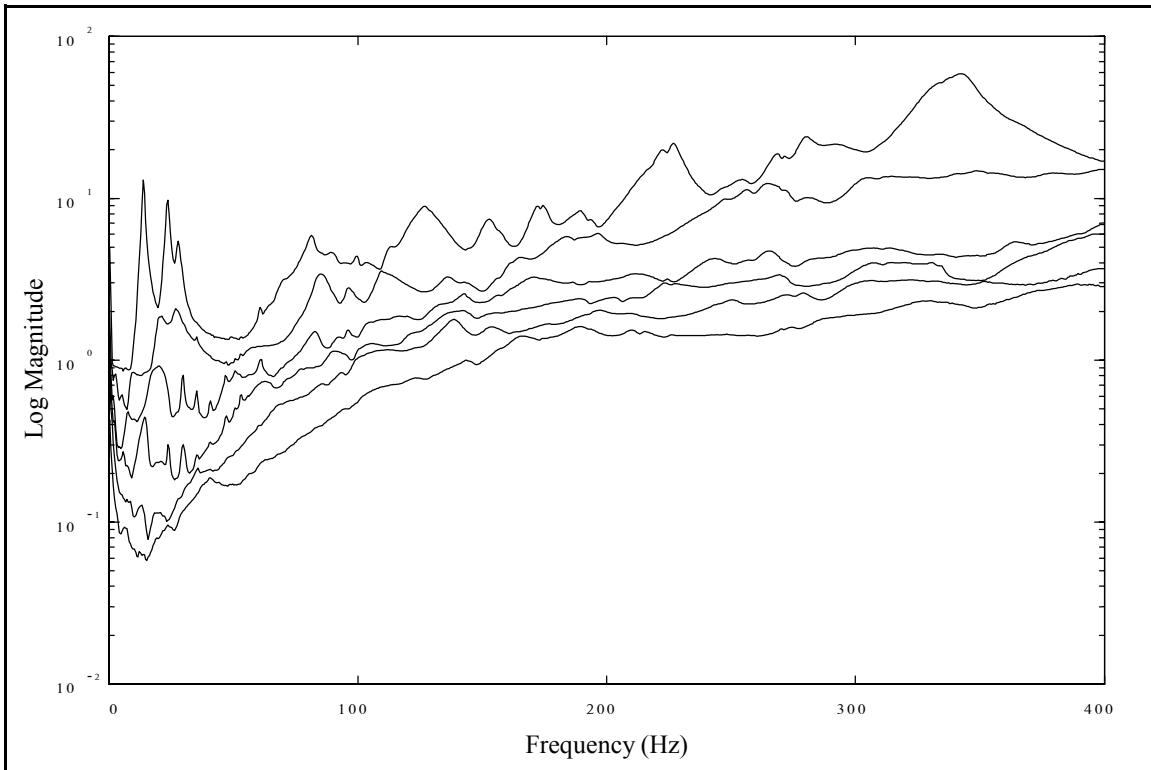
Figure 4-18(a). Machine Tool CMIF, Complex Calculation.
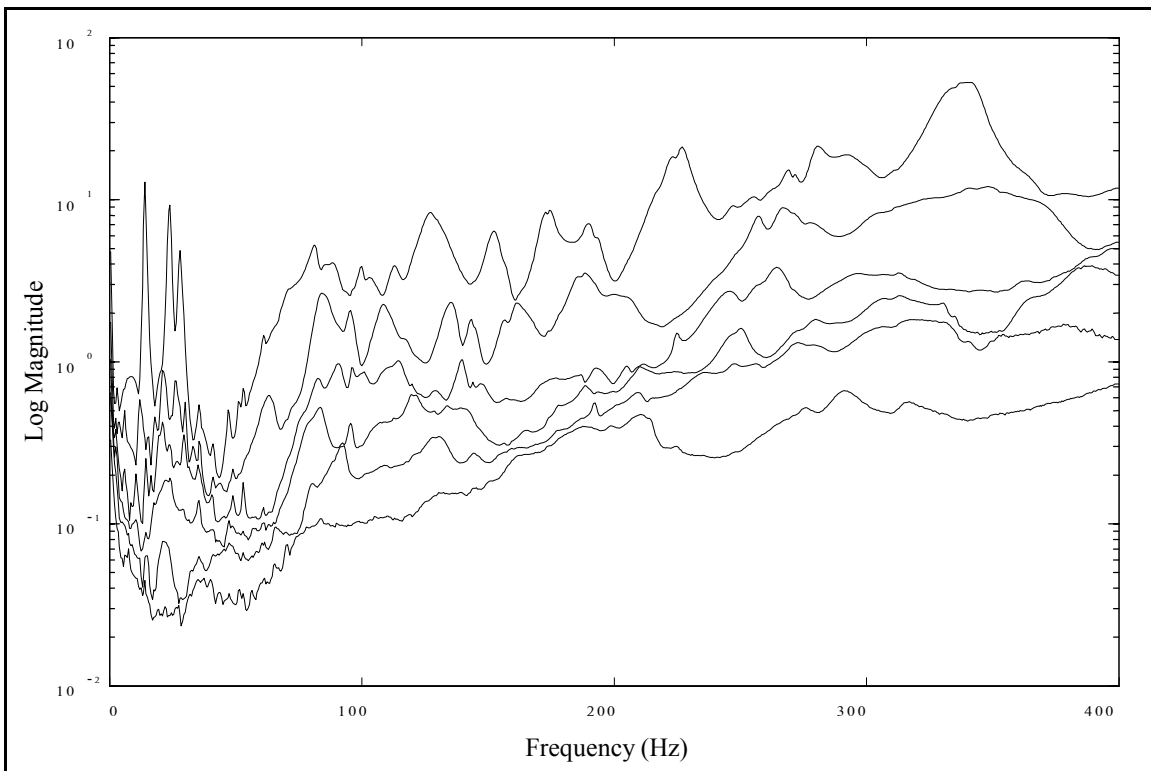
Figure 4-18(b). Machine Tool CMIF, Quadrature Calculation.

155

4.4 Composite Box Beams

A series of MRIT modal tests was conducted on seventeen composite box beams of varying composition and construction. The purpose of the tests was not for trouble-shooting or field testing, but for finite element model verification. The beams were made of lightweight composite materials and consisted of a flat top-plate and a U-shaped channel which were joined with adhesive. The beams were one meter in length and weighed about four pounds. The test geometry and reference locations are shown in Figure 4-19. The beam was divided into eleven equally spaced sections, with eight positions around the perimeter of each section. The test definition is listed in Table 4-8, and the test setup is shown in Figure 4-20. The beams were suspended on nylon fishing line between two pairs of vertical supports to simulate a free-free boundary condition

The first six beams were tested with a PC-based acquisition system, the rest were tested with an HP-35670A analyzer and the MRIT I-BASIC program which was introduced in Section 2.5. Using the PC system, the time to conduct a test was about 7 hours. Using the MRIT I-BASIC system, the test time was reduced to about 4 hours, with 3-1/2 hours for collecting measurements and 1/2 hour for transferring data files. The primary factor in the time savings was the input channel autoranging process. The point number incre-menting, data filename updating, and Test-Log file writing also reduced the test time.

Several sine-sweep measurements were also conducted on each beam to evaluate its linearity. However, attaching a shaker to the beam had a significant influence on the dynamics of the system. This condition is revealed by comparing the driving point FRFs

from the sine-sweeps and the impact test. Figure 4-22 compares the (111,*z*) and (15,*y*)

driving point FRFs between the sine-sweep and the impact test.[†] The FRFs exhibit

significant differences that are not just a shift of frequencies, but also a substantial change

of the dynamic characteristics of the system. Figure 4-23(a) compares the driving point

FRFs for the impact test, and the peaks of these two FRFs correlate as expected. Figure

4-23(b) compares the driving point FRFs for the sine-sweeps, and these measurements

exhibit a significant shift of the peaks. Since only one shaker was connected to the beam

at a time for the sine-sweeps, the dynamics of the beam must also be dependent on the

location of the shaker.

Several factors contribute to the observed phenomenon. The beams are lightweight,

which means that any mass loading will possibly have a substantial effect. The mass

loading effect of the small accelerometers used for the impact tests are consistent for all

the measurements. However, the mass loading effects of the load cell is dependent on the

direction of the measurements. The beams are rather flexible, especially at the ends on

the flange of the top-plate. The effects of the load cell in the direction of the measure-

ment are minimized, but an inertial force is generated by the mass of the load cell in the

directions transverse to the measured direction. The conclusion of these measurements is

that testing the beams with shaker inputs is not suitable, and impact testing is the appro-

priate method for these beams.

---

† The data set from the last beam is used in this section. All beams exhibited similar behavior.

As discussed in Section 3.4.2, impacting in three directions at all points on the beam was not possible (e.g., points along the center line of the top-plate in the y-direction). Of the 264 potential DOFs, 148 were measurable, which are shown in Figure 4-21. The slave DOF method is a suitable vector completion technique for this case. The measured and completed modes shapes of the first vertical and horizontal bending modes are shown in Figures 4-24 and 4-25, respectively. (Note that the top-plate has been artificially separated from the U-channel to clarify displaying of the mode shapes.) For the vertical mode, the z-direction DOFs at position 8 were determined from the z-direction DOFs at position 7, and the z-direction DOFs at position 4 were determined from the z-direction DOFs at position 5. For the horizontal mode, the y-direction DOFs at position 2 were determined from the y-direction DOFs at positions 1 and 3, and the y-direction DOFs at position 6 were determined from the y-direction DOFs at position 5 and 7.

The complex and quadrature calculation CMIFs of this data set are shown in Figure 4-26. For the beam tests, CMIF was used as a preliminary procedure, which was followed with an MDOF parameter estimation method.

No. References	3
No. Impact Locations	148
Data Acquisition System	PC with multi-channel front-end hardware or 4-channel programmable analyzer
Impactor	lightweight impact hammer
Reference Transducers	(3) lightweight accelerometers (10 mV/g)
Frequency Range	200 - 1000 Hz at 1 Hz

Table 4-8. Composite Box Beam Test Definition.
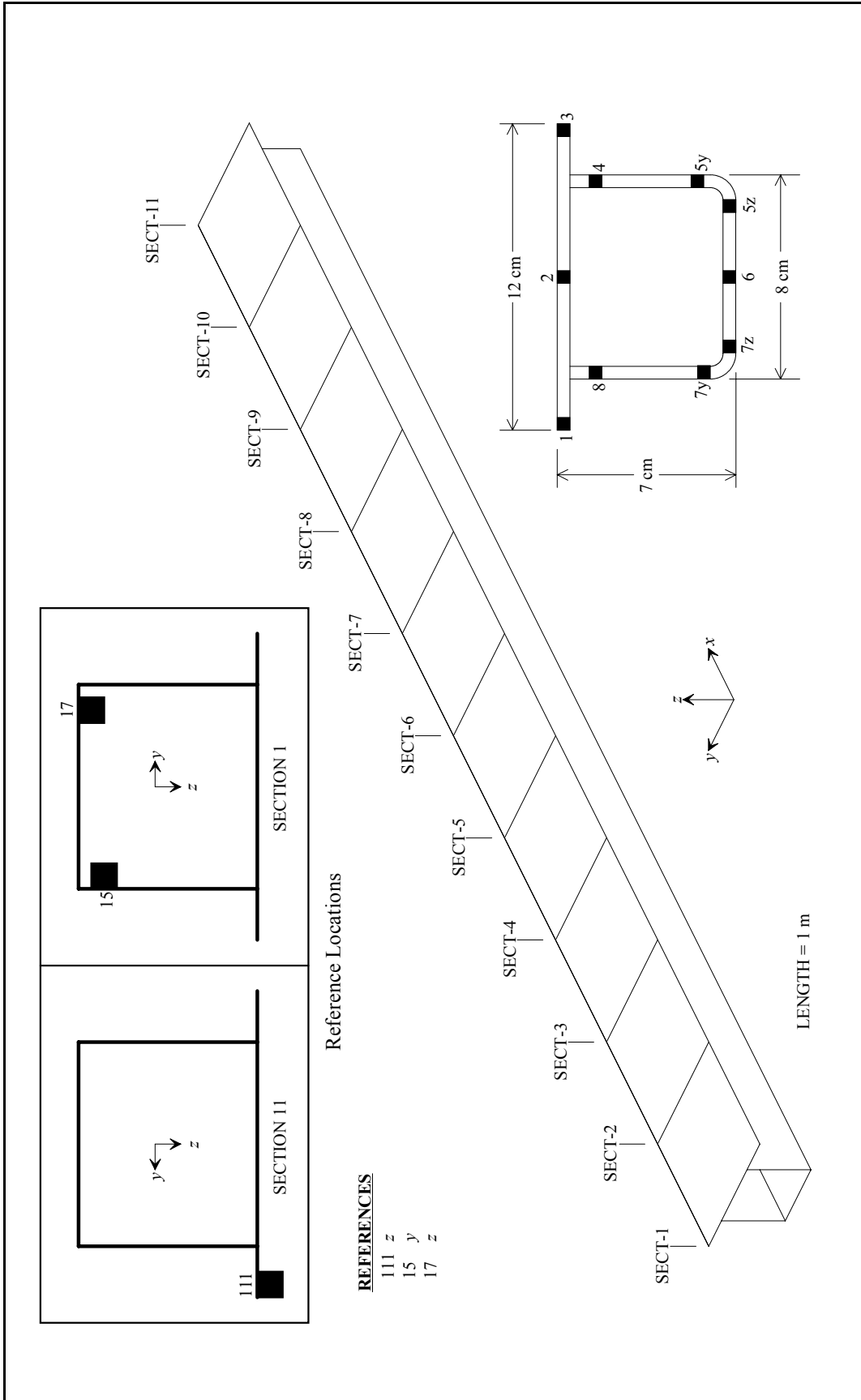
Figure 4-19. Composite Box Beam Geometry and Reference Locations.

159
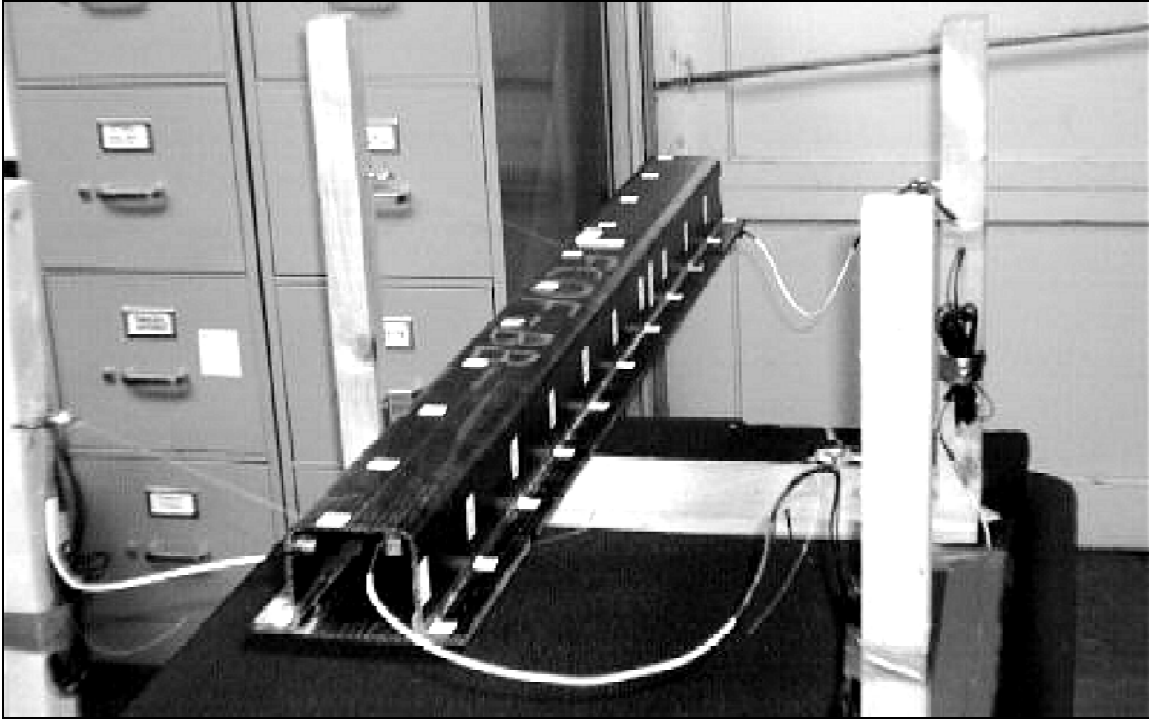
Figure 4-20. Composite Box Beams Test Case.
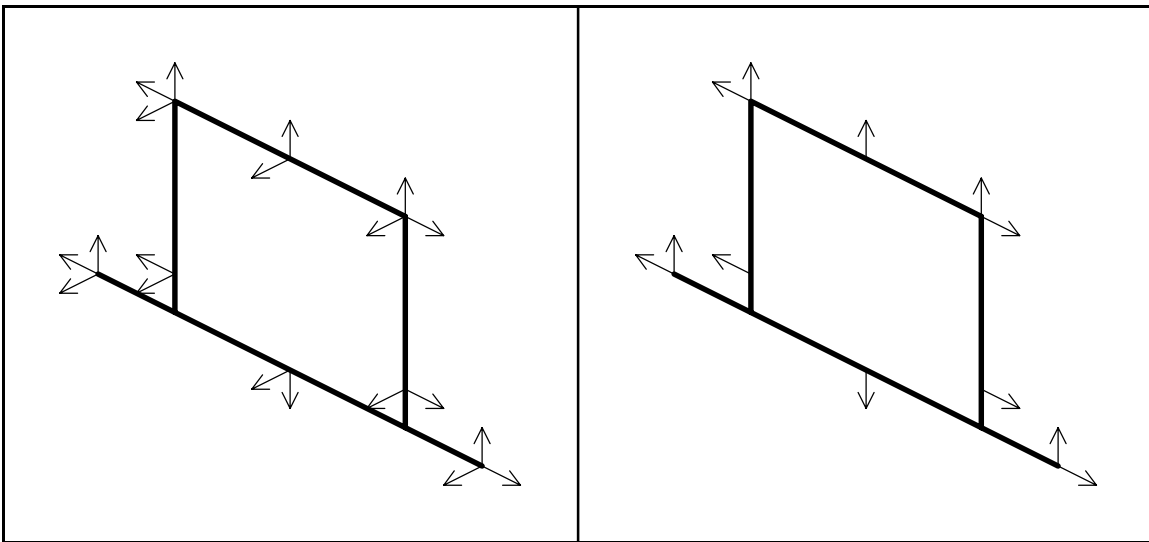
Figure 4-21(a). Measurable DOFs for Sections 1 and 11.

Figure 4-21(b). Measurable DOFs for Sections 2 to 10.
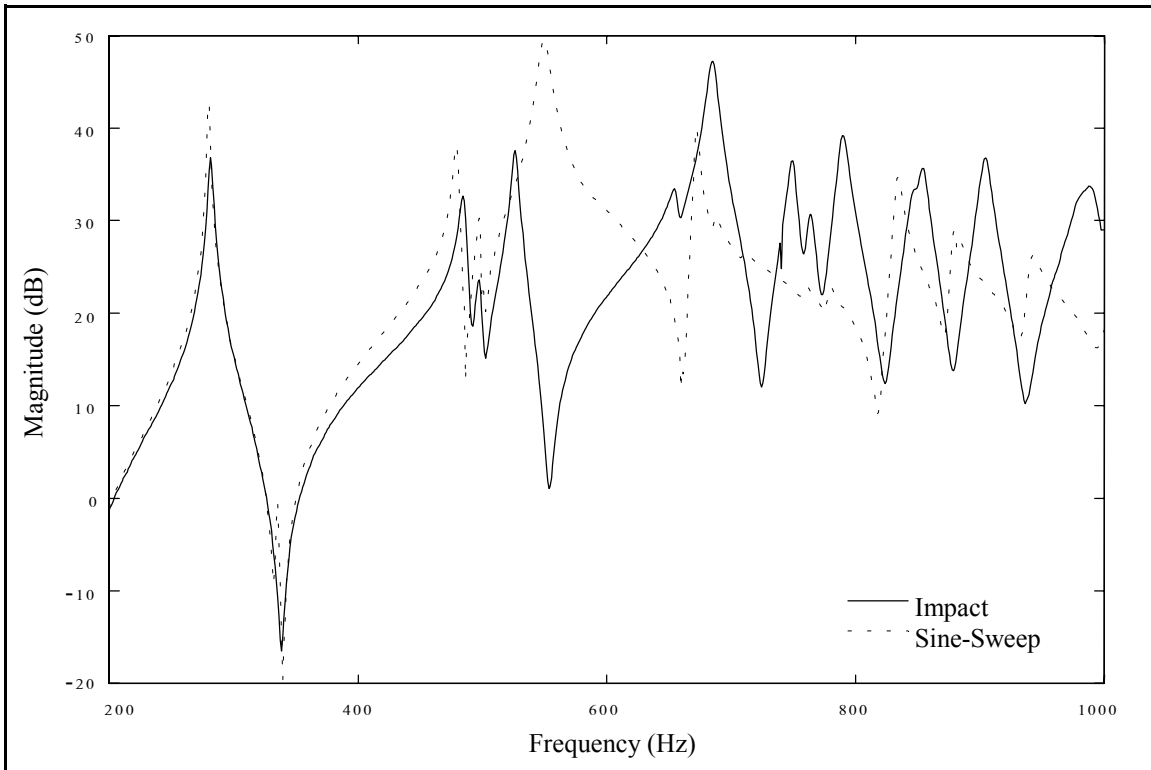
Figure 4-22(a). Impact and Sine-Sweep Driving Point FRFs at (111,*z*).
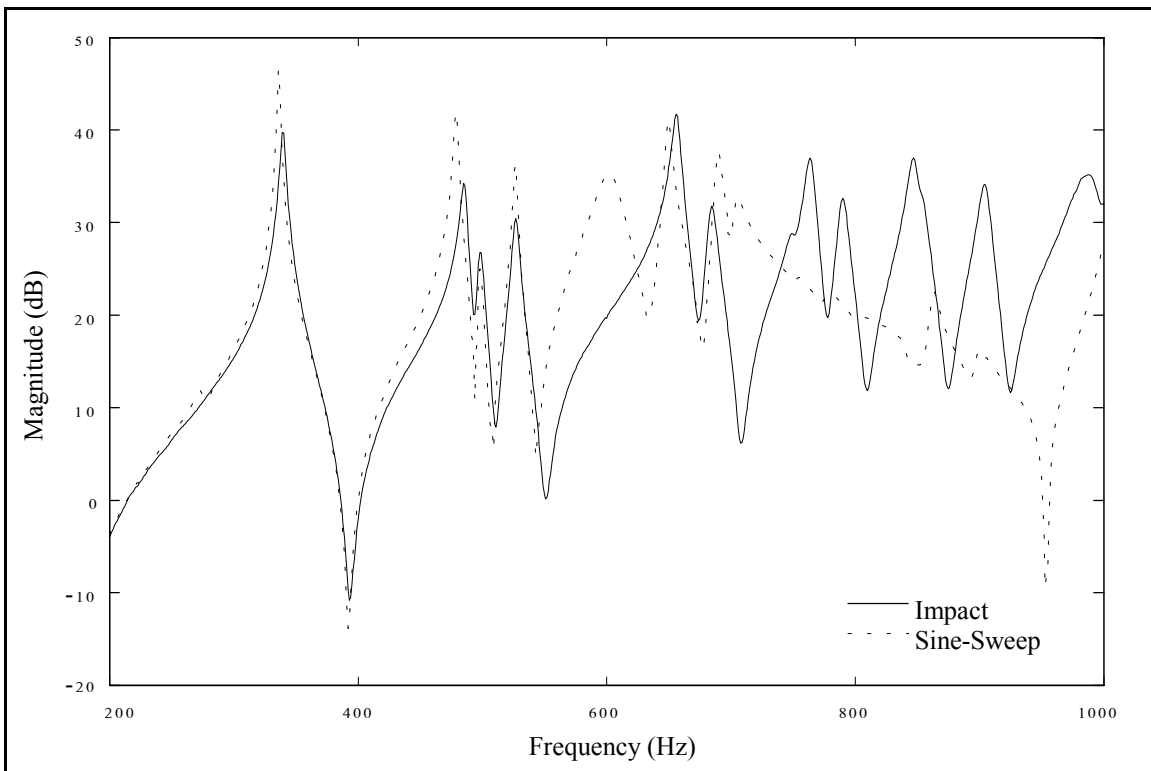
Figure 4-22(b). Impact and Sine-Sweep Driving Point FRFs at (15,*y*).

161
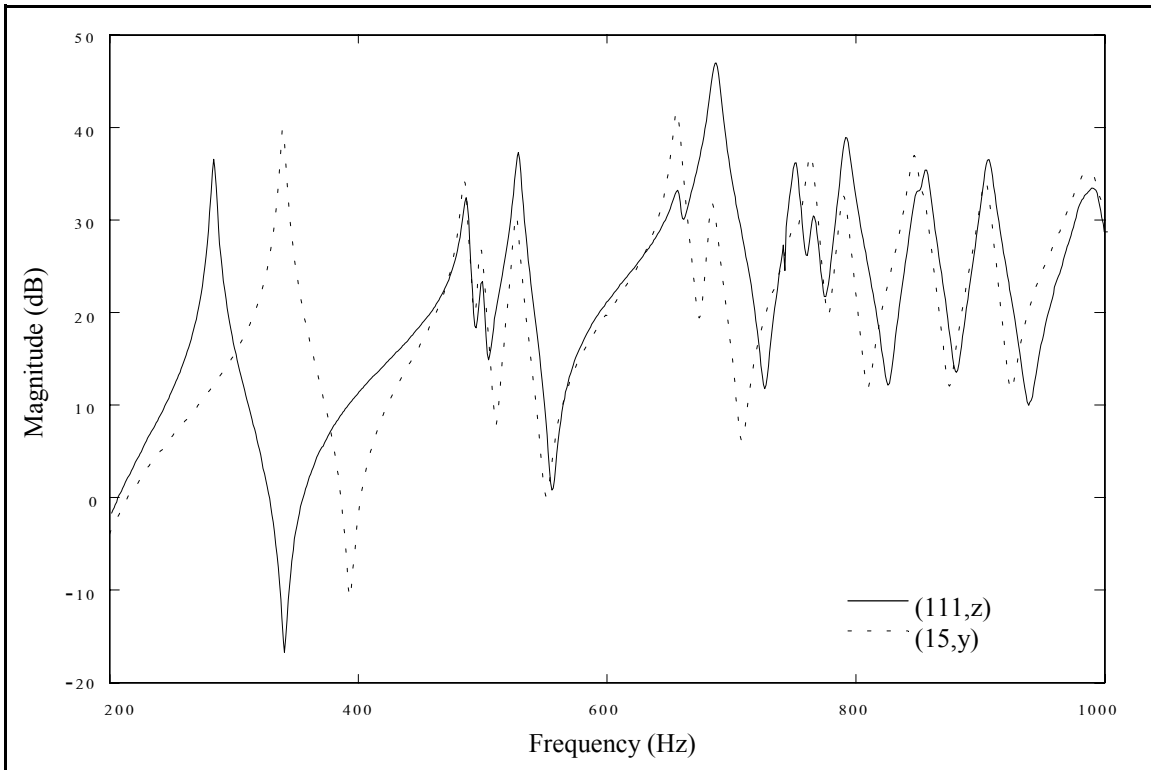
Figure 4-23(a). Impact Driving Point FRFs at (111,z) and (15,*y*).
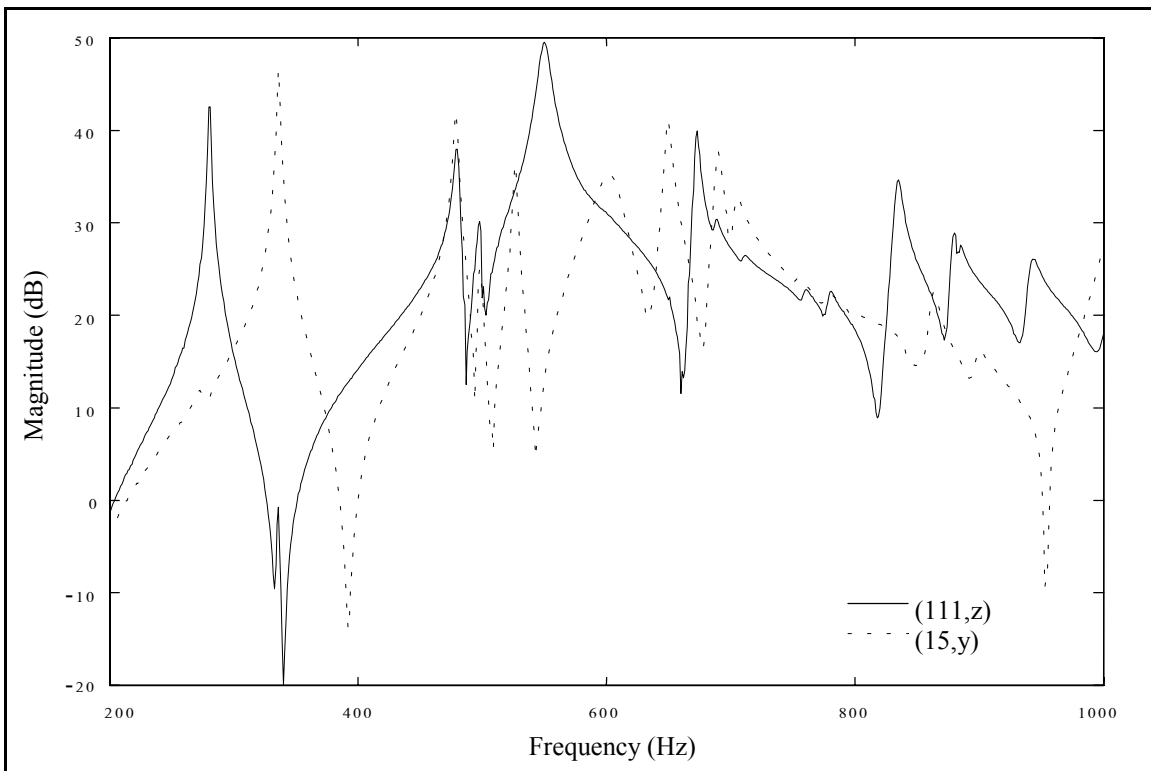
Figure 4-23(b). Sine-Sweep Driving Point FRFs at (111,z) and (15,*y*).

162
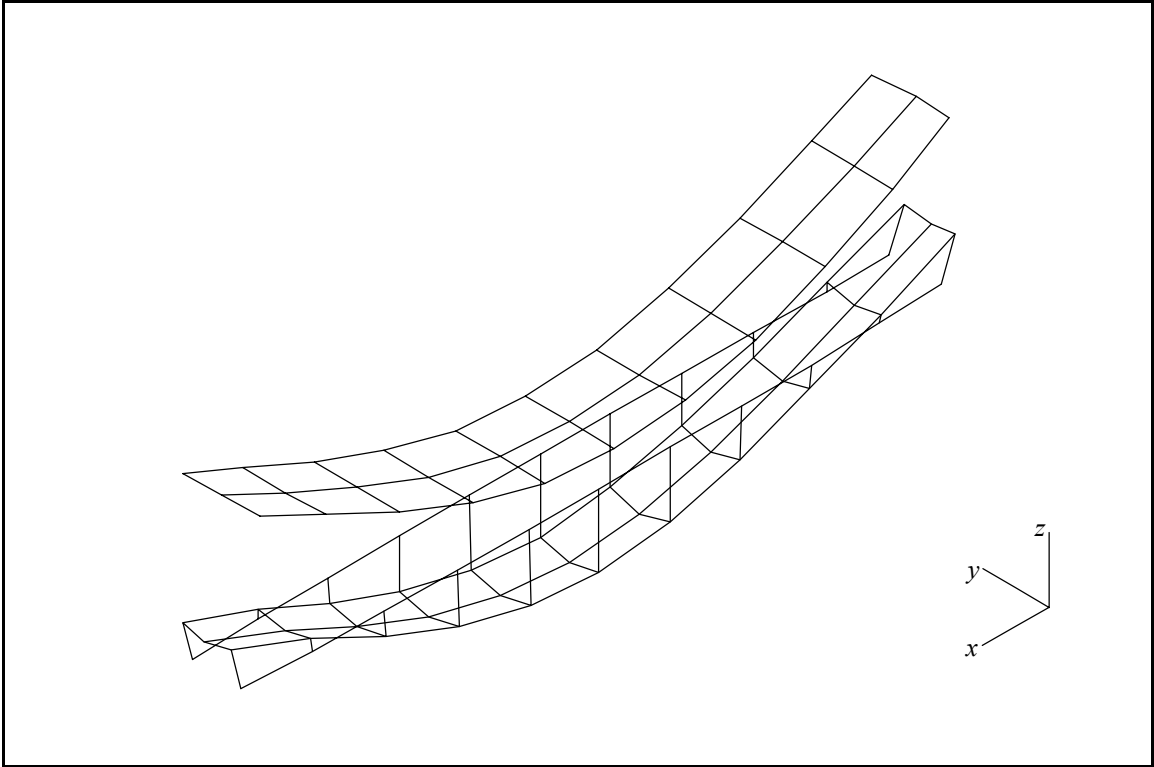
Figure 4-24(a). Composite Box Beams Measured Vertical Bending Mode Shape.
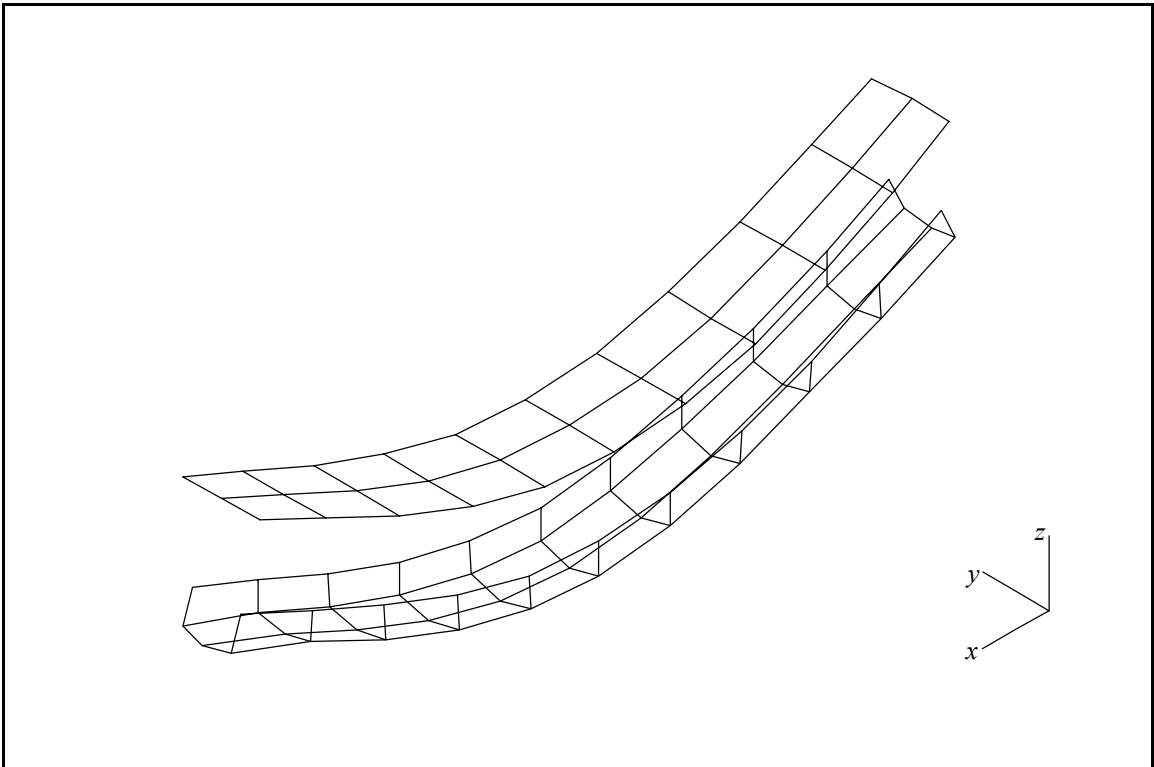
Figure 4-24(b). Composite Box Beams Completed Vertical Bending Mode Shape.

163
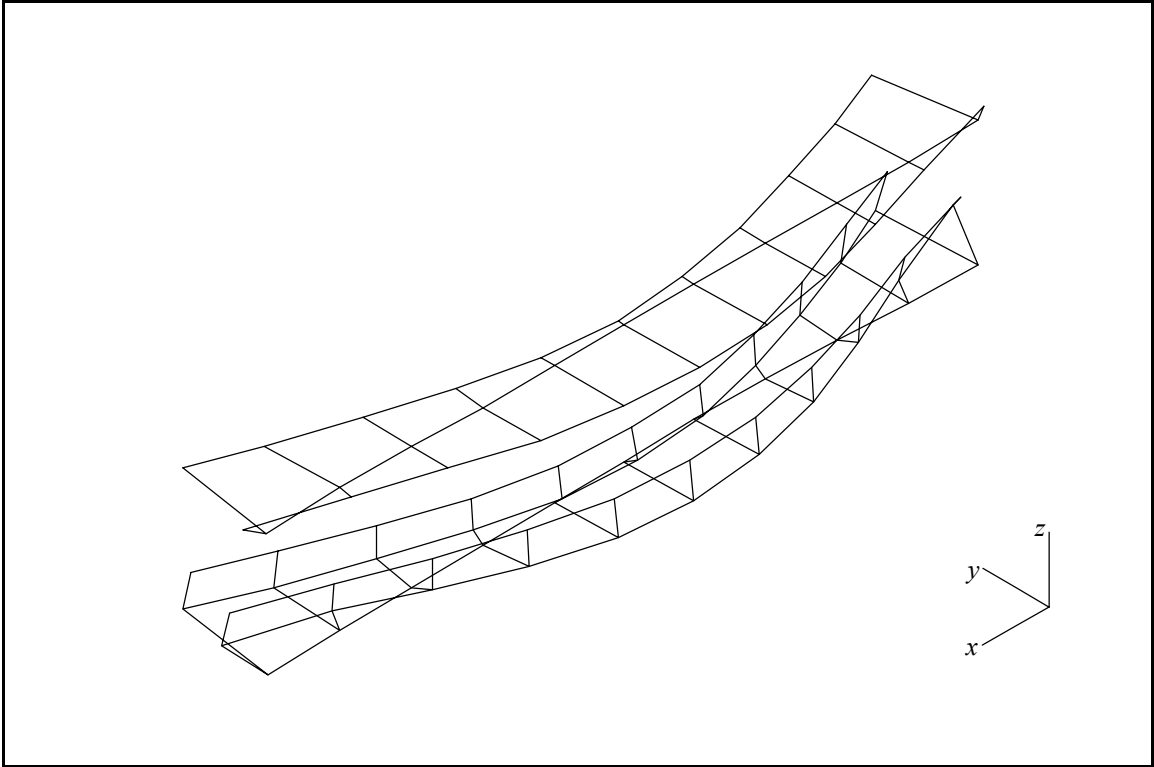
Figure 4-25(a). Composite Box Beams Measured Horizontal Bending Mode Shape.
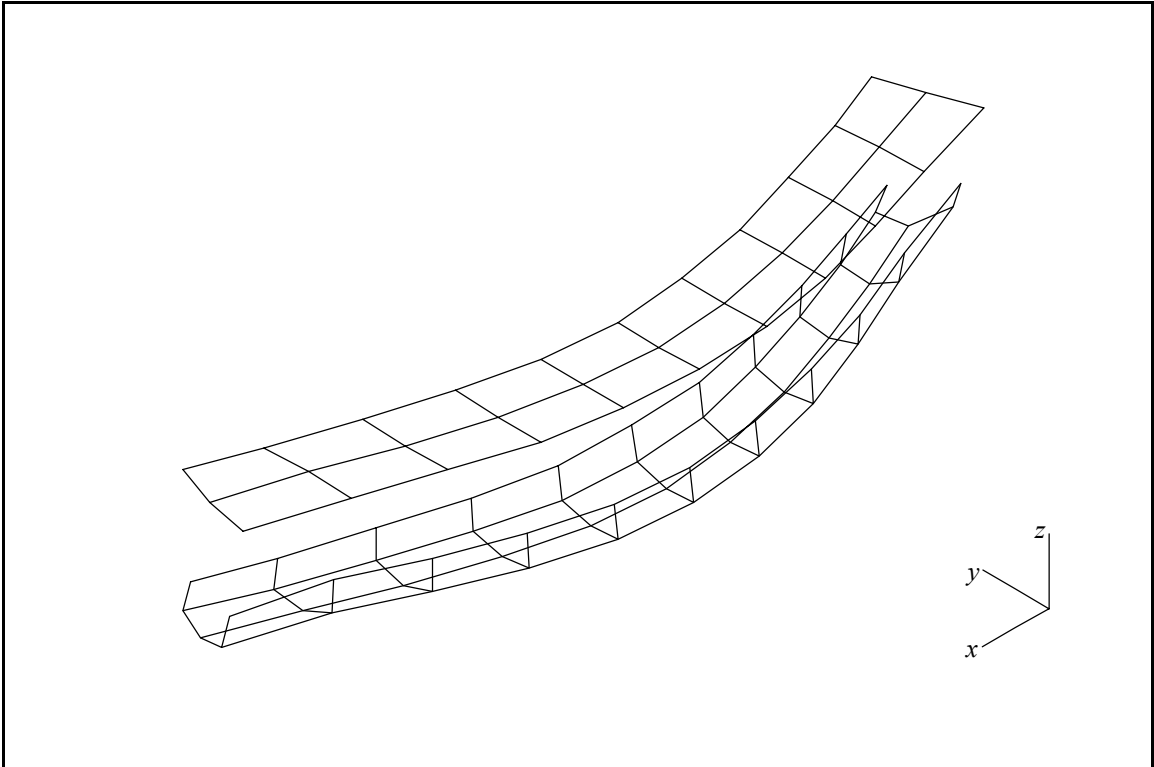
Figure 4-25(b). Composite Box Beams Completed Horizontal Bending Mode Shape.

164
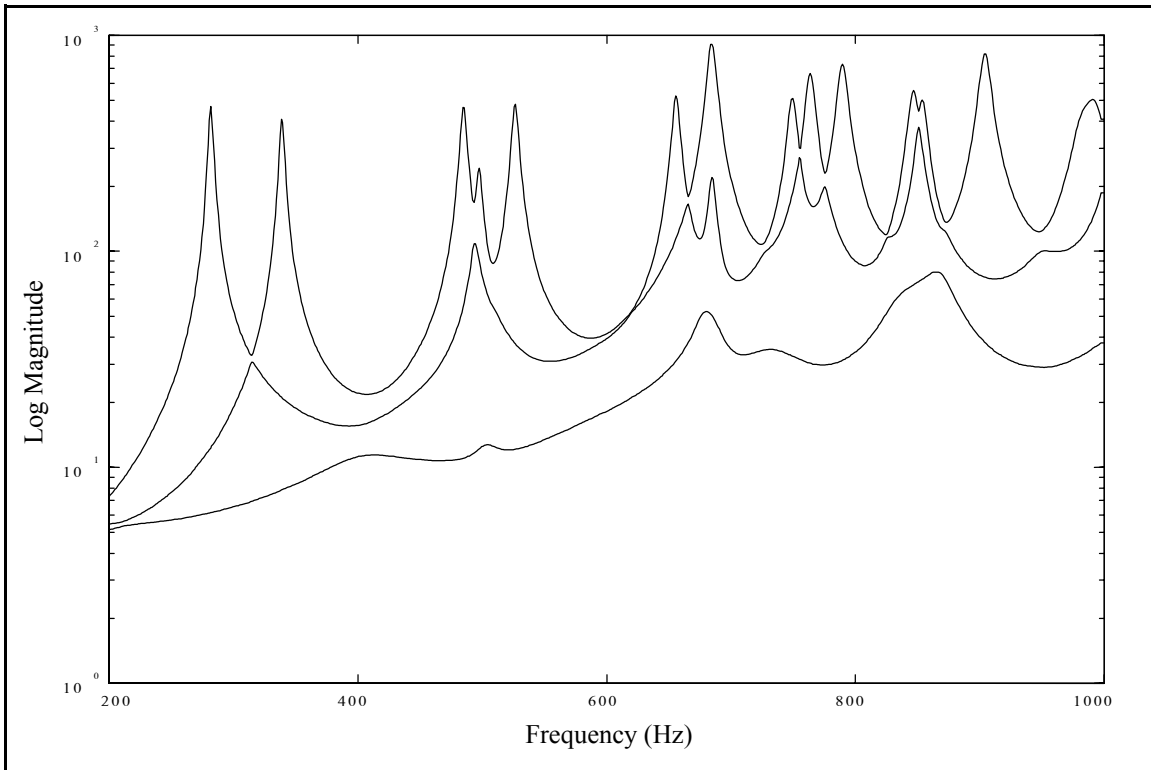
Figure 4-26(a). Composite Box Beams CMIF, Complex Calculation.
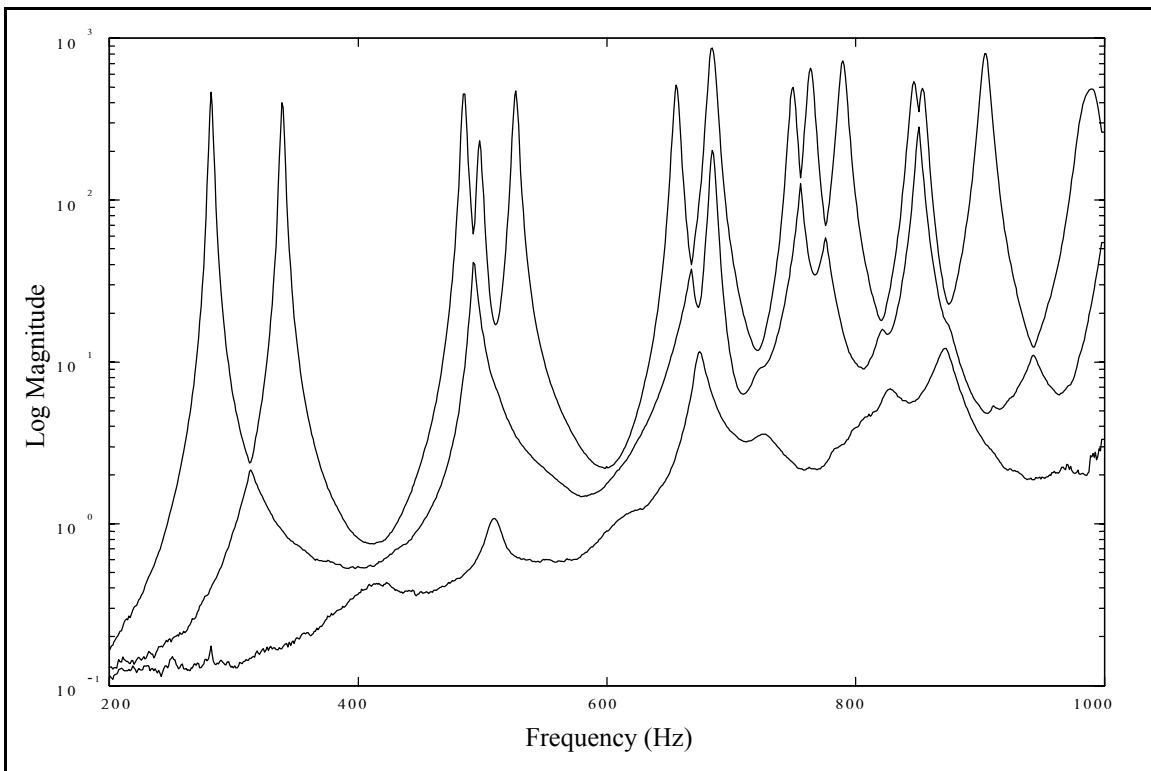
Figure 4-26(b). Composite Box Beams CMIF, Quadrature Calculation.

165

4.5   Squeeze Film Damper Test Rig

The squeeze film damper (SFD) test rig consists of an electric motor, a coupling, a spindle onto which a bearing is installed, an instrumentation ring, a steel housing structure, and a concrete base. The front view of the SFD test rig pictured in Figure 4-27 shows the housing, spindle tip, and instrumentation ring. An MRIT modal test was conducted on these components of the system for the purpose of troubleshooting, the test definition is listed in Table 4-9. The motor, spindle, and housing are affixed to the base, and the rig assembly was test in-situ, but a bearing was not installed during the test. The test geometry and reference locations are shown in Figure 4-28.

The instrumentation ring has a 12-inch outer diameter and an 8-inch inner diameter and surrounds the spindle tip. There are sixteen test geometry points equally spaced around the circumference of the ring. Impacting the instrumentation ring in the radial direction was not possible because of the limited space between the ring and the spindle tip. The components could not be disassembled for testing because the modes of the complete system were of interest. To measure the mode shapes of the instrumentation ring, impacts were made normal to the face of the ring (in the axial or z-direction) with the impact hammer and on the inner edge of the ring in a skewed direction with the Modal Punch, as indicated in Figure 4-29. In order to impact on the edge of the ring, a V-shaped groove was machined into a standard, steel impact tip. This groove was then positioned on the inner edge of the ring, and the tip of the spindle aligned the angle of the input. The tangential components of the mode shapes were still unmeasurable. The radial component could be calculated from the axial and skewed components using the coordinate

166

transformation method described in Section 3.4.1. The transformation, which is derived from Equations 3-34 and 3-35, is nonorthogonal and is determined from the geometry, as shown in Figure 4-30.

$$
\left\{ \begin{array}{c} \Psi_a \\ \Psi_s \end{array} \right\} = \left[\begin{array}{cc} 1 & 0 \\ \cos\theta & \sin\theta \end{array} \right] \left\{ \begin{array}{c} \Psi_a \\ \Psi_r \end{array} \right\} \quad \text{and} \quad \left\{ \begin{array}{c} \Psi_a \\ \Psi_r \end{array} \right\} = \left[\begin{array}{cc} 1 & 0 \\ \frac{-1}{\tan\theta} & \frac{1}{\sin\theta} \end{array} \right] \left\{ \begin{array}{c} \Psi_a \\ \Psi_s \end{array} \right\} \tag{4-2}
$$

where, $\quad \Psi_1 = \Psi_a \qquad\qquad \Psi_x = \Psi_a \qquad\qquad \theta = 0$

$\qquad\qquad\qquad \Psi_2 = \Psi_s \qquad\qquad \Psi_y = \Psi_r \qquad\qquad \theta_2 = \theta = 60°$

The CMIFs of this data set are shown in Figure 4-31. In Figure 4-31(a), the first CMIF curve is predominantly two peaks with very high relative magnitudes, and the other modes have peaks in the second CMIF curve. In Figure 4-31(b), the quadrature calculation has changed the relative magnitudes of the peaks such that more modes have peaks in the first CMIF curve.

No. References	5
No. Impact Locations	66
Data Acquisition System	PC with multi-channel front-end hardware
Impactor	1-lb impact hammer and Modal Punch
Reference Transducers	(5) accelerometers (10,100 mV/g)
Frequency Range	0 - 3200 Hz at 8 Hz

Table 4-9. Squeeze Film Damper Rig Test Definition.

Figure 4-27. Squeeze Film Damper Rig Test Case.

REFERENCES

1	*y*
5	*x*
5	*z*
17	*y*
18	*x*

17 HOUSING

RING

1

SPINDLE

18

5

y

z   *x*

Note: The housing is 27 x 18 inches.
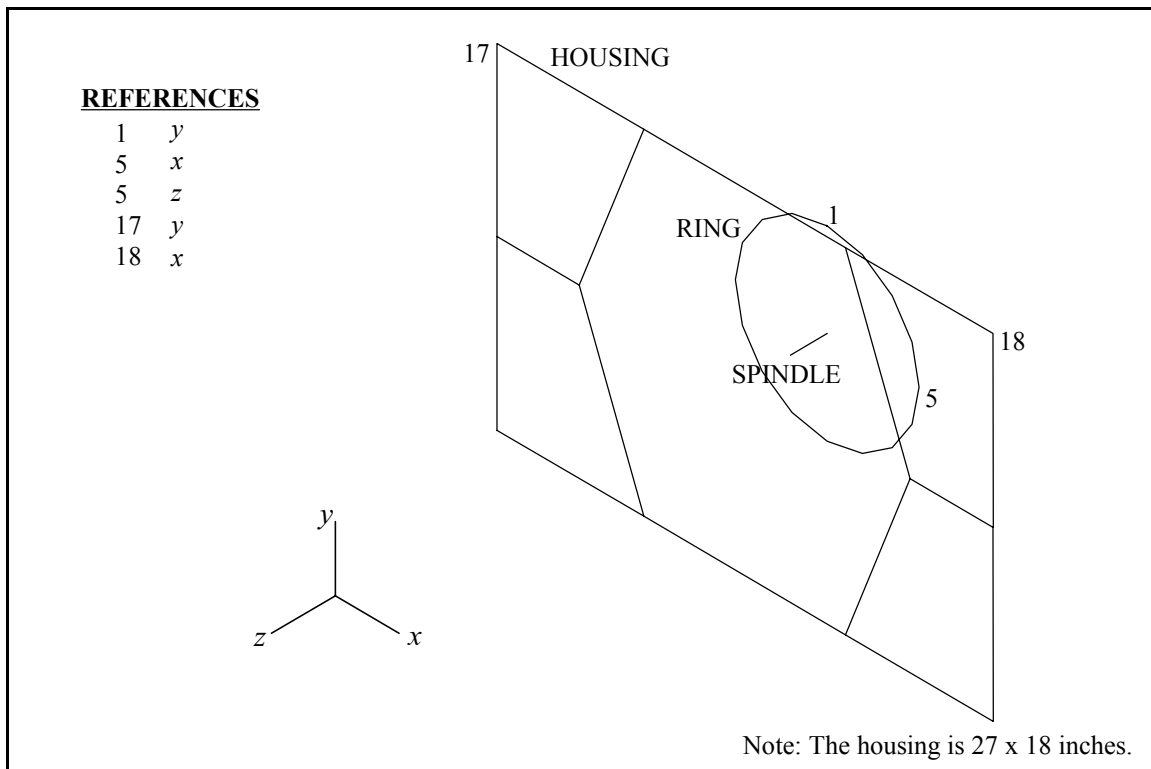
Figure 4-28. Squeeze Film Damper Rig Geometry and Reference Locations.
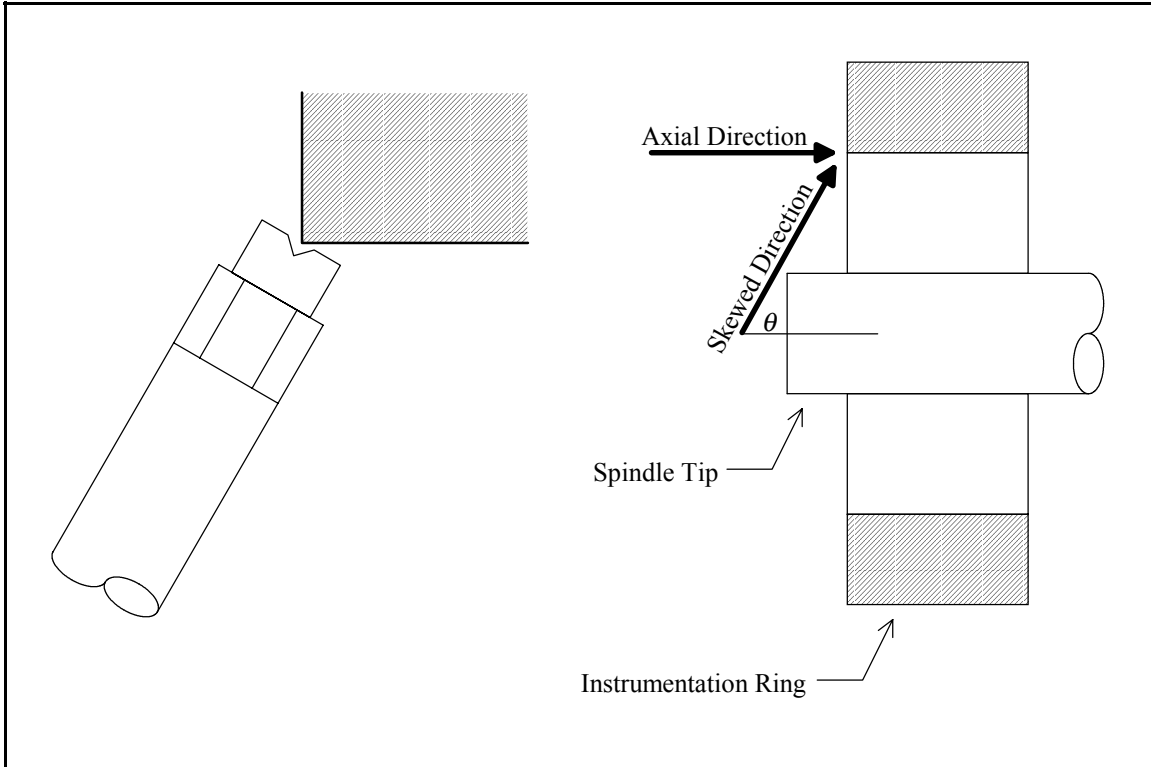
Figure 4-29. Skewed Direction Impacts on Instrumentation Ring.
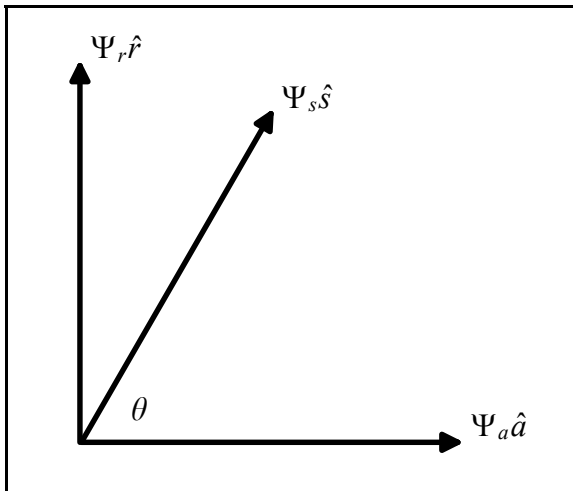
a is the axial direction
s is the skewed direction
r is the radial direction
Ψ_a is the axial component
Ψ_s is the skewed component
Ψ_r is the radial component

Figure 4-30. Skewed Direction Impacts Coordinate Transformation.
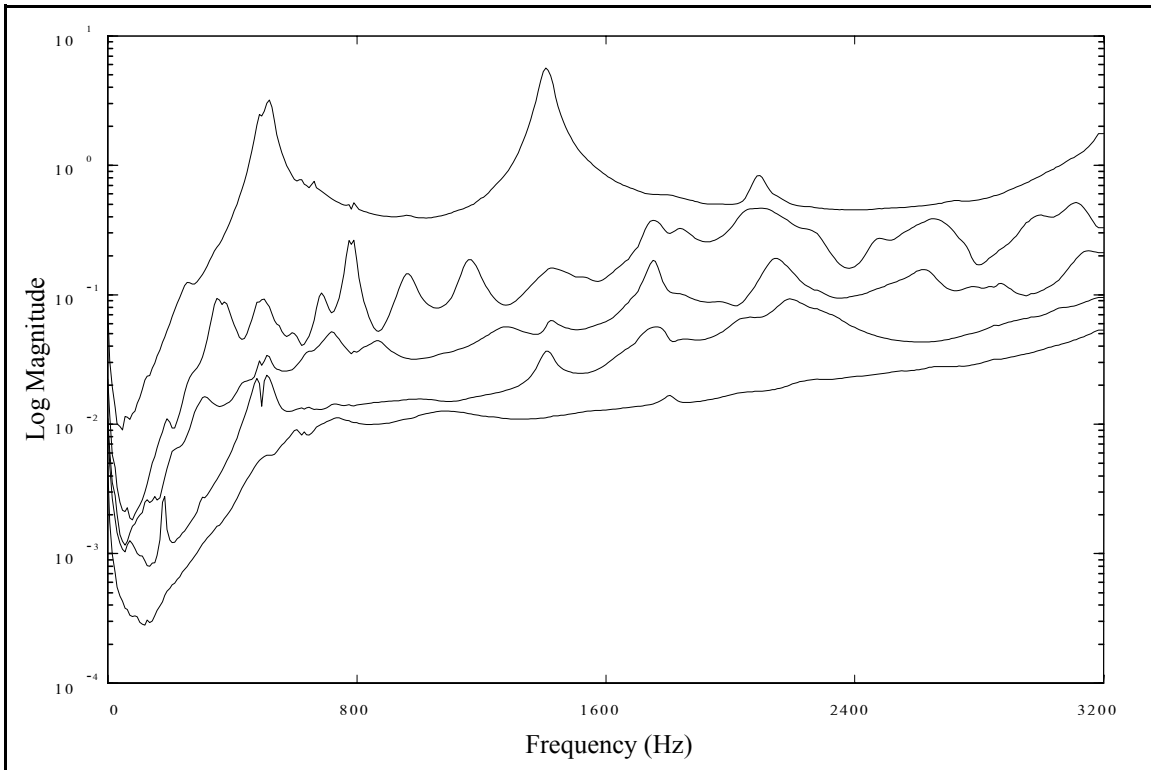
Figure 4-31(a). Squeeze Film Damper Rig CMIF, Complex Calculation.
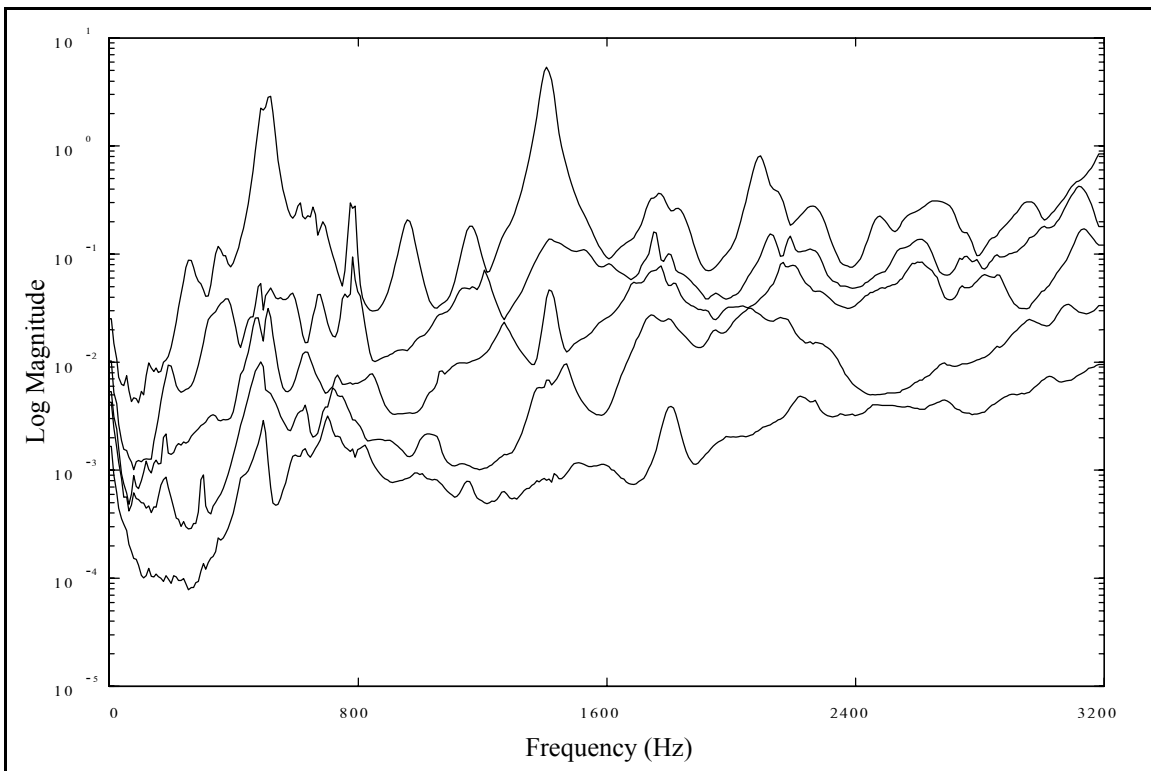
Figure 4-31(b). Squeeze Film Damper Rig CMIF, Quadrature Calculation.

170

4.6   Automobile Rear-Axle

A unique application of the MRIT method was to measure the mode shapes of an automobile rear-axle in its case. The rear-axle assembly was removed from the automobile and suspended with shock cord, and the test definition is listed in Table 4-10. Figure 4-32 shows a schematic of the test system, the reference locations, and the animation geometry. The axle was enclosed in a cylindrical case, which made it inaccessible to an impact hammer. To impact on the axle, 1/4-inch holes were drilled at 2-inch intervals along the length of the case in two perpendicular directions. The Modal Punch was fitted with a steel extension tip, as pictured in Figure 4-33, which was inserted into the holes to impact on the axle through the case. Reference accelerometers were located on the wheel hubs and on the gears in the differential. Measurements were made on the axle and the case, but the DOFs on the gears were not included in the animation geometry. This modal test would be very difficult and impractical, if at all possible, using the MIMO test method. The CMIFs of this data set, shown in Figure 4-34, exhibit several sets of nearly repeated modes of multiplicity three and four, and CMIF can separate these modes.

No. References	6
No. Impact Locations	76
Data Acquisition System	PC with multi-channel front-end hardware
Impactor	standard impact hammer and Modal Punch
Reference Transducers	(4) accelerometers, with 2 triaxes
Frequency Range	0 - 800 Hz at 1 Hz

Table 4-10. Automobile Rear-Axle Test Definition.
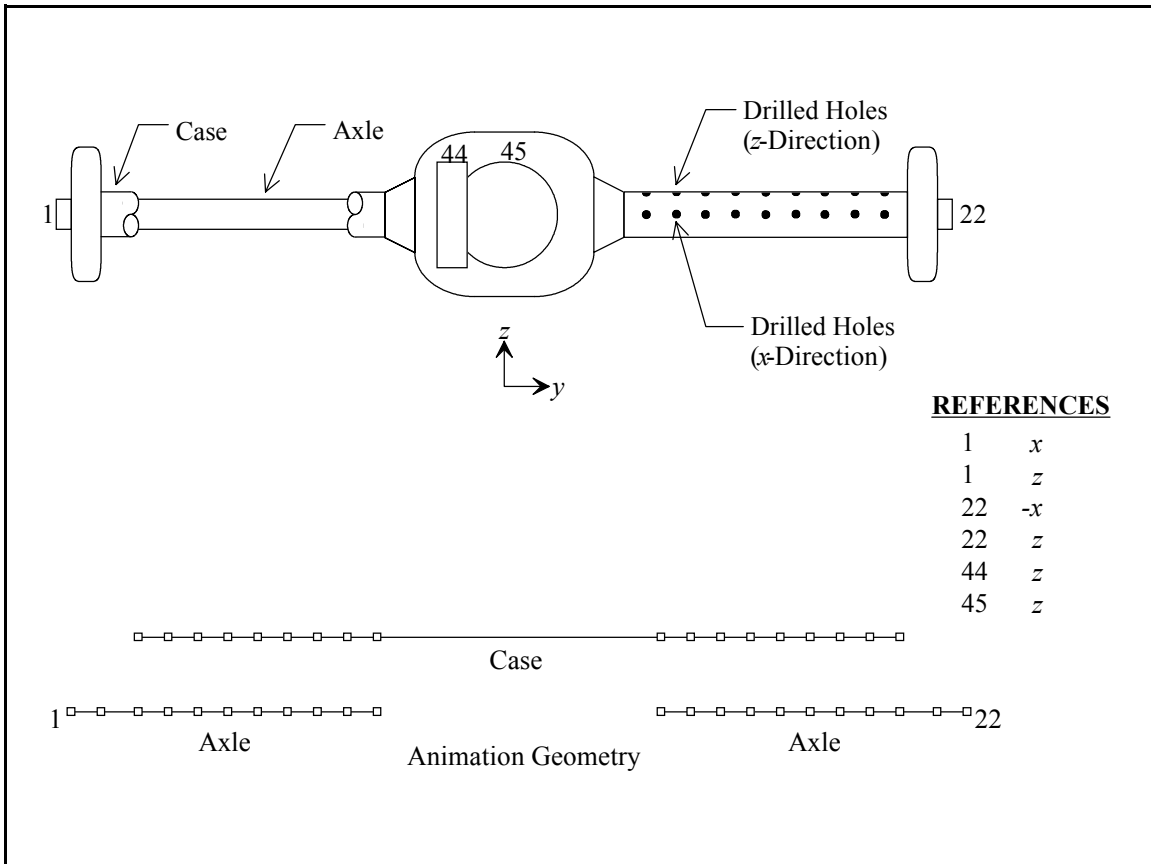
Figure 4-32. Automobile Rear-Axle Test Case, Geometry and Reference Locations.
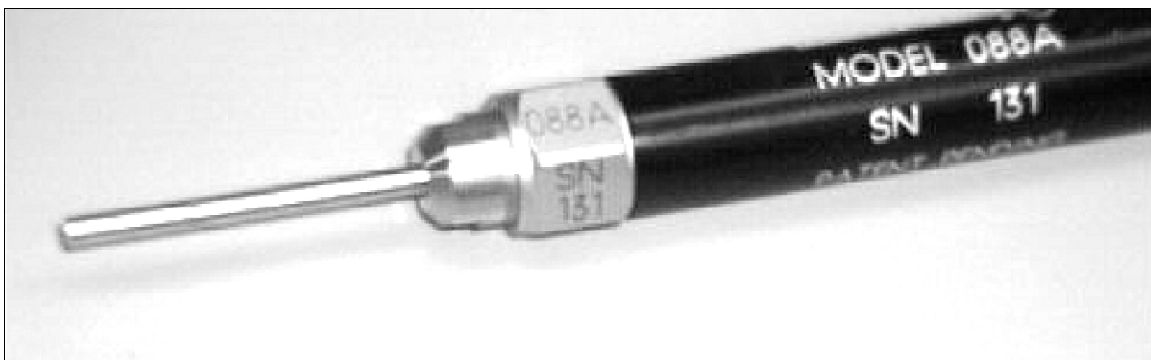
Figure 4-33. The Modal Punch with Extension Tip.
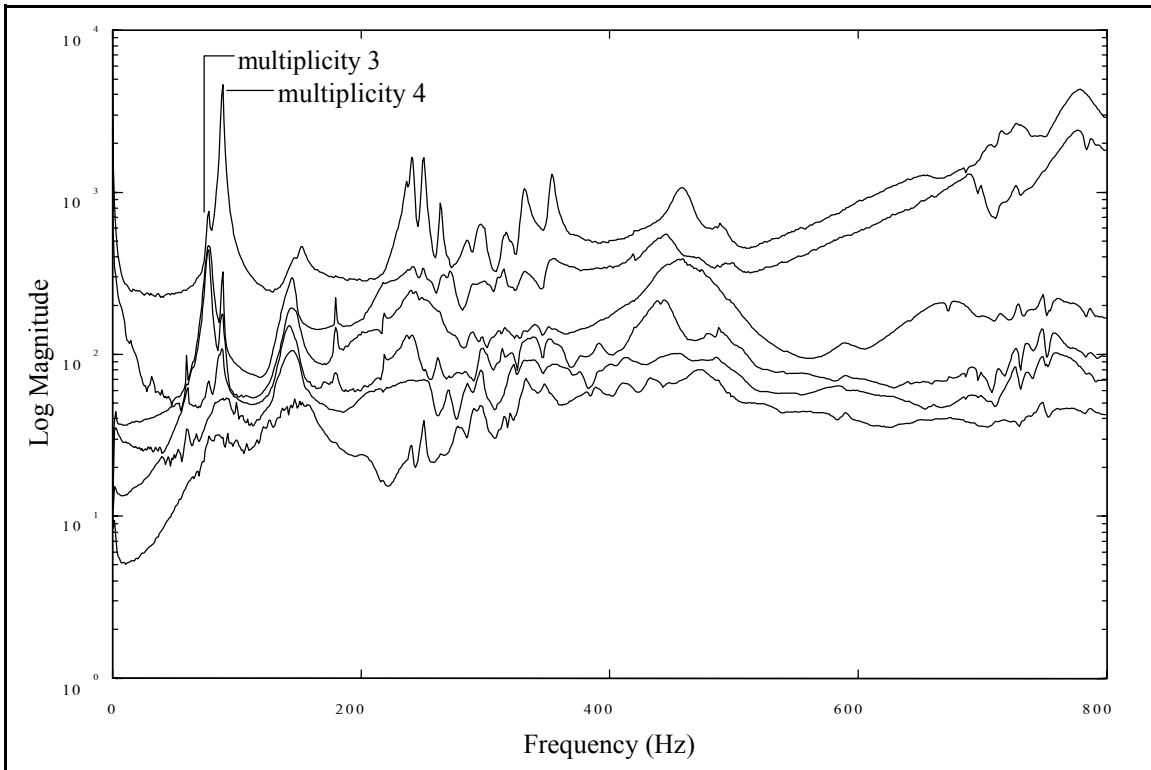
Figure 4-34(a). Automobile Rear-Axle CMIF, Complex Calculation.
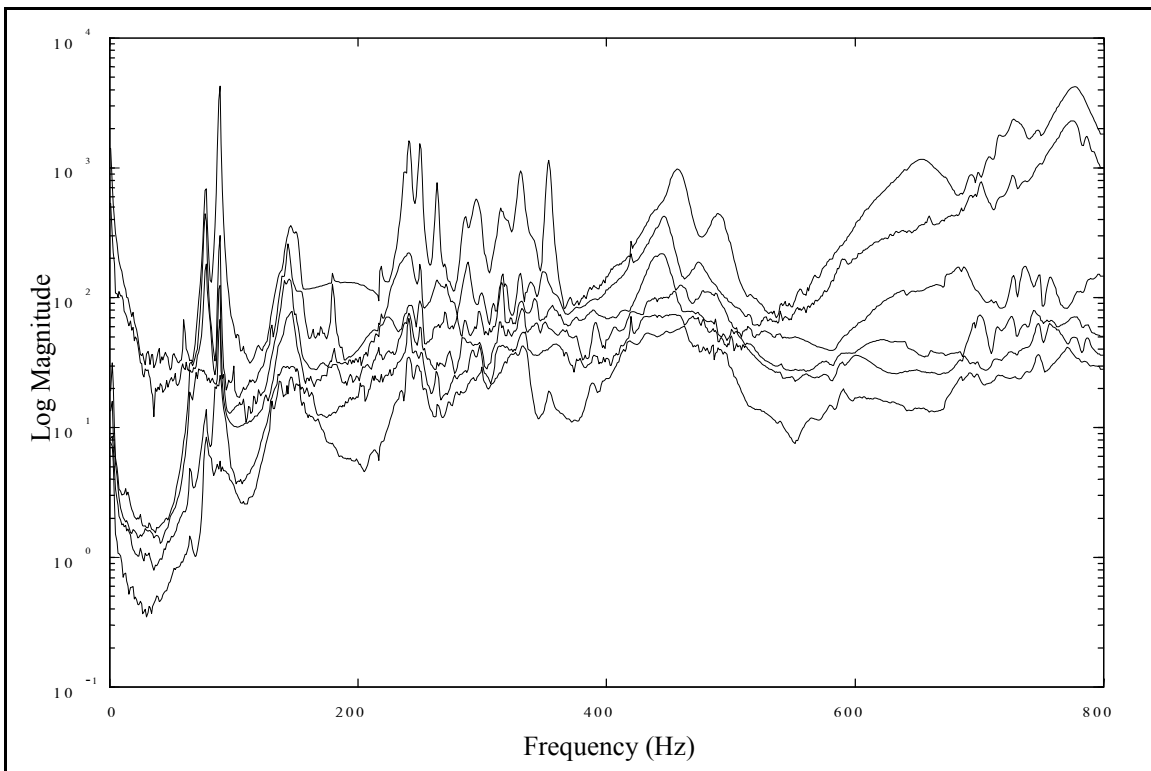
Figure 4-34(b). Automobile Rear-Axle CMIF, Quadrature Calculation.

173

4.7 Turbine Blade

The MRIT method was used to conduct an acoustic modal[43,44] test on a small turbine blade, as a preliminary procedure for other testing. The purpose of this test was to determine the resonant frequencies and mode shapes, which would then be used to identify areas of large deflections for strain measurements. Since the test object was small and lightweight, MIMO testing with shakers was not a practical method and mass loading of accelerometers was an appreciable concern. For this MRIT test case, the reference transducers were omni-directional microphones which were positioned above the turbine blade, and the testing was conducted in an anechoic room. The test definition is listed in Table 4-11, and the test setup is shown in Figure 4-35. The test object was clamped in a fixture at both ends for fixed boundary conditions. The test geometry is shown in Figure 4-36, and impacts were made normal the curved surface. The impactor used for this test, which also shown in Figure 4-35, is quite small and is not swung like a hammer. Instead, the head is pull backed, bending the flexible shaft, and then released to impact the object. The CMIFs of this data set are shown in Figure 4-37, and the modes identified included the sixth bending and third torsion.

No. References	5
No. Impact Locations	64
Data Acquisition System	PC with multi-channel front-end hardware
Impactor	miniature, flexible impact hammer
Reference Transducers	(5) microphones
Frequency Range	0 - 12.8 kHz at 16 Hz

Table 4-11. Turbine Blade Test Definition.
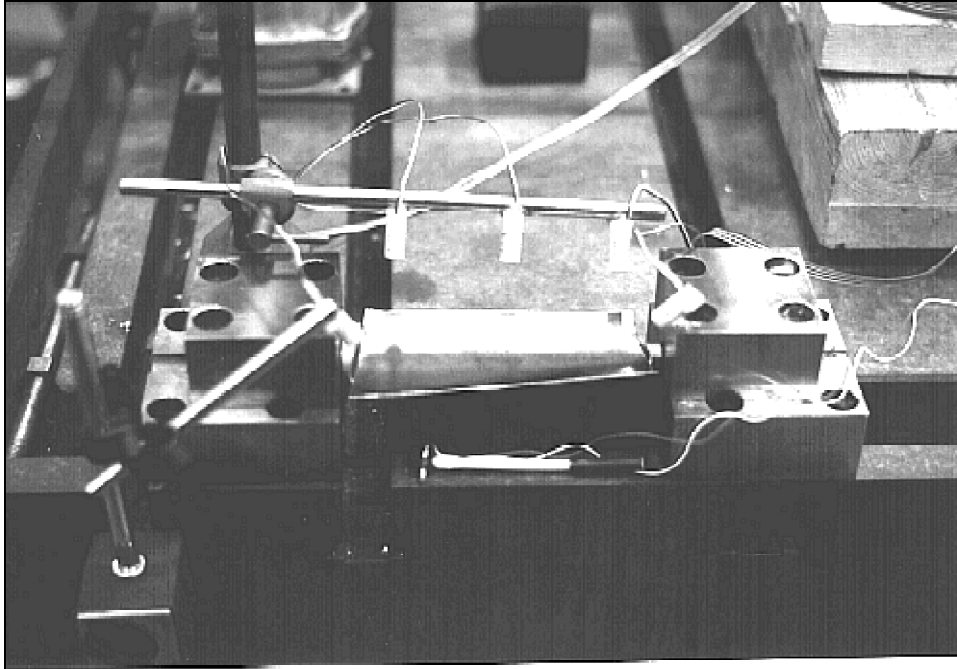
Figure 4-35. Turbine Blade Test Case.

Overall Dimensions : 2-1/4 x 6-1/4 inches.
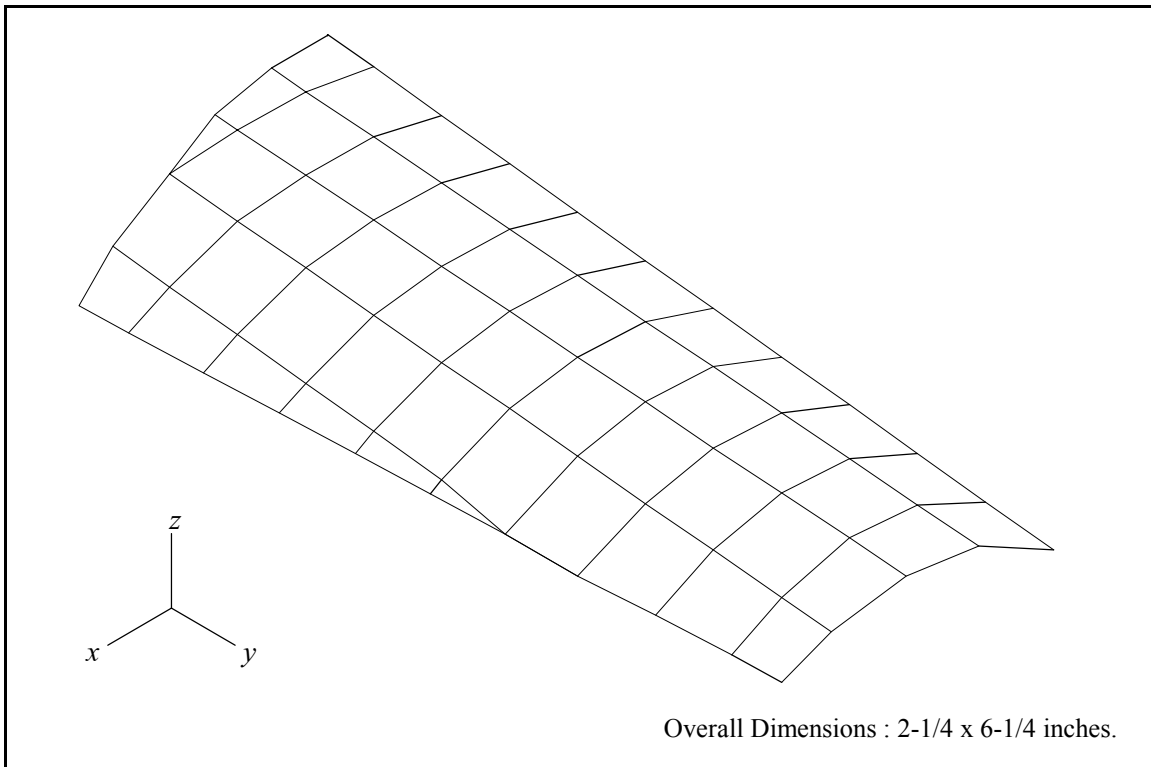
Figure 4-36. Turbine Blade Geometry.
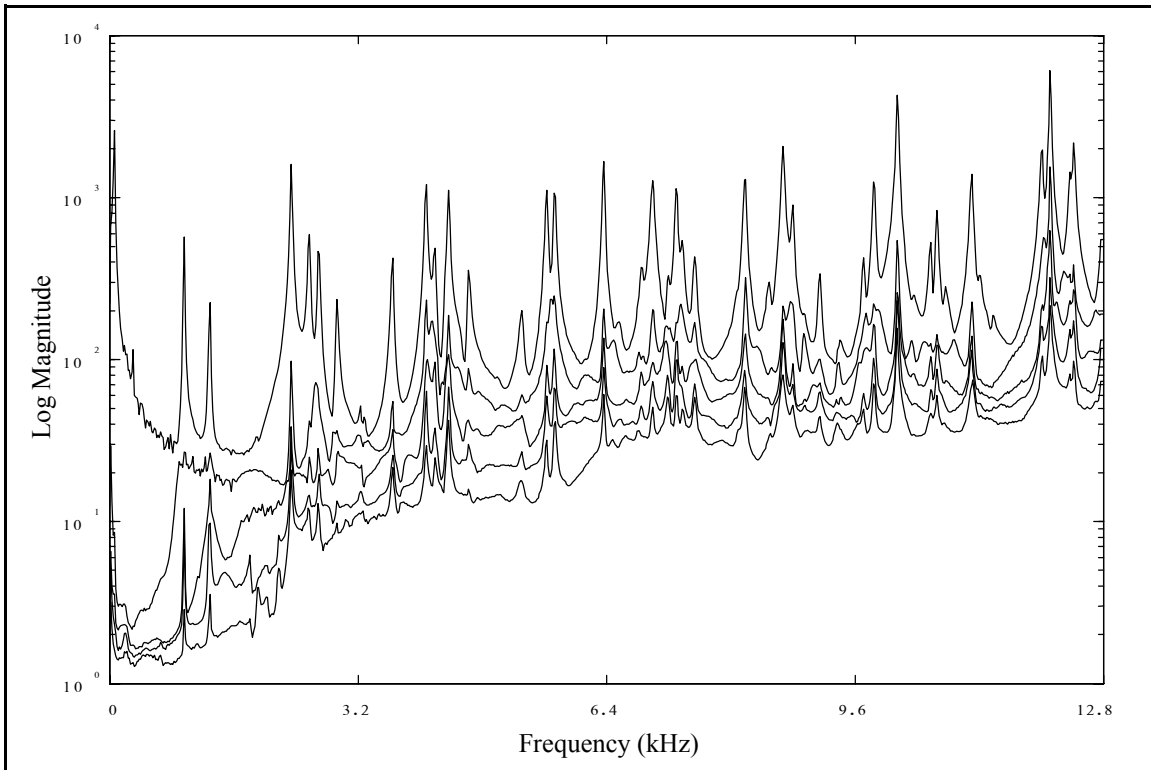
Figure 4-37(a). Turbine Blade CMIF, Complex Calculation.
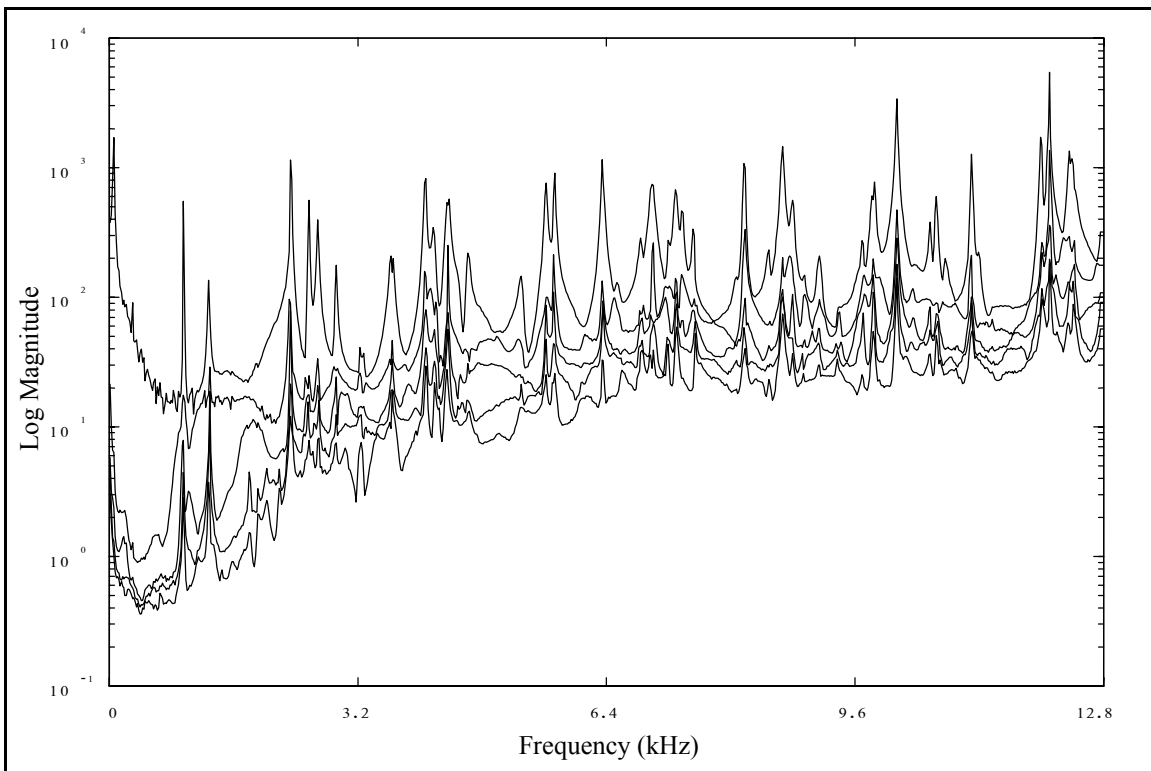
Figure 4-37(b). Turbine Blade CMIF, Quadrature Calculation.

176

4.8   Concrete Bridge

An MRIT modal test was conducted on a short-span, prestressed concrete bridge, which is pictured in Figure 4-38. The bridge was tested as part of a research project for developing an experimental technique for estimating the flexibility matrix of such structures. The bridge had a span of 29 feet, a width of 24 feet, and weighed 30 tons. The test geometry and reference locations are shown in Figure-39, measurements were made only normal the top surface. This bridge, which was built in the 1950's in Athens County, Ohio, was scheduled for demolition the day after the test, and because of the time constraints, MRIT was the only feasible testing method. In addition, only one lane of the bridge could be tested because the other lane had to remained open to traffic. Measurements were collected between the passages of vehicles, and the test was completed by three people in about four hours. Preliminary analysis of the measurements was done on-site with the CMIF analysis method on a laptop PC. The CMIFs of this data set are shown in Figure 4-40. This test case is a noteworthy example of field testing, as a gasoline-powered, electric generator was required to power the analyzer and computer at the remote site . The bridge was constructed from inverted T-shaped beams, and several of these were removed for additional MRIT tests in the laboratory.

No. References	3
No. Impact Locations	27
Data Acquisition System	4-channel programmable analyzer
Impactor	12-lb impact sledge-hammer
Reference Transducers	(3) seismic accelerometers (1000 mV/g)
Frequency Range	0 - 200 Hz at .25 Hz

Table 4-12. Concrete Bridge Test Definition.
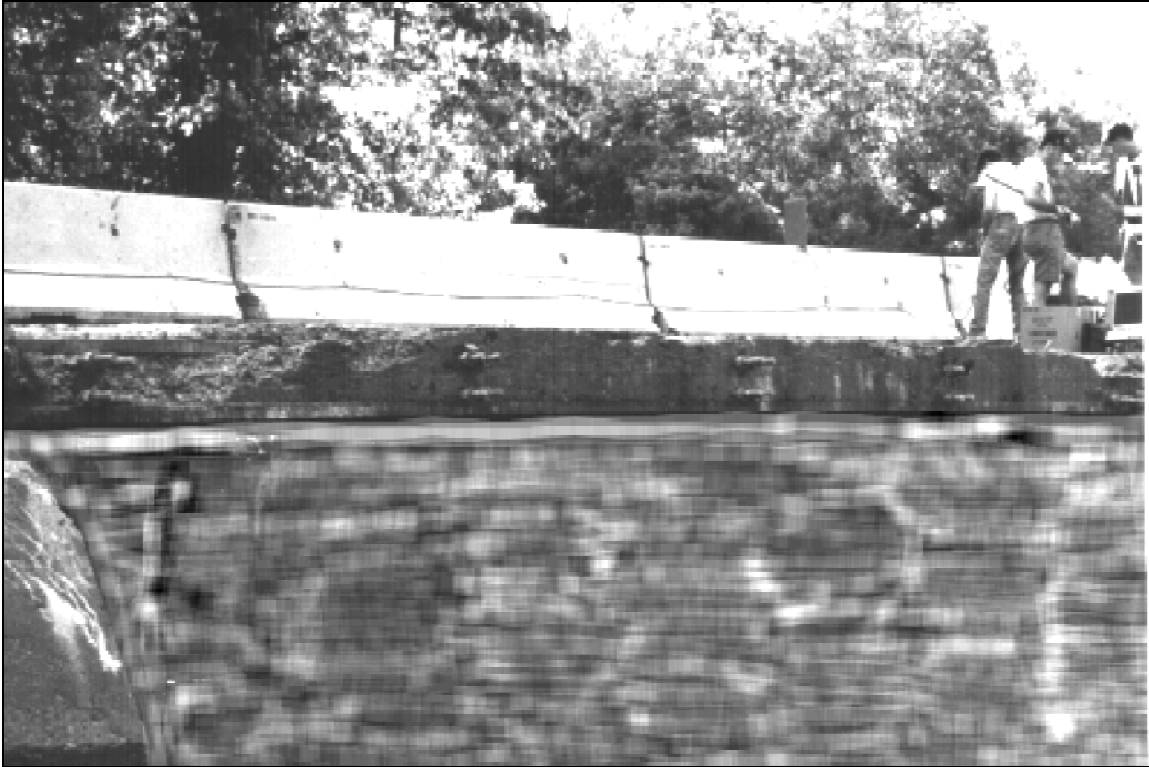
Figure 4-38. Concrete Bridge Test Case.
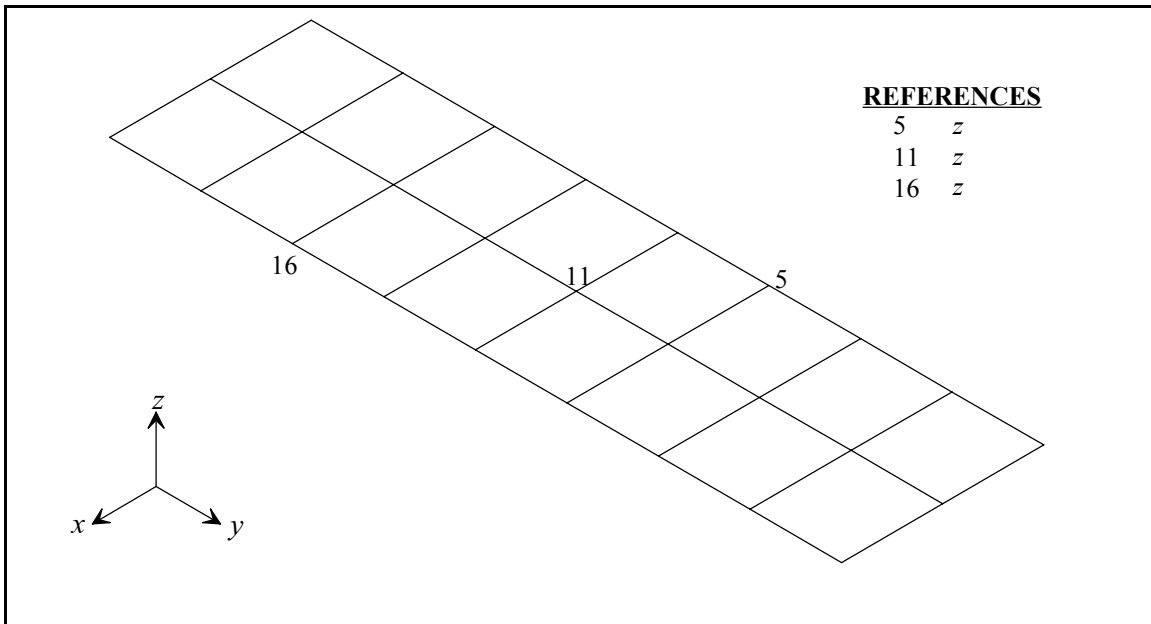
Figure 4-39. Concrete Bridge Geometry and Reference Locations.
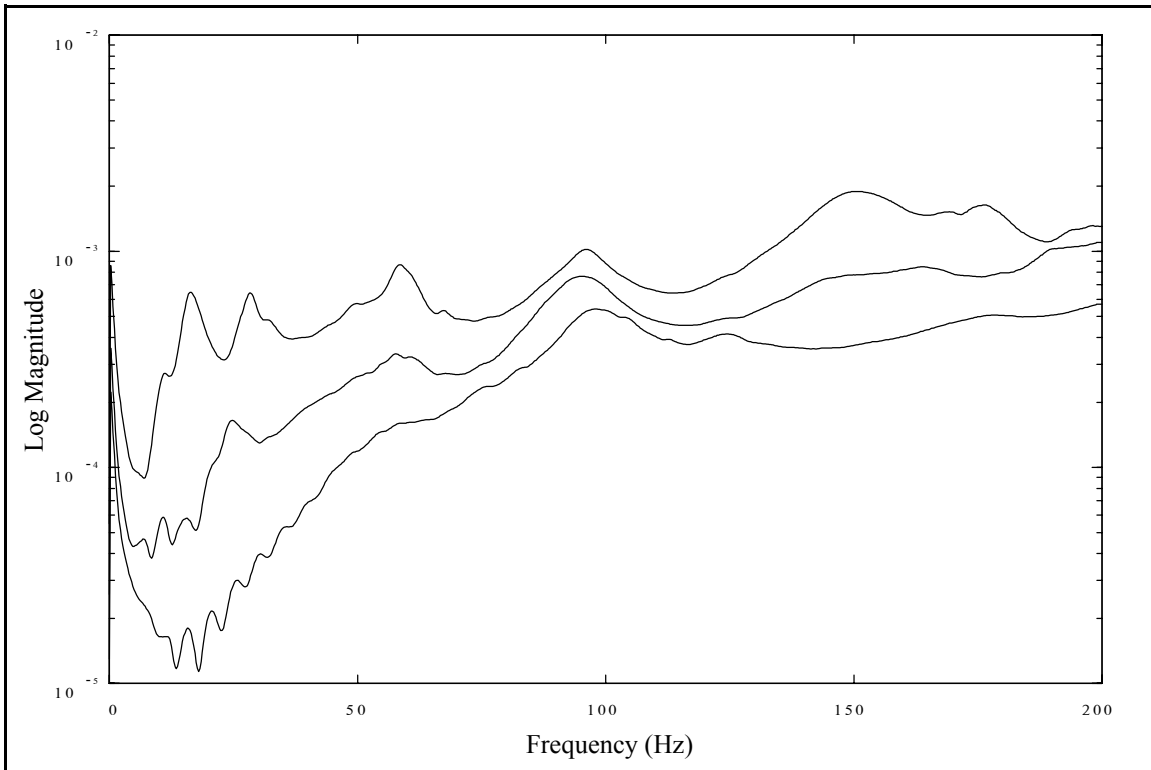
Figure 4-40(a). Concrete Bridge CMIF, Complex Calculation.
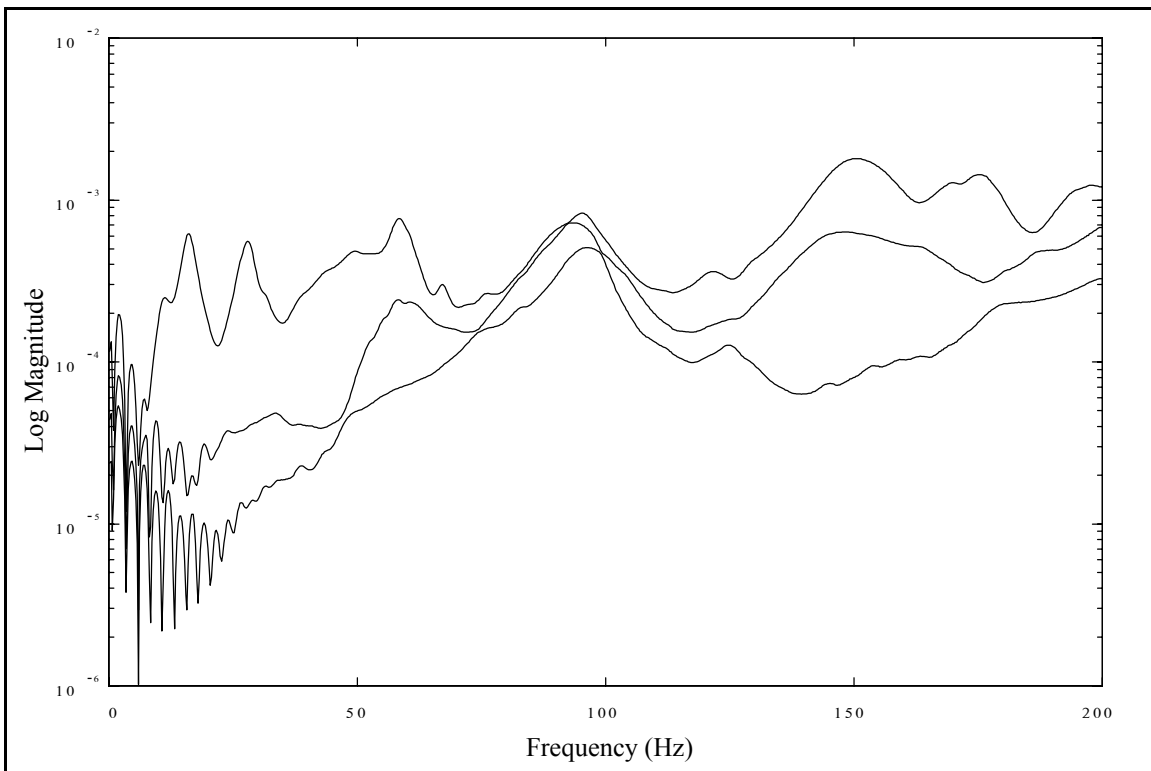
Figure 4-40(b). Concrete Bridge CMIF, Quadrature Calculation.

179

4.9 Rotating Machinery

In Section 2.3.2, several techniques for removing periodic noise components from response signals were described. This type of signal processing is applicable to an impact test of rotating machinery while in operation. Testing a system while in operation may be necessary if its dynamics vary with operating conditions. For instance, the properties of the bearings may be dependent on the rotational speed. The small rotating rig pictured in Figure 4-41 is the system for this test case. The reference transducers were proximity probes positioned to measure the vertical and horizontal deflections of the shaft, and impacts were made on the disk in the vertical and horizontal directions. The periodic components in the response are created by the run-out of the shaft and unbalance. The run-out is caused by any variance of the circular cross-section of the shaft. A time domain curve-fitting algorithm was used to estimate the frequency, amplitude and phase of the periodic components of the response signals.

Figure 4-42 is the measured time record for the vertical response due to the vertical input. The blocksize is 2048 points and the pretrigger delay is 50 percent of the sampling period. The first half of the time record is processed to estimate the parameters of the periodic components. The impact occurred at the midpoint of the sampling period, and the second half of the time record, also shown in Figure 4-43(a), contains the response due the impact plus the periodic response. The response after the periodic content has been removed is shown in Figure 4-43(b), this is the response due to only the impact. Next, an exponential window is applied to the processed response, as shown in Figure 4-43(c), and then is Fourier transformed. Only the second half of the impact time record

is transformed to the input autopower spectrum. This procedure is repeated for each average.

Figure 4-44(a) is the FRF of the vertical response and the vertical input with the applied signal processing. Figure 4-44(b) is the same FRF using the unprocessed response in Figure 4-43(a). The exponential window was applied, but the periodic components were not removed. The vertical lines indicate the regions of the FRF where the periodic components in the response are evident. As this example demonstrates, the response to periodic excitation sources can be removed from FRF measurements with signal processing.
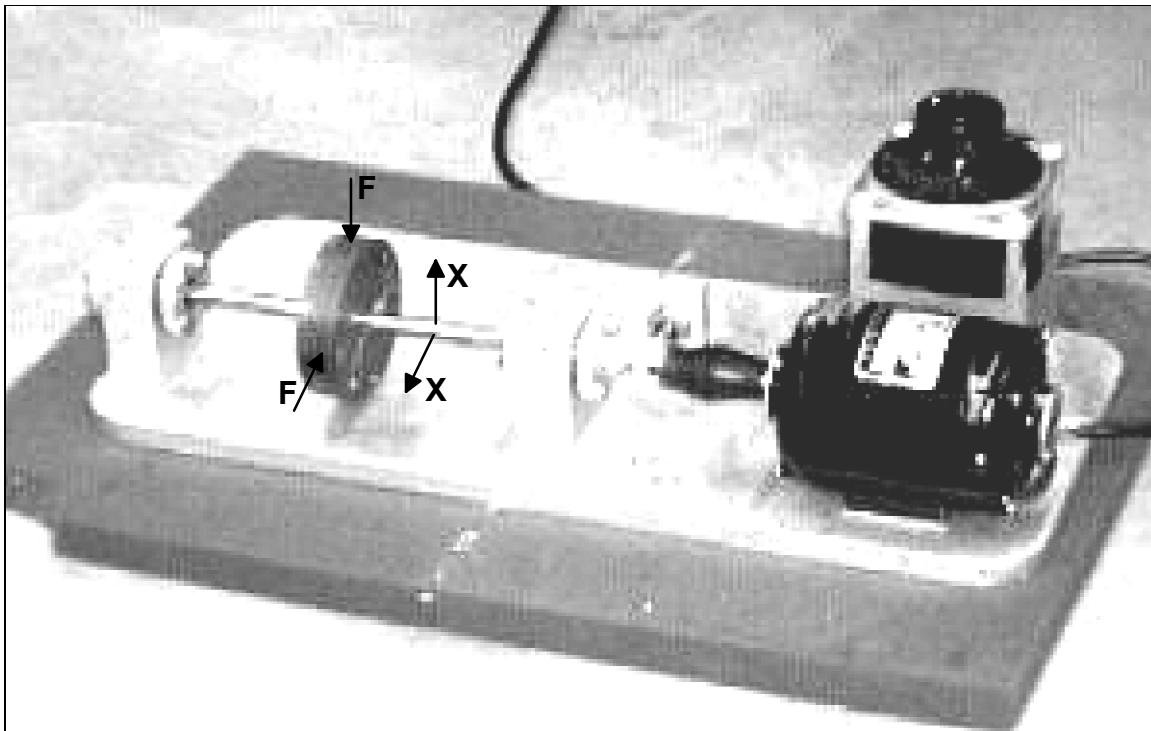
Figure 4-41. Rotating Machinery Test Case.
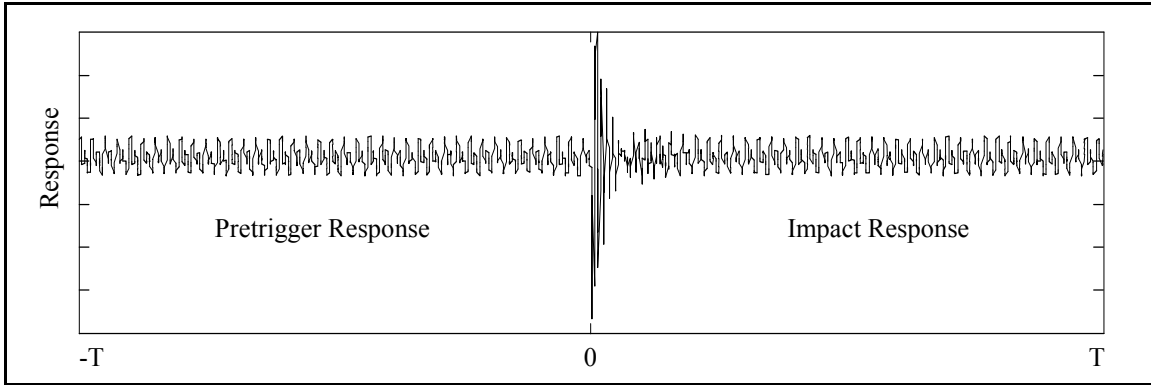
Figure 4-42. Rotating Machinery Pretrigger and Impact Response.
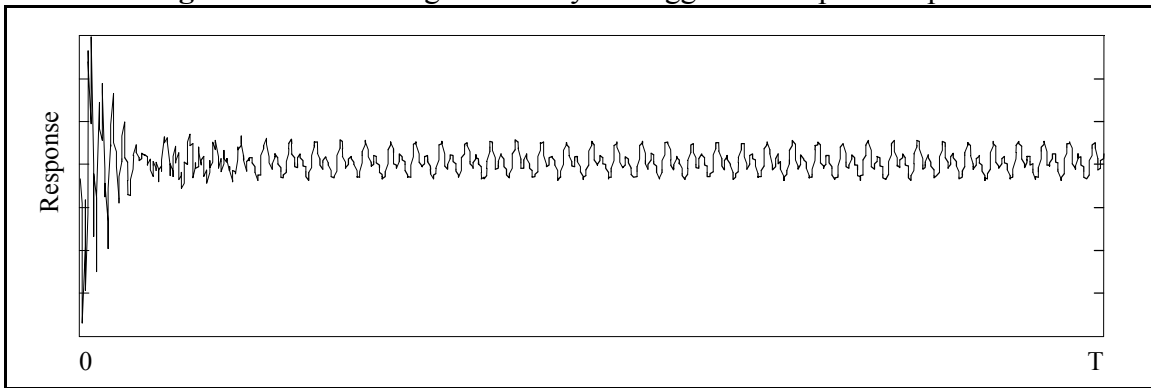
Figure 4-43(a). Impact Response, before Signal Processing.
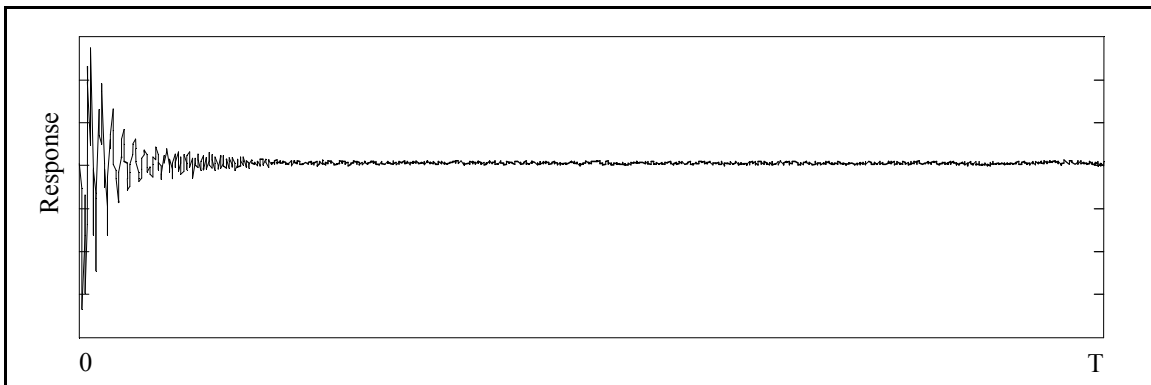
Figure 4-43(b). Impact Response, after Signal Processing.
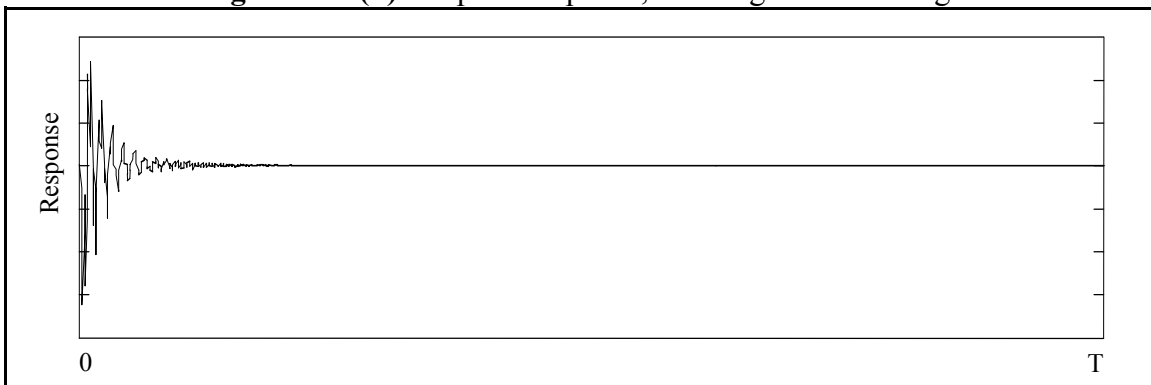
Figure 4-43(c). Impact Response, after Signal Processing and Windowing.

182
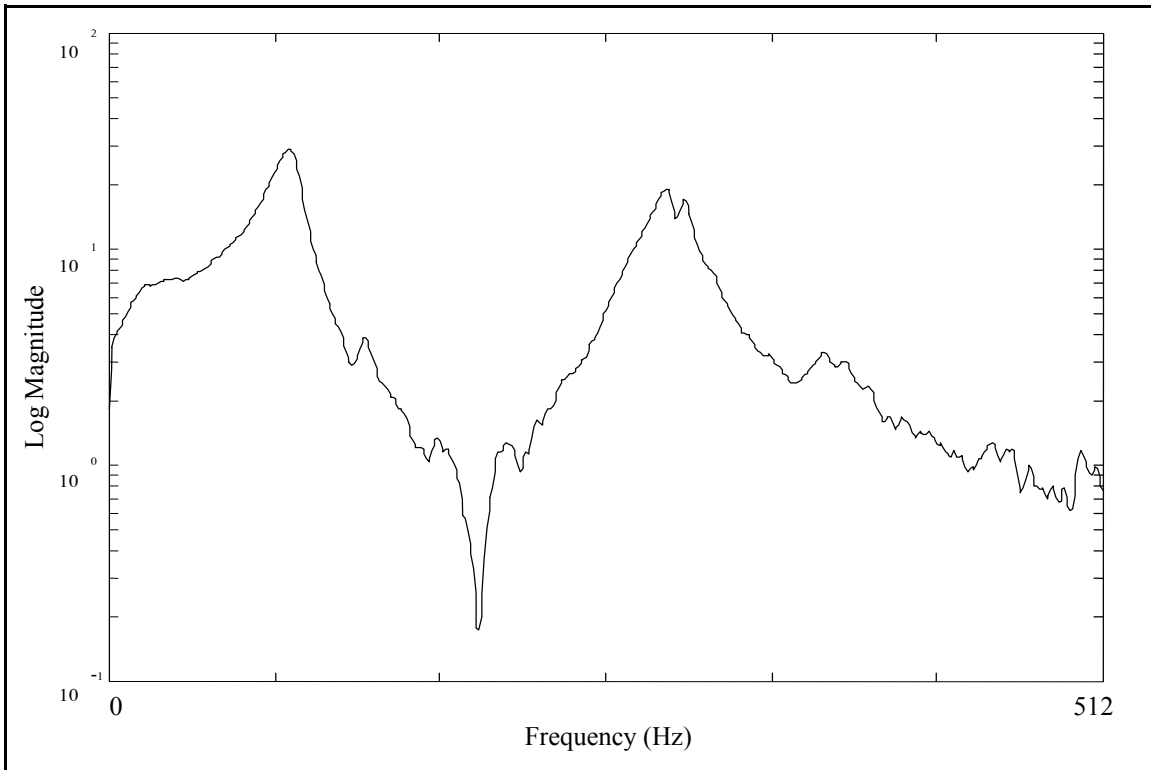
Figure 4-44(a). Rotating Machinery FRF, with Signal Processing.
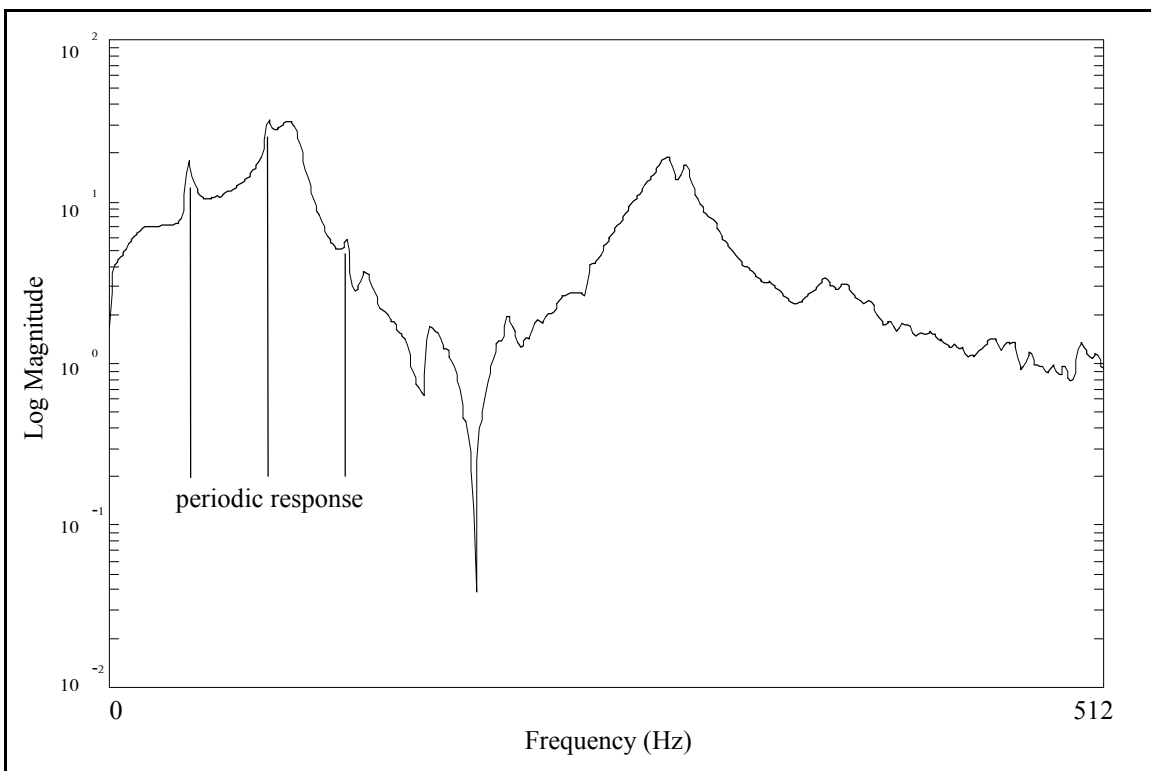
Figure 4-44(b). Rotating Machinery FRF, without Signal Processing.

183

4.10 Chapter Summary

The analytical systems and the circular plate are included to demonstrate the CMIF analysis method and its associated parameter estimation techniques. The one DOF system validates the SDOF algorithms for estimating poles and modal scale factors and the exponential window correction. The five DOF system demonstrates that acceptable results are obtained for an MDOF system and provides some insight on the effects and results CMIF. The five DOF system and circular plate test cases also demonstrate the capability of CMIF to detect and process repeated modes. The circular plate data set contains an unexpected occurrence of the CMIF crossover effect in which a crossover occurs at a peak in the CMIF. Although the CMIF analysis method is generally very straightforward, there are instances when evaluation techniques are necessary to select a valid set of CMIF peaks. The circular plate data set was also used to display some of the effects and results of the CMIF processing options.

The experimental test cases are offered as a sample of the diverse possibilities for MRIT applications. Some of these test were conducted as part of research projects, while others were done only for this thesis work. All of these tests were accomplished in a practical manner, with limited equipment, and by people with varying levels of impact testing experience. In each case the MRIT method produced an FRF data set from which acceptable modal parameters could be estimated for the purpose of the test. Listed below is a summary of the important features of the test cases which illustrate some aspect of Multiple Reference Impact Testing.

Types of test systems: from rather small objects, such as the turbine blade, to rather large structures, such as the bridge; systems in operation such as the rotating machinery.

Types of impactors: flexible, miniature impactor for the turbine blade; lightweight, hand-held impact hammer for the circular plate and composite box beams; standard-size, hand-held impact hammer for the rear-axle and rotating machinery; 1-lb hand-held impact hammer for the machine tool and SFD rig; 12-lb impact sledge-hammer for the bridge; instrumented punch for the SFD rig and the rear-axle.

Reference transducers: microphones for the turbine blade; proximity probes for the rotating machinery; different types and sizes of accelerometers for the other test cases.

Field testing: machine tool, SFD rig, bridge.

Troubleshooting: machine tool, SFD rig,

Alternative to MIMO: composite box beams, turbine blade, rear-axle, bridge.

Vector completion methods: slave DOFs for the composite box beams; coordinate transformation for the SFD rig.

The rotating machinery test case also demonstrates the signal processing steps to remove the response components due to periodic excitation sources from impact data. This procedure requires either customized data acquisition programming or post-processing. The capability to perform the signal processing in real-time on the acquisition system would be favorable. Otherwise, the actual measurements for this type of impact test would entail collecting several sets of time records for each impact location, and post-processing the data to compute FRFs. For this test case, the latter procedure was used.

Chapter 5   Conclusions and Recommendations

Impact testing procedures and applications have been established over many years, and it is still a widely used modal testing method. MRIT is an enhancement of impact testing that provides a practical method for measuring multiple reference FRFs that does not require a multiple-input FRF estimator. Because MRIT requires minimal setup time and testing equipment and is adaptable to many testing conditions, it is very well suited for troubleshooting and field testing. The availability of portable testing equipment has promoted the utility of MRIT, and implementation of MRIT can be further improved with custom testing software.

Although impact testing is a very practical and efficient procedure, specialized testing techniques and some skill and experience are necessary to successfully conduct an impact test. The most significant limitation of the MRIT method in particular is unobtainable measurements due to physical constraints of a test system. In most cases, this limitation is acceptable, and techniques are available to lessen the effects. However, there are instances when this limitation is prohibitive, such as systems with very irregular surfaces. In these cases, roving response testing may be a more suitable method than MRIT.

The CMIF analysis method is an appropriate parameter estimation companion for MRIT because it is a straightforward procedure that efficiently processes multiple reference FRFs to produce mode shapes and frequencies. Although CMIF is an approximate

method and uses SDOF estimation algorithms, it typically produces satisfactory results. In many troubleshooting applications, CMIF produces information that is sufficient for the purpose. In other situations, CMIF could possibly be used as a preliminary procedure, followed by more detailed analysis. Just as an MRIT data set can be processed with any parameter estimation method, the CMIF analysis method can also be used for other types of data sets. In addition, coordinate transformation and a few basic vector completion techniques are available for many of the types of unmeasurable DOFs commonly encountered with MRIT.

An issue related to the CMIF analysis method that needs to be addressed is the arbitrary phase shift of enhanced FRFs caused by complex left singular vectors, which seems to adversely effect the pole and scaling estimation. The simplest technique to avoid this situation is to always use left singular vectors from the quadrature FRF matrix in the eFRF calculation. Another technique could be to normalize the complex left singular vectors to remove any phase shift prior to the eFRF calculation.

The MRIT Acquisition and Analysis software developed during the course of this work implement most of the concepts and procedures presented in this thesis. Yet issues remain for further investigation and implementation, such as real-time signal processing for removing periodic components and convenient vector completion. In addition, any further refinements to the measurement process or equipment will further promote the utility of the MRIT method.

This thesis has presented a survey of issues related to Multiple Reference Impact Testing. In order to successfully utilize MRIT, the fundamental principles and practical limitations must be understood. The essential conclusion is that although MRIT has some shortcomings, these are generally outweighed by its benefits. MRIT has been and will continue to be a popular testing method, because it is an effective testing method for many applications.

References

[1]   W.A. Fladung, D.L. Brown, *Multiple Reference Impact Testing*, Proceedings of the Seventeenth International Seminar on Modal Analysis, 1992, pp. 257-272.

[2]   R.W. Rost, *Investigation of Multiple Input Frequency Response Function Estimation Techniques for Modal Analysis*, Doctoral Dissertation, University of Cincinnati, 1985, 219 pp.

[3]   R.J. Allemang, *Investigation of Some Multiple Input/Output Frequency Response Function Experimental Modal Analysis Techniques*, Doctoral Dissertation, University of Cincinnati, 1980, 358 pp.

[4]   L.P. Lauffer, M.D. Tucker, *Multi-Point Transient Modal Testing,* Proceedings of the Fifth International Modal Analysis Conference, 1987, pp. 394-398.

[5]   T. Vinh, I.H. Tawfiq, *Polyreference Method of Modal Analysis Using Impact Testing*, Proceedings of the Florence Modal Analysis Conference, 1991, pp. 221-227.

[6]   E. Betti, *Il nouvo Cimento*, Ser. 2, Vols. 7 and 8, 1872.

[7]   J.C. Maxwell, *Scientific Papers*, Cambridge, Vol. 1, p. 598, 1890.

[8]   J.S. Bendat, A.G. Piersol, *Random Data: Analysis and Measurement Procedures*, John Wiley and Sons, Inc., 1971, 407 pp.

[9]   E.O. Brigham, *The Fast Fourier Transform and its Applications*, Prentice-Hall, Inc., 1988, 448 pp.

[10]   S. R. Ibrahim, E.C. Mikulcik, *A Method for the Direct Identification of Vibration Parameters from the Fee Response*, Shock and Vibration Bulletin, Vol. 47, Part 4, 1977, pp. 183-198.

[11]   C.D. Van Karsen, *A Survey of Excitation Techniques for Frequency Response Function Measurement*, Masters Thesis, University of Cincinnati, 1987, 81 pp.

[12]   A. Soom, B.J. Wang, T. Trachler, *Energy Transfer During Impact Testing*, Proceedings of the Fourth International Modal Analysis Conference, 1986, pp. 1424-1431.

[13] D.L. Brown, W.G. Halvorsen, *Impulse Technique for Structural Frequency Response Testing*, Sound and Vibration, Vol.11, No. 11, 1977, pp. 8-21.

[14] D. Corelli, D.L. Brown, *Impact Testing Considerations*, Proceedings of the Second International Modal Analysis Conference, 1984, pp. 735-742.

[15] K.G. McConnell, *Errors in Using Force Transducers*, Proceedings of the Eighth International Modal Analysis Conference, 1990, pp. 884-890.

[16] W.A. Fladung, R.W. Rost, J.B. Poland, *The Modal Punch: A New Impacting Development*, Proceedings of the Twelfth International Modal Analysis Conference, 1994, pp. 1034-1040.

[17] W.A. Fladung, R.W. Rost, D.L. Brown, *Further Developments of Multiple Reference Impact Testing*, Proceedings of the Twelfth International Modal Analysis Conference, 1994, pp. 1026-1033.

[18] D.L. Brown, R.D. Zimmerman, R.J. Allemang, M. Mergeay, *Parameter Estimation Techniques for Modal Analysis*, SAE Paper Number 790221, SAE Transactions, Vol. 88, Sect. 1, 1979, 19 pp.

[19] R.J. Allemang, D.L. Brown, W.A. Fladung, *Modal Parameter Estimation: A Unified Matrix Polynomial Approach*, Proceedings of the Twelfth International Modal Analysis Conference, 1994, pp. 501-513.

[20] A.V. Oppenheim, R.W. Schafer, *Digital Signal Processing*, Prentice-Hall, Inc., 1975, 585 pp.

[21] R.C. Sohaney, J.M. Nieters, Pr*oper Use of Weighting Functions for Impact Testing*, Proceedings of the Third International Modal Analysis Conference, 1985, pp. 1102-1106.

[22] H. Van der Auweraer, P. Vanherck, P. Sas, R. Snoeys, *Accurate Modal Analysis Measurements with Programmed Sine Wave Excitation*, Mechanical Systems and Signal Processing, Vol. 1, No. 3, 1987, pp. 293-300.

[23] D. J. Ewins, *Modal Testing: Theory and Practice*, Research Studies Press, Ltd., John Wiley and Sons, Inc., 1984, 269 pp.

[24] Hewlett-Packard, *HP Instrument BASIC Users Handbook Version 2.0*, 1992.

[25] Hewlett-Packard, *HP-IB Programmer's Guide*, 1992.

[26] Hewlett-Packard, *Using HP Instrument BASIC with the HP 35670A*, 1992.

[27] Hewlett-Packard, *HP-IB Programming with the HP 35670A*, 1992.

[28] Hewlett-Packard, *Standard Data Format Utilities: User's Guide*, 1993.

[29] Vold, H., Kundrat, J., Rocklin, T., Russell, R., *A Multi-Input Modal Estimation Algorithm for Mini-Computers*, SAE Paper Number 820194, SAE Transactions, Vol. 91, Sect. 1, Jan. 1982, 7 pp.

[30] Juang, J.-N., Pappa, R.S., *An Eigensystem Realization Algorithm for Modal Parameter Identification and Model Reduction*, AIAA Journal of Guidance, Control, and Dynamics, Vol. 8, No. 4, 1985, pp. 620-627.

[31] F. Lembregts, R. Snoeys, J. Leuridan, *Application and Evaluation of Multiple Input Modal Parameter Estimation*, Journal of Analytical and Experimental Modal Analysis, Vol. 2, No. 1, 1987, pp. 19-31.

[32] C.Y. Shih, Y.G. Tsuei, R.J. Allemang, D.L. Brown, *A Frequency Domain Global Parameter Estimation Method for Multiple Reference Frequency Response Measurements*, Mechanical Systems and Signal Processing, Vol. 2, No. 4, 1988, pp. 367-377.

[33] C.Y. Shih, Y.G. Tsuei, R.J. Allemang, D.L. Brown, *Complex Mode Indicator Function and Its Applications to Spatial Domain Parameter Estimation*, Proceedings of the Seventh International Modal Analysis Conference, 1989, pp. 533-540.

[34] W. Leurs, *Modal Parameter Estimation Based on the Complex Mode Indicator Functions*, Proceedings of the Eleventh International Modal Analysis Conference, 1993, pp. 1035-1041.

[35] G. Strang, *Linear Algebra and Its Applications*, 3rd ed., Harcourt Brace Jovanich, Inc., 1988, 505 pp.

[36] R.J. Allemang, *Vibrations: Analytical and Experimental Modal Analysis*, UC-SDRL-CN-20-263-662, University of Cincinnati, Mar. 1994, 184 pp.

[37] S.J. Shelley, *Investigation of Discrete Modal Filters for Structural Dynamics Applications*, Doctoral Dissertation, University of Cincinnati, 1991, 269 pp.

[38] S.M. Crowley, *Expanding Test Mode Shapes for Better Visualization*, Proceedings of the Florence Modal Analysis Conference, 1991, pp. 593-599.

[39] C.W. Englehardt, D.L. Hunt, *User Manual for TFORM Mode Shape Transformation Program*, SDRC, Inc., Mar. 1989.

[40] J. Crowley, D. Brown, G.T. Rocklin, *Uses of Rigid Body Calculations in Test*, Proceedings of the Fourth International Modal Analysis Conference, 1986, pp. 487-491.

[41] The MathWorks Inc., *MATLAB User's Guide*, March, 1991.

[42] SDRC I-Deas, *Core Utilities User's Guide*, Section XIV, Universal Datasets, 1990.

[43] R.J. Allemang, W.R. Shapton, *Using Modal Techniques to Guide Acoustic Signature Analysis*, SAE Paper Number 780106, SAE Transactions, Vol. 87, Sect. 1, 1978, 9 pp.

[44] D.L. Brown, R.J. Allemang, *Modal Analysis Techniques Applicable to Acoustic Problem Solution*, Inter-Noise, 1978, pp. 909-914.